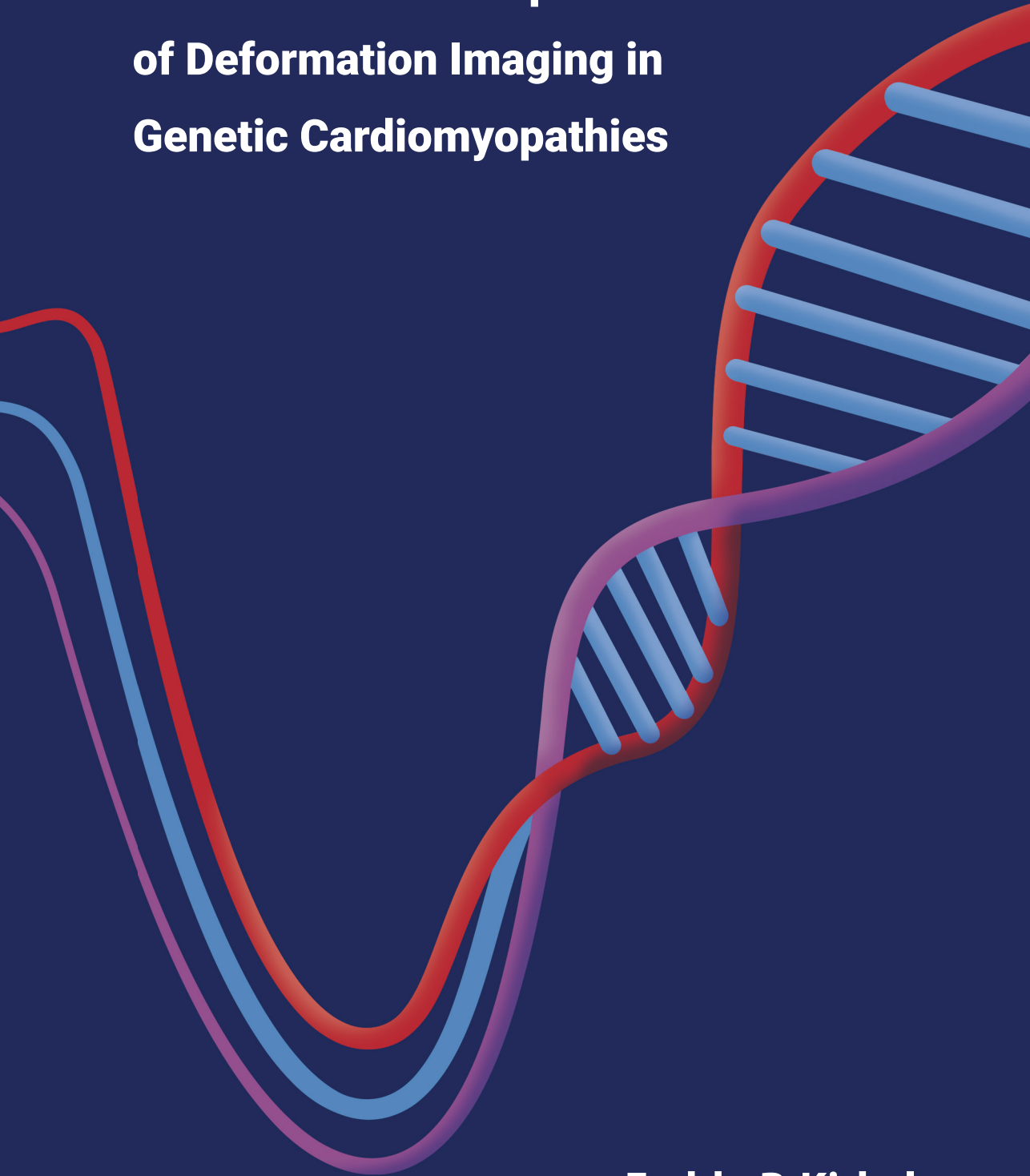


Towards Clinical Implementation of Deformation Imaging in Genetic Cardiomyopathies



Feddo P. Kirkels

**TOWARDS CLINICAL IMPLEMENTATION OF DEFORMATION
IMAGING IN GENETIC CARDIOMYOPATHIES**

Feddo P. Kirkels

ISBN: 978-94-6506-077-4

Provided by thesis specialist Ridderprint, ridderprint.nl

Printing: Ridderprint

Layout and design: Puck Paassen, persoonlijkproefschrift.nl

Financial support by the Dutch Heart Foundation for the publication of this thesis is gratefully acknowledged.

Copyright © F.P. Kirkels, 2024

All rights reserved. No part of this thesis may be reproduced, stored in a retrieval system, or transmitted in any form or by any means without prior permission of the copyright owner.

Towards Clinical Implementation of Deformation Imaging in Genetic Cardiomyopathies

Klinische Implementatie van Deformatiebeeldvorming in Erfelijke Hartspierziekten

(met een samenvatting in het Nederlands)

Proefschrift

ter verkrijging van de graad van doctor aan de
Universiteit Utrecht
op gezag van de
rector magnificus, prof. dr. H.R.B.M. Kummeling,
ingevolge het besluit van het college voor promoties
in het openbaar te verdedigen op

dinsdag 11 juni 2024 des middags te 4.15 uur

door

Feddo Pieter Kirkels

geboren op 27 mei 1993
te Utrecht

Promotoren

Prof. dr. F.W. Asselbergs

Prof. dr. ir. J.E. Lumens

Copromotoren

Dr. M.J. Cramer

Dr. A.J. Teske

Beoordelingscommissie

Prof. dr. S.A.J. Chamuleau

Prof. dr. P.A.F.M. Doevendans

Prof. dr. M.C. Post

Prof. dr. J.P. van Tintelen

Prof. dr. B.K. Velthuis

TABLE OF CONTENTS

Introduction

Chapter 1	General Introduction and Thesis Outline	9
-----------	---	---

Part I. Deformation imaging methods in ARVC

Chapter 2	Improving Diagnostic Value of Echocardiography in Arrhythmogenic Right Ventricular Cardiomyopathy Using Deformation Imaging <i>JACC Cardiovasc Imaging. 2021;14(12):2481-2483.</i>	25
Chapter 3	Right Ventricular Functional Abnormalities in Arrhythmogenic Cardiomyopathy: Association With Life-Threatening Ventricular Arrhythmias <i>JACC Cardiovasc Imaging. 2021;14(5):900-910.</i>	31

Part II. Characterizing the disease substrate underlying deformation abnormalities

Chapter 4	Electromechanical Substrate Characterization in Arrhythmogenic Cardiomyopathy Using Imaging-Based Patient-Specific Computer Simulations <i>Europace. 2021;23(Suppl1):i153-i160.</i>	59
Chapter 5	Uncertainty Quantification of Regional Cardiac Tissue Properties in Arrhythmogenic Cardiomyopathy Using Adaptive Multiple Importance Sampling <i>Frontiers in Physiology. 2021;12:738926.</i>	79
Chapter 6	Monitoring of Myocardial Involvement in Early Arrhythmogenic Right Ventricular Cardiomyopathy Across the Age Spectrum <i>J Am Coll Cardiol. 2023;82(9):785-97.</i>	103

Part III. Towards clinical implementation of deformation imaging

Chapter 7	Echocardiographic Deformation Imaging for Early Detection of Genetic Cardiomyopathies: A Systematic Review <i>J Am Coll Cardiol. 2022;79(6):594-608.</i>	127
Chapter 8	The Added Value of Abnormal Regional Myocardial Function for Risk Prediction in Arrhythmogenic Right Ventricular Cardiomyopathy <i>Eur Heart J Cardiovasc Imaging. 2023;24(12):1710-1718.</i>	163

Discussion

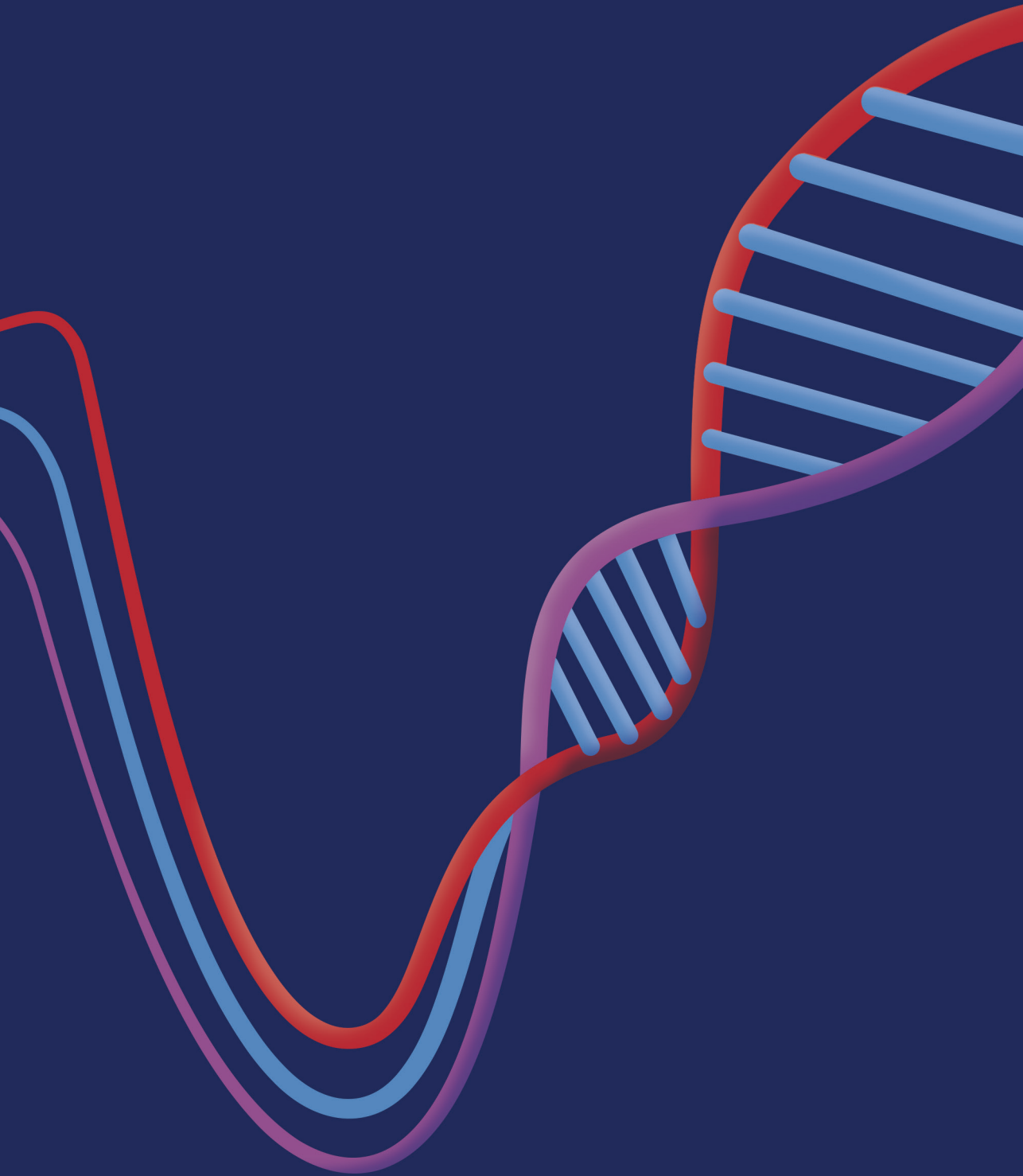
Chapter 9	General Discussion and Future Perspectives	185
-----------	--	-----

Addendum: Left sided wall stress causing arrhythmia

Chapter 10	Prevalence of Mitral Annulus Disjunction and Mitral Valve Prolapse in Patients With Idiopathic Ventricular Fibrillation <i>J Am Heart Assoc. 2022;11(16):e025364.</i>	201
------------	--	-----

Appendices

Nederlandstalige samenvatting	222
List of publications	226
Dankwoord/Acknowledgements	228
Curriculum Vitae	234



CHAPTER 1

General Introduction and Thesis Outline

INTRODUCTION

Sudden cardiac death (SCD) resulting from cardiac arrest represents a major public health concern worldwide, accounting for an estimated 15-20% of all deaths.¹ Particularly in young, seemingly healthy individuals, it is an event with devastating impact. Families and physicians are left with many unanswered questions: Did we miss any signs? Could it have been prevented? And who else is at risk? It was estimated that in the Netherlands, every three days an individual below the age of 40 dies of SCD.² While in older patients coronary artery disease is the most common cause of SCD, typical causes in the young are congenital heart disease, heritable electrical disease and heritable cardiomyopathy. Arrhythmogenic right ventricular cardiomyopathy (ARVC), subject of a large part of this thesis, is a relatively common cause of SCD within the latter category. However, both at autopsy and in survivors of sudden cardiac arrest, a substantial amount of cardiac arrests remains unexplained. When no underlying cause is identified after extensive diagnostic testing, patients are diagnosed with idiopathic ventricular fibrillation. This subset of patients is subject of the addendum of this thesis.

Arrhythmogenic Right Ventricular Cardiomyopathy

ARVC is a genetic cardiomyopathy which is characterized by progressive loss of primarily right ventricular myocardium and its substitution by fibrous and fatty tissue.³ Over the years, several terms were introduced related to this disease. The original term, arrhythmogenic right ventricular dysplasia, refers to the developmental disorder (“dysplasia”) that this disease was thought to be at the time. Later, ARVD was recognized as a progressive disease which develops after birth (“cardiomyopathy”) and after a transition period with the term ARVD/C, it was replaced with ARVC. While the classical and most comprehensively described phenotype primarily affects the right ventricle (RV), a proportion of patients has predominant LV disease. In recent years, the term arrhythmogenic cardiomyopathy (AC) was introduced to cover the whole spectrum of biventricular involvement. In this thesis, the terms AC and ARVC are used interchangeably, but focus is on the classical predominant RV phenotype.

Genetic background

Early observations of familial disease clustering suggested a genetic basis for ARVC. The Greek physician couple Nikos Protonotarios and Adalena Tsatsopoulou recognized that individuals on the Greek island of Naxos had a form of ARVC in conjunction with a cardiocutaneous syndrome (wooly hair and palmoplantar keratosis).⁴ In 2000, genetic linkage analysis of patients with so-called Naxos disease started an important breakthrough in defining the genetic background of ARVC.⁵ The typical phenotype is explained by similar junction structures in myocardial and epidermal tissue. Genetic variants in the gene encoding for plakoglobin were the first disease causing genetic variants identified in patients with ARVC. Plakoglobin is a component of the cardiac desmosome, which is responsible for cell-to-cell adhesion of cardiomyocytes (*Figure 1*). In subsequent years, more desmosomal variants were linked to ARVC and nowadays likely-(pathogenic) variants are identified in the majority of patients. Most of these disease causing variants in ARVC are inherited in an autosomal dominant pattern. Currently, the most common ARVC-associated gene is plakophilin-2 (PKP2), which was identified in about half of the ARVC patients in the Netherlands and the USA.⁶ However, also genetic variants in non-desmosomal proteins can cause ARVC, suggesting other pathogenic mechanisms in a final common pathway leading to myocardial fibrosis, fat infiltration and ventricular arrhythmias.⁷

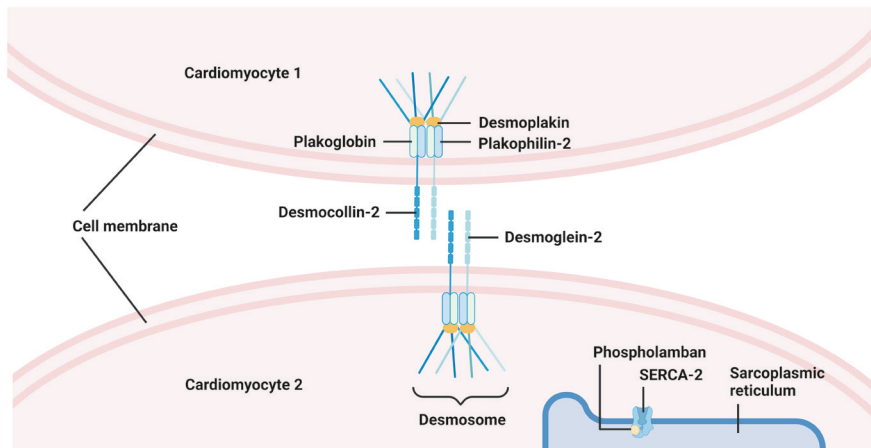


Figure 1. The cardiac desmosome

The cardiac desmosome provides mechanical cell-cell contact by connecting the cytoskeletons between cardiac myocytes. The encoded proteins (genes) associated with ARVC are divided into desmosomal (the most common being Plakophilin-2, or PKP2) and non-desmosomal proteins (for instance Phospholamban, or PLN).

Pathophysiology

The exact pathophysiological mechanism of ARVC is still a matter of debate. Besides the characteristic histopathologic pattern of fibrofatty replacement of myocardium, patchy inflammatory infiltrates are often observed in association with dying myocytes, suggesting that the pathologic process may be immunologically mediated. Wall thinning and aneurysmal dilatation are typically localized in the inflow tract (subtricuspid region) and outflow tract (infundibular region) of the RV.³ While the initial report of ARVC described the RV apex as typical localization for disease manifestation, more recent data showed that the apex is only involved in end-stage disease. On the other hand, the revised “triangle of dysplasia” includes the posterolateral wall of the LV as early affected region.⁸ It is thought that genetically abnormal desmosomes lead to disruption of intercellular junctions with myocyte detachment and cell death. This process of mechanical uncoupling occurs in reaction to mechanical wall stress and is aggravated by for instance physical exercise.⁹ The fibrofatty tissue that replaces myocardium forms a substrate for ventricular arrhythmias by slowing intra-ventricular conduction and through scar-related macro-reentry circuits, similar to that in myocardial infarction. Besides mechanical coupling, the desmosome also plays a crucial role in electrical coupling of cardiomyocytes by interacting with gap junctions and the sodium channel complex within the intercalated disc.¹⁰ Complex mechanisms operating at this molecular and cellular level may also contribute to occurrence of life-threatening ventricular arrhythmias in ARVC.

Clinical presentation

The estimated prevalence of ARVC is around 1:2000 to 1:5000 in the general population.⁹ Inheritance is characterized by incomplete penetrance and varying disease expression. There is age-related penetrance, whereby patients typically become symptomatic between the second and fourth decade of life.⁶ Clinical presentation of ARVC is variable and may include palpitations, exercise-induced (pre-)syncope, chest pain, and dyspnea. However, life-threatening arrhythmias

and SCD may also be the first clinical manifestation.¹¹ The clinically overt stage is preceded by a “concealed phase” in which no, or only subtle electrical or structural disease manifestation can be identified. The “electrical phase” is characterized by T-wave inversions and terminal QRS prolongation on electrocardiogram (ECG), premature ventricular complexes (PVCs) and ventricular tachycardia originating from the RV. In the “structural phase”, changes on tissue level lead to regional wall motion abnormalities and in the end-stage potentially heart failure.¹²

Diagnosis

No single test has sufficient sensitivity and specificity to serve as gold standard for ARVC diagnosis. To standardize the clinical diagnosis, a combination of clinical tests was defined in the Task Force Criteria (TFC) from 1994, and later modified in 2010.¹³ Criteria were divided into six categories: structure/function, tissue characterization, repolarization abnormalities, depolarization abnormalities, arrhythmias, and family history. Criteria considered to have high specificity were classified as major, other criteria as minor. At least two major, 1 major with 2 minor, or 4 minor criteria are required for a definite diagnosis. In general, low specificity of abnormalities associated with ARVC confronts clinicians with the challenge of differentiating ARVC from conditions like idiopathic RV outflow tract tachycardia, cardiac sarcoidosis and other causes of a volume overloaded RV. (Table 1)

Treatment and risk stratification

With no curative treatment options, current therapeutic strategies aim for symptom reduction and prevention of disease progression and SCD. Restriction of intense sports activity is regarded important in both ARVC patients and family members at risk, since exercise has been shown to provoke arrhythmias and accelerate disease progression. Unfortunately, it remains unclear to what extent exercise should be reduced to prevent harmful effects, while maintaining the physical and mental health benefits of exercise in general.^{14,15} Despite limited supportive data, beta-blockers are currently recommended in all patients since adrenergic stimulation seems to play a role in provoking ventricular arrhythmias.¹⁶ A central component of clinical management of ARVC patients and family members at risk is consideration of an implantable cardioverter defibrillator (ICD). Patients who benefit most from an ICD are those who have had an episode of ventricular fibrillation or sustained ventricular tachycardia. It remains a clinical challenge to select patients who will benefit from primary preventive ICD implantation. Different multivariable models have been developed to assist clinicians in this decision, of which the ARVC risk calculator published in 2019 (www.ARVCrisk.com) is currently the most extensively validated model.¹⁷ This tool estimates the 5-year risk of developing a first episode of sustained ventricular arrhythmia in patients with a definite ARVC diagnosis according to the 2010 TFC.

Family screening

Since ARVC is an inherited cardiomyopathy, family members of ARVC patients may be at risk of developing the disease. With the identification ARVC-causing genetic variants, integration of targeted genetic testing into clinical practice is proliferating. Given the autosomal dominant inheritance, first-degree relatives have a 50% chance of carrying the genetic predisposition for ARVC. However, even in family members carrying the same pathogenic variant as the index patient, cardiac screening is a major challenge because of incomplete penetrance and variable disease expression. Since life-threatening arrhythmias can already occur early in the disease, detection of the earliest signs of disease manifestation in family members is an ongoing quest.

Currently, life-long follow-up with intervals of 2-3 years is recommended in all family members at risk.¹⁸ The diagnostic framework is provided by the 2010 TFC and requires frequent ECG and Holter monitoring and repeated cardiac imaging with CMR or echocardiography. However, since disease manifestation in family members may be subtle, conventional diagnostics included in the 2010 TFC may lack sensitivity to reveal the earliest structural and functional changes.

Table 1. 2010 Task Force criteria proposed by Marcus et al¹³

Global or regional dysfunction and structural alterations	
2D-echo	
Major	Presence of a regional RV akinesia, dyskinesia, or aneurysm and 1 of the following (enddiastole) <ul style="list-style-type: none"> • PLAX RVOT ≥ 32 mm (corrected for BSA: PLAX RVOT/BSA ≥ 19 mm/m²) or • PSAX RVOT ≥ 36 mm (corrected for BSA: PLAX RVOT/BSA ≥ 21 mm/m²) or • RV-FAC $\leq 33\%$
Minor	Presence of a regional RV akinesia, dyskinesia, or aneurysm and 1 of the following (enddiastole): <ul style="list-style-type: none"> • PLAX RVOT ≥ 29 to < 32 mm (corrected for BSA: PLAX RVOT/BSA ≥ 16 to < 19 mm/m²) or • PSAX RVOT ≥ 32 to < 36 mm (corrected for BSA: PSAX RVOT ≥ 18 to < 21 mm/m²) or • RV-FAC $> 33\%$ to $\leq 40\%$
MRI	
Major	Presence of a regional RV akinesia or dyskinesia, or dyssynchronous RV contraction and 1 of the following: <ul style="list-style-type: none"> • Ratio of RV-EDV to BSA ≥ 110 ml/m² (male) ≥ 100 ml/m² (female) or • RVEF $\leq 40\%$
Minor	Presence of a regional RV akinesia or dyskinesia, or dyssynchronous RV contraction and 1 of the following: <ul style="list-style-type: none"> • Ratio of RV-EDV to BSA ≥ 100 to < 110 ml/m² (male) ≥ 90 to < 100 ml/m² (female) or • RVEF $> 40\%$ to $\leq 45\%$
RV angiography	
Major	Presence of regional RV akinesia, dyskinesia, or aneurysm
Tissue characterization	
Major	Residual myocytes $< 60\%$ by morphometric analysis (or $< 50\%$ if estimated), with fibrous replacement of the RV free wall myocardium in ≥ 1 sample, with or without fatty replacement of tissue on endomyocardial biopsy
Minor	Residual myocytes 60-75% by morphometric analysis (or 50% to 65% if estimated), with fibrous replacement of the RV free wall myocardium in ≥ 1 sample, with or without fatty replacement of tissue on endomyocardial biopsy
Repolarization abnormalities (ECG)	
Major	Inverted T waves in right precordial leads (V_1 , V_2 , and V_3) or beyond in individuals >14 years of age (in the absence of complete RBBB QRS ≥ 120 ms)
Minor	Inverted T waves in leads V_1 and V_2 in individuals >14 years of age (in the absence of complete RBBB) or Inverted T waves in leads in V_4 - V_6 or Inverted T waves in leads V_1 - V_4 in individuals >14 years of age in the presence of complete RBBB

Table 1. 2010 Task Force criteria proposed by Marcus et al¹³ (continued)

Depolarization abnormalities (ECG)	
Major	Epsilon wave (reproducible low-amplitude signals between end of QRS complex to onset of the T wave) in the right precordial leads (V_1 - V_3)
Minor	Late potentials by SA-ECG in ≥ 1 of 3 parameters in the absence of a QRS duration of 110 ms on the standard ECG <ul style="list-style-type: none"> • Filtered QRS duration (fQRS) ≥ 114 ms • Duration of terminal QRS < 40 μV (low-amplitude signal duration) ≥ 38 ms • Root-mean-square voltage of terminal 40 ms ≤ 20 μV Terminal activation duration of QRS ≥ 55 ms measured from the nadir of the S wave to the end of the QRS, including R' , in V_1 , V_2 , or V_3 , in the absence of complete RBBB
Ventricular arrhythmias	
Major	Nonsustained or sustained ventricular tachycardia of LBBB morphology with superior axis (negative or indeterminate QRS in leads II, III, and aVF and positive in lead aVL)
Minor	Nonsustained or sustained ventricular tachycardia of RV outflow configuration, LBBB morphology with inferior axis (positive QRS in leads II, III, and aVF and negative in lead aVL) or of unknown axis >500 premature ventricular complexes per 24 hours (Holter)
Family history	
Major	ARVC definite diagnosis confirmed in a first-degree relative who meets current 2010 Task Force criteria ARVC definite diagnosis confirmed pathologically at autopsy or surgery in a first-degree relative Identification of a pathogenic ARVC related mutation categorized as associated or probably associated with ARVC. Plakoglobin (JUP), Desmoplakin (DSP), Plakophilin-2 (PKP2), Desmoglein-2 (DSG2), Desmocollin-2 (DSC2), transforming growth factor beta-3 (TGF β 3), and transmembrane protein 43 (TMEM43)
Minor	History of ARVC in a first-degree relative in whom it is not possible or practical to determine whether the family member meets current Task Force criteria ARVC confirmed pathologically or by current Task Force Criteria in second-degree relative Premature sudden death (<35 years of age) due to suspected ARVC in a first-degree relative

Definite ARVC diagnosis requires: 2 major, 1 major + 2 minor or 4 minor criteria from different categories of the abovementioned criteria, in the absence of another cause of disease. Abbreviations: ARVC = arrhythmogenic right ventricular cardiomyopathy, ECG = electrocardiography, PLAX/PSAX = parasternal long/short axis view, RVOT = RV outflow tract, BSA = body surface area, RBBB/LBBB = right/left bundle branch block.

Echocardiographic deformation imaging

Echocardiographic deformation imaging has been proposed as an additional method for detection of early disease manifestation in ARVC.¹⁹ This technique has developed over the past two decades as a sensitive method for quantitative assessment of both global and regional contractile function of myocardial tissue. Acoustic markers called “speckles” are tracked in a two-dimensional image plane to estimate relative changes in myocardial length through

the cardiac cycle. Changes are expressed in percentages of lengthening or shortening over time and referred to as myocardial strain (*Figure 2*). Reproducibility of deformation imaging is superior compared to multiple conventional functional measures. Besides, it is more robust compared to visual assessment of regional wall motion abnormalities, which is especially challenging in the thin walled RV and highly dependent on experience of the observer. When compared to other high-end imaging modalities, the non-invasive nature, low cost and wide availability of echocardiographic deformation imaging are important advantages for routine clinical practice.

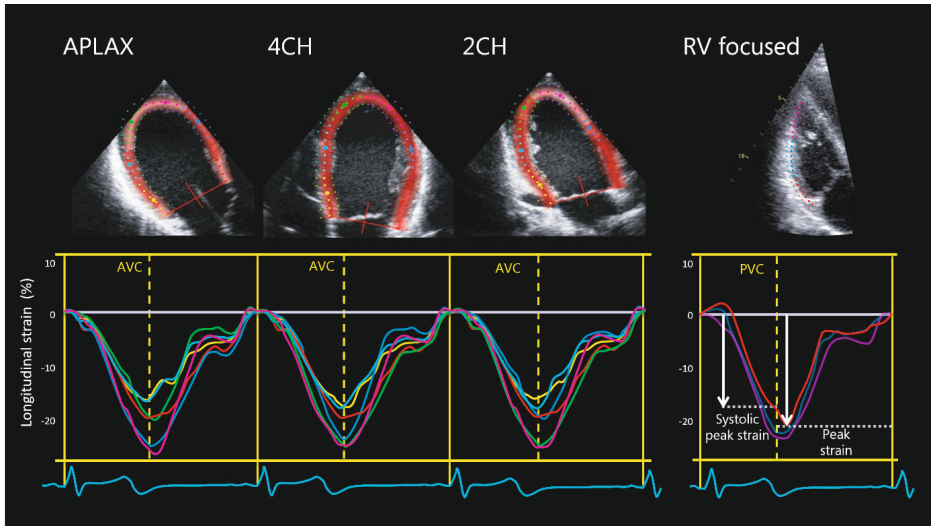


Figure 2. Echocardiographic speckle tracking deformation imaging

In the left ventricle, ventricular wall motion is tracked in the apical long axis (APLAX) view, the apical 4-chamber (4CH) and apical 2-chamber (2CH) view. In the right ventricle (RV), the free wall is tracked in an RV-focused 4CH view. The aortic valve closure (AVC) and pulmonic valve closure (PVC) mark the end of the systole. Longitudinal strain is expressed in percentages of lengthening or shortening over time. Longitudinal strain is displayed for 18 LV segments and for 3 RV free wall segments. Systolic peak strain is the peak negative strain occurring up to the moment of valve closure.

Previous studies have repeatedly demonstrated the potential value of deformation imaging in ARVC. It was demonstrated that this technique may help to reveal early disease manifestation in desmosomal genetic variant carriers without an overt ARVC phenotype.^{12,20,21} One study from our own institute identified characteristic deformation patterns in the subtricuspid segment of the RV free wall, known as the first affected region in ARVC. These abnormal patterns were seen in half of the genetic variant carriers without overt signs of disease by conventional diagnostics.¹² The CircAdapt model, a computer simulation model of the heart and circulation developed at Maastricht University, was used to link deformation abnormalities to a possible underlying disease substrate of reduced contractility and increased stiffness (*Figure 3*). The abnormal deformation pattern with delayed onset to shortening, reduced peak strain and post-systolic shortening was a robust finding²² which turned out to be a precursor of disease progression.²³

While abnormal subtricuspid deformation patterns were not yet linked to arrhythmic outcome, researchers from Oslo did relate deformation abnormalities to arrhythmic events in the patients history.^{24,25} They reported strong correlations between RV and LV mechanical dispersion, measures of regional heterogeneity in contraction, and arrhythmic events. A combination of increased mechanical dispersion, T-wave inversions on the ECG, and a history of high intensity exercise was proposed to characterize a high risk profile regarding incidence of ventricular arrhythmias.

Although many studies have confirmed the added value of deformation imaging, the technique is still not widely implemented in clinical practice. A possible contributor to this lagging implementation may be that many deformation methods have been used in single center studies without external validation. Second, most studies focus on deformation imaging as a single parameter, while added value should better be tested in a clinical practice based multimodality approach.

In this thesis, ARVC is used as a disease model to demonstrate the road to clinical implementation of deformation imaging in genetic cardiomyopathies in general. It focusses both on detection and characterization of the early disease substrate as well as on arrhythmic risk stratification in patients and family-members at risk. Two major clinical challenges for clinicians which go hand in hand.

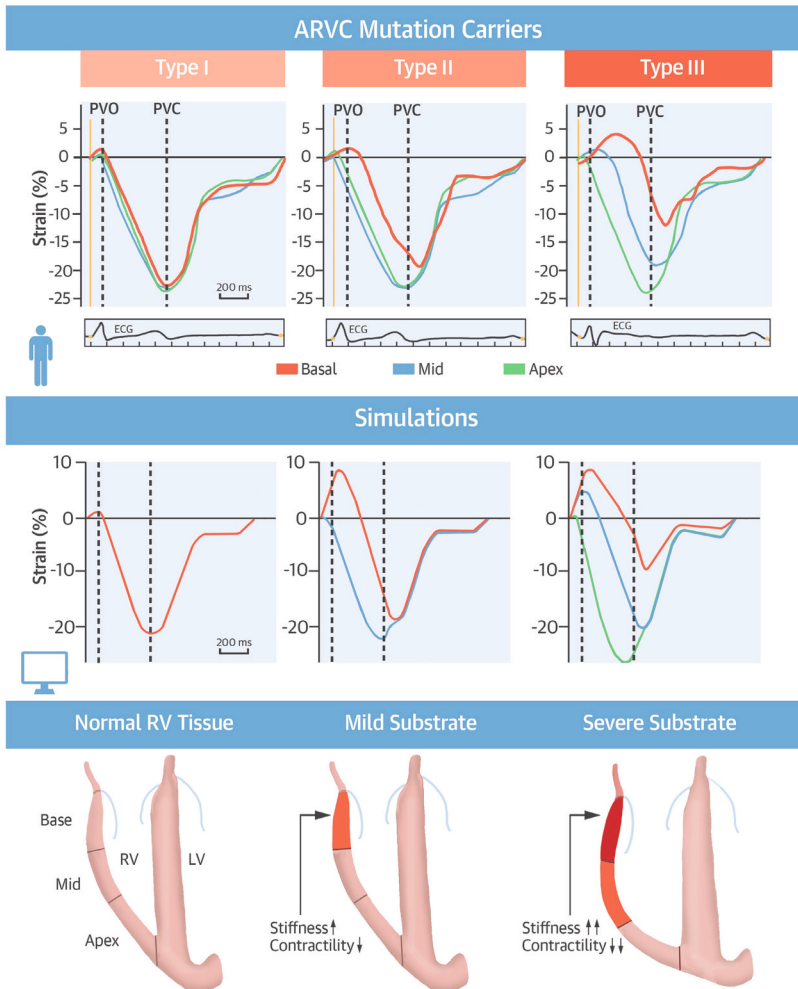


Figure 3. RV deformation patterns

Using deformation imaging and computer simulation, 3 distinctive characteristic RV longitudinal deformation patterns were identified by researchers from our institute in 2016.¹² (Left) Type I normal deformation as seen in healthy controls. (Middle) Type II, characterized by delayed onset of shortening, reduced systolic peak strain, and minor post-systolic shortening. This pattern was reproduced by the computer simulation of severely reduced contractility and mildly increased passive stiffness in the basal (subtricuspid) RV segment. (Right) Type III, characterized by little or no systolic peak strain, predominantly systolic stretching, and major post-systolic shortening. This pattern was reproduced by introducing severely reduced contractility and severely increased passive stiffness in the basal segment. ECG = electrocardiogram; PVO/PVC = pulmonary valve opening/closure. (Copyright 2016 by Elsevier; reprinted with permission)

THESIS OUTLINE

Part I. Deformation imaging methods in ARVC

In a clinical evaluation of the diagnostic 2010 TFC, conventional echocardiography lacked sensitivity for ARVC diagnosis.²⁶ This could be partly caused by visual assessment of RV wall motion abnormalities, prerequisite to fulfill a criterion, which is difficult and highly dependent on the observer's experience. In **Chapter 2**, we investigated whether inclusion of RV deformation could lead to better detection of ARVC patients by echocardiography compared to conventional echocardiographic methods. While previous studies in ARVC patients and family members from Utrecht identified characteristic regional RV deformation patterns, studies performed in Oslo focused on RV mechanical dispersion, a measure for regional heterogeneity in contraction. Both methods have been successfully applied in subsequent cohorts in the center where they were developed, but were never externally validated. **Chapter 3** describes an external validation study for both methods, designed in a way that a single, newly trained observer applied both methods in both cohorts. Besides, we combined data from Utrecht and Oslo to evaluate incremental value of combining the two methods in association to the occurrence of life-threatening ventricular arrhythmia.

Part II. Characterizing the disease substrate underlying deformation abnormalities

Although the gold standard for characterization of the disease substrate in ARVC is based on histology on tissue acquired by autopsy or biopsy of the thin walled RV, this is not an option in most patients. Deformation abnormalities most likely reflect the local tissue substrate, as was previously supported by simulations with the CircAdapt computer model.¹² In this study, a general disease substrate of reduced contractility and increased stiffness was demonstrated. In part II of this thesis, we describe the steps from a general disease simulation to a patient-specific approach with possible clinical applications. This patient-specific cardiac model was used as a so-called Digital Twin, a virtual representation of reality based on a comprehensive physical and functional description of the heart. The idea was to use this Digital Twin to gain more insight in the structural disease substrate in early-stage ARVC. So in a way to use it as a non-invasive myocardial biopsy. The ultimate goal was to try to distinguish arrhythmogenic substrates from the more benign tissue abnormalities leading to deformation abnormalities. In **Chapter 4** we apply this patient-specific approach in the cohort of desmosomal pathogenic variant carriers in which the general disease model was first described.²⁷ Deformation data were used as input and the model estimates the underlying disease substrate in a specific patient. **Chapter 5** describes the introduction of uncertainty to model estimations. Since both measurements and model estimations introduce uncertainty, this was a necessary step towards longitudinal follow-up of the disease substrate. In **Chapter 6**, we combined deformation measurements and model estimations to investigate age-related penetrance of ARVC in a longitudinal cohort of patients and family-members without overt structural abnormalities. In a position statement from 2010, it was suggested that serial screening of relatives can be stopped at the age of 50-60 years, due to completed penetrance.²⁸ By monitoring structural progression and occurrence of events in different age groups, we evaluated if penetrance was indeed completed in the older group.

Part III. Towards clinical implementation of deformation imaging

Part III of this thesis is focused on proceeding deformation imaging into routine clinical practice. Although echocardiographic deformation imaging has already been in use for

over two decades, the technique is still not widely implemented in clinical practice. An important step towards wide implementation could be inclusion in clinical guidelines, which requires convincing evidence of the added value of deformation imaging. One important strength of deformation imaging is that it is a more sensitive method for detection of early disease manifestation compared to conventional global imaging parameters. In **Chapter 7**, we summarized all available evidence regarding the value of deformation imaging in early detection of genetic cardiomyopathies in relatives. While the value of deformation imaging as a stand-alone index has been extensively published, there is a lack of clinical practice based multi-modality studies. Inclusion in clinical guidelines requires evidence of added value in a real-world setting. In other words, it should improve current clinical practice. In **Chapter 8** we used ARVC as a model to investigate added value of deformation imaging for arrhythmic risk prediction in a multimodality approach. We integrated deformation imaging with the validated ARVC risk calculator¹⁷ to test added value in a clinical practice based approach.

Addendum: left-sided wall stress causing arrhythmia

In **Chapter 10** we provide an addendum to this thesis. Where the *subtricuspid* region is a weak spot in the RV, the *submitral* region can be a similar weak spot in the LV. In both cases, the hypothesis is that high mechanical stress on a thin wall can cause life-threatening arrhythmias. Dedicated imaging may help to identify these weak spots. On the right side, ARVC is an important contributor to this weak spot (desmosomal fragility). On the left side, mitral annular disjunction (MAD), defined as atrial displacement of the mitral valve hinge point may cause a weak spot (*Figure 4*). In the affected area, the thin atrial wall has to withstand the high wall stress which is normally applied to the thick LV wall. This condition recently received increasing attention in relation to unexplained ventricular arrhythmia.^{29,30} In this chapter, we reanalyzed cardiac magnetic resonance images of patients who survived an unexplained cardiac arrest with special attention to the mitral valve area.

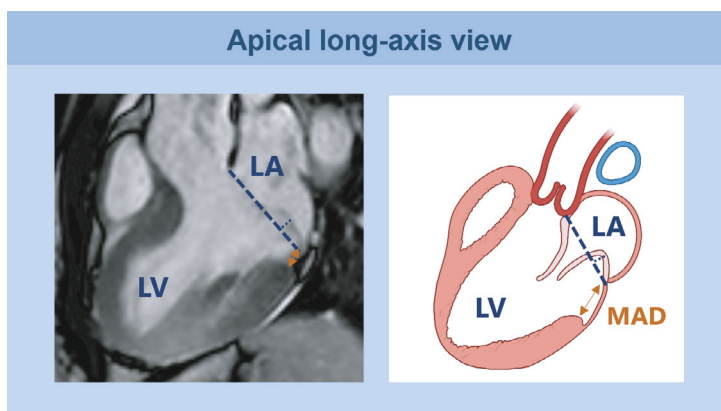


Figure 4. Mitral annular disjunction

Mitral annular disjunction (MAD) and mitral valve prolapse at end-systole in the longitudinal 3-chamber view on cardiac magnetic resonance imaging (left panel) and in a schematic overview (right panel). The orange arrow indicates the longitudinal MAD distance along the atrial wall. The dashed line connects the annular hinge points and represents the annular plane. The dotted line perpendicular on the annular plane measures the mitral valve prolapse. LA = left atrium, LV = left ventricle.

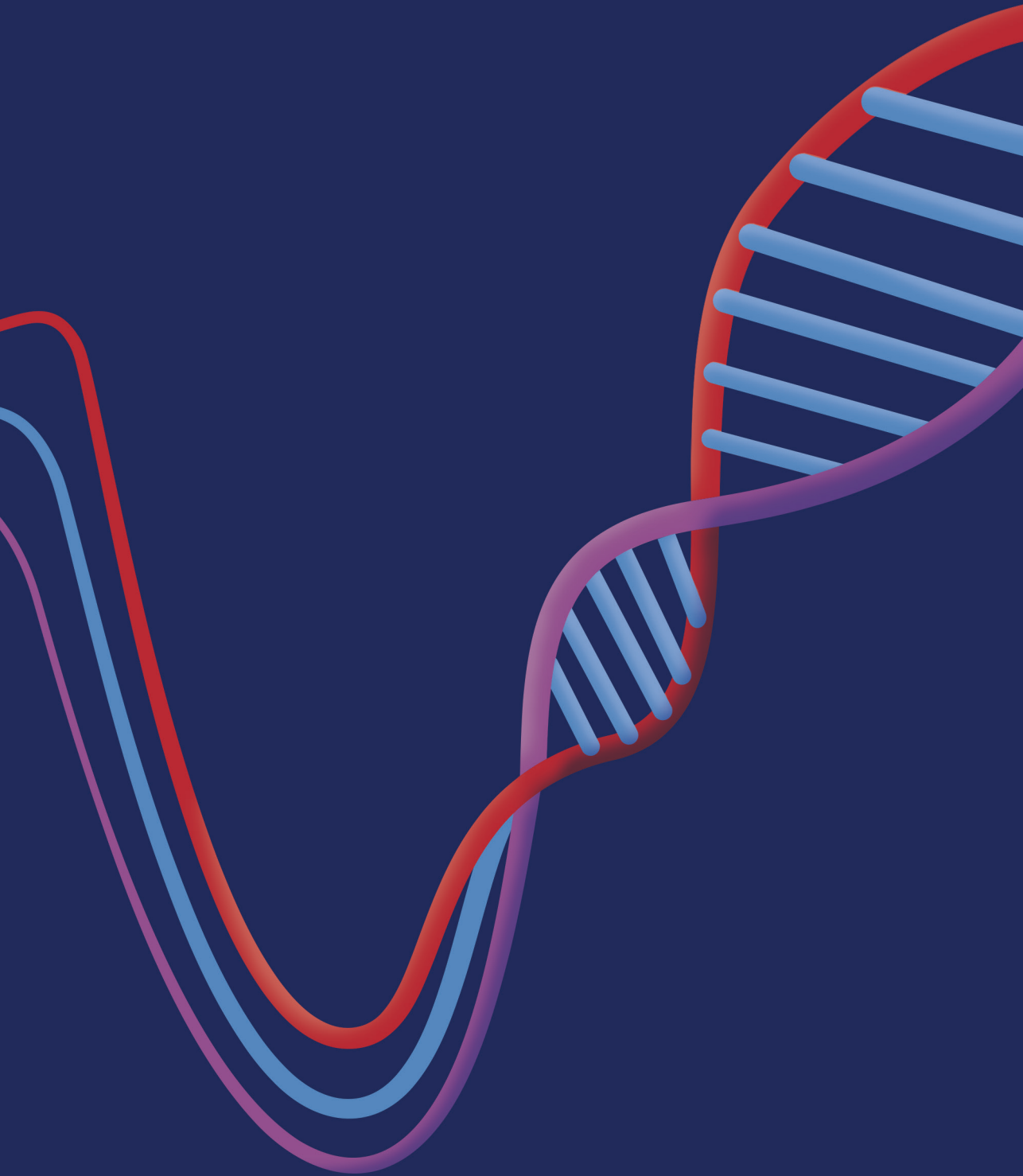
REFERENCES

1. Hayashi M, Shimizu W, Albert CM. The spectrum of epidemiology underlying sudden cardiac death. *Circ Res*. 2015;116(12):1887–906.
2. Vaartjes I, Hendrix A, Hertogh EM, et al. Sudden death in persons younger than 40 years of age: Incidence and causes. *Eur J Cardiovasc Prev*. 2009;16(5):592–6.
3. Marcus FI, Fontaine GH, Guiraudon G, et al. Right ventricular dysplasia: a report of 24 adult cases. *Circulation*. 1982;65(2):384–98.
4. Protonotarios N, Tsatsopoulou A, Patsourakos P, et al. Cardiac abnormalities in familial palmoplantar keratosis. *Heart*. 1986;56(4):321–6.
5. McKoy G, Protonotarios N, Crosby A, et al. Identification of a deletion in plakoglobin in arrhythmogenic right ventricular cardiomyopathy with palmoplantar keratoderma and woolly hair (Naxos disease). *Lancet*. 2000;355(9221):2119–24.
6. Groeneweg JA, Bhonsale A, James CA, et al. Clinical Presentation, Long-Term Follow-Up, and Outcomes of 1001 Arrhythmogenic Right Ventricular Dysplasia/Cardiomyopathy Patients and Family Members. *Circ Cardiovasc Genet*. 2015;8(3):437–46.
7. Austin KM, Trembley MA, Chandler SF, et al. Molecular mechanisms of arrhythmogenic cardiomyopathy. *Nat Rev Cardiol*. 2019;16(9):519–37.
8. Te Riele ASJM, James CA, Philips B, et al. Mutation-positive arrhythmogenic right ventricular dysplasia/cardiomyopathy: The triangle of dysplasia displaced. *J Cardiovasc Electrophysiol*. 2013;24(12):1311–20.
9. Corrado D, Link MS, Calkins H. Arrhythmogenic Right Ventricular Cardiomyopathy. Jarcho JA, editor. *N Engl J Med*. 2017;376(1):61–72.
10. Delmar M, McKenna WJ. The Cardiac Desmosome and Arrhythmogenic Cardiomyopathies. *Circ Res*. 2010;107(6):700–14.
11. Thiene G, Nava A, Corrado D, Rossi L, Pennelli N. Right Ventricular Cardiomyopathy and Sudden Death in Young People. *N Engl J Med*. 1988;318(3):129–33.
12. Mast TP, Teske AJ, Walmsley J, et al. Right Ventricular Imaging and Computer Simulation for Electro-mechanical Substrate Characterization in Arrhythmogenic Right Ventricular Cardiomyopathy. *J Am Coll Cardiol*. 2016;68(20):2185–97.
13. Marcus FI, McKenna WJ, Sherrill D, et al. Diagnosis of arrhythmogenic right ventricular cardiomyopathy/Dysplasia: Proposed modification of the task force criteria. *Circulation*. 2010;121(13):1533–41.
14. James CA, Bhonsale A, Tichnell C, et al. Exercise increases age-related penetrance and arrhythmic risk in arrhythmogenic right ventricular dysplasia/cardiomyopathy-associated desmosomal mutation carriers. *J Am Coll Cardiol*. 2013;62(14):1290–7.
15. Lie ØH, Deigaard LA, Saberniak J, et al. Harmful Effects of Exercise Intensity and Exercise Duration in Patients With Arrhythmogenic Cardiomyopathy. *JACC Clin Electrophysiol*. 2018;4(6):744–53.
16. Corrado D, Wichter T, Link MS, et al. Treatment of Arrhythmogenic Right Ventricular Cardiomyopathy/Dysplasia. *Circulation*. 2015;132(5):441–53.
17. Cadrin-Tourigny J, Bosman LP, Nozza A, et al. A new prediction model for ventricular arrhythmias in arrhythmogenic right ventricular cardiomyopathy. *Eur Heart J*. 2019;40(23):1850–8.

18. Towbin JA, McKenna WJ, Abrams DJ, et al. 2019 HRS expert consensus statement on evaluation, risk stratification, and management of arrhythmogenic cardiomyopathy. *Heart Rhythm*. 2019;16(11):e301–72.
19. Haugaa KH, Basso C, Badano LP, et al. Comprehensive multi-modality imaging approach in arrhythmogenic cardiomyopathy - an expert consensus document of the European Association of Cardiovascular Imaging. *Eur Heart J Cardiovasc Imaging*. 2017;18(3):237–53.
20. Teske AJ, Cox MGPJ, Te Riele ASJM, et al. Early detection of regional functional abnormalities in asymptomatic ARVD/C gene carriers. *J American Soc Echocardiogr*. 2012;25(9):997–1006.
21. Réant P, Hauer AD, Castelletti S, et al. Epicardial myocardial strain abnormalities may identify the earliest stages of arrhythmogenic cardiomyopathy. *Int J Cardiovasc Imaging*. 2016;32(4):593–601.
22. Taha K, Mast TP, Cramer MJ, et al. Evaluation of Disease Progression in Arrhythmogenic Cardiomyopathy: The Change of Echocardiographic Deformation Characteristics Over Time. *JACC Cardiovasc Imaging*. 2019;13(2):631–4.
23. Mast TP, Taha K, Cramer MJ, et al. The Prognostic Value of Right Ventricular Deformation Imaging in Early Arrhythmogenic Right Ventricular Cardiomyopathy. *JACC Cardiovasc Imaging*. 2019;12(3):446–55.
24. Sarvari SI, Haugaa KH, Anfinson OG, et al. Right ventricular mechanical dispersion is related to malignant arrhythmias: A study of patients with arrhythmogenic right ventricular cardiomyopathy and subclinical right ventricular dysfunction. *Eur Heart J*. 2011;32(9):1089–96.
25. Leren IS, Saberniak J, Haland TF, Edvardsen T, Haugaa KH. Combination of ECG and Echocardiography for Identification of Arrhythmic Events in Early ARVC. *JACC Cardiovasc Imaging*. 2017;10(5):503–13.
26. Bosman LP, Cadrin-Tourigny J, Bourfiss M, et al. Diagnosing arrhythmogenic right ventricular cardiomyopathy by 2010 task force criteria: Clinical performance and simplified practical implementation. *Europace*. 2020;22(5):787–96.
27. van der Pols MJ, Mast TP, Loh P, et al. Clinical characterisation and risk stratification of patients with arrhythmogenic right ventricular dysplasia/cardiomyopathy ≥ 50 years of age. *Netherlands Heart Journal*. 2016;24(12):740–7.
28. Charron P, Arad M, Arbustini E, et al. Genetic counselling and testing in cardiomyopathies: a position statement of the European Society of Cardiology Working Group on Myocardial and Pericardial Diseases. *Eur Heart J*. 2010;31(22):2715–26.
29. Dejgaard LA, Skjølsvik ET, Lie ØH, et al. The Mitral Annulus Disjunction Arrhythmic Syndrome. *J Am Coll Cardiol*. 2018;72(14):1600–9.
30. Essayagh B, Sabbag A, El-Am E, Cavalcante JL, Michelena HI, Enriquez-Sarano M. Arrhythmic mitral valve prolapse and mitral annular disjunction: pathophysiology, risk stratification, and management. *Eur Heart J*. 2023;44(33):3121–35.

PART I.

Deformation imaging methods in ARVC



CHAPTER 2

Improving Diagnostic Value of Echocardiography in Arrhythmogenic Right Ventricular Cardiomyopathy Using Deformation Imaging

Feddo P. Kirkels, Laurens P. Bosman, Karim Taha, Maarten J. Cramer, Jeroen F. van der Heijden, Richard N.W. Hauer, Folkert W. Asselbergs, Anneline S.J.M. te Riele, Arco J. Teske

*JACC Cardiovasc Imaging. 2021;14(12):2481-2483.
Research letter*

INTRODUCTION

Arrhythmogenic Right Ventricular Cardiomyopathy (ARVC) is an inherited cardiomyopathy diagnosed by a complex set of tests defined in the 2010 Task Force Criteria (TFC).¹ This includes echocardiography, which combines measures of right ventricular (RV) dilatation and function with subjective visual wall motion assessment to obtain diagnostic criteria. However, a recent clinical validation study of the TFC demonstrated that these echocardiographic criteria lack sensitivity for ARVC diagnosis.² Subtle wall motion abnormalities can be missed by visual assessment, hampering diagnosis. In contrast, echocardiographic deformation imaging is known for its high sensitivity for detection of wall motion abnormalities. The performance of deformation imaging within the TFC for ARVC diagnosis remains however unknown. We performed a head-to-head comparison of the diagnostic value of TFC visual wall motion assessment versus deformation imaging in a real-world cohort of consecutive patients evaluated for ARVC.

METHODS

The study population was derived from a recently published study on TFC performance, which included 160 consecutive patients who were referred for ARVC evaluation at the UMC Utrecht, the Netherlands, between 2009-2011.² Of those, we included 59 patients who underwent an echocardiogram according to our current protocol³ on a single vendor, allowing deformation analysis. The study was approved by the local ethics board.

In absence of a gold standard test for diagnosis of ARVC, the reference standard was diagnosis by consensus of 3 independent ARVC experts (JvdH/RH/AtR) who re-evaluated all available patient data, beyond the scope of the TFC, including a median follow-up of 5.9 years IQR[2.7-7.6 years] after the echocardiographic examination.²

All echocardiograms were performed with a Vivid 7 or E9 scanner and post-processed with EchoPac v.202 (GE Healthcare, Horten, Norway). The original clinical assessment of RV outflow tract dimensions, fractional area change and wall motion was used to determine conventional echocardiographic TFC.¹ In addition, RV deformation patterns of the subtricuspid area³ were obtained by two experienced operators (FK/KT) blinded for clinical data. Deformation patterns were scored as either normal or abnormal, according to the presence of regional mechanical dysfunction (type II/III, as previously described in detail).³ We evaluated the effect of replacing visual wall motion assessment with deformation imaging on the sensitivity, specificity and C-statistic of the echocardiographic TFC for ARVC diagnosis. (*Figure 1A*)

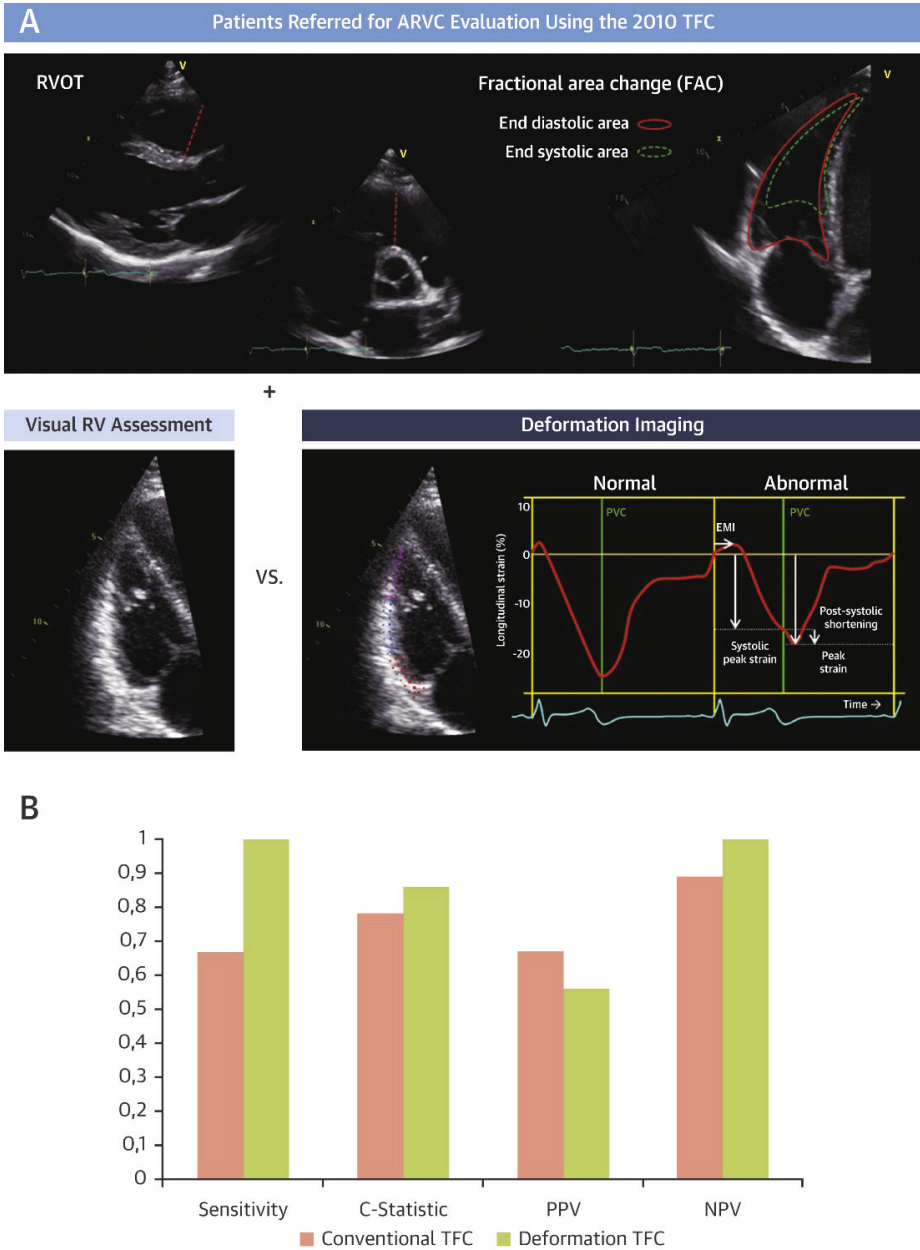


Figure 1. ARVC evaluation according to the echocardiographic 2010 TFC
(A) ARVC evaluation according to the echocardiographic 2010 TFC by using visual wall motion assessment vs. deformation imaging. An RV-focused 4-chamber view was used to classify local deformation patterns as normal or abnormal.³ **(B)** Diagnostic performance of echocardiographic TFC when using conventional visual assessment compared to deformation imaging.

RESULTS

Of 59 patients (age 38 ± 17 years, 49% male), the experts diagnosed 15 (25%) with ARVC. Conventional echocardiographic TFC, either minor or major, were observed in 10 (67%) patients. Using deformation imaging instead of visual wall motion assessment led to 5 (33%) additional detections of ARVC, whereas none were reclassified to normal. Consequently, deformation imaging increased sensitivity from 67% to 100%, while specificity decreased from 89% to 73%. The C-statistic increased from 0.78, 95%CI (0.64-0.91) to 0.86, 95%CI (0.80-0.93). (Figure 1B)

Of note, half ($n=6/12$) of the patients with “false positive” abnormal deformation patterns were at risk family members of ARVC patients. They all developed new TFC during follow-up and 4 of them later fulfilled criteria for a definite diagnosis. Therefore, it can be debated whether the deformation abnormalities in these patients were truly “false positive” or, more likely, reflective of a very early sign of disease in these patients.³ Deformation imaging detected all patients who developed the diagnosis during follow-up, and including these patients resulted in an increased specificity (80%) and C-statistic (0.74, 95%CI [0.62-0.86] to 0.90, 95%CI [0.84-0.96]).

DISCUSSION AND CONCLUSION

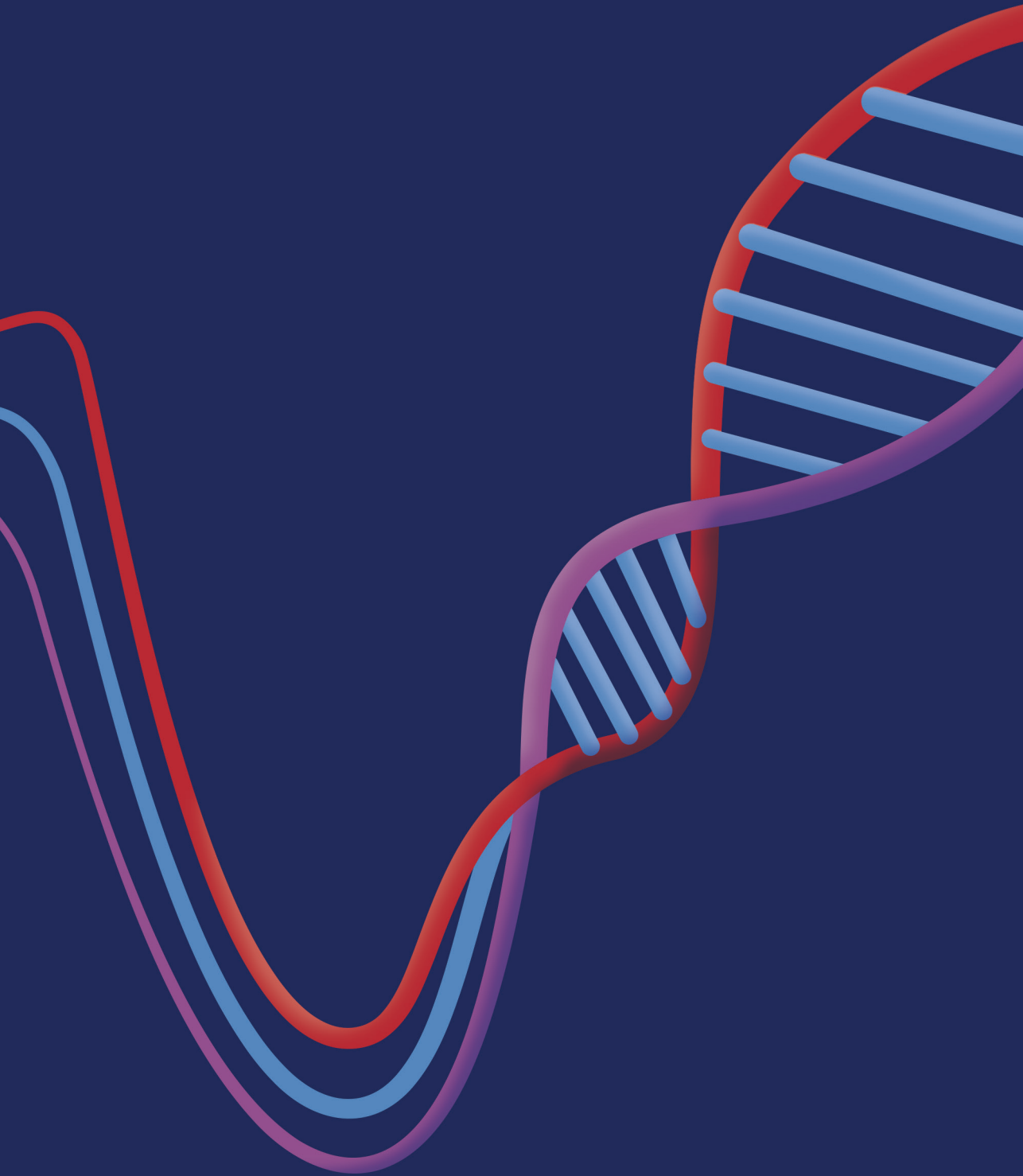
We showed that RV deformation is highly sensitive for diagnosing ARVC, and improves the diagnostic performance of echocardiographic TFC when replacing the visual wall motion assessment. When the original 1994 TFC were revised in 2010, hypokinesia was disregarded as a criterion and only akinesia/dyskinesia remained.¹ This was necessary to prevent overdiagnosing of the disease, but consequently led to a loss in sensitivity. As wall motion abnormalities are a prerequisite to fulfil a criterion, the diagnostic performance of echocardiography depends primarily on visual assessment of RV wall motion abnormalities, which is difficult and highly dependent on the observer’s experience. Replacing visual assessment by deformation imaging offers a solution for this loss in sensitivity, while also being less subjective.

In the present study, all patients who were diagnosed with ARVC by the expert panel were detected by RV deformation abnormalities. The cohort size and absence of a true gold standard test for ARVC were limitations in our study design. Because deformation imaging is not able to reliably distinguish ARVC from other RV related disease as a stand-alone index, such diagnostic dilemmas should always be conducted in a clinical multi-modality approach like the TFC. Using deformation imaging instead of visual wall motion assessment improved the overall performance of echocardiographic TFC for diagnosing ARVC.

Acknowledgements: This work was supported by the Netherlands Cardiovascular Research Initiative, an initiative with support of the Dutch Heart Foundation (grant number CVON2015-12 eDETECT). Dr Te Riele is supported by the Dutch Heart Foundation (grant number 2015T058) and the UMC Utrecht Fellowship Clinical Research Talent. Dr Asselbergs is supported by UCL Hospitals NIHR Biomedical Research Centre.

REFERENCES

1. Marcus FI, McKenna WJ, Sherrill D, et al. Diagnosis of arrhythmogenic right ventricular cardiomyopathy/Dysplasia: Proposed modification of the task force criteria. *Circulation*. 2010;121(13):1533–41.
2. Bosman LP, Cadrin-Tourigny J, Bourfiss M, et al. Diagnosing arrhythmogenic right ventricular cardiomyopathy by 2010 task force criteria: Clinical performance and simplified practical implementation. *Europace*. 2020;22(5):787–96.
3. Mast TP, Teske AJ, Walmsley J, et al. Right Ventricular Imaging and Computer Simulation for Electro-mechanical Substrate Characterization in Arrhythmogenic Right Ventricular Cardiomyopathy. *J Am Coll Cardiol*. 2016;68(20):2185–97.



CHAPTER 3

Right Ventricular Functional Abnormalities in Arrhythmogenic Cardiomyopathy: Association With Life-Threatening Ventricular Arrhythmias

*Feddo P. Kirkels, Øyvind H. Lie, Maarten J. Cramer, Monica Chivulescu, Christine Rootwelt-Norberg,
Folkert W. Asselbergs, Arco J. Teske, Kristina H. Haugaa*

JACC Cardiovasc Imaging. 2021;14(5):900-910.

ABSTRACT

Objectives

In this study, we aimed to perform an external validation of the value of RV deformation patterns and RV mechanical dispersion in patients with arrhythmogenic cardiomyopathy (AC). Secondly, we assessed the association of these parameters with life threatening ventricular arrhythmia (VA).

Background

Subtle RV dysfunction assessed by echocardiographic deformation imaging is valuable in AC diagnosis and risk prediction. Two different methods have emerged, the RV deformation pattern recognition and RV mechanical dispersion, but these have neither been externally validated nor compared.

Methods

We analysed AC probands and mutation-positive family members, matched from two large European referral centers. We performed speckle tracking echocardiography, whereby we classified the subtricuspid deformation patterns from normal to abnormal and assessed RV mechanical dispersion from 6 segments. We defined VA as sustained ventricular tachycardia, appropriate ICD therapy, or aborted cardiac arrest.

Results

We included 160 subjects, 80 from each center (43% proband, 55% female, aged 41 ± 17 years). VA had occurred in 47 (29%) subjects. In both cohorts, patients with a history of VA showed abnormal deformation patterns (96% and 100%) and had greater RV mechanical dispersion (53 ± 30 ms vs. 30 ± 21 ms, $p < 0.001$ for the total cohort). Both parameters were independently associated to VA (adjusted OR 2.71, 95% CI (1.47 – 5.00) per class step-up and 1.26, 95% CI (1.07 – 1.49) per 10 ms, respectively). The association with VA significantly improved when adding RV mechanical dispersion to pattern recognition (NRI 0.42, $p = 0.02$ and IDI 0.06, $p = 0.01$).

Conclusion

We externally validated two RV dysfunction parameters in AC. Adding RV mechanical dispersion to RV deformation patterns significantly improved the association with life-threatening VA, indicating incremental value.

INTRODUCTION

Arrhythmogenic cardiomyopathy (AC, also known as arrhythmogenic right ventricular cardiomyopathy (ARVC)) is an inheritable cardiomyopathy, characterized by life-threatening ventricular arrhythmias (VA) and progressive cardiac failure.¹ In the classical phenotype, pathogenic mutations encoding for desmosomal proteins lead to primarily right ventricular (RV) myocyte loss and replacement by fibrofatty tissue.^{2,3}

Already in the early stage of the disease, life-threatening arrhythmias can occur, making it a leading cause of sudden cardiac death amongst young, seemingly healthy, individuals.^{2,3,4} Early detection of the disease is thus of great importance. Currently, AC is diagnosed according to a complex set of criteria, defined in the 2010 revised Task Force Criteria (TFC), in which cardiac imaging has an important role.⁵

In addition to conventional imaging parameters, as incorporated in the 2010 TFC, echocardiographic deformation imaging has been described for detection of subtle phenotypic expressions in early AC as well as for risk prediction regarding ventricular arrhythmias.⁶⁻¹¹ The technique has been applied to the RV in AC patients in different ways: by recognition of deformation patterns of the RV subtricuspid area^{6,7}, and by using the mechanical dispersion, a measure of heterogeneous contraction, as a parameter of disease expression⁸⁻¹⁰. These two methods have successfully been tested in separate cohorts of the centers where they were developed, but are not yet implemented in clinical care outside of these centers. In order to advance RV deformation imaging closer to standard clinical care in AC, it is pivotal to show that these results are not only achieved in one center. To date, the value of RV deformation patterns and mechanical dispersion has never been externally validated. Furthermore, the association between RV deformation patterns and ventricular arrhythmias has not been investigated previously, and it is not known whether the two methods measure essentially the same phenomenon or if combining the two methods adds value to risk stratification of VA.

We aimed to perform an external validation of the association between RV deformation patterns and disease stage in AC. Furthermore, we aimed to validate mechanical dispersion as a marker of ventricular arrhythmias. Finally, we wanted to explore the added value of combining the parameters.

METHODS

Study design and population

This study was conducted in two academic referral centers for AC in Europe. We used an AC cohort from the University Medical Center Utrecht in the Netherlands and an age- and sex matched AC cohort from the Oslo University Hospital in Norway. Probands underwent genetic testing as described previously¹², and cascade genetic screening was performed in family members of genotype positive probands. The Utrecht cohort consisted of 80 AC probands and genotype positive family members with an echocardiographic examination including RV deformation imaging in Utrecht between 2006 and 2015, who have been reported previously.⁶ During this period, 87 subjects were evaluated, of which 7 were excluded due to inadequate image quality for RV deformation analyses. The Oslo cohort also consisted of 80 AC probands and genotype positive family members. By matching to the Utrecht subjects based on age and sex, the Oslo subjects were selected from a previously reported cohort of 144 subjects which

were referred between 1997 and 2016.¹³ Due to inadequate image quality for RV deformation analyses, 4 subjects were replaced by other matched subjects from the Oslo cohort during the matching process. For the purpose of external validation, the two cohorts were kept separated first. The association between RV deformation patterns and disease stage was determined in the Oslo cohort and compared to the Utrecht cohort, where the method was initially developed. The external validity of the association between RV mechanical dispersion and arrhythmic events was tested in the Utrecht cohort and compared to the Oslo cohort. Subsequently, the two cohorts were merged to compare both RV deformation techniques and to explore added value of combining them in the total cohort. The study was approved by both local institutional ethics review boards and complies with the declaration of Helsinki.

Collection of data

Clinical characteristics

We recorded clinical characteristics at inclusion, including demographics, anti-arrhythmic or beta blocker medication, presence of an ICD, and history of cardiac syncope (sudden loss of consciousness followed by spontaneous sudden awakening). By applying the 2010 TFC⁵, we determined fulfilment of a definite AC diagnosis. Date of inclusion was defined as the date of first complete echocardiographic examination suitable for performing deformation imaging.

Electrocardiography

We performed standard 12-lead ECG recording and 24-hour Holter monitoring at inclusion. The extent of T-wave inversions (TWI), presence of epsilon waves and increased terminal activation duration (TAD) were recorded according to the 2010 TFC. Arrhythmias were recorded on either 12-lead ECG, Holter or ICD monitoring.⁵ The amount of premature ventricular complexes per 24 hours on Holter monitoring was documented and non-sustained ventricular tachycardia was defined as consecutive runs of ≥ 3 ventricular beats >100 beats/min for <30 s.¹⁴

Echocardiography

We performed echocardiography, using a GE Vivid 7, E9 or E95 scanner (GE Healthcare, Horten, Norway). Cine-loops were stored for post-processing with EchoPac version 202 (GE Healthcare). We assessed structural and functional abnormalities defined in the 2010 TFC⁵ and parameters from the EACVI consensus paper.¹⁵

Details on acquisition of the RV focused 4-chamber view and post-processing in echocardiographic speckle tracking deformation imaging were previously described more extensively.¹⁶⁻¹⁸ We assessed the subtricuspid deformation pattern in a single wall tracing of the RV lateral free wall, which was automatically divided into a basal, mid, and apical segment. Timing of the pulmonary valve closure was assessed by Doppler traces in the RV outflow tract, obtained in the parasternal short-axis view. The following deformation parameters were measured in the basal segment: time to onset of shortening (or electro-mechanical interval (EMI))¹⁹, systolic peak strain²⁰ and the amount post-systolic shortening²¹ (*definitions in supplementary material*). Based on these parameters, a distinction into three different deformation patterns has previously been observed in AC and simulated using a computer model.⁶ (*Figure 1, panel A*) For RV mechanical dispersion, we used a 6-segment RV model, including both the lateral wall and the interventricular septum. It was calculated as the standard deviation (SD) of the segmental time intervals from onset Q/R on the surface ECG to maximum shortening, represented by the automatically detected peak negative strain.^{8,9} (*Figure 1, panel*

B) The left ventricular (LV) global longitudinal strain (GLS) was calculated in a 16-segment LV model.²²⁻²⁴ RV free wall longitudinal strain was calculated as the averaged peak systolic strain from 3 RV free wall segments. All measurements were performed by a single observer blinded to clinical outcome, who was newly trained in both RV deformation imaging techniques and not involved in the initial development of the methods. Intra- and inter-observer variability of deformation imaging parameters was assessed by reanalysing 20 echocardiographic studies in both the Utrecht and Oslo database. (*Supplementary material*)

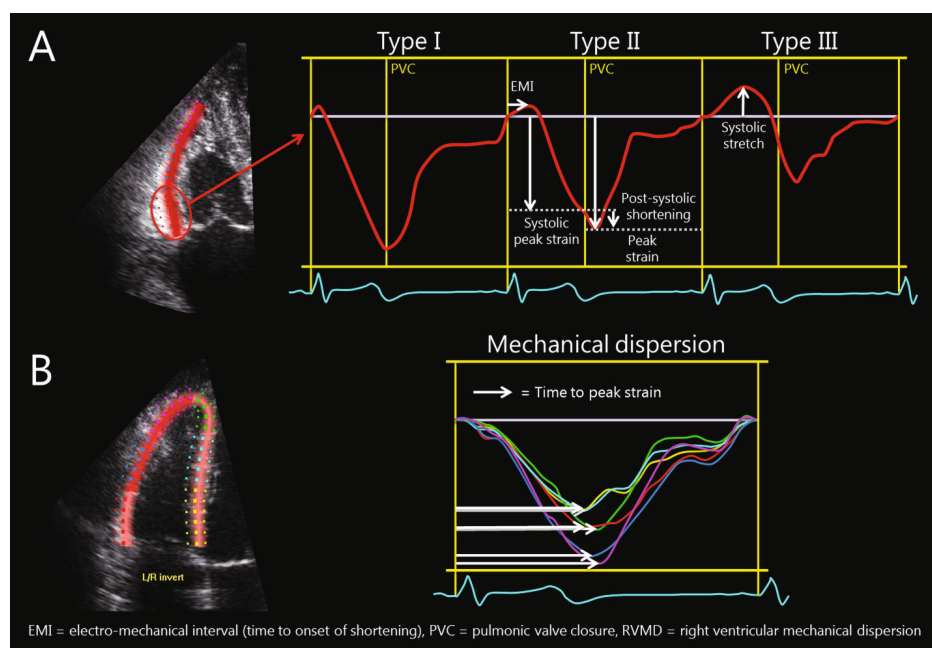


Figure 1. Echocardiographic deformation imaging of the RV

RV deformation pattern recognition of the basal segment and RV mechanical dispersion performed on an RV focused 4-chamber view. **Panel A:** Based on predefined criteria, a division into 3 different deformation patterns is identified.⁶ Type I is normal deformation; type II is characterized by delayed onset of shortening, reduced systolic peak strain and minor post-systolic shortening; type III is characterized by little or no systolic peak strain, predominantly systolic stretching and major post-systolic shortening. **Panel B:** For RV mechanical dispersion, a 6-segment model of the RV was used, including both the lateral wall and the interventricular septum. It was calculated as the standard deviation (SD) of the segmental time intervals from onset Q/R on the surface ECG to peak negative strain and expressed in milliseconds.^{8,9} Horizontal arrows indicate the time interval until peak shortening for each segment.

Cardiac magnetic resonance imaging

Cardiac magnetic resonance (CMR) imaging was performed on a 1.5-T scanner, as published previously and according to standard AC protocols.^{6,12} Available data were analysed for structural abnormalities fulfilling 2010 TFC.⁵ Conventional CMR measurements included RV end-diastolic volume indexed for BSA (RVEDVi) and RV ejection fraction (RVEF). Contrast-enhanced images with administration of gadolinium were acquired for detection of myocardial fibrosis in both ventricles, presenting as late gadolinium enhancement.

Outcomes

All arrhythmic events were adjudicated retrospectively from the time of echocardiographic assessment. Life-threatening ventricular arrhythmia was defined as a documented history of sustained ventricular tachycardia, aborted cardiac arrest or appropriate ICD therapy. The division into three different disease stages was based on the presence of subsets of the 2010 TFC, as described previously.^{5,6} In brief, subjects in the *structural* stage presented with minor or major 2010 TFC for structural abnormalities on echocardiography or CMR. Subjects categorized in the *electrical* stage fulfilled no structural criteria but had minor or major ECG abnormalities (repolarization and/or depolarization) and/or history of ventricular arrhythmias as defined by the 2010 TFC. *Subclinical* subjects were defined as fulfilling neither structural, nor electrical 2010 TFC.

Statistical analysis

Analyses were performed with SPSS statistics for Windows 21 (IBM corp., Armonk, New York) and Stata/SE version 16.0 (Statacorp, College Station, Texas). Continuous data were presented as mean \pm SD and categorical variables were presented as frequencies (percentage of cases). Continuous variables were compared by independent Student's t-tests and categorical data by χ^2 or Fisher's exact tests. The association to VA was assessed by the area under the receiver operator characteristics curve (AUC). Odds ratios (OR) and 95% confidence intervals (CI) were calculated for RV deformation patterns and mechanical dispersion using univariable and multivariable logistic regression. The incremental value of combining RV deformation patterns with mechanical dispersion was assessed by reclassification analysis by integrated diagnostic improvement (IDI) and continuous net reclassification improvement (NRI), and the AUCs of different models were compared. Mechanical dispersion was dichotomized at an optimal cut-off derived from a single threshold regression analysis. This threshold was defined as the point estimate that best classified two groups with the most diverging odds ratios. Intra- and inter-observer variability was expressed by kappa statistics or intraclass correlation coefficient, as appropriate. P-values were two-sided and values <0.05 were considered significant.

RESULTS

Clinical characteristics

We included 160 patients (55% female, aged 41 ± 17 years), comprising 68 probands and 92 mutation positive family members, from 86 different families. Plakophilin-2 (PKP2) was the most common pathogenic mutation in both the Oslo and Utrecht cohort (90% and 89%, respectively). Most probands ($n = 55$ (81%)) and part of the family members ($n = 42$ (46%)) fulfilled a definite 2010 TFC AC diagnosis.⁵ Life-threatening ventricular arrhythmia had occurred in 47 (29%) of the subjects, with similar rates in the Oslo and Utrecht cohort (25 (31%) vs. 22 (28%), $p = 0.60$); as documented sustained ventricular tachycardia in 37, aborted cardiac arrest in 8, and appropriate ICD therapy in 2. More patients from the Oslo cohort were categorized in the electrical disease stage (25 (31%) vs. 13 (16%), $p = 0.03$), whereas the other disease stages were equally represented in both cohorts. (Table 1)

Table 1. Clinical characteristics and comparison per center

	All (n=160)	Oslo (n=80)	Utrecht (n=80)	p-value
Age, yrs	40.6 ± 16.8	40.9 ± 16.1	40.4 ± 17.6	0.87
Female, n(%)	88 (55)	44 (55)	44 (55)	1.00
Probands, n(%)	68 (43)	40 (50)	28 (35)	0.06
BSA, m ²	1.9 ± 0.2	1.9 ± 0.2	1.9 ± 0.2	0.31
Definite AC, n(%)	97 (61)	47 (59)	50 (63)	0.63
AA medication, n(%)	44 (28)	12 (15)	32 (40)	<0.001
Beta blockers, n(%)	60 (38)	27 (34)	33 (41)	0.33
Mutation, n(%)	139 (87)	59 (75)	80 (100)	<0.001
PKP2, n(%)	124 (78)	53 (67)	71 (89)	0.001
ICD, n(%)	20 (14)	7 (9)	13 (19)	0.07
Syncope, n(%)	40 (25)	30 (38)	10 (13)	<0.001
VA, n(%)	47 (29)	25 (31)	22 (28)	0.60
Disease stage, n(%)				
• Subclinical	36 (23)	15 (19)	21 (26)	0.26
• Electrical	38 (24)	25 (31)	13 (16)	0.03
• Structural	86 (54)	40 (50)	46 (58)	0.34

Values are, n (%), mean ± standard deviation. Abbreviations: AA = anti arrhythmic, AC = arrhythmogenic cardiomyopathy, BSA = body surface area, ICD = implantable cardioverter-defibrillator, PKP2 = plakophilin-2, VA = life-threatening ventricular arrhythmia.

Ventricular arrhythmias

Patients with VA were predominantly males (n = 28, 60%) and were significantly older (46.4 ± 13.9 vs. 38.2 ± 16.8 years, p = 0.002). Only two (2%) of the mutation-positive family members had experienced the arrhythmic outcome at evaluation (*Table 2, analyses separated by center are enclosed in the supplementary material*). Patients with VA had worse conventional echocardiographic parameters at inclusion, except for LVEF (*Table 3*).

RV subtricuspid deformation patterns were similarly distributed within the two cohorts (*Figure 2, panel A*) and were more abnormal in patients with VA. Among VA patients, 46 (98%) had an abnormal RV deformation pattern type II (n = 16 (34%)) or type III (n = 30 (64%)). Odds for VA significantly increased with each step-up in type (OR 3.91, 95%CI (2.23 – 6.85), p <0.001), also when adjusted for age at outcome adjudication (OR 3.55, 95%CI (1.97 – 6.42), p <0.001).

Table 2. Clinical characteristics and electrocardiographic parameters of patients without and with life-threatening arrhythmia

	All (n=160)	No VA (n=113)	VA (n=47)	p-value
Age, yrs	41 ± 17	38 ± 17	46 ± 14	0.002
Female, n(%)	88 (55)	69 (61)	19 (40)	0.01
Probands, n(%)	68 (43)	23 (20)	45 (96)	<0.001
BSA, m ²	1.9 ± 0.2	1.9 ± 0.2	2.0 ± 0.2	<0.001
Definite AC, n(%)	97 (61)	57 (50)	40 (85)	<0.001
AA medication, n(%)	44 (28)	16 (14)	28 (60)	<0.001
Beta blockers, n(%)	60 (38)	35 (31)	25 (53)	0.008
Mutation, n(%)	139 (87)	103 (92)	36 (77)	0.008
PKP2, n(%)	124 (78)	94 (84)	30 (64)	0.005
ICD, n(%)	20 (14)	2 (2)	18 (44)	<0.001
Syncope, n(%)	40 (25)	23 (20)	17 (36)	0.04
HR, bpm	61 ± 12	63 ± 13	56 ± 10	<0.001
TWI major, n(%)	45 (28)	22 (20)	23 (49)	<0.001
Epsilon wave, n(%)	13 (8)	5 (5)	8 (17)	0.008
TAD>55ms, n(%)	37 (25)	22 (21)	15 (37)	0.04
PVC>500, n(%)	43 (27)	33 (30)	10 (22)	0.32
Disease stage, n(%)				
• Subclinical	36 (23)	36 (32)	0 (0)	<0.001
• Electrical	38 (24)	31 (27)	7 (15)	0.09
• Structural	86 (54)	46 (41)	40 (85)	<0.001

Values are, n (%), mean ± standard deviation. Abbreviations: AA = anti arrhythmic, AC = arrhythmogenic cardiomyopathy, BSA = body surface area, HR = heart rate, ICD = implantable cardioverter-defibrillator, PKP2 = plakophilin-2, PVC = premature ventricular complex, TAD = terminal activation duration, TWI = T-wave inversion, VA = life-threatening ventricular arrhythmia.

Patients with VA had more pronounced RV mechanical dispersion (53 ± 30 vs. 30 ± 21 ms, $p < 0.001$). This difference was evident in both cohorts (45 ± 25 vs. 26 ± 15 ms, $p < 0.001$ in the Oslo cohort and 63 ± 33 vs. 34 ± 25 ms, $p < 0.001$ in the Utrecht cohort). (Figure 2, panel B) Every 10 ms increase in RV mechanical dispersion increased the odds of observing VA by 45% (OR 1.45, 95%CI (1.23 – 1.71), $p < 0.001$). When adjusted for age, the increased odds was comparable (OR 1.41, 95%CI (1.18 – 1.69), $p < 0.001$). The optimal cut-off for RV mechanical dispersion to detect patients with a history of VA was 24 ms (OR 1.06, 95%CI (0.96 – 1.18) per 10 ms increment < 24 ms and 1.57, 95%CI (1.45 – 1.71) per 10 ms increment > 24 ms).

The AUC significantly decreased when dichotomizing RV mechanical dispersion, compared to using it as a continuous variable (0.71, 95%CI (0.64 – 0.77) vs. 0.78, 95%CI (0.71 – 0.86), $p = 0.01$). Therefore, RV mechanical dispersion was used only as a continuous variable.

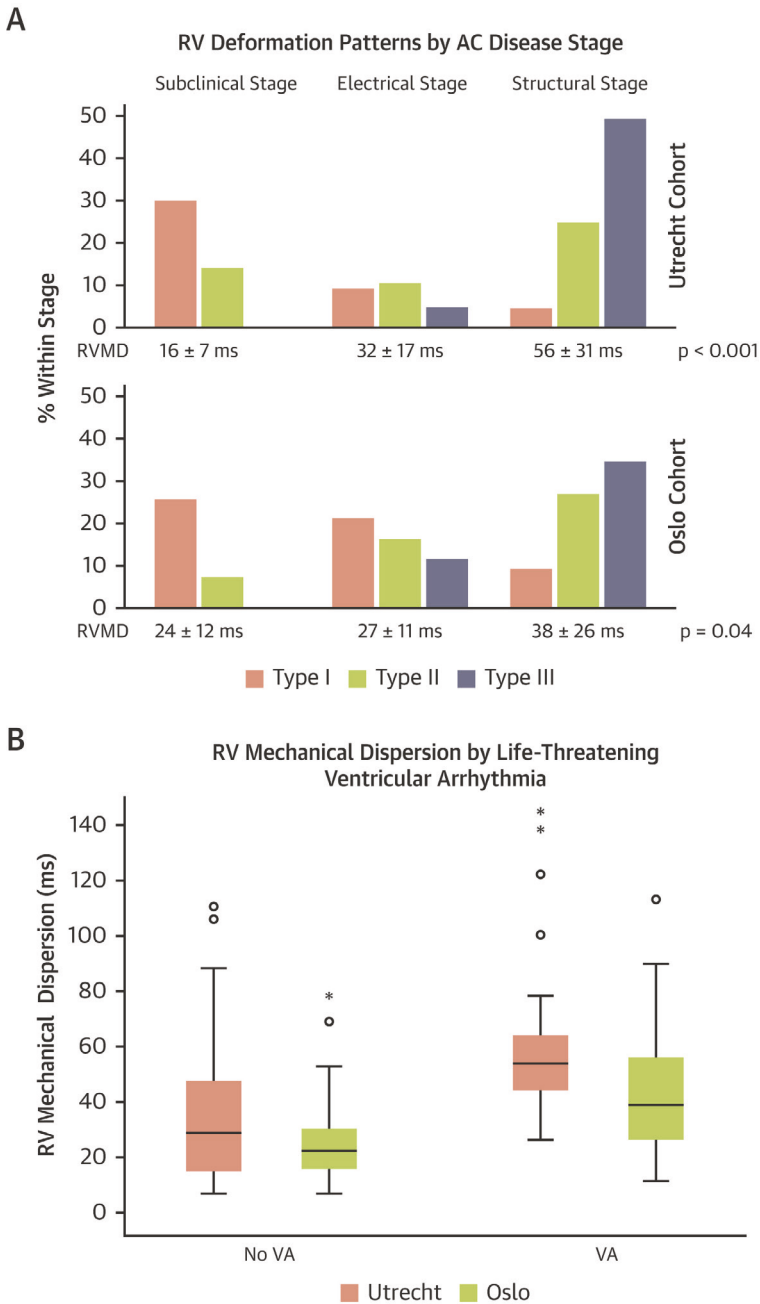


Figure 2. External validation of methods

To appreciate the external validity of the RV deformation methods, results are displayed separately for both cohorts. **Panel A:** Distribution of RV deformation patterns over three different disease. Below each disease stage, the RV mechanical dispersion (RVMD) is reported as mean ± standard deviation. **Panel B:** Distribution of RV mechanical dispersion for patients with and without a history of life-threatening ventricular arrhythmia (VA).

Table 3. Cardiac imaging parameters of patients without and with life-threatening arrhythmia

Echocardiography	All (n=160)	No VA (n=113)	VA (n=47)	p-value
RVD, mm	41 ± 10	38 ± 7	48 ± 12	<0.001
RVFAC, %	38 ± 11	42 ± 9	29 ± 9	<0.001
RV deformation pattern I, n(%)	43 (27)	42 (37)	1 (2)	<0.001
RV deformation pattern II, n(%)	56 (35)	40 (35)	16 (34)	0.87
RV deformation pattern III, n(%)	61 (38)	31 (27)	30 (64)	<0.001
RV _{FW} SL, %	-19.3 ± 7.6	-21.4 ± 6.5	-14.0 ± 7.7	<0.001
• Peak systolic strain basal, %	-14 ± 9	-16 ± 9	-8 ± 8	<0.001
• Peak systolic strain mid, %	-20 ± 8	-22 ± 7	-14 ± 8	<0.001
• Peak systolic strain apical, %	-24 ± 8	-26 ± 7	-20 ± 10	<0.001
RVMD, ms	37 ± 26	30 ± 21	53 ± 30	<0.001
RVOT, mm	35 ± 8	32 ± 6	40 ± 9	<0.001
TAPSE, mm	21 ± 4	22 ± 4	18 ± 5	<0.001
LVEF, %	57 ± 7	57 ± 6	56 ± 9	0.31
GLS, %	-18.1 ± 3.4	-18.7 ± 2.8	-16.7 ± 4.2	0.003
CMR	(n=129)	(n=95)	(n=34)	
RVEF, %	46 ± 13	49 ± 12	37 ± 13	<0.001
RVEDVi, ml	110 ± 41	99 ± 31	148 ± 48	<0.001
LGE, n (%)	34 (27)	14 (15)	20 (59)	<0.001

Values are, n (%), mean ± standard deviation. Abbreviations: CMR = cardiac magnetic resonance, EDVi = end diastolic volume indexed, EF = ejection fraction, FAC = fractional area change, GLS = global longitudinal strain, LGE = late gadolinium enhancement, LV = left ventricle, MD = mechanical dispersion, RV = right ventricle, RVD = right ventricular diameter, RV_{FW}SL = right ventricular free wall longitudinal strain, RVOT = right ventricular outflow tract, TAPSE = tricuspid annular plane systolic excursion.

ROC analysis showed a reasonable association between deformation pattern recognition and VA (AUC 0.74, 95%CI (0.66 – 0.82)) and between RV mechanical dispersion and VA (AUC 0.78, 95%CI (0.71 – 0.86)), when used separately. We observed no difference between the associations in the Oslo and Utrecht cohort for both pattern recognition (AUC 0.77, 95%CI (0.68 – 0.86) vs. 0.72, 95%CI (0.61 – 0.83), p = 0.49), and RV mechanical dispersion (AUC 0.76, 95%CI (0.65 – 0.88) vs. 0.81, 95%CI (0.72 – 0.91), p = 0.50).

All deformation analyses showed excellent intra- and inter-observer agreement. (*Supplementary material*)

Combining the two RV deformation methods

RV deformation patterns and RV mechanical dispersion were partially concordant, but also independently associated with VA (adjusted OR 2.71, 95%CI (1.47 – 5.00) per step-up and 1.26, 95%CI (1.07 – 1.49) per 10 ms increment, respectively). Patients with abnormal deformation patterns (type II or III) had increased odds for VA (OR 27.21, 95%CI (3.62 – 204.63)) and within this

subgroup odds for VA increased by 30% for each 10 ms increase in RV mechanical dispersion (OR 1.30, 95%CI (1.11 – 1.53) per 10 ms increase). (*Central illustration*)

When applying the RV mechanical dispersion in the group with normal or type II deformation patterns, the odds of VA increased by approximately 45% for each 10 ms increase in dispersion (OR 1.46, 95%CI (1.08 – 1.96)). Classification significantly improved when adding RV mechanical dispersion to pattern recognition (NRI 0.42, $p = 0.02$ and IDI 0.06, $p = 0.01$). The association increased from AUC 0.74, 95%CI (0.66 – 0.82) to 0.80, 95%CI (0.73 – 0.87), $p = 0.001$. (*Figure 3*) This association was similar to the association between CMR markers and arrhythmia. (*Table 4*)

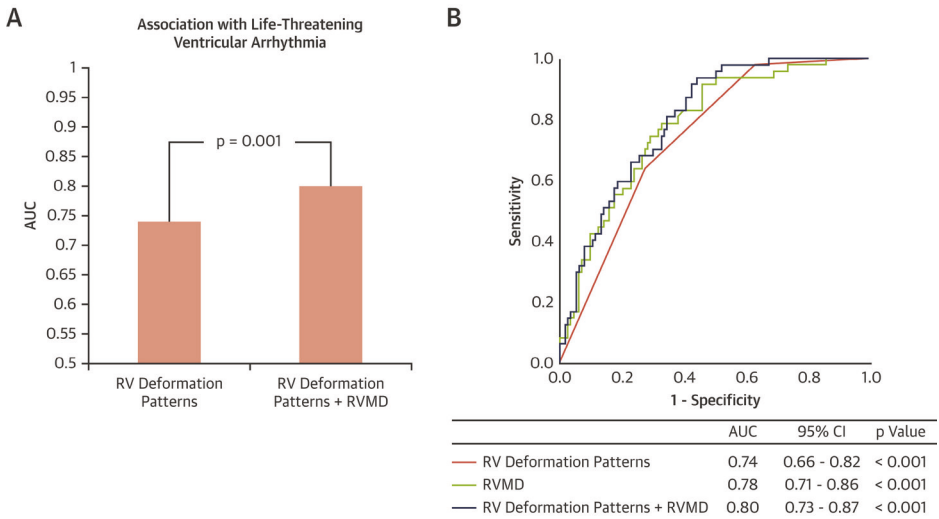


Figure 3. Comparison of models

Panel A: An improved association with life-threatening ventricular arrhythmia was found when combining RV deformation patterns and RV mechanical dispersion (RVMD), compared to taking only RV deformation patterns into account. This is expressed by an increase in area under the curve (AUC), when comparing ROC statistics.

Panel B: Display of the ROC curves of the individual and combined RV deformation methods.

Table 4. Association to arrhythmia of CMR vs. the combined RV deformation imaging approach

	AUC (95% CI) CMR marker	vs. RV deformation imaging	p-value
RVEF (n=99)	0.73 (0.61 – 0.85)	0.74 (0.63 – 0.84)	0.95
RVEDVi (n=92)	0.81 (0.69 – 0.93)	0.77 (0.66 – 0.87)	0.53
LGE (n=125)	0.73 (0.63 – 0.82)	0.76 (0.67 – 0.84)	0.58

Abbreviations: AUC = area under the receiver operator characteristic, CI = confidence interval, CMR = cardiac magnetic resonance, EDVi = end diastolic volume indexed, EF = ejection fraction, LGE = late gadolinium enhancement, RV = right ventricular.

DISCUSSION

This study provides an external validation of the use of RV deformation pattern recognition and RV mechanical dispersion in AC patients and mutation positive family members. Both abnormal deformation patterns and prolonged RV mechanical dispersion were independent markers of patients with a history of VA, highlighting the role of deformation analyses in the echocardiographic assessment of AC patients. *Combining* the two parameters increased the association to VA, indicating an independent and incremental value of these techniques which may help risk stratification of AC patients.

RV deformation patterns

This study, for the first time, links abnormal RV deformation patterns to arrhythmic events. Previous studies have focused on the use of RV deformation patterns for early detection of AC disease manifestation and the correlation with clinical disease stages, based on the presence of 2010 TFC.^{6,19} Subsequently, prognostic value of the patterns was shown for prediction of disease progression, defined as development of new 2010 TFC during follow-up⁷, and structural progression on echocardiography²⁵.

The distribution of deformation patterns over disease stages of increasing severity was similar in both cohorts and in line with previous results⁶, and it was therefore considered a successful external validation. (*Figure 2*) We found clearly abnormal deformation patterns in the RV subtricuspid segment in a significant number of subjects without any electrical or structural 2010 TFC, indicating presence of mechanical dysfunction already in an early stage of the disease.⁶

Importantly, abnormal RV deformation patterns had an excellent sensitivity for detection of patients with VA, with a negative predictive value of 0.98. Specificity was suboptimal when taking only past events into account. A prospective setting is however needed, since abnormalities now classified as false-positive might be indicators of a risk of future life-threatening arrhythmic events.

RV mechanical dispersion

We observed a marked increase in RV mechanical dispersion for patients with VA in both cohorts with no difference by ROC comparison, suggesting mechanical dispersion as an externally valid marker of VA.

Mean RV mechanical dispersion was higher in the Utrecht cohort, partly caused by several outliers. (*Figure 2, panel B*) The association between RV mechanical dispersion and arrhythmia was in line with previous reports on patients with early AC disease¹² and exercise induced arrhythmias.²⁶

Previous studies and a consensus document on multi-modality imaging in AC have suggested cut-offs for RV mechanical dispersion.^{8,9,15} We observed that dichotomizing at the optimal threshold resulted in a significant loss of information, indicating better abilities of mechanical dispersion used as a continuous parameter.

Combining the two RV deformation methods

Previously, it was not clear whether the two RV deformation methods assess the same underlying pathology, and comparative data were not available. By applying both methods on the total cohort and associating them to the same definition of arrhythmic outcome, this

study was the first to enable a direct comparison. Both RV deformation pattern recognition and mechanical dispersion were independently associated with VA. Importantly, the classification of patients with a history of VA significantly improved when adding the RV mechanical dispersion to pattern recognition. This implies that the two techniques are complementary and may reflect different pro-arrhythmogenic properties of the myocardium. We chose the clinically most intuitive approach to first evaluate the categorical parameter (deformation patterns), and add the continuous variable (mechanical dispersion). Although deformation patterns and RV mechanical dispersion are both obtained from longitudinal deformation in the same echocardiographic view, there are two important reasons for their unique value. First, mechanical dispersion focusses on heterogeneity in global RV contraction, whereas the deformation pattern is considered to reflect focal substrates in one segment. The usually less affected interventricular septum is included in RV mechanical dispersion for a more robust calculation of the standard deviation and to detect globally delayed contraction of the RV lateral wall. Second, patterns include information of both timing and strain amplitude, whereas strain amplitude has no direct influence on mechanical dispersion. The two methods, therefore, have independent strengths and weaknesses. The pattern approach is sensitive to subtle abnormalities in the subtricuspid segment which may be associated with increased arrhythmic risk. In both cohorts, the subtricuspid segment showed to be first affected in AC, which is in line with previous reports.²⁷ However, prominent involvement of other RV segments has also been reported in AC^{28,29} and focussing on one segment is accompanied by the risk of missing information. Importantly, whereas the subtricuspid deformation pattern is not able to detect progression to other RV segments, RV mechanical dispersion will increase along with more extensive disease and helps stratifying between intermediate and high arrhythmic risk.

Clinical implications

External validation of RV deformation pattern recognition and mechanical dispersion is a crucial step towards including them in routine clinical assessment and in clinical risk stratification in AC patients. This study was the first attempt to externally validate the value of these methods. For external validation of the combined approach, a third cohort will be needed.

Current risk stratification tools do not include regional and subtle RV function, but only the global RV function from RVEF by CMR.³⁰ Deformation imaging contributes as a sensitive marker of early structural and functional abnormalities and may improve risk stratification as shown in this study. The overall association with arrhythmia was similar to CMR markers, but the easily available echocardiography has many practical advantages, especially in patients who cannot undergo CMR imaging.

The increasing use of cascade genetic screening will confront clinicians with an expanding group of asymptomatic patients and relatives with an important arrhythmic risk.¹³ We showed that a normal RV deformation pattern can identify low risk subjects with excellent negative predictive value. In clinical practice, an initial impression of the deformation pattern can be determined with a brief qualitative determination. Patients with normal deformation patterns would not require quantitative analysis by mechanical dispersion. In patients with borderline abnormal deformation patterns, RV mechanical dispersion may be used for further stratification. In patients with clearly abnormal deformation patterns, a high mechanical dispersion will imply high risk of ventricular arrhythmias. A stepwise approach using both RV deformation indices is superior as it allows identification of a group of low-risk individuals as well as further arrhythmic risk stratification in others. (*Central illustration*)

Limitations

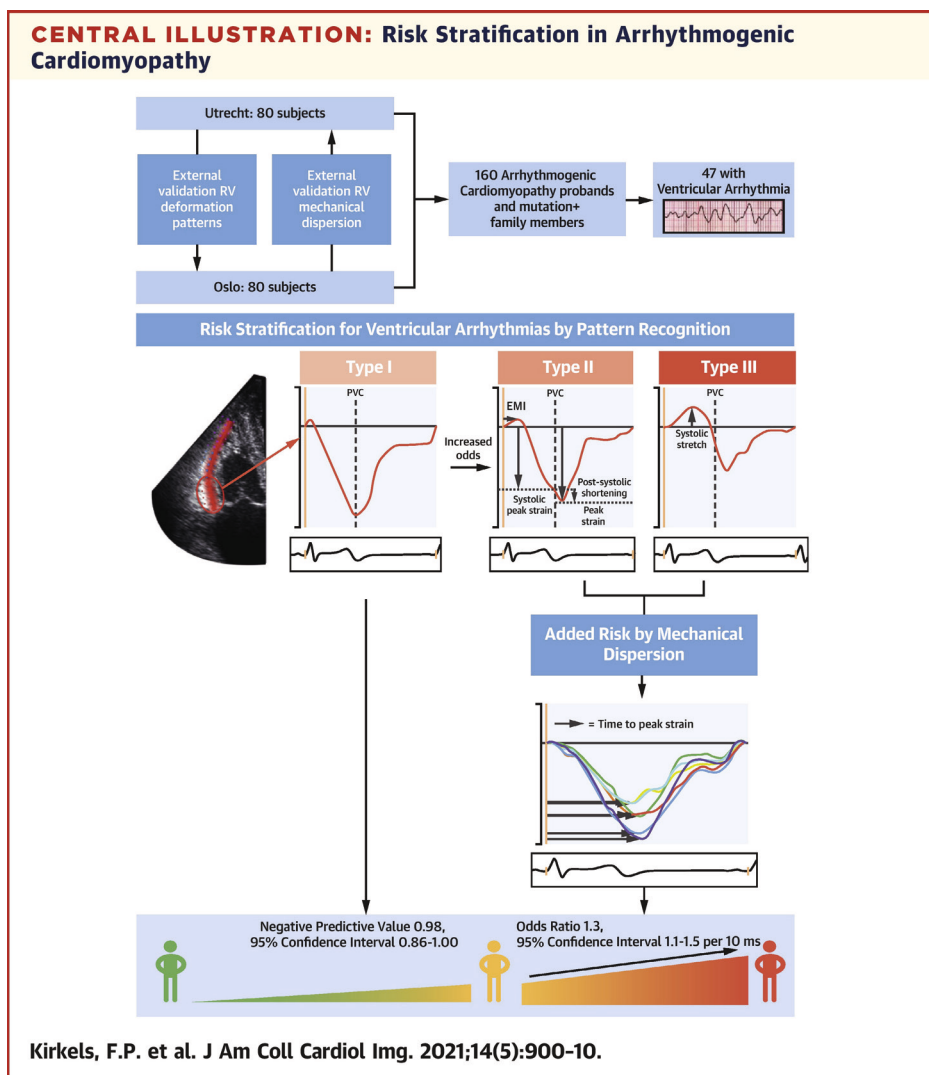
This study had a cross-sectional design with retrospective outcome adjudication with inherent limitations. The predictive value of the investigated parameters should be assessed in a prospective trial. RV deformation imaging reflects partly the same RV functional status as other echocardiographic and CMR indices and a multimodality approach will probably offer the best results. To investigate the clinical impact of RV deformation measurements, the additive predictive value should be explored with regard to the existing risk calculation model.³⁰

A single observer performed all deformation analyses in this study. We considered this a strength for the external validation of the methodology. Although our inter-observer variability analysis showed excellent agreement, this approach may represent a limitation for the clinical external validation.

Subjects evaluated at higher age were more likely to have experienced an event. However, also when adjusted for age, RV deformation abnormalities were associated with substantial increase in odds for history of VA. Implantation of ICDs caused a risk of bias for detection of arrhythmic events, but due to the low number of appropriate ICD therapies this risk is considered to be low in the current study.

Data from family members may not be independent. However, since we included patients from 86 different families, we considered it unlikely that overall results were influenced by dependence within single families. A comparison with healthy controls was not performed in this study, but can be found for RV deformation patterns⁶ and mechanical dispersion⁸ separately in previous studies.

The majority of patients had PKP2 mutations which may limit the extrapolation to other genetic causes of AC.



Central illustration. Risk stratification in arrhythmogenic cardiomyopathy (AC)

We enrolled 160 arrhythmogenic cardiomyopathy (AC) probands and mutation-positive family members from two large European referral centers, of which 47 had experienced life-threatening ventricular arrhythmia (VA). **(top)** We performed speckle tracking echocardiography, whereby we classified the subtricuspid deformation patterns from normal to abnormal and assessed RV mechanical dispersion from 6 segments. Both methods were first externally validated and compared to the cohort where the method was developed. **(top left)** Subsequently, a combined approach was developed, in which a normal deformation pattern (type I) was associated with an excellent negative predictive value (NPV), requiring no further analyses. **(bottom left)** In patients with an abnormal deformation pattern (type II or III), mechanical dispersion further stratified between intermediate and high arrhythmic risk. **(bottom right)**

CONCLUSION

This study is the first to externally validate the use of RV deformation pattern recognition and RV mechanical dispersion in AC. RV deformation patterns and mechanical dispersion were independently associated with life-threatening ventricular arrhythmia. Importantly, we observed an added value of combining mechanical dispersion and RV deformation patterns for optimal detection of patients with a history of VA. Future larger prospective studies should investigate the value of combining both parameters in a multimodality risk prediction approach.

PERSPECTIVES

Clinical competencies

The use of cascade genetic screening in arrhythmogenic cardiomyopathy is presenting clinicians with an expanding group of asymptomatic genotype positive relatives with an important arrhythmic risk. Deformation imaging detects early structural and functional abnormalities indicating increased risk of ventricular arrhythmias and may help risk stratification in early disease.

Translational outlook

Deformation imaging in the easily available echocardiographic assessment has become part of daily clinical practice in many centers. We compared two cohorts of patients with arrhythmogenic cardiomyopathy from two different centers and externally validated two methods of deformation imaging. Both methods showed validity for detection of early structural and functional abnormalities and the combination of the methods increased clinical risk stratification of patients with arrhythmogenic cardiomyopathy.

Acknowledgements: The authors would like to thank Margareth Ribe and Maria Ruud for their work as research coordinators. This work was supported by the Norwegian Research Council (project 288438). Folkert Asselbergs is supported by UCL Hospitals NIHR Biomedical Research Centre.

REFERENCES

1. Marcus FI, Fontaine GH, Guiraudon G, et al. Right ventricular dysplasia: A report of 24 adult cases. *Circulation*. 1982;65(2):384-98.
2. Thiene G, Nava A, Corrado D, Rossi L, Pennelli N. Right Ventricular Cardiomyopathy and Sudden Death in Young People. *N Engl J Med*. 1988;318(3):129-133.
3. Corrado D, Link M, Calkins H. Arrhythmogenic Right Ventricular Cardiomyopathy. *N Engl J Med*. 2017;376:61-72.
4. Groeneweg JA, Bhonsale A, James CA, et al. Clinical Presentation, Long-Term Follow-Up, and Outcomes of 1001 Arrhythmogenic Right Ventricular Dysplasia/Cardiomyopathy Patients and Family Members. *Circ Cardiovasc Genet*. 2015;8(3):437-446.
5. Marcus FI, McKenna WJ, Sherrill D, et al. Diagnosis of arrhythmogenic right ventricular cardiomyopathy/Dysplasia: Proposed modification of the task force criteria. *Circulation*. 2010;121(13):1533-1541.
6. Mast TP, Teske AJ, Walmsley J, et al. Right Ventricular Imaging and Computer Simulation for Electromechanical Substrate Characterization in Arrhythmogenic Right Ventricular Cardiomyopathy. *J Am Coll Cardiol*. 2016;68(20):2185-2197.
7. Mast TP, Taha K, Cramer MJ, et al. The Prognostic Value of Right Ventricular Deformation Imaging in Early Arrhythmogenic Right Ventricular Cardiomyopathy. *JACC Cardiovasc Imaging*. 2019;12(3):446-455.
8. Sarvari SI, Haugaa KH, Anfinson OG, et al. Right ventricular mechanical dispersion is related to malignant arrhythmias: A study of patients with arrhythmogenic right ventricular cardiomyopathy and subclinical right ventricular dysfunction. *Eur Heart J*. 2011;32(9):1089-1096.
9. Leren IS, Saberniak J, Haland TF, Edvardsen T, Haugaa KH. Combination of ECG and Echocardiography for Identification of Arrhythmic Events in Early ARVC. *JACC Cardiovasc Imaging*. 2017;10(5):503-513.
10. Lie ØH, Rootwelt-Norberg C, Dejgaard LA, et al. Prediction of Life-Threatening Ventricular Arrhythmia in Patients With Arrhythmogenic Cardiomyopathy: A Primary Prevention Cohort Study. *JACC Cardiovasc Imaging*. 2018;11(10):1377-1386.
11. Malik N, Win S, James CA, et al. Right Ventricular Strain Predicts Structural Disease Progression in Patients With Arrhythmogenic Right Ventricular Cardiomyopathy. *J Am Heart Assoc*. 2020 (E-pub ahead of print). (doi: 10.1161/JAHA.119.015016)
12. Saberniak J, Leren IS, Haland TF, et al. Comparison of patients with early-phase arrhythmogenic right ventricular cardiomyopathy and right ventricular outflow tract ventricular tachycardia. *Eur Heart J Cardiovasc Imaging*. 2017;18(1):62-69.
13. Chivulescu M, Lie ØH, Popescu BA, et al. High penetrance and similar disease progression in probands and in family members with arrhythmogenic cardiomyopathy. *Eur Heart J*. 2020;41(14):1401-1410.
14. Peachey H, Pedersen CT, Kay GN, et al. EHRA/HRS/APHRs Expert Consensus on Ventricular Arrhythmias. *Heart Rhythm*. 2014;11(10):166-196.
15. Haugaa KH, Basso C, Badano LP, et al. Comprehensive multi-modality imaging approach in arrhythmogenic cardiomyopathy-an expert consensus document of the European Association of Cardiovascular Imaging. *Eur Heart J Cardiovasc Imaging*. 2017;18(3):237-253
16. Mast TP, Teske AJ, Doevendans PA, Cramer MJ. Current and future role of echocardiography in arrhythmogenic right ventricular dysplasia/cardiomyopathy. *Cardiol J*. 2015;22(4):362-374.

17. Teske AJ, De Boeck BWL, Melman PG, Sieswerda GT, Doevendans PA, Cramer MJM. Echocardiographic quantification of myocardial function using tissue deformation imaging, a guide to image acquisition and analysis using tissue Doppler and speckle tracking. *Cardiovasc Ultrasound*. 2007;5:27.
18. Badano LP, Koliás TJ, Muraru D, et al. Standardization of left atrial, right ventricular, and right atrial deformation imaging using two-dimensional speckle tracking echocardiography: A consensus document of the EACVI/ASE/Industry Task Force to standardize deformation imaging. *Eur Heart J Cardiovasc Imaging*. 2018;19(6):591-600.
19. Mast TP, Teske AJ, Te Riele AS, et al. Prolonged Electromechanical Interval Unmasks Arrhythmogenic Right Ventricular Dysplasia/Cardiomyopathy in the Subclinical Stage. *J Cardiovasc Electrophysiol*. 2016;27(3):303-314.
20. Teske AJ, Cox MG, De Boeck BW, Doevendans PA, Hauer RN, Cramer MJ. Echocardiographic Tissue Deformation Imaging Quantifies Abnormal Regional Right Ventricular Function in ARVD/C. *J Am Soc Echocardiogr*. 2009;22(8):920-927.
21. Teske AJ, Cox MG, Te Riele AS, et al. Early detection of regional functional abnormalities in asymptomatic ARVD/C gene carriers. *J Am Soc Echocardiogr*. 2012;25(9):997-1006.
22. Collier P, Phelan D, Klein A. A Test in Context: Myocardial Strain Measured by Speckle-Tracking Echocardiography. *J Am Coll Cardiol*. 2017;69(8):1043-1056.
23. Voigt J-U, Pedrizzetti G, Lysyansky P, et al. Definitions for a common standard for 2D speckle tracking echocardiography: consensus document of the EACVI/ASE/Industry Task Force to standardize deformation imaging. *J Am Soc Echocardiogr*. 2015;28(2):183-193.
24. Edvardsen T, Haugaa KH. Imaging assessment of ventricular mechanics. *Heart*. 2011;97(16):1349-1356.
25. Taha K, Mast TP, Cramer MJ, et al. Evaluation of Disease Progression in Arrhythmogenic Cardiomyopathy: The Change of Echocardiographic Deformation Characteristics Over Time. *J Am Coll Cardiol Img*. 2020;13(2):631-634.
26. Claeys M, Claessen G, Claus P, et al. Right ventricular strain rate during exercise accurately identifies male athletes with right ventricular arrhythmias. *Eur Heart J Cardiovasc Imaging*. 2020;21(3):282-290.
27. Te Riele AS, James CA, Philips B, et al. Mutation-positive arrhythmogenic right ventricular dysplasia/cardiomyopathy: the triangle of dysplasia displaced. *J Cardiovasc Electrophysiol*. 2013;24(12):1311-1320.
28. Czimbalmoš C, Csecs I, Dohy Z, et al. Cardiac magnetic resonance based deformation imaging: role of feature tracking in athletes with suspected arrhythmogenic right ventricular cardiomyopathy. *Int J Cardiovasc Imaging*. 2019;35(3):529-538.
29. Pieles GE, Grosse-Wortmann L, Hader M, et al. Association of Echocardiographic Parameters of Right Ventricular Remodeling and Myocardial Performance With Modified Task Force Criteria in Adolescents With Arrhythmogenic Right Ventricular Cardiomyopathy. *Circ Cardiovasc Imaging*. 2019;12(4):e007693.
30. Cadrin-Tourigny J, Bosman LP, Nozza A, et al. A new prediction model for ventricular arrhythmias in arrhythmogenic right ventricular cardiomyopathy. *Eur Heart J*. 2019;40(23):1850-1858.

SUPPLEMENTARY MATERIAL

Supplement: deformation imaging methods

RV deformation patterns

Details on image acquisition and post-processing in echocardiographic deformation imaging were previously described extensively.^{1,2} Deformation graphs were derived by speckle tracking of the endocardial border of the RV lateral free wall in a focused apical 4-chamber view.¹ After manual tracing, the wall was divided automatically into the basal, mid and apical segment. Multiple parameters were calculated and combined into a 3 type model. (*Figure 1, panel A*) The first parameter is the time to onset of shortening, also called the electro-mechanical interval (EMI). The EMI is defined as the time interval between the first deflection on the surface ECG and the onset of local myocardial shortening, as measured by 2D-speckle tracking.³ Second parameter is the systolic peak strain value, the maximum negative strain value between pulmonary valve opening and closure.⁴ Timing of the pulmonary valve closure was assessed in the parasternal short-axis view by Doppler tracing of the RVOT. The last parameter included in this combined model is the post-systolic index, defined as the percentage of shortening occurring after closure of the pulmonary valve. This index is calculated by taking the post-systolic shortening as a percentage of the global peak longitudinal strain.⁴

By using cut-offs of the previously mentioned parameters, the three types are distinguished. Type I is a normal deformation pattern, as seen in healthy controls, characterized by an EMI ≤ 90 ms, systolic peak strain $\geq |-20\%|$ and $\leq 10\%$ post-systolic shortening. Type II is characterized by delayed onset of shortening (>90 ms), reduced systolic peak strain ($< |-20\%|$ and $\geq |-10\%|$) and minor post-systolic shortening ($>10\%$). Type III strain patterns are characterized by little or no systolic peak strain ($< |-10\%|$), predominantly systolic stretching and major post-systolic shortening.⁴

Mechanical dispersion

The method for obtaining the mechanical dispersion from echocardiographic deformation imaging has been elaborated previously.^{5,6} Speckle tracking of the endocardium was performed in the 3 apical views for the LV and in the apical 4-chamber view for the RV.^{5,7} The LV was divided in a 16-segment model and the RV in a 6-segment model. The operator manually adjusted incorrectly tracked segments, and excluded them in the case of subsequently failed tracking. As a derivative of the contraction duration, time to peak negative strain was defined as the time from first deflection in the QRS complex on surface ECG to maximum LV and RV shortening by strain. Mechanical dispersion was calculated as the standard deviation (SD) of the segmental time intervals from onset Q/R on the surface ECG to peak negative strain, and expressed in milliseconds. The LV mechanical dispersion (LVMD) was calculated over all 16 segments and the RV mechanical dispersion (RVMD) over 6 segments, retaining the septal segments.⁶

Supplementary table 1. Intra- and inter-observer variability in deformation imaging measurements

		Utrecht			Oslo
		INTRA_1	INTRA_2	INTER_1_2	INTER
GLS	ICC + 95%CI	0.95 (0.81;0.98)	0.96 (0.91;0.98)	0.94 (0.89;0.96)	0.92 (0.81;0.97)
LVMD	ICC + 95%CI	0.96 (0.91;0.99)	0.99 (0.96;0.99)	0.92 (0.86;0.96)	0.87 (0.71;0.95)
RVMD	ICC + 95%CI	0.87 (0.71;0.95)	x	0.84 (0.64;0.93)	0.91 (0.78;0.96)
RV patterns	difference	3/20	0/20	3/40	2/20
	K	0.74	1.00	0.87	0.85
		p <0.001	p <0.001	p <0.001	p <0.001
	weighted K	0.78	1.00	0.89	0.89
		p <0.001	p <0.001	p <0.001	p <0.001

Abbreviations: CI = confidence interval, GLS = global longitudinal strain, ICC = intraclass correlation coefficient, K = kappa statistic, LV = left ventricle, MD = mechanical dispersion, RV = right ventricle

Supplementary table 2. Clinical characteristics comparison of patients without and with history of life-threatening arrhythmia at inclusion, separated by center.

	All	No VA	VA	p-value
	(n=160)	(n=113)	(n=47)	
	(n=80)	(n=55)	(n=25)	
	(n=80)	(n=58)	(n=22)	
Age, yrs (n = 160)	40.6 ± 16.8	38.2 ± 17.4	46.4 ± 13.9	0.002
Oslo (n = 80)	40.9 ± 16.1	38.8 ± 16.9	45.5 ± 13.4	0.06
Utrecht (n = 80)	40.4 ± 17.6	37.7 ± 17.9	47.5 ± 14.7	0.03
Female, n(%) (n = 160)	88 (55)	69 (61)	19 (40)	0.01
Oslo (n = 80)	44 (55)	31 (56)	13 (52)	0.90
Utrecht (n = 80)	44 (55)	38 (66)	6 (27)	0.002
Probands, n(%) (n = 160)	68 (43)	23 (20)	45 (96)	<0.001
Oslo (n = 80)	40 (50)	16 (29)	24 (96)	<0.001
Utrecht (n = 80)	28 (35)	7 (12)	21 (96)	<0.001
BSA, m ² (n = 158)	1.9 ± 0.2	1.9 ± 0.2	2.0 ± 0.2	<0.001
Oslo (n = 79)	2.0 ± 0.2	1.9 ± 0.2	2.0 ± 0.2	0.06
Utrecht (n = 79)	1.9 ± 0.2	1.8 ± 0.2	2.0 ± 0.2	0.008
Definite AC, n(%) (n = 160)	97 (61)	57 (50)	40 (85)	<0.001
Oslo (n = 80)	47 (59)	29 (53)	18 (72)	0.11
Utrecht (n = 80)	50 (63)	28 (48)	22 (100)	<0.001
AA med., n(%) (n = 160)	44 (28)	16 (14)	28 (60)	<0.001
Oslo (n = 80)	12 (15)	5 (9)	7 (28)	0.03
Utrecht (n = 80)	32 (40)	11 (19)	21 (96)	<0.001
BB, n(%) (n = 160)	60 (38)	35 (31)	25 (53)	0.008
Oslo (n = 80)	27 (34)	20 (36)	7 (28)	0.46
Utrecht (n = 80)	33 (41)	15 (26)	18 (82)	<0.001
Mutation, n(%) (n = 159)	139 (87)	103 (92)	36 (77)	0.008
Oslo (n = 79)	59 (75)	45 (83)	14 (56)	0.009
Utrecht (n = 80)	80 (100)	58 (100)	22 (100)	-

Supplementary table 2. Clinical characteristics comparison of patients without and with history of life-threatening arrhythmia at inclusion, separated by center. (continued)

	All (n=160) (n=80) (n=80)	No VA (n=113) (n=55) (n=58)	VA (n=47) (n=25) (n=22)	p-value
PKP2, n(%) (n = 159)	124 (78)	94 (84)	30 (64)	0.005
Oslo (n = 79)	53 (67)	43 (80)	10 (40)	<0.001
Utrecht (n = 80)	71 (89)	51 (88)	20 (91)	0.71
ICD, n(%) (n = 148)	20 (14)	2 (2)	18 (44)	<0.001
Oslo (n = 80)	7 (9)	0 (0)	7 (28)	<0.001
Utrecht (n = 68)	13 (19)	2 (4)	11 (69)	<0.001
Syncope, n(%) (n = 160)	40 (25)	23 (20)	17 (36)	0.04
Oslo (n = 80)	30 (38)	18 (33)	12 (48)	0.19
Utrecht (n = 80)	10 (13)	5 (9)	5 (23)	0.09

Values are, n (%), mean \pm standard deviation. Abbreviations: AA med. = anti arrhythmic medication, BB = beta blockers, AC = arrhythmogenic cardiomyopathy, BSA = body surface area, ICD = implantable cardioverter-defibrillator, PKP2 = plakophilin-2, VA = life-threatening ventricular arrhythmia

Supplementary table 3. Electrocardiographic parameter comparison between patients without and with history of life-threatening arrhythmia at inclusion, separated by center.

	All (n=160) (n=80) (n=80)	No VA (n=113) (n=55) (n=58)	VA (n=47) (n=25) (n=22)	p-value
HR, bpm (n = 158)	60.6 \pm 12.3	62.6 \pm 12.7	55.8 \pm 9.6	<0.001
Oslo (n = 78)	60.0 \pm 11.9	62.4 \pm 11.6	55.0 \pm 11.0	0.009
Utrecht (n = 80)	61.1 \pm 12.6	62.8 \pm 13.7	56.8 \pm 7.9	0.02
TWI major, n(%) (n = 160)	45 (28)	22 (20)	23 (49)	<0.001
Oslo (n = 80)	22 (28)	10 (18)	12 (48)	0.006
Utrecht (n = 80)	23 (29)	12 (21)	11 (50)	0.01
TWI minor, n(%) (n = 159)	17 (11)	12 (11)	5 (11)	0.99
Oslo (n = 80)	9 (11)	6 (11)	3 (12)	0.89
Utrecht (n = 79)	8 (10)	6 (11)	2 (9)	0.85
ϵ wave, n(%) (n = 159)	13 (8)	5 (5)	8 (17)	0.008
Oslo (n = 80)	4 (5)	1 (2)	3 (12)	0.06
Utrecht (n = 79)	9 (11)	4 (7)	5 (23)	0.05*
TAD>55ms, n(%) (n = 148)	37 (25)	22 (21)	15 (37)	0.04
Oslo (n = 80)	7 (9)	3 (6)	4 (16)	0.12
Utrecht (n = 68)	30 (44)	19 (37)	11 (69)	0.02
NSVT, n(%) (n = 80)*	24 (30)	14 (26)	10 (40)	0.19
Oslo (n = 80)				
Utrecht (n = 0)				

Supplementary table 3. Electrocardiographic parameter comparison between patients without and with history of life-threatening arrhythmia at inclusion, separated by center. (continued)

	All (n=160) (n=80) (n=80)	No VA (n=113) (n=55) (n=58)	VA (n=47) (n=25) (n=22)	p-value
PVC>500, n(%) (n = 158)	43 (27)	33 (30)	10 (22)	0.32
Oslo (n = 79)	17 (22)	13 (24)	4 (16)	0.42
Utrecht (n = 79)	26 (33)	20 (35)	6 (29)	0.62
VT major, n(%) (n = 160)	29 (18)	4 (4)	25 (53)	<0.001
Oslo (n = 80)	10 (13)	2 (4)	8 (32)	<0.001
Utrecht (n = 80)	19 (24)	2 (3)	17 (77)	<0.001
VT minor, n(%) (n = 160)	57 (36)	36 (32)	21 (45)	0.12
Oslo (n = 80)	32 (40)	16 (29)	16 (64)	0.003
Utrecht (n = 80)	25 (31)	20 (35)	5 (23)	0.31
SAECG abn.I, n(%) (n = 75)**	43 (57)	25 (50)	18 (72)	0.07
Oslo (n = 75)				
Utrecht (n = 0)				

Values are, n (%), mean \pm standard deviation. Abbreviations: HR = heart rate, NSVT = non-sustained ventricular tachycardia, PVC = premature ventricular complex, TAD = terminal activation duration, SAECG = signal averaged electrocardiogram, TWI = T-wave inversion, VA = ventricular arrhythmia, VT = ventricular tachycardia.

* Occurrence of NSVT was not systematically documented in Utrecht and thus only available for patients from the Oslo cohort.

** SAECG was not routinely performed in Utrecht and thus only available for patients from the Oslo cohort.

Supplementary table 4. Cardiac imaging parameter comparison between patients without and with history of life-threatening arrhythmia at inclusion, separated by center.

	All (n=160) (n=80) (n=80)	No VA (n=113) (n=55) (n=58)	VA (n=47) (n=25) (n=22)	p-value
EF, % (n = 160)	56.7 \pm 6.7	57.1 \pm 5.8	55.7 \pm 8.5	0.31
Oslo (n = 80)	56.5 \pm 6.6	56.6 \pm 6.0	56.3 \pm 7.9	0.89
Utrecht (n = 80)	56.9 \pm 6.9	57.7 \pm 5.7	55.1 \pm 9.3	0.14
GLS, % (n = 159)	-18.1 \pm 3.4	-18.7 \pm 2.8	-16.7 \pm 4.2	0.003
Oslo (n = 79)	-18.2 \pm 3.3	-18.7 \pm 2.4	-17.1 \pm 4.6	0.10
Utrecht (n = 80)	-18.0 \pm 3.5	-18.7 \pm 3.2	-16.2 \pm 3.7	0.003
LVMD, ms (n = 159)	41.2 \pm 19.8	37.4 \pm 19.4	50.2 \pm 18.0	<0.001
Oslo (n = 79)	39.6 \pm 14.0	35.8 \pm 10.9	47.8 \pm 16.5	0.002
Utrecht (n = 80)	42.7 \pm 24.3	38.8 \pm 24.8	52.9 \pm 19.7	0.02
RVD, mm (n = 160)	40.8 \pm 9.5	37.9 \pm 6.5	47.9 \pm 11.5	<0.001
Oslo (n = 80)	40.7 \pm 8.9	38.3 \pm 4.7	45.9 \pm 13.0	0.008
Utrecht (n = 80)	41.0 \pm 10.1	37.5 \pm 7.9	50.1 \pm 9.5	<0.001

Supplementary table 4. Cardiac imaging parameter comparison between patients without and with history of life-threatening arrhythmia at inclusion, separated by center. (continued)

	All (n=160) (n=80) (n=80)	No VA (n=113) (n=55) (n=58)	VA (n=47) (n=25) (n=22)	p-value
RVFAC, % (n = 159)	37.9 ± 10.5	41.5 ± 8.9	29.3 ± 9.3	<0.001
Oslo (n = 80)	38.6 ± 10.2	41.1 ± 7.6	30.9 ± 11.0	<0.001
Utrecht (n = 79)	37.3 ± 10.9	40.9 ± 9.9	27.4 ± 6.3	<0.001
RV deformation pattern I, n(%)	43 (27)	42 (37)	1 (2)	<0.001
Oslo (n = 80)	24 (30)	24 (44)	0 (0)	<0.001
Utrecht (n = 80)	19 (24)	18 (31)	3 (5)	0.01
RV deformation pattern II, n(%)	56 (35)	40 (35)	16 (34)	0.87
Oslo (n = 80)	28 (35)	18 (33)	10 (40)	0.53
Utrecht (n = 80)	28 (35)	22 (38)	6 (27)	0.37
RV deformation pattern III, n(%)	61 (38)	31 (27)	30 (64)	<0.001
Oslo (n = 80)	28 (35)	13 (24)	15 (60)	0.002
Utrecht (n = 80)	33 (41)	18 (31)	15 (68)	0.003
RV _{FW} SL, % (n = 160)	-19.3 ± 7.6	-21.4 ± 6.5	-14.0 ± 7.7	<0.001
Oslo (n = 80)	-20.7 ± 7.5	-22.6 ± 6.5	-16.4 ± 7.8	<0.001
Utrecht (n = 80)	-17.9 ± 7.5	-20.3 ± 6.3	-11.3 ± 6.7	<0.001
RVMD, ms (n = 160)	36.8 ± 26.3	29.9 ± 21.1	53.4 ± 30.0	<0.001
Oslo (n = 80)	31.8 ± 20.5	25.9 ± 15.4	44.7 ± 24.5	0.001
Utrecht (n = 80)	41.8 ± 30.2	33.6 ± 24.8	63.3 ± 33.1	<0.001
RVOT, mm (n = 158)	34.5 ± 7.8	32.2 ± 6.1	40.2 ± 8.6	<0.001
Oslo (n = 78)	35.1 ± 6.7	33.4 ± 5.4	39.1 ± 7.7	0.002
Utrecht (n = 80)	33.9 ± 8.8	31.1 ± 6.6	41.4 ± 9.5	<0.001
TAPSE, mm (n = 159)	20.7 ± 4.4	21.6 ± 3.6	18.4 ± 5.3	<0.001
Oslo (n = 80)	22.4 ± 4.1	23.2 ± 3.3	20.6 ± 5.2	0.03
Utrecht (n = 79)	19.0 ± 4.0	20.1 ± 3.2	15.8 ± 4.1	<0.001
CMR	(n=129)	(n=95)	(n=34)	
Oslo	(n=69)	(n=47)	(n=22)	
Utrecht	(n=60)	(n=48)	(n=12)	
RVEF, % (n = 99)	45.9 ± 13.1	48.6 ± 12.0	37.4 ± 13.0	<0.001
Oslo (n=41)	48.4 ± 11.6	50.1 ± 10.5	43.6 ± 12.9	0.07
Utrecht (n = 58)	44.2 ± 13.9	47.4 ± 12.7	30.1 ± 9.0	<0.001
RVEDVi, ml (n = 92)	109.8 ± 40.8	98.6 ± 31.0	147.7 ± 47.5	<0.001
Oslo (n = 38)	107.8 ± 39.6	94.7 ± 26.5	140.0 ± 48.7	0.01
Utrecht (n = 54)	111.2 ± 41.9	101.0 ± 33.5	156.3 ± 47.1	<0.001
LGE, n (%) (n = 124)	34 (27)	14 (15)	20 (59)	<0.001
Oslo (n = 64)	13 (20)	4 (10)	9 (41)	0.003
Utrecht (n = 60)	21 (34)	10 (20)	11 (92)	<0.001

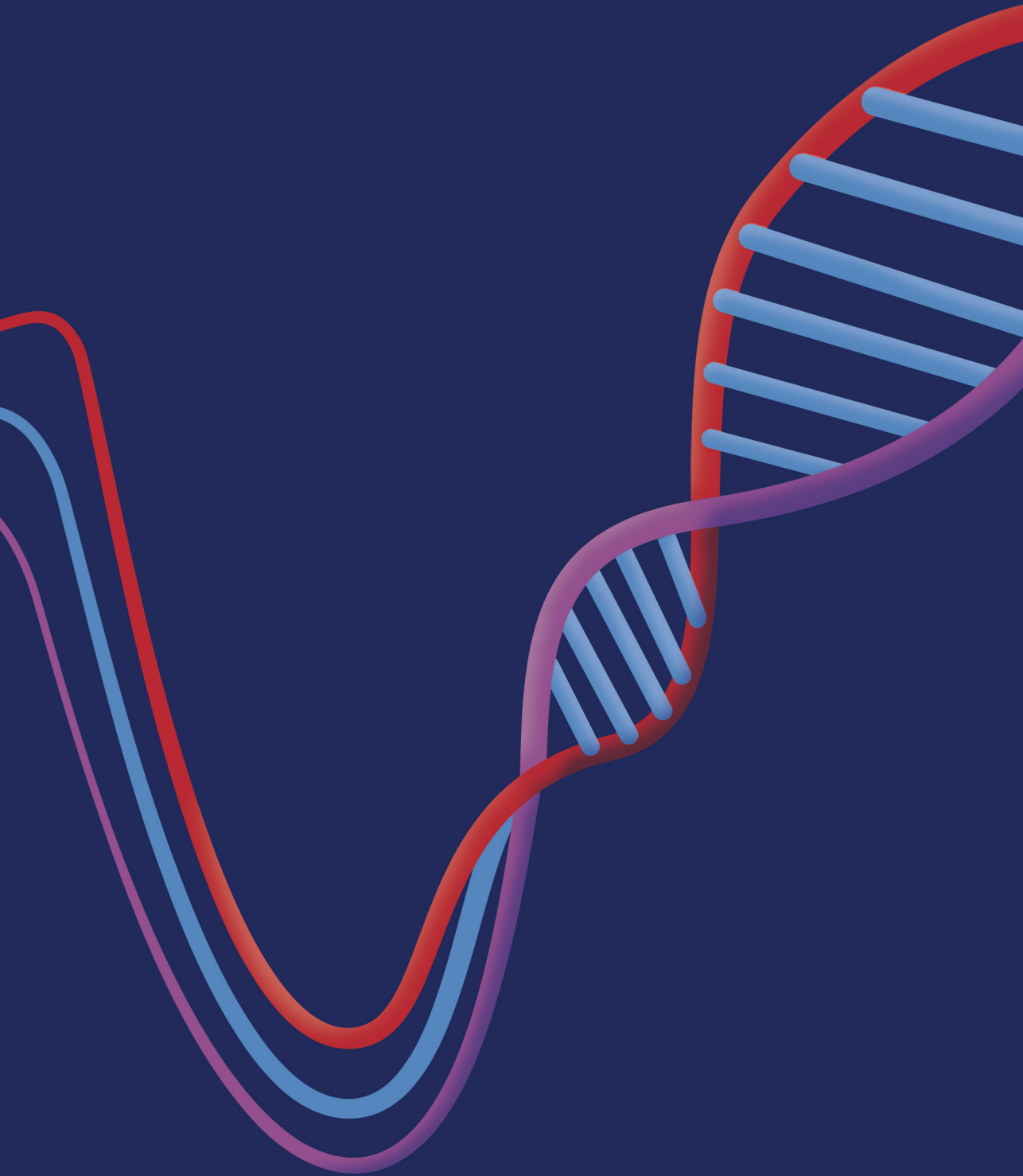
Values are, n (%), mean ± standard deviation. Abbreviations: CMR = cardiac magnetic resonance, EDVi = end diastolic volume indexed, EF = ejection fraction, FAC = fractional area change, GLS = global longitudinal strain, LGE = late gadolinium enhancement, LS = longitudinal strain, LV = left ventricle, MD = mechanical dispersion, RV = right ventricle, RVD = right ventricular diameter, RVOT = right ventricular outflow tract, TAPSE = tricuspid annular plane systolic excursion.

REFERENCES OF THE SUPPLEMENTARY MATERIAL

1. Mast TP, Teske AJ, Doevendans PA, Cramer MJ. Current and future role of echocardiography in arrhythmogenic right ventricular dysplasia/cardiomyopathy. *Cardiol J*. 2015;22(4):362-374.
2. Teske AJ, De Boeck BWL, Melman PG, Sieswerda GT, Doevendans PA, Cramer MJM. Echocardiographic quantification of myocardial function using tissue deformation imaging, a guide to image acquisition and analysis using tissue Doppler and speckle tracking. *Cardiovasc Ultrasound*. 2007;5:27.
3. Mast TP, Teske AJ, Te Riele AS, et al. Prolonged Electromechanical Interval Unmasks Arrhythmogenic Right Ventricular Dysplasia/Cardiomyopathy in the Subclinical Stage. *J Cardiovasc Electrophysiol*. 2016;27(3):303-314.
4. Mast TP, Teske AJ, Walmsley J, et al. Right Ventricular Imaging and Computer Simulation for Electromechanical Substrate Characterization in Arrhythmogenic Right Ventricular Cardiomyopathy. *J Am Coll Cardiol*. 2016;68(20):2185-2197.
5. Sarvari SI, Haugaa KH, Anfinson OG, et al. Right ventricular mechanical dispersion is related to malignant arrhythmias: A study of patients with arrhythmogenic right ventricular cardiomyopathy and subclinical right ventricular dysfunction. *Eur Heart J*. 2011;32(9):1089-1096.
6. Leren IS, Saberniak J, Haland TF, Edvardsen T, Haugaa KH. Combination of ECG and Echocardiography for Identification of Arrhythmic Events in Early ARVC. *JACC Cardiovasc Imaging*. 2017;10(5):503-513.
7. Edvardsen T, Haugaa KH. Imaging assessment of ventricular mechanics. *Heart*. 2011;97(16):1349-1356.

PART II.

**Characterizing the disease substrate underlying
deformation abnormalities**



CHAPTER 4

Electromechanical Substrate Characterization in Arrhythmogenic Cardiomyopathy Using Imaging-based Patient-specific Computer Simulations

Feddo P. Kirkels, Nick van Osta*, Aurore Lyon, Tijmen Koopsen, Tim A.M. van Loon, Maarten J. Cramer, Arco J. Teske, Tammo Delhaas, Joost Lumens*

** The first two authors contributed equally*

Europace. 2021;23(Suppl1):i153-i160.

ABSTRACT

Aims

Arrhythmogenic Cardiomyopathy (AC) is an inherited cardiac disease, characterized by life-threatening ventricular arrhythmias and progressive cardiac dysfunction. The aim of this study is to use computer simulations to non-invasively estimate the individual patient's myocardial tissue substrates underlying regional right ventricular (RV) deformation abnormalities in a cohort of AC mutation carriers.

Methods

In 68 AC mutation carriers and 20 control subjects, regional longitudinal deformation patterns of the RV free wall (RVfw), interventricular septum (IVS) and left ventricular free wall (LVfw) were obtained using speckle-tracking echocardiography. We developed and used a patient-specific parameter estimation protocol based on the multi-scale CircAdapt cardiovascular system model to create virtual AC subjects. Using the individual's deformation data as model input, this protocol automatically estimated regional RVfw and global IVS and LVfw tissue properties.

Results

The computational model was able to reproduce clinically measured regional deformation patterns for all subjects, with highly reproducible parameter estimations. Simulations revealed that regional RVfw heterogeneity of both contractile function and compliance were increased in subjects with clinically advanced disease compared to mutation carriers without clinically established disease ($17\pm 13\%$ vs. $8\pm 4\%$, $p=0.01$ and $18\pm 11\%$ vs. $10\pm 7\%$, $p<0.01$, respectively). No significant difference in activation delay was found.

Conclusion

Regional RV deformation abnormalities in AC mutation carriers were related to reduced regional contractile function and tissue compliance. In clinically advanced disease stages, a characteristic apex-to-base heterogeneity of tissue abnormalities was present in the majority of the subjects, with most pronounced disease in the basal region of the RVfw.

INTRODUCTION

Arrhythmogenic cardiomyopathy is an inherited heart muscle disorder characterized by fibrofatty replacement of primarily the right ventricular (RV) myocardium, which predisposes to ventricular arrhythmias and sudden cardiac death in young individuals.^{1,2} Variable disease expression is found in familial AC³, ranging from sudden cardiac death (SCD) in young individuals to a lifelong absence of any phenotype. To prevent apparently healthy AC mutation carriers from SCD, early detection of potentially pro-arrhythmic tissue substrates is important.

Using speckle-tracking echocardiography, our groups⁴ found distinct regional RV deformation abnormalities in AC mutation carriers. Predominantly the basal (subtricuspid) part of the RV free wall was affected, even in the absence of electrocardiographic or structural 2010 Task Force Criteria (TFC)⁵. Using computer simulations, it was hypothesized that these deformation abnormalities resulted from a decreased contractility and an increased stiffness within this segment. In a follow-up study, these RV deformation abnormalities were found to be associated with AC disease progression.⁶ Another approach, as reported by Sarvari et al.⁷ showed that RV mechanical dispersion, defined as the standard deviation in time-to-peak strain, is a marker for arrhythmic events in AC patients. The latter study demonstrate the prognostic value of RV longitudinal strain, while the disease substrates underlying the deformation abnormalities remain unknown. Together with the first study by Mast et al.⁴, these studies suggest that identification of the disease substrate causing RV deformation abnormalities could be used to better understand disease progression and support risk stratification. Patient-specific characterization of the electromechanical disease substrates in early-stage AC may lead to better arrhythmic risk stratification and ultimately to the identification of possible therapeutic targets, thereby enabling personalized medicine. Since invasive tissue characterization is accompanied by important risks, and is rarely performed, non-invasive ways of tissue characterization should be investigated.

The aim of this study is to non-invasively estimate the pathophysiological substrates underlying regional deformation abnormalities in the individual AC mutation carrier, using imaging-based patient-specific computer simulations. We use a parameter estimation protocol based on a previously established framework⁸ which simulates myocardial deformation to identify regional tissue properties.

METHODS

Patient Cohort

This study was performed on a previously reported consecutive cohort of pathogenic desmosomal mutation carriers, who were evaluated at the UMC Utrecht in the Netherlands between 2006 and 2015.⁴ During this period, 87 subjects carrying a pathogenic plakophilin-2 (PKP2), desmoglein-2 (DSG2), or desmoplakin (DSP) mutation were evaluated. Additionally, 20 healthy volunteers were included as control subjects. The study was approved by the local institutional ethics review board.

The echocardiographic protocol has been detailed elsewhere.⁹ Briefly, all echocardiographic data were obtained on a Vivid 7 or Vivid E9 ultrasound machine (GE Vingmed Ultrasound, Horten, Norway) using a broadband M3S transducer and were analysed for fulfilling 2010 TFC for structural abnormalities.⁵ Only exams during sinus rhythm were eligible for inclusion.

Conventional 2-, 3-, and 4-chamber views, as well as an RV-focused apical 4-chamber view, were used to visualize the RV lateral free wall (RVfw), interventricular septum (IVS), and LV free wall (LVfw). Cine-loops were stored for offline two-dimensional speckle tracking using EchoPAC v. 202 (GE Vingmed Ultrasound, Horten, Norway). A single observer, blinded to clinical information, obtained segmental longitudinal strain curves of the RVfw and the LV.

In this study, we focused on regional heterogeneity of RVfw tissue abnormalities because the RVfw is the most affected area in pathogenic desmosomal mutation carriers.¹⁰ Therefore, three segmental deformation patterns of the RVfw (i.e. apical, mid-ventricular and basal) were used to personalize the computational model (Figure 1). Additionally, two global deformation patterns of the LVfw and IVS were used to ensure realistic mechanical boundary conditions for the RVfw in terms of ventricular interaction. Global LVfw and IVS deformation patterns were obtained by averaging the 12 LVfw and 6 IVS segmental deformation curves, respectively, using the standardized 18-segment model.¹¹

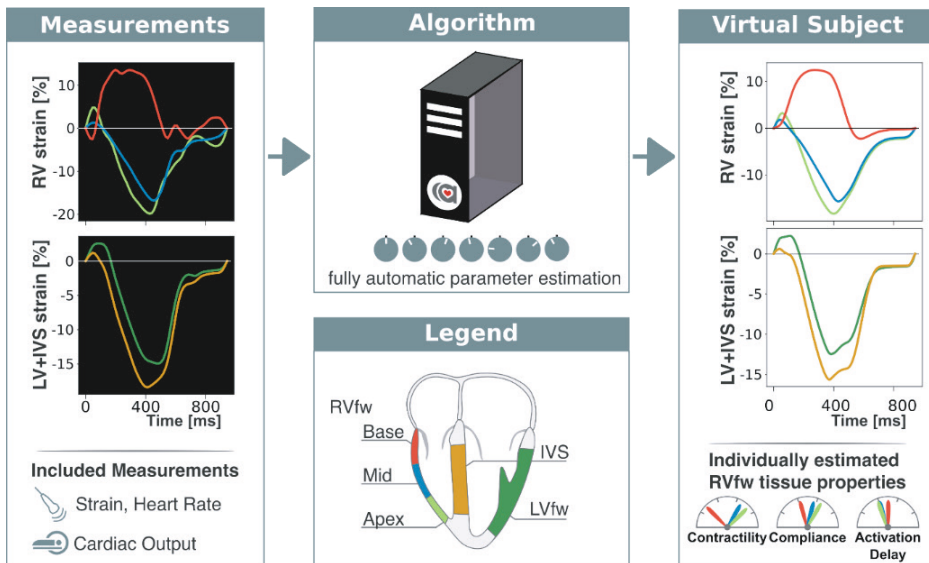


Figure 1. Methodology

Right ventricular (RV), interventricular septal (IVS), and left ventricular (LV) strain were obtained using speckle-tracking echocardiography, and cardiac output was obtained using cardiovascular magnetic resonance imaging (CMR). Using a fully automatic estimation protocol, virtual subjects reproducing the clinical measures were generated and local tissue properties were extracted.

Cardiac magnetic resonance imaging (CMR) was performed on a 1.5-T scanner (Achieva, Philips Healthcare, Best, the Netherlands), according to standard AC protocol¹², and included measurements of the RV end-diastolic volume, RV ejection fraction, and LV ejection fraction. LV stroke volume was used to personalize cardiac output (CO) in the computer simulations.

For further analysis, RV disease substrates were categorized by three different non-invasive imaging approaches, which have been published previously:

1. Following the revised 2010 TFC⁵, AC can be divided into three consecutive clinical stages: a) subclinical (concealed) stage with absence of any 2010 TFC, except for harbouring a pathogenic mutation; b) electrical stage, with only electrocardiographic (ECG) or Holter abnormalities; and c) structural stage, with structural abnormalities on non-invasive imaging, regardless of the history of ventricular arrhythmias or presence of ECG or Holter abnormalities.^{5,13}
2. Based on the pattern of basal RVfw deformation following the predefined criteria published by Mast et al.⁴ A Type-I pattern is defined as normal deformation; a Type-II pattern is characterized by delayed onset of shortening, reduced systolic peak strain and minor post-systolic shortening; a Type-III pattern is characterized by little or no systolic peak strain, predominantly systolic stretching and major post-systolic shortening.
3. Based on RV mechanical dispersion (RVMD), an index of segmental heterogeneity in contraction in the RVfw and IVS. RVMD was calculated on 6 segments of the RV, including the IVS, and defined as the standard deviation of the segmental time intervals from onset Q/R on the surface ECG to peak negative strain.⁷ A previously established cut-off value of 30ms¹⁴ was used in this study to define a group with low and high RVMD.

Computer Simulations

Regional RV, IVS, and LV myocardial deformation were simulated using the CircAdapt model¹⁵, which is a closed-loop lumped parameter computer model of the human heart and circulation. It enables simulation of cardiac hemodynamics and regional wall mechanics, using a phenomenological model describing active and passive myofibre mechanics.¹⁶ Ventricular interactions are modelled using the TriSeg model using the concept of conservation of energy.¹⁷ LVfw and IVS were modelled as a single segment representing the mechanics of the entire wall. Three RVfw segments representing the apical, mid-ventricular, and basal regions were modelled using the previously validated MultiPatch model.¹⁶

Patient-Specific Simulation Protocol

Computer simulations were personalized by automatically tuning model parameters to optimize the modelled myofibre strain to measured longitudinal strain (*Figure 1*). A parameter subset with 21 parameters essential for modelling regional RVfw, IVS, and LVfw deformation in AC mutation carriers was previously identified⁸ and shown in *Supplementary Table 1*. CO and heart rate (HR) were direct input parameters of the model and thereby set from the measurements. The former was obtained from CMR data, while the latter was obtained from the RV focused 4-chamber view. The other 19 parameters describe the size of the RVfw, IVS, and LVfw (3 model parameters), myocardial twitch duration and thus relative systolic duration (1 parameter), and three regional tissue properties per myocardial segment being contractility, compliance, and activation delay (i.e. 15 model parameters in total).

Objective function

The objective function describes the agreement between modelled and measured strain. Measured strain is by definition relative to the stretch on $t = t_0$, which is defined as the onset of the QRS complex, obtained from ECG. This cannot be modelled in CircAdapt. Therefore,

modelled segmental strain is shifted in time to best match strain around $t = t_0$. Modelled strain is obtained from the modelled sarcomere length l_s , using

$$\epsilon_{model,seg} = \left(\frac{l_{s,seg}}{l_{s,seg}|_{t=t_0}} - 1 \right) \cdot 100\% \quad (1)$$

Using the objective function, goodness of the simulation is quantified relative to the measurements. It is unknown which strain indices identify the strain. Therefore, the used objective function is based on the full strain curve. To reduce the effect of drift, and reduce the effect of the atria on the estimate, only strain is used from start of QRS complex up to 50% of relaxation. The modelled onset of shortening is matched with the measured onset of shortening. The quadratic difference of each segment is defined as

$$A_{seg}^2 = \frac{\int_{t_{onsetQRS}}^{t_{50relax}} \left(\epsilon_{model,seg} - \epsilon_{meas,seg} \right)^2 dt}{t_{50relax} - t_{onsetQRS}} \quad (2)$$

The used segments are the apical, mid, and basal segment of the RVfw, and the LVfw and IVS strain.

To prevent the parameter estimation protocol from exploring non-physiological area in the input space, a maximum mean left atrial pressure is added as a penalty function. There are signs of increased atrial volumes in this cohort¹⁸, but no invasive pressure measurements are available. Therefore, we cannot rule out increased diastolic pressures. No pulmonary hypertension was observed in this cohort, so it can be assumed that the mean left atrial pressure (mLAP) not exceeds 15 mmHg.¹⁹ To constrain our simulation results to physiological values without having too much effect on the estimation protocol, we use a threshold mLAP of $p_{thres} = 25 \text{ mmHg}$. This is implemented as a penalty function

$$e_{pressure} = \begin{cases} \bar{p}_{la} - p_{thres} & \text{if } \bar{p}_{la} > p_{thres} \\ 0 & \text{else} \end{cases} \quad (3)$$

The final objective function results in

$$e^2 = \frac{1}{3} \cdot \left(1/3 \frac{A_{RVapex}^2}{\alpha^2} + 1/3 \frac{A_{RVmid}^2}{\alpha^2} + 1/3 \frac{A_{RVbase}^2}{\alpha^2} + \frac{A_{IVS}^2}{\alpha^2} + \frac{A_{LVfw}^2}{\alpha^2} \right) + \frac{e_{pressure}^2}{\beta^2} \quad (4)$$

With $\alpha = 1\%$ and $\beta = 1 \text{ mmHg}$

Parameter Estimation protocol

Parameters were individually estimated using a parameter estimation framework previously described in more detail.⁸ This framework estimates model parameters using the clinical data as described above and results in a virtual subject that reproduces the clinical data. In brief, the parameter estimation framework consisted of two steps. First, with CO and HR set to the measured values, 5000 quasi-random Monte Carlo simulations were performed from which the best 60 simulations were used as initial candidate solutions. Second, these candidate

simulations were optimized using the stochastic multi-swarm particle swarm optimization (MSPSO).^{20,21} MSPSO is an evolutionary algorithm, where a population of candidate solutions moves through the input space driven by their history and the history of a changing subpopulation. Eventually, this parameter estimation protocol results in a virtual patient, from which regional tissue properties can be extracted.

Local tissue properties

RVfw contractility, compliance, and activation delay were extracted from the resulting virtual patient simulations and the heterogeneity of these tissue properties was investigated. Due to the nonlinearity, non-monotonicity, and non-additivity of the lumped system, the individual estimated parameters were not interpreted directly, but local tissue properties were derived from the simulated time signals of myofibre stress and strain. As the RVfw is typically most affected in desmosomal mutation carriers¹, we focus on the heterogeneity in regional RVfw tissue properties. To limit the degrees of freedom in the model, parameters in the LV and IVS were not estimated on a segmented level, but in a single segment representing the entire wall to include ventricular interaction.

Regional myocardial contractility, compliance, and activation delay were used to quantify regional mechanical tissue properties. In brief, segmental contractility was defined as the maximum rate of active stress rise $\max \frac{d\sigma_{act}}{dt}$, which can be seen as the equivalent of the maximum rate of ventricular systolic pressure rise (dp/dt_{max}) on a local tissue level. Segmental wall compliance was defined as the inverse slope of the end-diastolic passive myofibre stress ($d\sigma_{pas}$) and strain (ϵ) relationship, obtained using a preload manipulation. This is the regional equivalent of the slope of the global end-diastolic pressure-volume relation. Furthermore, regional activation delay was defined as the time delay of onset active stress development relative to the first activated segment. Their equations are given by

$$\text{Contractility} = \max \frac{d\sigma_{act}}{dt} \quad (5)$$

$$\text{Compliance} = \frac{d\epsilon}{d\sigma_{pas}} \quad (6)$$

$$t_{con} = t \Big|_{\max \frac{d\sigma_{act}}{dt}} \quad (7)$$

$$\text{Activation Delay} = t_{con} - \frac{\sigma_{act} \Big|_{t_{con}}}{\text{Contractility}} - t_{RA \text{ activation}} \quad (8)$$

Reproducibility

To determine reproducibility, a separate validation set was used. Two separate observers blinded to clinical data performed deformation analysis twice in nine subjects with a pathogenic desmosomal mutation, resulting in four different deformation datasets per patient.

Each dataset was used three times as input for the parameter estimation framework described above. Inter- and intra-observer agreement, as well as the uniqueness of parameter estimation were determined using the intraclass correlation coefficient (ICC).²² To calculate this coefficient, the average estimation of patient i was considered the true estimation (α_i) and the errors origin from inter-observer variability $\epsilon_{o,i}$, intra-observer variability $\epsilon_{m,i}$, and inter-simulation variability $\epsilon_{e,i}$.

$$Y_{o,m,e,i} = \alpha_i + \epsilon_{o,i} + \epsilon_{m,i} + \epsilon_{e,i} \quad (9)$$

The interclass correlation coefficient for each of the error origins is

$$ICC_{type} = \frac{\sigma_{\alpha}^2}{\sigma_{\alpha}^2 + \sigma_{\epsilon_{type}}^2} \quad (10)$$

Statistical analysis and Computational Setup

Continuous data were presented as mean \pm SD. Normal distribution was tested using the Shapiro-Wilk test. Comparison between subgroups of continuous variables was done using a one-way analysis of variance, t-test, Kruskal-Wallis, or Mann-Whitney U test as appropriate. Bonferroni correction was used to adjust for multiple comparisons. All statistical analyses were performed in Python 3.6.4 using the packages *SciPy* (modified BSD License) and *statsmodels* (modified BSD License).

The CircAdapt model was coded in C++ and compiled using MSVC 14.1. All other code was written in Python and interpreted with Python 3.6.4. The parameter estimation protocol was written for single thread computation. The estimation of subjects ran parallel on Windows 10 system (AMD Ryzen Threadripper 3970X 32-Cores 4.5GHz and 128GB RAM).

RESULTS

From the 87 AC mutation carriers who were evaluated, 3 subjects were excluded due to inadequate echocardiographic imaging quality and 16 were excluded due to missing CMR data. All remaining exams were obtained during sinus rhythm. The 68 AC mutation carriers included in this study (18 probands and 50 family members) had a mean age of 39 ± 17 years and 41 (60%) were female. Among the different pathogenic mutations, PKP2 was most common in this cohort (90%). A total of 20 control subjects (9 (45%) females, mean age 28 ± 6 years) were also included in the study. Using the 2010 TFC, 18 (26%) mutation carriers were classified in the subclinical stage, 15 (22%) in the electrical stage, and 35 (51%) in the structural stage. The median time between echocardiography and CMR was 26 days (interquartile range (-7, 398 days)). (Table 1)

Table 1. Clinical characteristics

	Controls (n = 20)	Subclinical Stage (n = 18)	Electrical Stage (n = 15)	Structural Stage (n = 35)	
Age, yrs	28 ± 6	27±14	40±17 [§]	44±16 [^]	p<0.001
Female	9 (45%)	11 (61%)	12 (80%)	18 (51%)	
BSA, m ²	1.87±0.17	1.80±0.21	1.84±0.17	1.91±0.22	p=0.280
Proband	0 (0%)	0 (0%)	0 (0%)	18 (53%)	
AC diagnosis	0 (0%)	0 (0%)	5 (33%)	35 (100%)	
2010 TFC (major or minor)					
Structural criteria		0 (0%)	0 (0%)	35 (100%)	
Depolarization criteria		1 (6%)	12 (80%)	17 (49%)	
Repolarization criteria		1 (6%)	3 (20%)	20 (57%)	
Arrhythmia criteria		0 (0%)	5 (33%)	32 (91%)	
Mutations					
PKP2 mutation		15 (83%)	14 (93%)	32 (91%)	
DSG2 mutation		3 (17%)	1 (7%)	2 (6%)	
DSP mutation		0 (0%)	0 (0%)	1 (3%)	
CMR					
CO, L/min/m ²	3.7±0.6	3.3±0.5	3.5±0.6	3.2±0.8	p=0.041
RV-EDVi, mL/m ²	108±17	87±17	94±12	132±41*	p<0.01
LV-EDVi, mL/m ²	98±14	85±13	93±14	91.8±15	p=0.063
RVEF, %	54±6	56±8	51±6	36±11*	p<0.001
LVEF, %	61±7	58±4	57±7	56±9	p=0.182
Presence of LGE	0 (0%)	0 (0%)	0 (0%)	20 (57%)	
Echocardiography					
HR	62±10	67±16	63±11	58±9	p=0.088
LV-GLS, %	-21.1±1.7	-20.0±1.7	-19.0±3.0	-17.8±3.3*	p<0.001
LVEF, %	60.6±6.9	58.4±4.3	56.6±6.8	55.8±9.2	p=0.159
RV-GLS, %	-27.6±4.0	-25.4±3.6	-21.7±4.7 [§]	-15.0±5.6*	p<0.001
RV basal deformation pattern					
Type-I	20 (100%)	12 (67%)	4 (27%)	2 (6%)	
Type-II	0 (0%)	6 (33%)	8 (53%)	10 (29%)	
Type-III	0 (0%)	0 (0%)	3 (20%)	23 (66%)	
RVMD, ms	-	16.4±7.5 [^]	32.2±16.1	50±27	p<0.01

AC: Arrhythmogenic Cardiomyopathy; TFC: Task Force Criteria; PKP2: plakophilin-2; DSG2: desmoglein-2; DSP: desmoplakin; CMR: cardiovascular magnetic resonance imaging; CO: cardiac output; RV: right ventricle; LV: left ventricle; EDVi: end diastolic volume indexed for BSA; RVEF: right ventricular ejection fraction; LVEF: left ventricular ejection fraction; LGE: late gadolinium enhancement; HR: Heart rate; GLS: global longitudinal strain; RVMD: right ventricular mechanical dispersion; *: p<0.05 structural stage versus all other groups (Bonferroni correction) ; ^: p<0.05 structural stage versus control group and subclinical stage; §: p<0.05 electrical stage versus control

Typical examples of measured and simulated ventricular deformation curves in a control subject and subjects in the subclinical, electrical, and structural AC disease stages are shown in *Figure 2*. Most healthy controls ($n=20$, 100%) and subclinical stage subjects ($n=12$, 67%) had a Type-I deformation pattern and thus showed relatively homogeneous deformation patterns in the three RVfw segments. However, 6 (33%) subclinical subjects had an abnormal Type-II deformation pattern in the RVfw basal segment. Most subjects in the electrical stage showed heterogeneous deformation patterns with predominantly basal abnormalities (Type-II: $n=8$ (53%) and Type-III: $n=3$ (20%)), which were even more severe in the structural stage subjects (Type-II: $n=10$ (29%) and Type-III: $n=23$ (66%)).

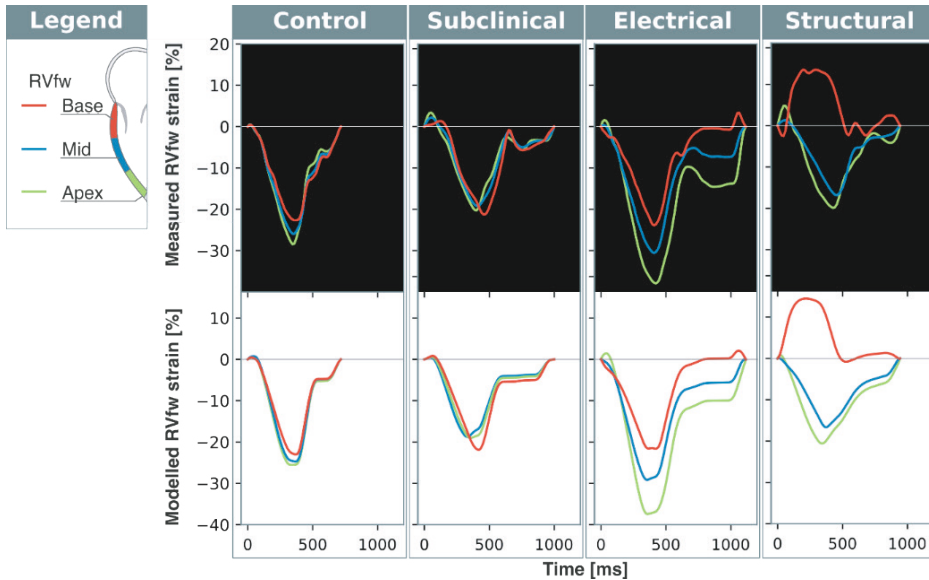


Figure 2. Typical regional right ventricular free wall (RVfw) strain patterns

Control subjects and most subjects in subclinical stage showed homogeneous strain patterns. Most subjects in the electrical and structural stage showed abnormal heterogeneous strain patterns.

Contractility

Overall, heterogeneity in regional RVfw contractility was higher in the electrical and structural stage groups compared to the subclinical stage and control groups (control: $9.98 \pm 4.27\%$; subclinical: $7.57 \pm 4.47\%$; electrical: $17.23 \pm 15.92\%$; structural: $16.94 \pm 13.28\%$, $p=0.011$). In general, the basal contractility was lower compared to the apical contractility (*Figure 3*). A few individuals ($n=9$, 13%), however, were found to have lower apical than basal contractility. No significant difference was found in average RVfw contractility (control: 363 ± 175 kPa/s; subclinical: 373 ± 131 kPa/s; electrical: 421 ± 167 kPa/s; structural: 442 ± 174 kPa/s) ($p=0.470$).

Compliance

Heterogeneity in regional RVfw compliance was increased in the electrical and structural stage groups compared to the subclinical stage and control groups (control: $9.16 \pm 4.84\%$; subclinical: $10.46 \pm 7.11\%$; electrical: $12.49 \pm 9.63\%$; structural: $18.45 \pm 11.00\%$, $p=0.002$). On average,

compliance was lower in the basal segment compared to the apical segment (Figure 3). Average RVfw compliance was not significantly different between the groups (control: 500 ± 325 %/kPa; subclinical: 551 ± 561 %/kPa; electrical: 1002 ± 723 %/kPa; structural: 742 ± 595 %/kPa, $p=0.094$).

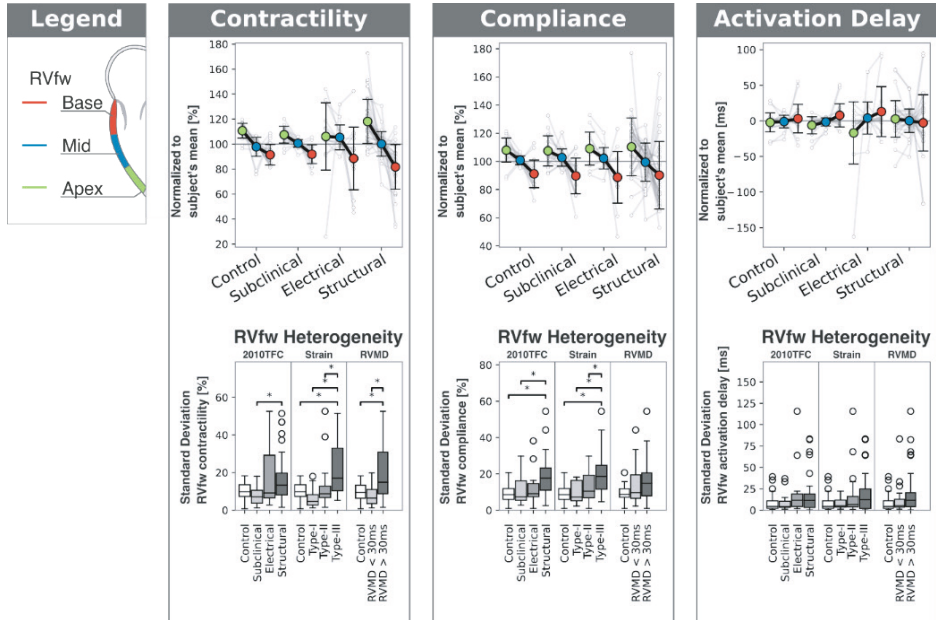


Figure 3. Estimated Tissue Properties

In the top row, RV regional estimations of contractility, compliance, and activation delay are shown relative to the mean value. In the bottom row, the standard deviation of these three properties is shown in a boxplot, characterized by 2010 TFC (subclinical, electrical, structural), strain morphology (Type-I, Type-II, and Type-III), and RV mechanical dispersion (RVMD). * indicates a significant difference with $p < 0.05$

Activation delay

No significant difference was found in heterogeneity of regional RVfw activation delay (control: 10 ± 11 ms; subclinical: 8.9 ± 10.1 ms; electrical: 21 ± 30 ms; structural: 18 ± 22 ms, $p=0.267$). However, the electrical and structural stage groups contained more individuals with a relatively late activated basal segment than the subclinical stage and control groups.

Basal deformation patterns

The simulations revealed that heterogeneity in RVfw contractility was increased in compared to the Type-I and control groups (control: $9.98 \pm 4.27\%$; Type-I: $6.52 \pm 5.20\%$; Type-II: $12.19 \pm 11.25\%$; Type-III: $21.81 \pm 14.09\%$, $p < 0.001$). Also, the heterogeneity in compliance was increased in the groups with Type-II and Type-III RV basal deformation patterns compared to the Type-I and control groups (control: $9.16 \pm 4.84\%$; Type-I: $9.43 \pm 5.78\%$; Type-II: $13.00 \pm 8.46\%$; Type-III: $20.63 \pm 11.74\%$, $p < 0.001$). No significant difference was found in activation delay (control: 10.0 ± 11.1 ms; Type-I: 8.4 ± 6.3 ms; Type-II: 16.6 ± 25.5 ms; Type-III: 21.3 ± 24.7 ms, $p=0.472$).

Right ventricular mechanical dispersion

Increased RVMD in pathogenic desmosomal mutation carriers was only related to increased heterogeneity in contractility ($20.0 \pm 14.7\%$) compared to the group with normal RVMD ($7.70 \pm 4.99\%$) ($p < 0.001$). Regional heterogeneities of both compliance and activation delay were not significantly different between subjects with low and high RVMD (compliance: $16.0 \pm 10.5\%$ vs $13.8 \pm 10.2\%$, $p = 0.054$; activation delay: $20.6 \pm 26.0\text{ms}$ vs $11.1 \pm 15.6\text{ms}$, $p = 0.195$).

Parameter estimation

The estimated RV tissue properties were highly reproducible, with a minimum inter- and intra-observer ICC of 0.91 and 0.86, respectively. Reproducibility of the simulations was sufficient, with a minimum ICC of 0.76. In all simulations of the same subject, the trend in local RVfw heterogeneity was similar. *Supplemental Table 2* shows the ICC of the estimated model parameters and *Supplemental Table 3* shows the ICC of the individual estimated tissue properties.

The simulations ran on average in 25 ± 10 hours per patient. The duration of the simulations depended on the heart rate, the quality of the initial subset, and the number of beats needed to find a hemodynamic stable simulation for each random state. The average dimensional error between modelled and measured strain was 0.84 ± 0.35 .

DISCUSSION

In this study, patient-specific simulations were successfully used to estimate regional RVfw tissue properties from echocardiographic deformation imaging data in 68 subjects with a pathogenic AC mutation and 20 control subjects. Regional heterogeneities of contractility and compliance in the RV free wall were largest in subjects in the structural disease stage. Our patient-specific simulations suggested that structural abnormalities according to the 2010 TFC were associated with an increased heterogeneity in RVfw myocardial tissue contractility and compliance. The most advanced disease substrates were found predominantly in the RVfw basal segment. To our knowledge, this is the first time that regional ventricular tissue properties are quantified using patient-specific simulations based on non-invasively measured longitudinal strain patterns. This method reveals potentially important information about myocardial disease substrates and thereby paves the way for personalized medicine.

In a previous study, we showed that desmosomal mutation carriers with more advanced AC disease stages have the most abnormal RV basal deformation pattern.⁴ In the same study, using computer simulations it was concluded that this abnormal mechanical behaviour of the RV cannot be explained by an electromechanical activation delay alone. Non-personalized simulations representing subgroups of AC mutation carriers showed that at least some degree of local mechanical dysfunction was needed to reproduce the measured RV deformation abnormalities. A recently published sensitivity analysis confirmed that model parameters related to both activation delay and mechanical dysfunction are essential to reproduce myocardial deformation using the CircAdapt model.⁸ The current study extends this previous work by estimating patient-specific myocardial substrates in all three RVfw segments and by including the LV mechanics for a more realistic approach of the patient's hemodynamics. These patient-specific simulations confirmed hypothesis that abnormal deformation patterns

are related to increased regional heterogeneity in contractility and compliance without a heterogeneity in activation delay.⁴

AC mutation carriers classified with structural abnormalities according to the 2010 TFC, being wall motion abnormalities such as akinesia, dyskinesia, or aneurysm in combination with RV dilatation or impaired RV systolic function measured by either CMR or echocardiography.⁵ These structural abnormalities result from fibrofatty replacements of the RV myocardium, which affects regional wall motion and eventually global RV systolic function.² Also our computer simulations revealed the largest heterogeneity of RVfw tissue properties in the patients with structural stage disease, with the basal region of the RVfw being most affected by the disease. The few structural stage subjects with a relatively low heterogeneity of RV tissue properties showed highly impaired RV deformation with decreased contractility and compliance in all three segments, suggesting highly advanced AC disease.

Our patient-specific simulations suggested that the RV apex-to-base heterogeneity of mechanical behaviour in the more advanced AC disease stages is mostly due to decreased basal contractility and compliance. Several potential causes for AC-related changes in active and passive myocardial tissue properties have been identified in clinical and pre-clinical studies. One is the fibrofatty replacement of the myocardium², which results in loss of contractile function and a change in passive tissue behaviour. Besides, Cerrone et al. found altered calcium transients in mice with a loss of PKP2 expression, including an increased calcium transient with an increased time-to-peak and a slower decay²³, suggesting a change in contractile function. To identify the exact (sub)cellular mechanisms underlying the regional RV deformation abnormalities in AC subjects beyond changes of tissue contractility and compliance, a more complex model of the myocardial electromechanics is needed.

In previous clinical studies, RVMD was associated with arrhythmic outcome.⁷ In our modelling study, a higher RVMD was associated with an increased heterogeneity of contractility in the RVfw, but not with myocardial compliance. These contractile abnormalities could reflect calcium handling abnormalities, which form a possible pro-arrhythmic substrate. Interestingly, using the classification defined by Mast et al.⁴, an abnormal Type-III deformation pattern was reproduced by both abnormal contractility and abnormal compliance. Where RVMD is based only on timing of the longitudinal strain, the pattern classification is based on information of both timing and amplitude. Our computer simulations suggest that both classifications can detect a different kind of tissue substrate.

An RVfw apex-to-base heterogeneity was already present in the deformation measurements of healthy controls, resulting in heterogeneity in estimated tissue properties. Some level of 'physiological' heterogeneity in deformation is to be expected, since regional differences of ventricular tissue properties, such as activation delay²⁴, action potential morphology²⁵, and wall thickness²⁶, also exist in healthy hearts. Because the control group and subclinical group have a similar heterogeneity in tissue properties, it can be assumed that the observed heterogeneity in regional RV tissue properties is not abnormal.

Study Limitations

Estimations are based on the average CO obtained from CMR and on regional LV and RV strain obtained from speckle tracking echocardiography. CMR volumes were used because they provided the most reliable non-invasive estimation of CO and ventricular volumes. Because the CMR and the echocardiographic examination cannot be performed simultaneously, there is a potential mismatch between the two measurements. This mismatch might result in

global under- or overestimation of ventricular tissue properties but is not expected to have a significant effect on the heterogeneity in RVfw tissue properties.

The deformation measurements were obtained from four different heartbeats. We did not correct for any measurement errors, such as timing errors between the four echo views, beat-to-beat variability, or respiration. Future studies could investigate how to design an objective function using strain indices or other measurements, such as valve timings, blood flow velocity or ejection fraction, to develop a more efficient fitting algorithm with an objective function invariant of measurement uncertainties.

Future Work

A longitudinal study, in which follow-up data is included, should be performed to reveal whether and how this disease substrate progresses in individuals, and whether any kind of disease evolution could be used for prediction of arrhythmic outcome in a clinical setting.

The majority of this retrospective study cohort consisted of PKP2 mutation carriers. Future prospective verification studies are needed to confirm our findings and to determine whether our results can be extrapolated to AC patients with a different genetic background. The CircAdapt model is not limited to modelling AC disease substrates, so future work could also explore to which extent this framework is applicable to identify disease substrates in other cardiac pathologies.

CONCLUSION

We presented a patient-specific modelling approach and showed its ability to reproduce regional ventricular deformation patterns and to estimate the underlying tissue properties in AC mutation carriers. Patient-specific simulations revealed that regional RV deformation abnormalities were related to reduced contractile function and tissue compliance. In most subjects, a characteristic apex-to-base heterogeneity of tissue abnormalities was present, whereby the basal region of the RVfw was most affected. Tissue abnormalities were most pronounced in the subjects with a clinically more advanced disease stage. Future studies should investigate whether simulation-based characterization of patient-specific disease substrates can be used for personalised prediction of AC disease progression or arrhythmic events.

REFERENCES

1. Thiene G, Nava A, Corrado D, Rossi L, Pennelli N. Right Ventricular Cardiomyopathy and Sudden Death in Young People. *N Engl J Med*. 1988;318(3):129-133.
2. Basso C, Corrado D, Marcus FI. Arrhythmogenic right ventricular cardiomyopathy. *Lancet*. 2009;(373):1289-300.
3. Groeneweg JA, Bhonsale A, James CA, et al. Clinical Presentation, Long-Term Follow-Up, and Outcomes of 1001 Arrhythmogenic Right Ventricular Dysplasia/Cardiomyopathy Patients and Family Members. *Circ Cardiovasc Genet*. 2015;8(3):437-46.
4. Mast TP, Teske AJ, Walmsley J, et al. Right Ventricular Imaging and Computer Simulation for Electromechanical Substrate Characterization in Arrhythmogenic Right Ventricular Cardiomyopathy. *J Am Coll Cardiol*. 2016;68(20):2185-97.
5. Marcus FI, McKenna WJ, Sherrill D, et al. Diagnosis of arrhythmogenic right ventricular cardiomyopathy/Dysplasia: Proposed modification of the task force criteria. *Circulation*. 2010;121(13):1533-41.
6. Mast TP, Taha K, Cramer MJ, et al. The Prognostic Value of Right Ventricular Deformation Imaging in Early Arrhythmogenic Right Ventricular Cardiomyopathy. *JACC Cardiovasc Imaging*. 2019;12(3):446-55.
7. Sarvari SI, Haugaa KH, Anfinson OG, et al. Right ventricular mechanical dispersion is related to malignant arrhythmias: A study of patients with arrhythmogenic right ventricular cardiomyopathy and subclinical right ventricular dysfunction. *Eur Heart J*. 2011;32(9):1089-96.
8. Van Osta N, Lyon A, Kirkels FP, et al. Parameter subset reduction for patient-specific modelling of arrhythmogenic cardiomyopathy-related mutation carriers in the CircAdapt model. *Philosophical Transactions of the Royal Society A*. 2020;378(2173):20190347.
9. Teske AJ, De Boeck BW, Melman PG, Sieswerda GT, Doevendans PA, Cramer MJ. Echocardiographic Quantification of Myocardial Function using Tissue Deformation Imaging, a Guide to Image Acquisition and Analysis using Tissue Doppler and Speckle Tracking. *Cardiovasc Ultrasound*. 2007;5(27).
10. Te Riele ASJM, James CA, Philips B, et al. Mutation-positive arrhythmogenic right ventricular dysplasia/cardiomyopathy: The triangle of dysplasia displaced. *J Cardiovasc Electrophysiol*. 2013;24(12):1311-20.
11. Voigt JU, Pedrizzetti G, Lysyansky P, et al. Definitions for a common standard for 2D speckle tracking echocardiography: consensus document of the EACVI/ASE/Industry Task Force to standardize deformation imaging. *Eur Heart J Cardiovasc Imaging*. 2015;16(1):1-11.
12. Dalal D, Tandri H, Judge DP, et al. Morphologic Variants of Familial Arrhythmogenic Right Ventricular Dysplasia/Cardiomyopathy. A Genetics-Magnetic Resonance Imaging Correlation Study. *J Am Coll Cardiol*. 2009;53(15):1289-99.
13. Te Riele ASJM, James CA, Rastegar N, et al. Yield of serial evaluation in at-risk family members of patients with ARVD/C. *J Am Coll Cardiol*. 2014;64(3):293-301.
14. Haugaa KH, Basso C, Badano LP, et al. Comprehensive multi-modality imaging approach in arrhythmogenic cardiomyopathy - an expert consensus document of the European Association of Cardiovascular Imaging. *Eur Heart J Cardiovasc Imaging*. 2017;18(3):237-53.
15. Arts T, Delhaas T, Bovendeerd P, Verbeek X, Prinzen F. Adaptation to Mechanical Load Determines Shape and Properties of Heart and Circulation: the CircAdapt Model. *Am J Physiol Heart Circ Physiol*. 2005;288:1943-54.

16. Walmsley J, Arts T, Derval N, et al. Fast Simulation of Mechanical Heterogeneity in the Electrically Asynchronous Heart Using the MultiPatch Module. *PLoS Comput Biol*. 2015;11:1–23.
17. Lumens J, Delhaas T, Kirn B, Arts T. Three-wall segment (TriSeg) model describing mechanics and hemodynamics of ventricular interaction. *Ann Biomed Eng*. 2009;37(11):2234–55.
18. Zghaib T, Bourfiss M, van der Heijden JF, et al. Atrial Dysfunction in Arrhythmogenic Right Ventricular Cardiomyopathy. *Circ Cardiovasc Imaging*. 2018;11(9):e007344.
19. Galiè N, Humbert M, Vachiery JL, et al. 2015 ESC/ERS Guidelines for the diagnosis and treatment of pulmonary hypertension. *Eur Heart J*. 2016 Jan 1;37(1):67–119.
20. Kennedy J, Eberhart R. Particle swarm optimization. In: *Proceedings of ICNN'95 - International Conference on Neural Networks*. IEEE; p. 1942–8.
21. Liang JJ, Suganthan PN. Dynamic multi-swarm particle swarm optimizer. In: *Proceedings 2005 IEEE Swarm Intelligence Symposium, 2005 SIS 2005*. IEEE; p. 124–9.
22. Koo TK, Li MY. A Guideline of Selecting and Reporting Intraclass Correlation Coefficients for Reliability Research. *J Chiropr Med*. 2016;15(2):155–63.
23. Cerrone M, Montnach J, Lin X, et al. Plakophilin-2 is required for transcription of genes that control calcium cycling and cardiac rhythm. *Nat Commun*. 2017;8(1):106.
24. Durrer D, Van Dam RTH, Freud GE, Janse MJ, Meijler FL, Arzbaecher RC. Total Excitation of the Isolated Human Heart. *Circulation*. 1970;41(6):899–912.
25. Antzelevitch C, Fish J. Electrical heterogeneity within the ventricular wall. *Basic Res Cardiol*. 2001;96:517–27.
26. Kawel-Boehm N, Maceira A, Valsangiacomo-Buechel ER, et al. Normal values for cardiovascular magnetic resonance in adults and children. *J Cardiovasc Magnetic Resonance*. 2015;17(1):29–52.

SUPPLEMENTARY MATERIAL

Supplemental Table 1. Parameter description

<i>Model parameter</i>	<i>Description</i>	<i>Location</i>	<i>Monte Carlo</i>	<i>PSO</i>
<i>SfAct Lv (kPa)</i>	Linear scaling factor for active stress	LV	(90,150)	(0,300)
<i>SfAct Sv (kPa)</i>		IVS	(90,150)	(0,300)
<i>SfAct RvApex (kPa)</i>		RVfw apex	(30,150)	(0,300)
<i>SfAct RvMid (kPa)</i>		RVfw mid	(30,150)	(0,300)
<i>SfAct RvBase (kPa)</i>		RVfw base	(30,150)	(0,300)
<i>k1 Lv (-)</i>	Non-linear scaling factor for passive stress	LV	(5,15)	(1,100)
<i>k1 Sv (-)</i>		IVS	(5,15)	(1,100)
<i>k1 RvApex (-)</i>		RVfw apex	(5,20)	(1,100)
<i>k1 RvMid (-)</i>		RVfw mid	(5,20)	(1,100)
<i>k1 RvBase (-)</i>		RVfw base	(5,20)	(1,100)
<i>dT Lv (ms)</i>	Activation delay of segment relative to estimated AV-delay	LV	(-25,25)	(-150,150)
<i>dT Sv (ms)</i>		IVS	(-25,25)	(-150,150)
<i>dT RvApex (ms)</i>		RVfw apex	(-25,50)	(-150,150)
<i>dT RvMid (ms)</i>		RVfw mid	(-25,50)	(-150,150)
<i>dT RvBase (ms)</i>		RVfw base	(-25,50)	(-150,150)
<i>AmRef Lv (cm²)</i>	Segment area at sarcomere length $L_s = 2\mu m$	LVfw	(0.8,1.2)*98	(0.5,2)*98
<i>AmRef Sv (cm²)</i>		IVS	(0.8,1.2)*49	(0.5,2)*49
<i>AmRef Rv (cm²)</i>		RVfw	(0.8,1.2)*129	(0.5,2)*129
<i>TimeFac (-)</i>	Scaling factor for myocardial twitch duration		(0.8,1.2)	(0.1,2)

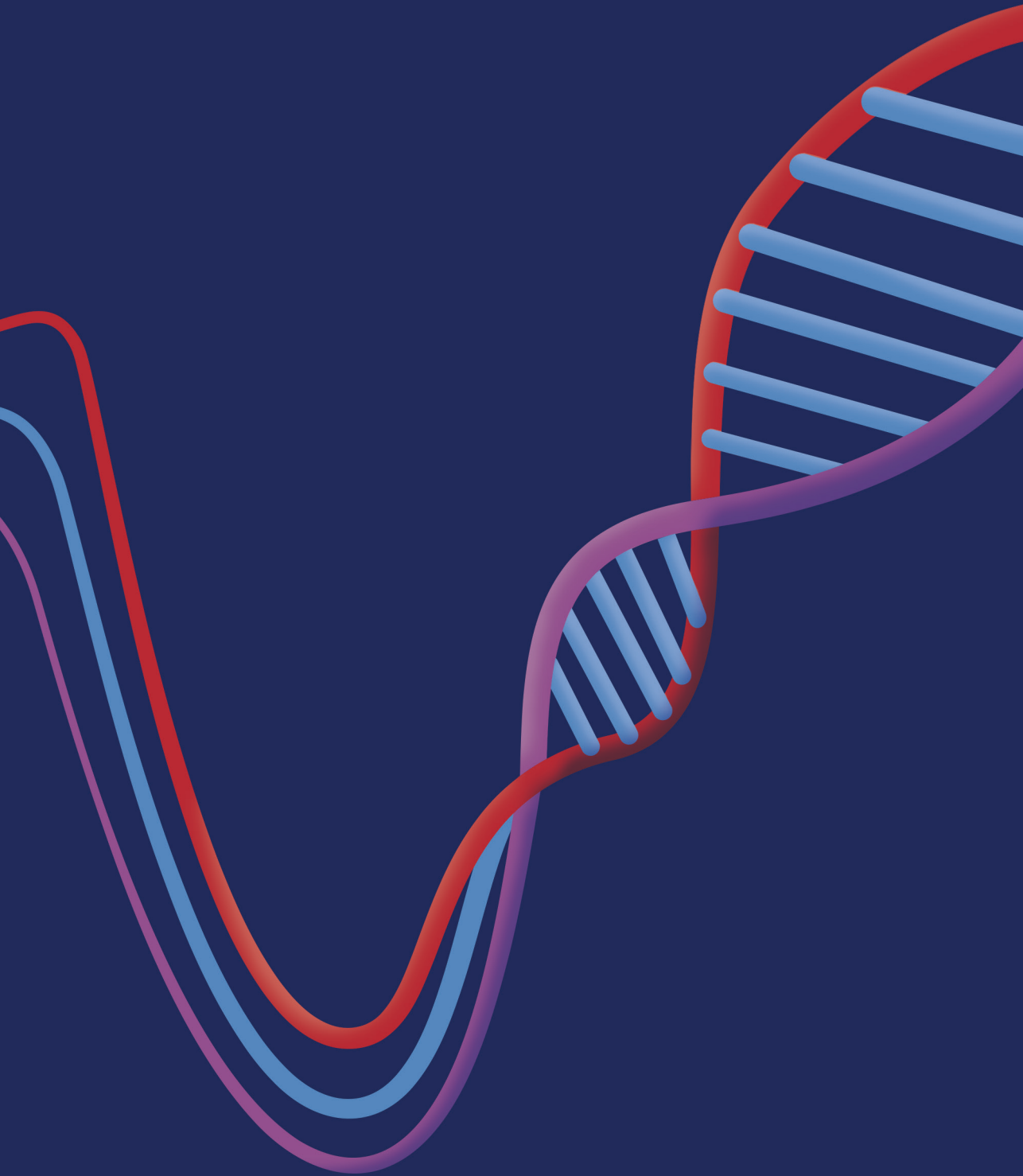
Supplemental Table 2. ICC of estimated model parameters

	SfAct LVfw	SfAct IVS	SfAct RVfw Apex	SfAct RVfw Mid	SfAct RVfw Bae	K1 LVfw	K1 IVS	K1 RVfw apex
<i>Inter</i>	0.85	0.86	0.93	0.92	0.85	0.98	0.94	0.97
<i>Intra</i>	0.71	0.68	0.92	0.92	0.84	0.95	0.90	0.83
<i>Model</i>	0.47	0.58	0.86	0.87	0.75	0.90	0.90	0.80

Supplemental Table 3. ICC of estimated tissue properties

	Contractility RVfw Apex	Contractility RVfw Mid	Contractility RVfw Base	Compliance RVfw Apex	Compliance RVfw Mid	Compliance RVfw Base	Delay RVfw Apex	Delay RVfw Mid	Delay RVfw base
<i>Inter</i>	0.98	0.96	0.95	0.97	0.98	0.96	0.96	0.95	0.94
<i>Intra</i>	0.95	0.93	0.95	0.88	0.97	0.97	0.87	0.89	0.94
<i>Model</i>	0.94	0.91	0.92	0.76	0.97	0.96	0.86	0.83	0.76

K1 RVfw mid	K1 RVfw base	dT LVfw	dT IVS	dT RVfw Apex	dT RVfw Mid	dT RVfw Base	AmRef LVfw	AmRef IVS	AmRef RVfw	TimeFac
0.90	0.91	0.88	0.97	0.95	0.96	0.94	0.99	0.89	0.95	0.99
0.85	0.89	0.81	0.80	0.89	0.94	0.96	0.96	0.82	0.97	0.91
0.69	0.73	0.56	0.63	0.74	0.96	0.95	0.92	0.76	0.92	0.93



CHAPTER 5

Uncertainty Quantification of Regional Cardiac Tissue Properties in Arrhythmogenic Cardiomyopathy Using Adaptive Multiple Importance Sampling

Feddo P. Kirkels, Nick van Osta*, Tim A.M. van Loon, Tijmen Koopsen, Aurore Lyon, Roel Meiburg, Wouter Huberts, Maarten J. Cramer, Tammo Delhaas, Kristina H. Haugaa, Arco J. Teske, Joost Lumens*

**The first two authors contributed equally*

Frontiers in Physiology. 2021;12:738926.

ABSTRACT

Introduction

Computational models of the cardiovascular system are widely used to simulate cardiac (dys) function. Personalization of such models for patient-specific simulation of cardiac function remains challenging. Measurement uncertainty affects accuracy of parameter estimations. In this study, we present a methodology for patient-specific estimation and uncertainty quantification of parameters in the closed-loop CircAdapt model of the human heart and circulation using echocardiographic deformation imaging. Based on patient-specific estimated parameters we aim to reveal the mechanical substrate underlying deformation abnormalities in patients with arrhythmogenic cardiomyopathy (AC).

Methods

We used adaptive multiple importance sampling to estimate the posterior distribution of regional myocardial tissue properties. This methodology is implemented in the CircAdapt cardiovascular modelling platform and applied to estimate active and passive tissue properties underlying regional deformation patterns, left ventricular volumes, and right ventricular diameter. First, we tested the accuracy of this method and its inter- and intraobserver variability using nine datasets obtained in AC patients. Second, we tested the trueness of the estimation using nine *in silico* generated virtual patient datasets representative for various stages of AC. Finally, we applied this method to two longitudinal series of echocardiograms of two pathogenic mutation carriers without established myocardial disease at baseline.

Results

Tissue characteristics of virtual patients were accurately estimated with a highest density interval containing the true parameter value of 9% (95% CI (0 – 79)). Variances of estimated posterior distributions in patient data and virtual data were comparable, supporting the reliability of the patient estimations. Estimations were highly reproducible with an overlap in posterior distributions of 89.9% (95% CI (60.1 – 95.9)). Clinically measured deformation, ejection fraction, and end-diastolic volume were accurately simulated. In presence of worsening of deformation over time, estimated tissue properties also revealed functional deterioration.

Conclusion

This method facilitates patient-specific simulation-based estimation of regional ventricular tissue properties from non-invasive imaging data, taking into account both measurement and model uncertainties. Two proof-of-principle case studies suggested that this cardiac digital twin technology enables quantitative monitoring of AC disease progression in early stages of disease.

INTRODUCTION

Computational models of the cardiovascular system are widely used to simulate cardiac (dys) function and related clinical application of therapies for cardiac disease.¹ Various attempts to generate a digital twin of the human heart have been made.² Previously, we proposed a framework to create a digital twin³ for quantification of the disease substrate underlying abnormal tissue deformation in patients with arrhythmogenic cardiomyopathy (AC).⁴

Inheritable AC primarily affects the right ventricle (RV) and predisposes to ventricular arrhythmias and sudden cardiac death in young individuals.^{5,6} Therefore, early disease detection is important. We previously determined an *in silico* disease substrate with decreased regional RV contractility and compliance, with the potential to predict disease progression on a patient-specific level.⁴ This method was, however, not able to include uncertainty present in both measurement and model.

Uncertainty will inevitably play a role in comparing estimated properties and thus Bayesian inference methods should be used to estimate the posterior distribution of model parameters, rather than only providing point estimates. Cardiovascular computational models are in general complex, meaning that the posterior distribution cannot be calculated analytically. Various techniques have been proposed to solve this problem, in which Markov chain Monte Carlo (MCMC) methods are often used.⁷⁻⁹ Adaptive multiple importance sampling (AMIS) is an important alternative to MCMC since it enables estimation of the posterior distribution in a model with a relatively high number of input parameters.^{10,11}

In this study, we apply AMIS to quantify parameter uncertainties in digital twins based on echocardiographic deformation imaging. We validate the methodology based on both *in silico* generated virtual data and datasets obtained from patients with AC and mutation positive family-members at risk of developing the disease. Furthermore, we use longitudinal series of echocardiograms in two AC patients to validate clinical applicability of this methodology.

MATERIALS AND METHODS

This section and *Figure 1* elucidate the methodology used to estimate parameters and related uncertainties using the CircAdapt model. First, we elaborate the mathematical basis and implementation of AMIS, which is generally applicable. Secondly, we describe the mathematical problem and introduce the included clinical measurements and the computational model used for the likelihood function. Finally, we explain the simulation protocol. The source code as well as the virtual patient datasets are available.

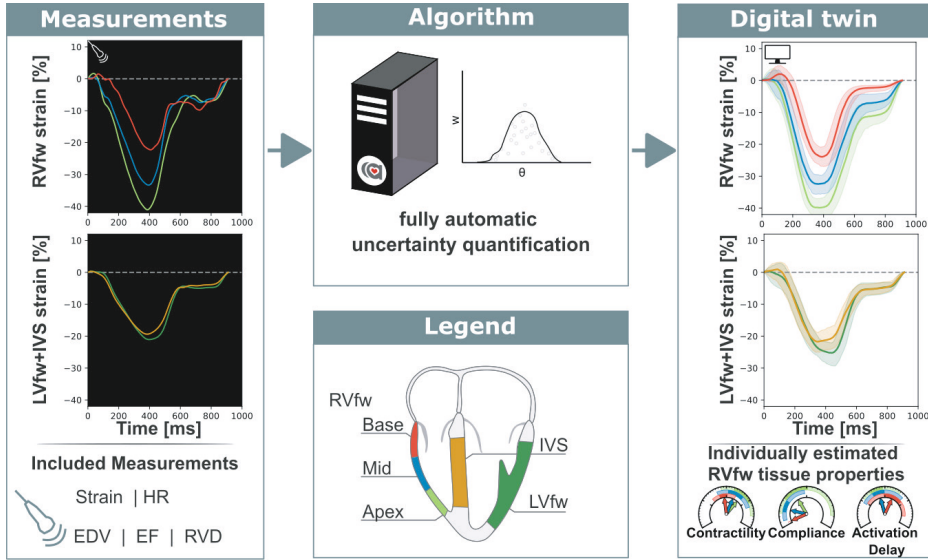


Figure 1. Non-invasive measurements were used as input for a fully automatic automated uncertainty quantification algorithm

This algorithm produced a digital twin based on estimated parameters with accompanying uncertainty. This digital twin can be used to get more insight in the estimated tissue properties. RVfw: right ventricle free wall; LVfw: left ventricle free wall; IVS: inter ventricular septum; HR: heart rate; EDV: end-diastolic volume; EF: ejection fraction; RVD: right ventricular diameter.

Mathematical basis of adaptive multiple importance sampling

We consider an n_θ -dimensional vector as a set of parameters θ of a numerical model $z = \mathcal{M}(\theta)$. This model $\mathcal{M}: \mathcal{R}^{n_\theta} \rightarrow \mathcal{R}^{n_z}$ maps the parameter vector to an n_z -dimensional vector of modelled data z . Measurement uncertainties are included in the likelihood function $p(z|\theta)$ representing the similarity between patient observation and model output. The posterior distribution $p(\theta|z)$ is the probability of having parameters θ given the observation z and is given by Bayes' rule as

$$p(\theta|z) = \frac{p(z|\theta)p(\theta)}{p(z)} \propto p(z|\theta)p(\theta), \quad (1)$$

with $p(\theta)$ the prior knowledge of the parameters and $p(z)$ the normalizing constant. No prior knowledge of the parameters $p(\theta)$ is known, so $p(\theta)$ was assumed to be uniform.

Importance sampling is an algorithm which estimates the posterior distribution $p(\theta|z)$.¹¹ The set of samples $\Theta = \{\theta \sim q(\theta)\}$ drawn from the proposal distribution $q(\theta)$ form an empirical estimation of the posterior distribution $p(\theta|z)$ in which each sample is weighted with the sample weight \mathcal{W} described by

$$w(\theta) \propto \frac{p(\theta|z)}{q(\theta)}. \quad (2)$$

The weights are normalized such that $\sum_{\theta \in \Theta} w(\theta) = 1$. Importance sampling is most effective when the proposal distribution $q(\theta)$ is close to the posterior distribution $p(\theta|z)$ such that variance in weight of the samples is small and the effective sample size is close to the actual sample size. Since no information was available on the posterior distribution, we used adaptive importance sampling in which the proposal distribution is iteratively updated to better describe the posterior distribution.¹¹

The computational cost of calculating the likelihood $p(z|\theta)$ in cardiovascular models is relatively high compared to the cost of calculating the probability density function of the proposal distribution $q(\theta)$, so the samples from all previous iterations were included in defining the proposal distribution $q(\theta)$ to optimally recycle past simulations following the adaptive multiple importance sampling (AMIS) (see *Figure 2*).¹⁰

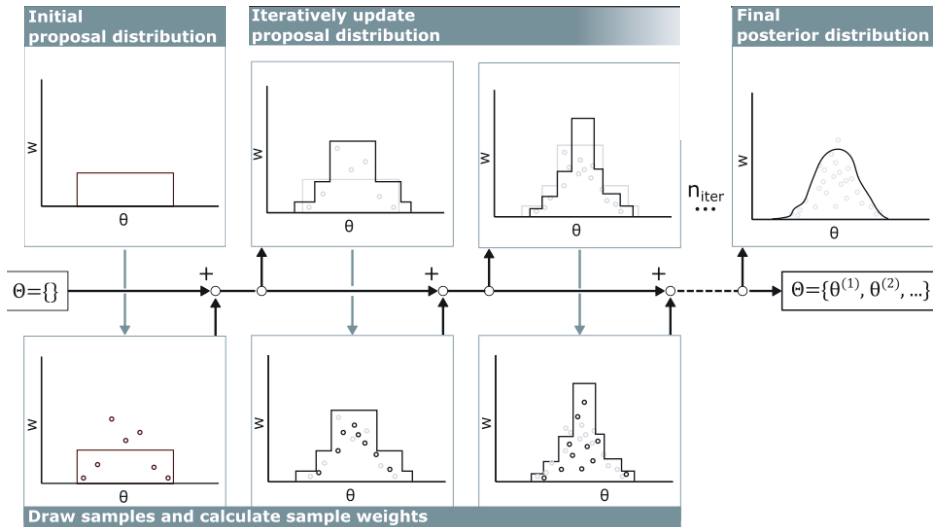


Figure 2. Visualization of adaptive multiple importance sampling

In the first iteration, samples θ are drawn from a uniform distribution and stored in the sample set Θ . For each sample, the corresponding sample weight w is calculated. Then, based on all previous samples θ in the sample set Θ and corresponding sample weight w , the next proposal distribution is defined and new samples are added to the sample set Θ . This iterates n_{iter} times.

Each iteration in this algorithm consists of two stages. First, samples are drawn from the proposal distribution and weights of all samples are updated. Second, the proposal distribution is updated based on the new sample weights.

Draw samples and calculate sample weights

At the start of each iteration i , 100 samples are drawn from the current proposal distribution $\pi_i(\theta)$. Samples are drawn without statistical dependencies between parameters, which may result in non-physiological combinations of parameters. For example, the model is not parameterized for a low contractile heart to be able to supply a high cardiac output (CO) and is therefore likely to become numerically unstable. To circumvent this, only a small uniform distribution around the reference is used as initial proposal distribution $q_0(\theta)$. AMIS will increase and decrease the search area of the proposal distribution and will move this to the area of interest in which physiological samples will be drawn close to the desired posterior distribution.

Each iteration, the weights are updated based on the proposal function and likelihood (Equation 2). The probability density function of all previous proposal distributions is given by the sum of all individual proposal distributions

$$q_i(\theta) = \frac{1}{N_{samples}} \sum_{i=0}^{n_{iter}-1} n_{samples, i} \cdot \pi_i(\theta), \quad (3)$$

with $n_{samples, i}$ the number of samples in iteration i and $N_{samples} = \sum_{i=0}^{n_{iter}-1} n_{samples, i}$ the total number of samples. Samples drawn from poorly performing proposal distributions are eliminated through the erosion of their low weights.¹⁰

The likelihood function is defined based on the normalized dimensionless summed squared error $X(\theta)^2$. This $X(\theta)^2$ is problem dependent and the X^2 used in this study is described in the section 'Problem description'. We assumed a non-informative uniform prior and neglected all interactions between individual errors. Furthermore, annealed adaptive importance sampling¹² was used to prevent the algorithm from premature convergence^{13,14}, resulting in a likelihood

$$p(z | \theta, T_i) \propto e^{-\frac{X(\theta)^2}{T_i}}, \quad (4)$$

in which $T_i \geq 1$ in each iteration i and represents the annealing temperature. This method is included to control convergence rate, thereby improving global search capabilities and limiting premature convergence towards local minima. The initial temperature is set to $T_{max} = 10$, and decreases each iteration i such that

$$T_{i+1} = \begin{cases} \min(10, T_i + \Delta X_{opt}^2) & \text{if } X^2 \text{ is improved} \\ \max(1, 0.8 \cdot T_i) & \text{else} \end{cases} \quad (5)$$

with ΔX_{opt}^2 the difference between the old and new X^2 of the best sample.

Update proposal distribution

Each iteration, the proposal distribution is updated based on all drawn samples in the sample set Θ and its corresponding weight W . In the updated proposal distributions, samples were drawn along the principal component axes of the weighted sample set Θ .

This protocol ran for at least 500 iterations. Additional iterations were performed in the case that the effective sample size $N_{eff} > 10 \cdot n_\theta$ was not fulfilled. The Kish effective sample size N_{eff} was used¹⁵, which is defined as

$$N_{eff} = \frac{\left[\sum_{\theta \in \Theta} w(\theta) \right]^2}{\sum_{\theta \in \Theta} \left(w(\theta)^2 \right)}. \quad (6)$$

Problem description

Clinical data

Patient-specific simulations were based on echocardiographic data from AC mutation carriers in various disease stages. Besides clinically measured LV and RV regional deformation imaging data, the LV end-diastolic volume (EDV), LV ejection fraction (EF) and right ventricular basal diameter (RVD) were used as model input. We used echocardiographic data of nine pathogenic AC mutation carriers which were evaluated in the University Medical Center Utrecht, the Netherlands. As previously described⁴, deformation analyses of these echocardiograms were performed twice by two observers to determine clinical inter- and intra-observer variability. Lastly, longitudinal datasets with >2 echocardiograms per patient at different time points were used to explore applicability of the model for follow-up of tissue properties over time. These longitudinal datasets were acquired from AC mutations carriers which were evaluated in the Oslo University Hospital, Norway.

All echocardiographic data were obtained on a Vivid 7, Vivid 9 or Vivid E95 ultrasound machine (GE Vingmed, Horten, Norway). The echocardiographic protocol was described previously.¹⁶ In this study, we focused on the right ventricular free wall (RVfw). This is typically the most affected area in AC mutation carriers¹⁷, which is expressed in typical deformation abnormalities (delayed onset of shortening, decreased peak systolic strain, post-systolic shortening, and increased RV mechanical dispersion).¹⁶ Therefore, deformation patterns of three RVfw segments (apical, mid-ventricular and basal) were used as input for our modelling framework (Figure 1).⁴ Additionally, LV free wall (LVfw) and interventricular septal (IVS) deformation patterns were included to ensure realistic mechanical boundary conditions for the RVfw in terms of ventricular interaction. These patterns were obtained by averaging the 12 LVfw and 6 IVS segmental deformation curves, respectively, using the standardized 18-segment model.¹⁸

Computational model of heart and circulation

Clinical measures were simulated using the CircAdapt model. This model is a fast biomechanical lumped parameter model of the heart and circulation. Via the one fibre model¹⁹, wall stress is related to cavity pressure. The TriSeg module allows inter-ventricular interaction over the IVS.²⁰ Phenomenological material laws prescribe the stress-strain relation in the spherical walls. The MultiPatch module allows for regional heterogeneity of tissue properties within a single wall²¹ and is used to describe the heterogeneity in the RVfw. Three segments were created in the RVfw to model the mechanics in the three different RVfw segments (apical, mid-ventricular, and basal).

The parameter subset θ included for estimation was based on a previous sensitivity analysis⁴ and is shown in *Table 1*. Parameters included were regional parameters describing the constitutive behaviour of active (SfAct) and passive stress (k1), activation delay (dT), reference wall area (AmRef), and global parameters relative systole duration (RSD), and CO. Heart rate (HR) in the model was set to match clinically measured HR to ensure equal cycle lengths in measured and modelled signals.

Strain was defined as the segmental displacement relative to its reference length at end diastole. Additionally, EF, EDV, and RVD were included. Modelled EDV was defined as the maximum cavity volume of the LV cavity assuming perfect valve behaviour. EF was defined as the ratio of stroke volume over maximum volume. RVD was defined as the maximum cavity diameter between the RVfw and IVS.

Table 1. parameters included in this study

Model parameter	Unit	Description	Sample distribution	Parameter range	N parameters	
SfAct	kPa	Active stress scaling factor	logit-uniform	(0, 1000)	5	(LVfw, IVS, RVapex, RVmid, RVbase)
k1	-	Stiffness exponent	logit-uniform	(1, 100)	5	(LVfw, IVS, RVapex, RVmid, RVbase)
dT	ms	Activation delay	logit-uniform	(-200, 800)	5	(LVfw, IVS, RVapex, RVmid, RVbase)
AmRef	cm^2	Eccentric hypertrophy	log-uniform	(0, ∞)	3	(LVfw, IVS, RVfw)
RSD	-	Global systolic duration scaling	log-uniform	(0, ∞)	1	Global
Q0	L/min	Cardiac Output	log-uniform	(0, ∞)	1	Global
					20	

Likelihood function

As shown in Equation 4, the likelihood function was based on the summed squared error X^2 . This error consists of the error in strain of the 5 segments and on the error in EF, EDV, and RVD. Because the measured diastolic strain is less reliable due to the drift affecting most of this phase, we only included strain during the systolic phase in this study. This systolic phase was

defined from the onset of the QRS complex until 100ms after peak strain of the segment with longest shortening phase.

To account for dependencies in strain, we included weighted dimensionless errors based on strain ($e_{\epsilon, seg}^2$), strain rate ($e_{\dot{\epsilon}, seg}^2$), and inter-segmental strain differences ($e_{\Delta\epsilon_{inter}}^2$). Errors in EF (e_{EF}^2), EDV (e_{EDV}^2) and RVD (e_{RVD}^2) were assumed independent, resulting in the χ^2 to be the sum of all individual weighted dimensionless errors e^2 :

$$\chi^2 = \sum_{seg \in segments} \left(e_{\epsilon, seg}^2 + e_{\dot{\epsilon}, seg}^2 \right) + \sum_{inter \in interseg} e_{\Delta\epsilon_{inter}}^2 + \sum_{m \in (EF, EDV, RVD)} e_m^2 \quad (7)$$

Standard deviations used to normalize each individual term were manually estimated *a priori* to meet differences between the inter- and intraobserver datasets. Standard deviations used to normalize EF, EDV, and RVD were set *a priori* in consultation with clinical partners.

RV tissue properties

To relate our simulations to clinical measures, four RV tissue properties were investigated, namely contractility, activation delay, compliance, and myocardial work. Segmental contractility was defined as the maximum rate of active stress rise, which can be seen as the equivalent of the maximum rate of ventricular systolic pressure rise (dP/dt_{max}) on a local tissue level. Segmental wall compliance was defined as the slope of the end-diastolic myofibre stress-strain relationship at time before first ventricular activation and can be interpreted as the regional equivalent of the slope of the global end-diastolic pressure-volume relation. Myocardial work density was defined as the area within the stress-strain loop and can be interpreted as the regional equivalent of global stroke work.

Simulation protocol

Uncertainty Quantification of Real Patient datasets

Nine clinical datasets in which the echocardiographic images were analysed twice by two independent observers were included to test reproducibility, leading to 36 datasets. For each individual dataset, parameters were estimated three times resulting in 108 estimations in total. Since no ground truth exists for estimated model parameters, only the reproducibility of estimations was evaluated. Three kinds of reproducibility were investigated, namely computational reproducibility, reproducibility including interobserver variability, and reproducibility including intraobserver variability. First, computational reproducibility was defined as the reproducibility of the exact same clinical dataset and quantified by the mutual information (MI) between two model parameter estimations. The same protocol was repeated three times with a different random seed. To calculate the MI, two distributions were discretized into 100 bins. The MI was then defined as the overlap divided by the union of the distributions. Secondly, reproducibility including interobserver variability was tested on the nine patient datasets, whereby a second blinded observer performed deformation imaging analysis on the same echocardiographic loops as the first observer. It was defined as MI between two estimated model parameter distributions from two datasets observed by the two different observers. Finally, reproducibility including intraobserver variability was quantified similarly from two different datasets, whereby the observer performed the deformation analysis again after at least two weeks, blinded to previous results. The median MI with 95% confidence interval (CI)

of all parameter estimations was reported. In case the estimations from different observations fully overlap, MI=100%. In case of no overlap at all, MI=0%.

Uncertainty Quantification of Virtual Patient datasets

To test the trueness of the estimation, *in silico* generated virtual patients were generated. To ensure these virtual patients to be representable for real AC patients, nine virtual patients were created based on the nine real patient datasets. For each real patient, the simulation with maximum likelihood was selected. The output of this simulation was used as virtual patient dataset, which was used as input of the modelling framework.

Trueness of the virtual estimations was tested by comparing the estimated distribution with the known true parameter values. For each parameter, the highest density interval (HDI) for which the true value is in the interval was calculated. The HDI was defined as the area of the distribution for which the posterior holds $p(\theta|z) > p(\theta_{true}|z)$. The distribution was approximated with a histogram with bin width defined by the Freedman-Diaconis rule.²² The HDI for each parameter should be near 0% meaning the true value is near the maximum a posteriori.

Application in longitudinal datasets

Two subjects with a baseline and two follow-up echocardiograms were selected (Table 2). For all six datasets, clinical data was extracted and the datasets were estimated independently of each other, similarly as described above. The two longitudinal sets of estimated tissue properties were investigated. Due to the retrospective nature of this study, LV EDV was only available at baseline. We assumed that it did not change during follow-up.

Table 2. Patient characteristics of the two subjects at baseline and follow-up used in the likelihood function

	Subject 1			Subject 2		
Time after baseline (yr)	0	4.5	9.1	0	5.2	7.3
LV EDV (mL)		112			150	
LV EF (%)	61	61	61	59	64	57
RVD (mm)	43	43	42	45	38	40

Code implementation

The CircAdapt model was written in C++. All other code was written in Python. Each individual dataset was solved sequentially and independently. The source code of the CircAdapt model has been made available before.³ All other source code is publicly available on Zenodo (<https://doi.org/10.5281/zenodo.5084657>). Datasets were estimated in parallel with Python 3.9.4 on a AMD Ryzen Threadripper 3970X.

RESULTS

Uncertainty Quantification of Real Patient datasets

Regional deformation characteristics were accurately simulated close to the measured deformation and with reasonable uncertainty ($X_{opt}^2=9.4$ (95% CI [5.4-20.9])). *Figure 3 (left)* shows a representative example. The modelled strain followed the pattern of clinically measured strain during systole and heterogeneity between the segments was well captured. A 1D representation of the convergence of the proposal distribution, corresponding to the estimated model parameters is shown in *Figure 4*. In the first 50 iterations, the proposal distribution decreased, increased, and moved to the area of interest. From the 50th iteration, most proposal distributions stabilized. This behaviour was also observed in estimations in other datasets.

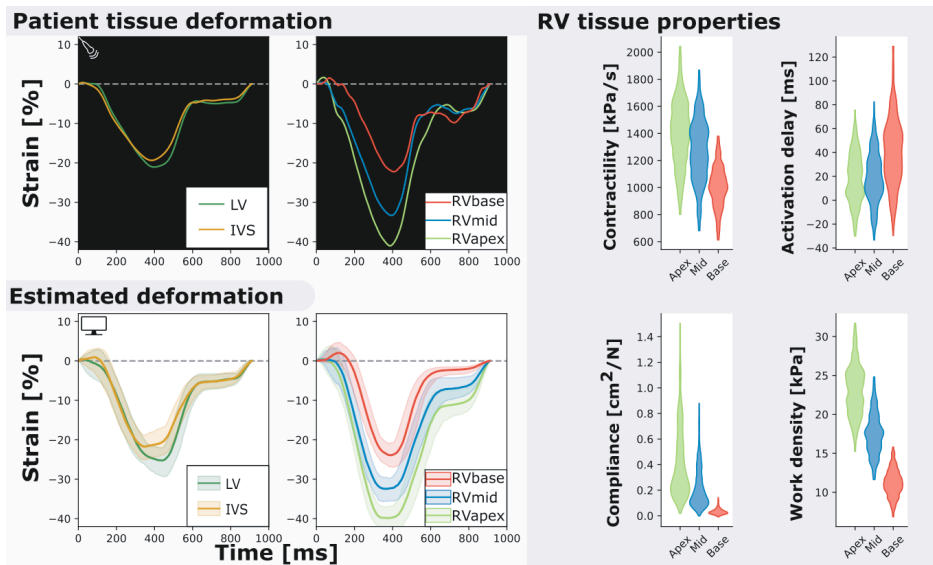


Figure 3. Measured and estimated strain of real subject (left) and violin plots of estimated parameters (right)

Deformation patterns and regional heterogeneity was well captured by the model. The best simulation in the sample set was in good agreement with to the patients dataset ($X_{opt}^2=8.9$).

The estimated posterior distributions of the model parameters (*Figure 4*) of most parameters were estimated with small variances, except for parameters SfAct and k1, because they were unidentifiable in some segments. The posterior correlation matrix (*Figure 5, top*) shows the correlation between estimated posterior distributions. Notable are the correlations between model parameters SfAct, k1, dT, and AmRef describing mechanics in the same wall segment. Additionally, there was a high correlation between different segments for the model parameters dT and AmRef. From the two global parameters, only RSD seemed to correlate with dT.

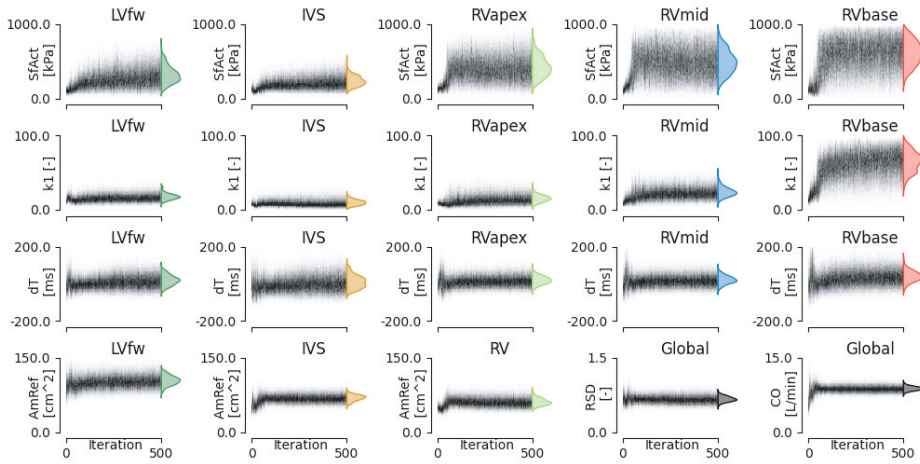


Figure 4. Convergence of estimated model parameters. The distributions on the right show the final estimated posterior distribution.

Figure 3 (right) shows the estimated regional RV model parameters and the RV tissue properties contractility, activation delay, compliance, and work density. The RV tissue properties were estimated with distributions with a smaller variance compared to the estimated model parameters. A decrease in basal contractility, compliance, and work density with respect to the apical and mid segment was found which is in line with the abnormal basal deformation pattern.

Figure 5 (bottom) shows the correlation between posterior model parameter distributions with the RV tissue properties contractility, compliance, and work density. Contractility was mostly correlated with SFact, AmRef, and CO. In the RVapex and RVmid, contractility was not only dependent on the parameters prescribing its own segmental mechanics, but also on the parameters prescribing other segmental mechanics. Similar results were observed for compliance, which was correlated with SFact, k1, and dT. Compliance showed no correlation with AmRef, RSD, and CO. Work density was mostly correlated with CO.

Estimated model parameters were highly reproducible. Computational reproducibility was found with an MI of 89.9% (95% CI (60.1 – 95.9)). The reproducibility error given inter- and intraobserver variability were estimated with an MI of 86.5% (95% CI (46.0 – 95.2)) and 85.9% (95% CI (43.7 – 95.3)), respectively.

Uncertainty Quantification of Virtual Patient datasets

Nine virtual patients were created based on the nine real-patient estimations. As an example, Figure 6 shows the virtual patient based on the patient results described above. Regional deformation characteristics were simulated close to the virtual patients deformation characteristics ($X^2_{opt} = 2.0$ (95% CI=(1.2 – 3.0))). The true parameter values were well captured by the estimated distributions. The HDI of the true parameter values was 9% (95% CI (0 – 79)). Heterogeneity in model parameters was well preserved. The width of the distribution in virtual fits was similar to that in the original patient estimation.

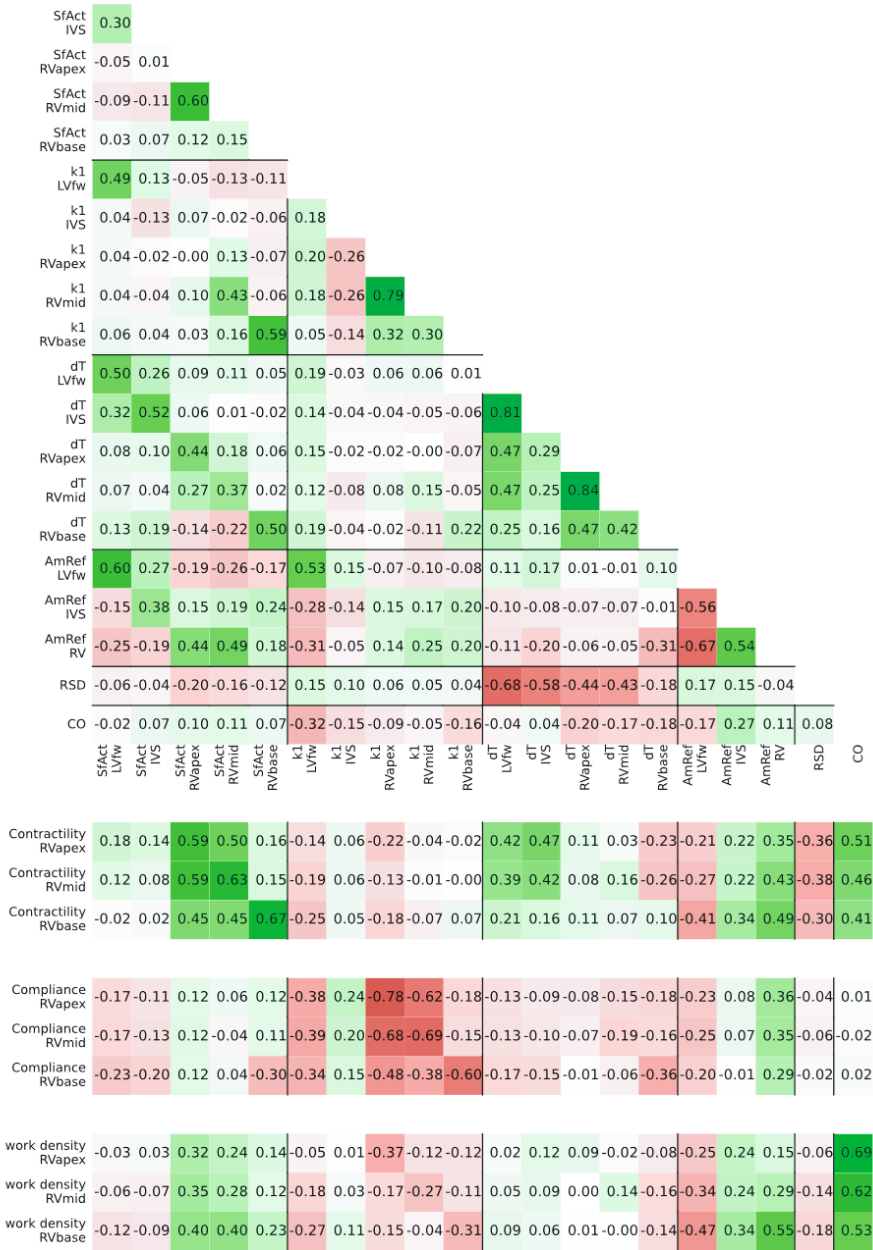


Figure 5. Posterior correlation matrix of the estimated model parameters (top) and the correlation between the posterior distribution of model parameters and derived tissue properties (bottom)

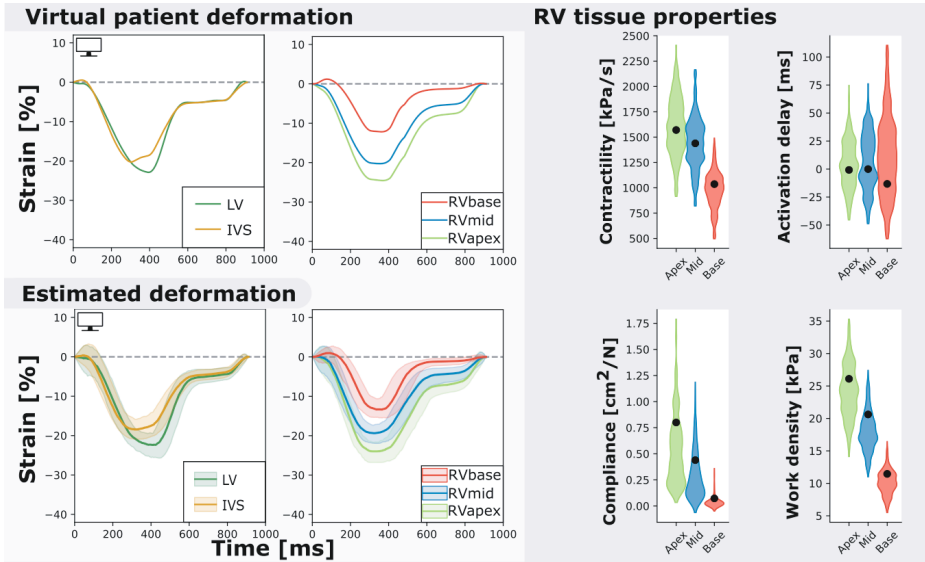


Figure 6. Measured and estimated strain of virtual subject (left) and violin plots of estimated parameters (right).

The estimated properties are close to the true properties of the virtual patient (black dot) and the heterogeneity is well captured. The best simulation in the sample set was closely related to the virtual patients dataset ($\chi^2_{opt} = 2.0$).

Application: Longitudinal datasets

Two subjects with a baseline and two follow-up echocardiograms were included in this study (Table 2). The first subject had a follow-up examination after 4.5 and 9.1 years and the second subject after 5.2 and 7.3 years. Results of these case studies are shown in Figure 7 and Figure 8.

Subject 1 developed an abnormal deformation pattern of the basal RV segment at last follow-up which was not seen at baseline. Computer simulations showed homogeneous RV contractility, activation delay, compliance, and work at baseline. In the last follow-up examination, an apex-to-base heterogeneity in compliance and work density was present.

Subject 2 showed normal RV deformation patterns at baseline and did not develop clear deformation abnormalities during follow-up. Contractility, activation delay, compliance, and work density were estimated homogeneously at baseline. In the final follow-up, a small apex-to-base heterogeneity in compliance was present.

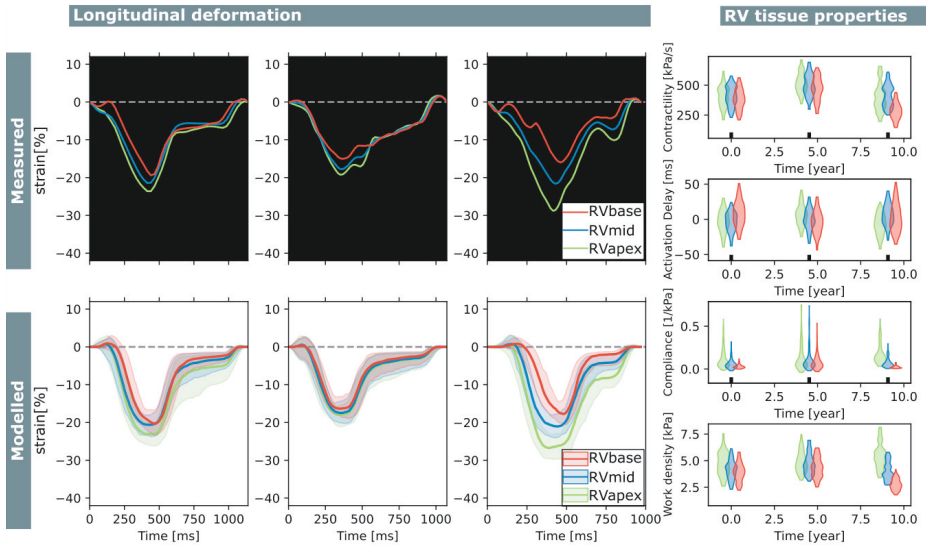


Figure 7. Longitudinal estimations subject 1

Echocardiographic deformation imaging was performed at baseline, and after 4.5 and 9.1 years of follow-up. Computer simulations showed homogeneous RV contractility, activation delay, compliance, and work at baseline. At last follow-up, subject 1 developed an abnormal deformation pattern of the basal RV. Estimation of RV tissue properties from these deformation data showed an apex-to-base heterogeneity in activation delay, compliance and work density.

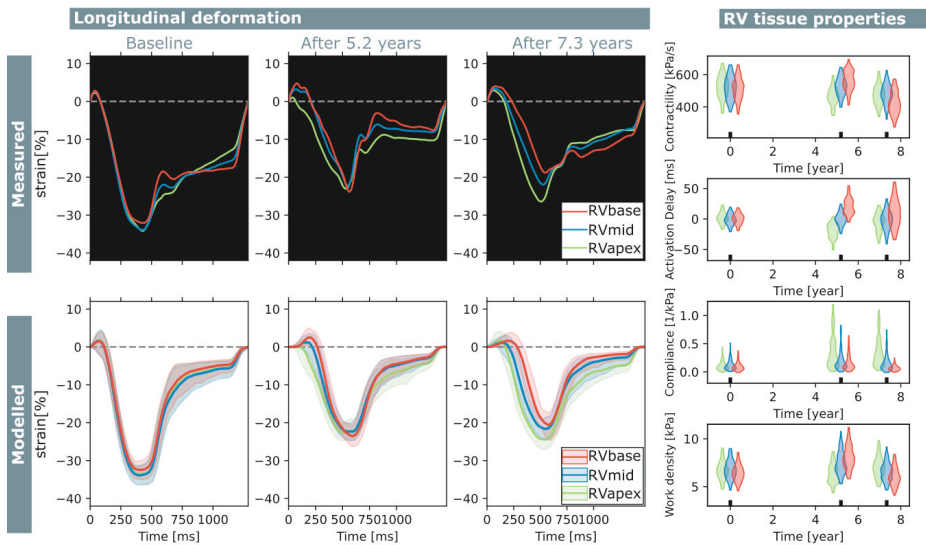


Figure 8. Longitudinal estimations subject 2

Echocardiographic deformation imaging was performed at baseline, and after 5.2 and 7.3 years of follow-up. Subject 2 had normal RV deformation patterns at baseline and did not develop clear deformation abnormalities during follow-up. Contractility, compliance, and work density were estimated homogeneously at baseline.

DISCUSSION

In this work, we successfully applied adaptive multiple importance sampling (AMIS) to estimate posterior distributions of model parameters describing local passive and active tissue behaviour based on echocardiographic deformation measurements. Estimated deformation closely resembled the clinically measured myocardial deformation with a realistic level of uncertainty originating from both the measurement and the model. Estimated RV tissue properties reflected progression of the disease substrate over time present in the clinical case studies.

Model-based inference

Personalization of cardiac computational models is becoming more popular and several approaches have been proposed. Schiavazzi et al.⁷ used MCMC to estimate model parameters in a simplified model of the single-ventricular heart in a close-looped circulation, based on clinically measured pressures and flows. Corrado et al.²³ used a Reduced Order Unscented Kalman Filter to estimate model parameters to optimize body surface potential maps and myocardial displacement. Meiburg et al.⁸ used the Unscented Kalman Filter to predict post-intervention hemodynamics after trans-aortic valve implantation. Zenker²⁴ used importance sampling to estimate model parameters in a cardiovascular model. Dhamala et al.²⁵ used high-dimensional Bayesian optimization for parameter personalization of a cardiac electrophysiological model. Coveney and Clayton²⁶ used history matching to calibrate the maximum conductance of ion channels and exchangers in two detailed models of the human atrial action potential against measurements of action potential biomarkers. Daly et al.²⁷ used sequential Monte Carlo Approximate Bayesian Inference to quantify the uncertainty amplification resulting in a cellular action potential model. Camps et al.²⁸ used the same technique to estimate key ventricular activation properties based on non-invasive electrocardiography and cardiac magnetic resonance imaging.

These studies used computational models with different levels of model complexity in both anatomical and physiological detail. Complex models allow personalisation with a high number of details, however, they suffer from a high-dimensional unknown space increasing the difficulty of personalization due to unidentifiability of the model parameters. This problem can be solved by reducing the complexity of the optimization problem by assuming global model parameters²⁹ or regional model parameters.³⁰ However, this does not reduce the computational cost and increases model discrepancy. It is suggested to use a surrogate model to approximate the exact posterior probability density function³¹, but this creates a new source of uncertainty. Including model discrepancy in the estimation often fails due to the non-identifiability between model parameter estimations and model discrepancy.³² The pseudo-true parameter value found by ignoring model discrepancy can still be valuable for clinical interpretation.

Another approach is to reduce the complexity of the model. Various lumped parameter models of the heart and circulation have been used for fast personalization.^{7,8,24} The cost of low complexity may lead to an increase in model discrepancy due to model assumptions and simplifications.³² It was, however, demonstrated before that the CircAdapt model is highly efficient in simulating regional mechanics and is able to simulate realistic hemodynamics.^{21,33} We previously showed that the CircAdapt model can simulate segmental mechanics with a similar spatial resolution as in clinical strain imaging measurements with low discrepancy.^{4,21} Therefore, we assume the CircAdapt model is a suitable model for modelling regional strain in AC patients.

In this study, we chose importance sampling because it is highly effective for complex high-dimensional models.¹¹ The computational cost of our model was approximately 1000 times higher compared to the calculation of the probability density of a sample drawn from the proposal distribution. Therefore, AMIS was the most suitable variant to optimally reuse all samples.¹⁰

Efficiency of AMIS heavily depends on the definition of the proposal distribution.¹¹ A wider proposal distribution ensures to visit the full input space of interest, but is accompanied by a risk of non-converging estimations due to the high number of samples with a low sample weight. On the other hand, a more narrowed search has the risk of finding a local minimum in which the wrong posterior is estimated, or the risk of collapsing when the weight of the found minimum drops to zero. As the number of samples goes to infinity, the sample weight will be equally distributed. However, for the limited number of samples drawn, an optimal balance should be found. We successfully implemented annealed adaptive importance sampling to prevent the model from premature convergence while still being able to narrow the proposal distribution in the later iterations. More research should go into defining the proposal distribution or the initial proposal distribution.

In this study, it took approximately 16h per dataset to converge. This time includes generating the proposal distributions, generating samples, running simulations, obtaining the likelihood function, and calculating the sample weights. The total duration mainly depends on the duration of each individual simulation, since the number of iterations in the estimations was equal or close to 500. The duration of each simulation depended on heart rate, numerical stability, and number of beats needed to get a hemodynamically stable solution. Computational time can be reduced in future studies, since AMIS allows parallel calculation of simulations. This reduction in computational time will be essential for clinical application of our method on a larger scale.

Uncertainty Quantification in Arrhythmogenic Cardiomyopathy

Cardiovascular models are, in general, complex models with a multitude of parameters. To create digital twins with the CircAdapt model, we used a parameter subset that we determined in a previous study.³ This subset includes model parameters related to regional RV contractile function, compliance, and activation delay. This is in line with functional and structural myocardial changes found in AC patients (e.g. fibro-fatty replacement of myocytes⁶, altered calcium handling³⁴, and fibrosis³⁵) and early generic simulation based hypotheses³⁶. These structural changes might cause abnormal electrical activation observed in patients with AC.³⁷ The RV tissue properties are useful to quantify the substrate, however, the model cannot distinguish the cellular origin of the substrate.

The likelihood function was based on our prior knowledge of the pathology. It is not trivial how to include this information as the amount of uncertainty and its dependencies is not known but heavily affects the posterior distribution. In this study, we limited the objectives in the likelihood function to only that information in the longitudinal study that our model can simulate realistically. The main contributor is regional RV strain, as regional deformation abnormalities are found in early stages of the disease.^{36,38–42} LV strain, RVD, LV EF, and LV EDV are included in the likelihood to personalize geometric properties of the model. Because of the complex geometry of the thin-walled RV, our 2D imaging methods did not provide a comprehensive measure of RV size and wall thickness. In future studies, 3D imaging methods might provide a more comprehensive inclusion of geometric variability of the RV. The RVD

was included to account for large geometrical differences between patients and geometrical changes over time. Wall volumes were not included in the parameter subset because they were unidentifiable given the available measurements.

Dependencies in strain were partially included by including strain rate and strain differences. Based on the used likelihood function, posterior distributions were estimated with a relatively wide variance (*Figure 4*), suggesting not all parameters are identifiable. The low reproducibility in some parameters (HDI 95% CI (0-79%)) is probably related to this unidentifiability. Heterogeneity in model parameters is, however, well preserved, suggesting that measurements that are sensitive to segment-averaged model parameters should also be included in the likelihood function. Further prospective studies could investigate the error propagation of dependent and independent uncertainties, whether all components of the likelihood are essential to include, and which other measurements should be included to increase the identifiability of the model parameters.

Derived tissue properties were estimated more precise and reproducible compared to model parameters, suggesting that different parameter combinations can result in the same hemodynamic state. Mechanics of the three RV segments were modelled with the same mathematical equations, however, they have different interactions with the surrounding walls as shown in *Figure 5*. Compliance in the basal segment was estimated more precise compared to the other segments (*Figure 6*). This results from the non-linear behaviour of the model, as basal model parameters were differently estimated due to basal deformation abnormalities. Therefore, compliance in the basal segment was less correlated with the other segments.

In this study, we used a single definition for myocardial contractility and compliance related to other more global definitions. There is no consensus on a single indicator for contractility and compliance, and often multiple (non-invasive) measures are used to get an impression. For contractility, the maximum pressure-time derivative dP/dt_{max} is the most commonly used index of contractility in the field of drug safety assessment.⁴³ Although this measure is preload and afterload dependent, the regional stress-time derivative as local equivalent gives insight in the regional differences in RV contractile function. Other global measures have been proposed to bypass preload and afterload dependencies, such as dP/dt_{max} at a specific pressure⁴³ or end-systolic pressure-volume relation⁴⁴. New techniques might be useful for future validation of RV tissue properties, such as shear wave imaging⁴⁵ to quantify cardiac stiffness.

The gold-standard assessment of RV stiffness (inverse of compliance) is the end-diastolic pressure-volume relation.⁴⁶ The local equivalent is the models material law describing the stress-sarcomere length relation. The actual amount of stress prescribed by this law depends on the sarcomere length during the cycle.¹⁹ Due to the complexity of the model, which includes mechanics based on sarcomere length, an accurate estimation of compliance is difficult. The compliance measure as used in this study only includes the compliance at the end diastolic sarcomere length and is therefore load-dependent. To obtain a load-independent measure, more information on the loading conditions should be included in the likelihood distribution.

Case study and future research directions

The two subjects included in the case study showed different behaviour over time. The first subject developed an abnormal basal RV deformation pattern during follow-up which was reflected in changes in estimated local tissue properties. The second subject did not develop clear deformation abnormalities, but did develop slight abnormal heterogeneity in tissue properties. In both cases, only small changes in estimations were observed from baseline

to follow-up. It has previously been shown that heterogeneity in deformation patterns has prognostic value for disease progression³⁸ and life-threatening arrhythmia³⁹. Although no further follow-up of these subjects was available, we can hypothesize our model might identify abnormal tissue substrates before this is clearly visible in deformation patterns. Further studies should investigate whether our approach is able to detect AC in an early stage and whether it has added prognostic value.

In this study, we estimated model parameters to predict tissue mechanics under mechanical loading similar to loading during measurement. To achieve this, we included CO in the parameter subset and EDV and EF in the likelihood function. The model could be used for predicting the behaviour of the heart under different loading conditions. This could facilitate the study of loading effects of drug interventions in the digital twin. Besides, the effect of exercise, which is an important modulator of phenotypic expression of AC⁴⁷, could be studied in the digital twin. For the latter, a virtual cardiac exercise performance test as proposed by Van Loon et al.⁴⁸ could be used to give more insight in the severity of the substrate and possible triggers for disease progressions. To allow the CircAdapt model to extrapolate its state to other loading conditions such as exercise, more information should be included.

Limitations

Uncertainties are assumed statistically independent and additive, however, this is in fact more complicated. Measurements have multiple sources for uncertainty. We have only included inter- and intra-observer variability of the speckle tracking imaging in our study. Global longitudinal strain has proven to be reproducible, however, it has been shown that beat-to-beat variability affects segmental peak strain, end systolic strain and post-systolic strain.⁴⁹ More research should elucidate the origin of this uncertainty, its effect on normalized strain morphology as included in our study, and how to optimally include uncertainty in defining the likelihood function. This could also facilitate inclusion of realistic noise on virtual patient datasets, which was outside the scope of this study.

AC is not only characterized by structural disease manifestation, but electrophysiologic substrates play an important role as well.⁵⁰ Currently, the CircAdapt model only contains the lumped effect of electrophysiology to describe the mechanical behaviour. Future studies could extend the model with a more detailed electromechanical coupling, such as proposed by Lyon et al.⁵¹, to be able to describe the electrophysiologic substrate.

CONCLUSION

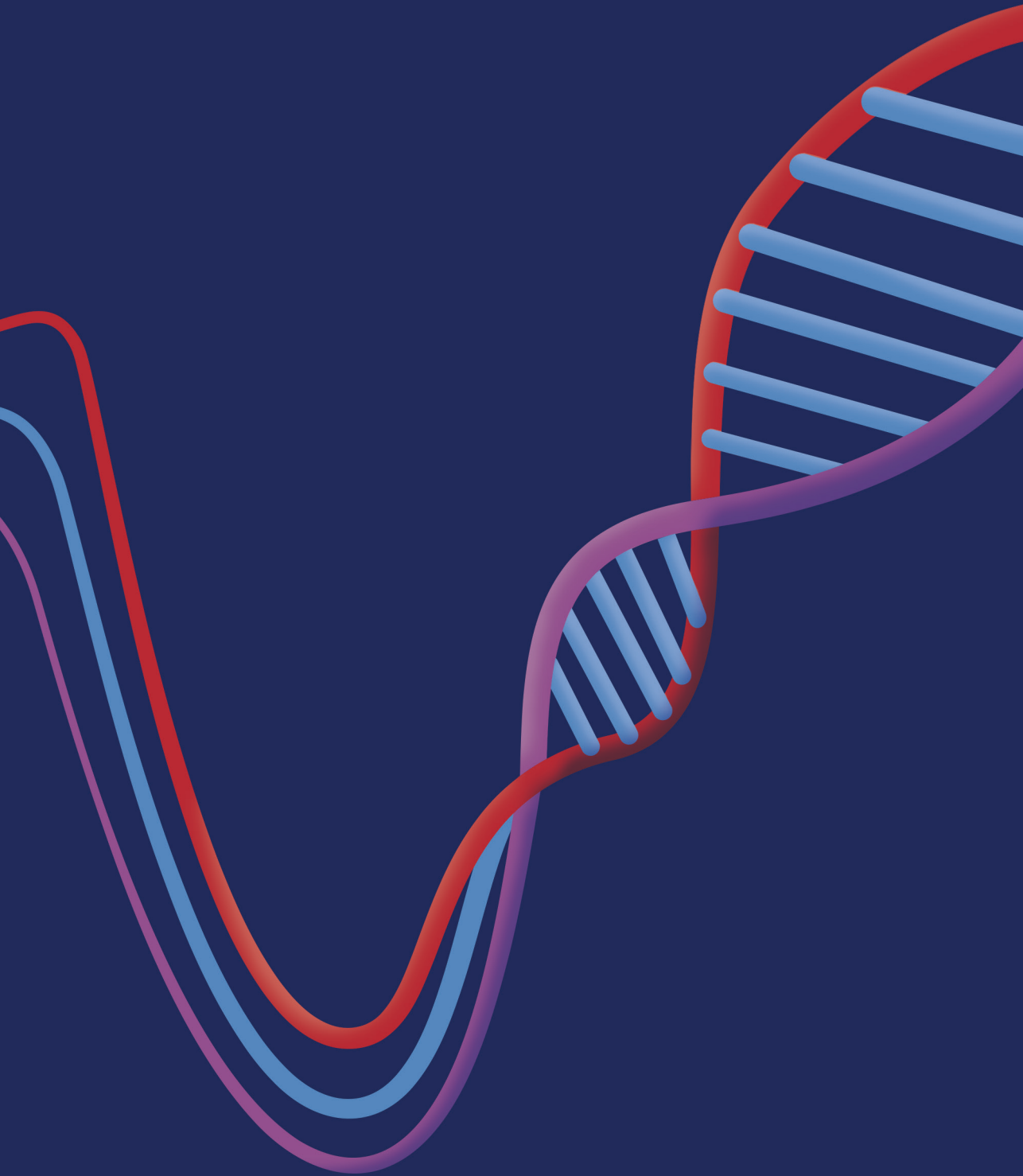
We presented a patient-specific modelling approach taking into account uncertainties. With this approach, we were able to reproduce regional ventricular deformation patterns and estimate the underlying tissue properties in AC mutation carriers with an acceptable level of uncertainty. Virtual estimations were precise and real-world estimations were highly reproducible. Two subjects in our case study revealed the evolution of early-stage AC disease over time using longitudinal follow-up datasets. Future studies should apply our method on a larger cohort and investigate the course of early stage RV disease development at individual as well as patient population levels.

REFERENCES

1. Niederer SA, Lumens J, Trayanova NA. Computational models in cardiology. *Nat Rev Cardiol*. 2019;16(2):100–11.
2. Corral-Acero J, Margara F, Marciniak M, et al. The ‘Digital Twin’ to enable the vision of precision cardiology. *Eur Heart J*. 2020;41(48):4556–64.
3. Van Osta N, Lyon A, Kirkels FP, et al. Parameter subset reduction for patient-specific modelling of arrhythmogenic cardiomyopathy-related mutation carriers in the CircAdapt model: Parameter Subset Reduction. *Philosophical Transactions of the Royal Society A*. 2020;378(2173):20190347.
4. Van Osta N, Kirkels FP, Lyon A, et al. Electromechanical substrate characterization in arrhythmogenic cardiomyopathy using imaging-based patient-specific computer simulations. *Europace*. 2021;23(Suppl1):i153-i160.
5. Thiene G, Nava A, Corrado D, Rossi L, Pennelli N. Right Ventricular Cardiomyopathy and Sudden Death in Young People. *N Engl J Med*. 1988;318(3):129–33.
6. Basso C, Corrado D, Marcus FI. Arrhythmogenic right ventricular cardiomyopathy. *Lancet*. 2009;(373):1289–300.
7. Schiavazzi DE, Baretta A, Pennati G, Hsia T, Marsden AL. Patient-specific parameter estimation in single-ventricle lumped circulation models under uncertainty. *Int J Numer Method Biomed Eng*. 2017;33(3).
8. Meiburg R, Zelis JM, van’t Veer JM, et al. Model-based aortic power transfer: A potential measure for quantifying aortic stenosis severity based on measured data. *Med Eng Phys*. 2021;90:66–81.
9. Dhamala J, Arevalo HJ, Sapp J, et al. Quantifying the uncertainty in model parameters using Gaussian process-based Markov chain Monte Carlo in cardiac electrophysiology. *Med Image Anal*. 2018;48:43–57.
10. Cornuet J, Marin J, Mira A, Robert CP. Adaptive Multiple Importance Sampling. *Scandinavian Journal of Statistics*. 2012;39(4):798–812.
11. Bugallo MF, Elvira V, Martino L, Luengo D, Miguez J, Djuric PM. Adaptive Importance Sampling: The past, the present, and the future. *IEEE Signal Process Mag*. 2017;34(4):60–79.
12. Li W, Lin G. An adaptive importance sampling algorithm for Bayesian inversion with multimodal distributions. *J Comput Phys*. 2015;294:173–90.
13. Černý V. Thermodynamical approach to the traveling salesman problem: An efficient simulation algorithm. *J Optim Theory Appl*. 1985;45(1):41–51.
14. Neal RM. Annealed importance sampling. *Stat Comput*. 2001;11(2):125–39.
15. Beskos A, Crisan D, Jasra A. On the stability of sequential Monte Carlo methods in high dimensions. *The Annals of Applied Probability*. 2014;24(4):1396–445.
16. Kirkels FP, Lie ØH, Cramer MJ, et al. Right Ventricular Functional Abnormalities in Arrhythmogenic Cardiomyopathy: Association With Life-Threatening Ventricular Arrhythmias. *JACC Cardiovasc Imaging*. 2021;14(5):900-910.
17. Marcus FI, McKenna WJ, Sherrill D, et al. Diagnosis of arrhythmogenic right ventricular cardiomyopathy/Dysplasia: Proposed modification of the task force criteria. *Circulation*. 2010;121(13):1533–41.

18. Voigt JU, Pedrizzetti G, Lysyansky P, et al. Definitions for a common standard for 2D speckle tracking echocardiography: consensus document of the EACVI/ASE/Industry Task Force to standardize deformation imaging. *Eur Heart J Cardiovasc Imaging*. 2015;16(1):1–11.
19. Arts T, Delhaas T, Bovendeerd P, Verbeek X, Prinzen FW. Adaptation to mechanical load determines shape and properties of heart and circulation: the CircAdapt model. *Am J Physiol Heart Circ*. 2005;288(4):H1943–54.
20. Lumens J, Delhaas T, Kirn B, Arts T. Three-wall segment (TriSeg) model describing mechanics and hemodynamics of ventricular interaction. *Ann Biomed Eng*. 2009;37(11):2234–55.
21. Walmsley J, Arts T, Derval N, et al. Fast Simulation of Mechanical Heterogeneity in the Electrically Asynchronous Heart Using the MultiPatch Module. *PLoS Comput Biol*. 2015;11:1–23.
22. Freedman D, Diaconis P. On the histogram as a density estimator: L 2 theory. *Zeitschrift für Wahrscheinlichkeitstheorie und Verwandte Gebiete*. 1981;57(4):453–76.
23. Corrado C, Gerbeau JF, Moireau P. Identification of weakly coupled multiphysics problems. Application to the inverse problem of electrocardiography. *J Comput Phys*. 2015;283:271–98.
24. Zenker S. Parallel particle filters for online identification of mechanistic mathematical models of physiology from monitoring data: performance and real-time scalability in simulation scenarios. *J Clin Monit Comput*. 2010;24(4):319–33.
25. Dhamala J, Bajracharya P, Arevalo HJ, et al. Embedding high-dimensional Bayesian optimization via generative modeling: Parameter personalization of cardiac electrophysiological models. *Med Image Anal*. 2020;62:101670.
26. Coveney S, Clayton RH. Fitting two human atrial cell models to experimental data using Bayesian history matching. *Prog Biophys Mol Biol*. 2018;139:43–58.
27. Daly AC, Cooper J, Gavaghan DJ, Holmes C. Comparing two sequential Monte Carlo samplers for exact and approximate Bayesian inference on biological models. *J R Soc Interface*. 2017;14(134):20170340.
28. Camps J, Lawson B, Drovandi C, et al. Inference of ventricular activation properties from non-invasive electrocardiography. *Med Image Anal*. 2021;73:102–43.
29. Davies V, Noè U, Lazarus A, et al. Fast Parameter Inference in a Biomechanical Model of the Left Ventricle by Using Statistical Emulation. *J R Stat Soc Ser C Appl Stat*. 2019;68(5):1555–76.
30. Dhamala J, Arevalo HJ, Sapp J, et al. Spatially Adaptive Multi-Scale Optimization for Local Parameter Estimation in Cardiac Electrophysiology. *IEEE Trans Med Imaging*. 2017;36(9):1966–78.
31. Paun LM, Colebank M, Qureshi U, Olufsen M, Hill N, Husmeier D. MCMC with delayed acceptance using a surrogate model with an application to cardiovascular fluid dynamics. *Proceedings of the International Conference on Statistics: Theory and Applications*. 2019.
32. Lei CL, Ghosh S, Whittaker DG, et al. Considering discrepancy when calibrating a mechanistic electrophysiology model. *Philosophical Transactions of the Royal Society A: Mathematical, Physical and Engineering Sciences*. 2020;378(2173):20190349.
33. Arts T, Lumens J, Kroon W, Delhaas T. Control of Whole Heart Geometry by Intramyocardial Mechano-Feedback: A Model Study. *PLoS Comput Biol*. 2012;8(2):e1002369.
34. van Opbergen CJM, Noorman M, Pfenniger A, et al. Plakophilin-2 Haploinsufficiency Causes Calcium Handling Deficits and Modulates the Cardiac Response Towards Stress. *Int J Mol Sci*. 2019;20(17):4076.

35. Tandri H, Saranathan M, Rodriguez ER, et al. Noninvasive detection of myocardial fibrosis in arrhythmogenic right ventricular cardiomyopathy using delayed-enhancement magnetic resonance imaging. *J Am Coll Cardiol*. 2005;45(1):98–103.
36. Mast TP, Teske AJ, Walmsley J, et al. Right Ventricular Imaging and Computer Simulation for Electro-mechanical Substrate Characterization in Arrhythmogenic Right Ventricular Cardiomyopathy. *J Am Coll Cardiol*. 2016;68(20):2185–97.
37. Haqqani HM, Tschabrunn CM, Betensky BP, et al. Layered Activation of Epicardial Scar in Arrhythmogenic Right Ventricular Dysplasia. *Circ Arrhythm Electrophysiol*. 2012;5(4):796–803.
38. Mast TP, Taha K, Cramer MJ, et al. The Prognostic Value of Right Ventricular Deformation Imaging in Early Arrhythmogenic Right Ventricular Cardiomyopathy. *JACC Cardiovasc Imaging*. 2019;12(3):446–55.
39. Sarvari SI, Haugaa KH, Anfinsen OG, et al. Right ventricular mechanical dispersion is related to malignant arrhythmias: A study of patients with arrhythmogenic right ventricular cardiomyopathy and subclinical right ventricular dysfunction. *Eur Heart J*. 2011;32(9):1089–96.
40. Leren IS, Saberniak J, Haland TF, Edvardsen T, Haugaa KH. Combination of ECG and Echocardiography for Identification of Arrhythmic Events in Early ARVC. *JACC Cardiovasc Imaging*. 2017;10(5):503–13.
41. Lie ØH, Rootwelt-Norberg C, Dejgaard LA, et al. Prediction of Life-Threatening Ventricular Arrhythmia in Patients With Arrhythmogenic Cardiomyopathy: A Primary Prevention Cohort Study. *JACC Cardiovasc Imaging*. 2018;11(10):1377–86.
42. Malik N, Win S, James CA, et al. Right ventricular strain predicts structural disease progression in patients with arrhythmogenic right ventricular cardiomyopathy. *J Am Heart Assoc*. 2020;9(7):e015016.
43. Sarazan RD, Mittelstadt S, Guth B, Koerner J, Zhang J, Pettit S. Cardiovascular Function in Nonclinical Drug Safety Assessment. *Int J Toxicol*. 2011;30(3):272–86.
44. Suga H, Sagawa K. Instantaneous Pressure-Volume Relationships and Their Ratio in the Excised, Supported Canine Left Ventricle. *Circ Res*. 1974;35(1):117–26.
45. Pernot M, Couade M, Mateo P, Crozatier B, Fischmeister R, Tanter M. Real-Time Assessment of Myocardial Contractility Using Shear Wave Imaging. *J Am Coll Cardiol*. 2011;58(1):65–72.
46. El Hajj MC, Viray MC, Tedford RJ. Right Heart Failure. *Cardiol Clin*. 2020;38(2):161–73.
47. Prior D, La Gerche A. Exercise and Arrhythmogenic Right Ventricular Cardiomyopathy. *Heart Lung Circ*. 2020;29(4):547–55.
48. van Loon T, Knackstedt C, Cornelussen R, et al. Increased myocardial stiffness more than impaired relaxation function limits cardiac performance during exercise in heart failure with preserved ejection fraction: a virtual patient study. *Eur Heart J Digital Health*. 2020;1(1):40–50.
49. Mirea O, Pagourelas ED, Duchenne J, et al. Variability and Reproducibility of Segmental Longitudinal Strain Measurement. *JACC Cardiovasc Imaging*. 2018;11(1):15–24.
50. Groeneweg JA, Bhonsale A, James CA, et al. Clinical Presentation, Long-Term Follow-Up, and Outcomes of 1001 Arrhythmogenic Right Ventricular Dysplasia/Cardiomyopathy Patients and Family Members. *Circ Cardiovasc Genet*. 2015;8(3):437–46.
51. Lyon A, Dupuis LJ, Arts T, et al. Differentiating the effects of β -adrenergic stimulation and stretch on calcium and force dynamics using a novel electromechanical cardiomyocyte model. *Am J Physiol Heart Circ*. 2020;319(3):H519–30.



CHAPTER 6

Monitoring of Myocardial Involvement in Early Arrhythmogenic Right Ventricular Cardiomyopathy Across the Age Spectrum

Feddo P. Kirkels, Nick van Osta*, Christine Rootwelt-Norberg, Monica Chivulescu, Tim van Loon, Eivind W Aabel, Anna I Castrini, Øyvind H. Lie, Folkert W. Asselbergs, Tammo Delhaas, Maarten J. Cramer, Arco J. Teske, Kristina H. Haugaa**, Joost Lumens ***

** Shared 1st authorship*

*** Shared last authorship*

J Am Coll Cardiol. 2023;82(9):785-97.

ABSTRACT

Background

Arrhythmogenic right ventricular cardiomyopathy (ARVC) is characterized by fibrofatty replacement of primarily the right ventricular (RV) myocardium, a substrate for life-threatening ventricular arrhythmias (VA). Repeated cardiac imaging of at-risk relatives is important for early disease detection. However, it is not known whether screening should be age-tailored.

Objectives

To assess the need for age-tailoring of follow-up protocols in early ARVC by evaluating myocardial disease progression in different age-groups.

Methods

We divided early-stage ARVC patients and genotype positive relatives without overt structural disease and VA at first evaluation into three groups: <30, 30-50 and ≥ 50 years old. Longitudinal biventricular deformation characteristics were used to monitor disease progression. To link deformation abnormalities to underlying myocardial disease substrates, Digital Twins were created using an imaging-based computational modelling framework.

Results

We included 313 echocardiographic assessments from 82 subjects (57% female, age 39 ± 17 years, 10% probands) during 6.7 ± 3.3 years follow-up. Left ventricular global longitudinal strain slightly deteriorated similarly in all age-groups (0.1%-point per year [95% CI 0.05-0.15]). Disease progression in all age-groups was more pronounced in the RV lateral wall, expressed by worsening in longitudinal strain (0.6%-point per year [95% CI 0.46-0.70]) and local differences in myocardial contractility, compliance and activation delay in the Digital Twin. Six patients experienced VA during follow-up.

Conclusion

Disease progression was similar in all age-groups and sustained VA also occurred in patients >50 years old without overt ARVC phenotype at first evaluation. Unlike recommended by current guidelines, our study suggests that follow-up of ARVC patients and relatives should not stop at older age.

INTRODUCTION

Arrhythmogenic right ventricular cardiomyopathy (ARVC) is a heritable cardiomyopathy characterized by fibrofatty replacement of primarily the right ventricular (RV) myocardium, providing a substrate for potentially life-threatening ventricular arrhythmias (VA).^{1,2} Variable disease expression is found in familial ARVC³, ranging from sudden cardiac death (SCD) in young individuals to a lifelong absence of any phenotype. To prevent SCD in apparently healthy carriers of disease causing genetic variants, early detection of potentially pro-arrhythmic tissue substrates is important to guide follow-up, anti-arrhythmic treatment, and timing of ICD-implantation.

ARVC has an age-related penetrance, whereby patients classically present in the third or fourth decade of life with symptomatic ventricular arrhythmias.³⁻⁷ However, with increased use of genetic testing for ARVC, carriers of a (likely-)pathogenic variant across all age-groups are recognized and included in extensive cardiac screening protocols, including non-invasive cardiac imaging examinations for detection of early disease. Presence and especially progression of functional abnormalities caused by structural disease of myocardial tissue is an important risk marker for occurrence of VA in ARVC.⁸⁻¹³ It is, however, currently not known whether structural disease progression occurs in all age-groups, hampering age-tailored follow-up protocols. In a position statement from 2010, it was suggested that serial screening of relatives can be stopped at the age of 50-60 years, due to completed penetrance.¹⁴ Therefore, we hypothesized that structural progression in early-stage ARVC occurs in early life and midlife, while progression above the age of 50 years old is limited.

Conventional echocardiographic measurements in combination with visual assessment of wall motion abnormalities, as described in the 2010 diagnostic task force criteria (TFC)¹⁵, lack sensitivity for detection of early structural disease substrates in ARVC.^{16,17} Over the past decade, echocardiographic deformation imaging has emerged as a valuable tool for both early detection and prognosis in ARVC.^{8,9,18-22} In this study, we used echocardiographic deformation imaging for monitoring of myocardial disease progression in patients with early-stage ARVC. To create a link between myocardial function and tissue substrates, we combined these clinical deformation imaging data with a recently developed patient-specific computer simulation technology.²³ This technology was used to create a series of Digital Twins of each patient's heart, providing unique insight in the development of regional RV tissue properties underlying the regional myocardial deformation abnormalities. Insight in the evolution of tissue substrates of individual patients may aid better prediction of unfavourable outcome.

By using echocardiographic deformation imaging and the related patient-specific simulations of cardiac mechanics, we aimed to evaluate structural progression in different stages of life in order to assess the need for age-tailoring of follow-up protocols in early-stage ARVC.

METHODS

Study design and population

We included a consecutive primary preventive cohort of ARVC patients and genotype positive family members evaluated at Oslo University Hospital, Rikshospitalet, Norway, between 1997 and 2021 with at least two clinical evaluations. Part of this cohort was reported in previous follow-up studies in ARVC patients.^{10,24} Patients with previous myocardial infarction and congenital heart disease were excluded. To focus on patients with early-stage structural disease, patients that met a major echocardiographic TFC at first evaluation were excluded. We also excluded patients who experienced sustained VA (defined as a documented history of sustained ventricular tachycardia, aborted cardiac arrest, or appropriated ICD therapy) at or prior to first evaluation.

Clinical characteristics were recorded at first evaluation. Subjects were divided into three age-groups (<30 years, 30-50 years and ≥50 years) based on their age at first evaluation, either for complaints or for family screening. Time to first VA was recorded prospectively from time of inclusion. End of observation was cardiac transplantation, death, or last-clinical follow-up by January 1, 2021.

All patients gave written informed consent. The study complied with the declaration of Helsinki and was approved by the Regional Ethical Committee of South-Eastern Norway.

Echocardiography

All available complete echocardiographic examinations in sinus rhythm between inclusion and last clinical follow-up were analysed. First evaluation was defined at the time of first echocardiography on compatible hardware (GE Vivid 7, E9, or E95, EchoPac 203, GE Vingmed, Horten, Norway). Presence of major echocardiographic TFC was determined at first evaluation for the purpose of patient selection. Left ventricular ejection fraction (LVEF) was measured by Simpson's biplane method and speckle tracking deformation imaging of both the LV and RV was performed in all examinations, according to previously described protocols.^{18,21,25,26} We assessed segmental RV deformation patterns in an RV-focused 4-chamber view, whereby a single-wall tracing of the RV free wall was automatically divided into a basal, mid, and apical segment. Timing of pulmonary valve closure was assessed by Doppler traces in the RV outflow tract, obtained in the parasternal short-axis view. The following deformation parameters were measured in each segment: time to onset of shortening (or electromechanical interval), systolic peak strain, and the amount of post-systolic shortening. These parameters were used to classify patients into three subgroups, each presenting with a distinct RV deformation pattern as described in previous studies.^{13,19} In brief, a Type I pattern is normal deformation; a Type II pattern is characterized by delayed onset of shortening, reduced systolic peak strain, and minor post-systolic shortening; and a Type III pattern is characterized by little or no systolic peak strain, predominantly systolic stretching, and major post-systolic shortening (*Central illustration, right upper panel*). The LV global longitudinal strain (GLS) was calculated as the peak negative strain from the averaged regional 16-segment LV model.²¹ RV free wall longitudinal strain (RV_{FW}-LS) was defined as the peak negative strain from the averaged regional RV free wall deformation characteristic. All measurements were performed by a single observer (FK) blinded to clinical information.

Computational simulations

To gain more insight into the course of myocardial disease development in individual patients, we created Digital Twins of the patient's heart at each follow-up, using our previously developed modelling framework.²³ In brief, this framework uses the patient's imaging data to personalize the well-established closed-loop CircAdapt model of the human heart and circulation.²⁷ This results in a series of patient-specific simulations of regional cardiac mechanics and global hemodynamics for each patient.

Besides LV and RV deformation data, this framework uses LV end diastolic volume, LVEF and RV end-diastolic diameter as input. Taking measurement uncertainty into account, the estimated tissue properties are represented as a probability distribution. Three myocardial tissue properties were estimated for each RV segment: contractility, compliance, and mechanical activation delay. Given the interindividual differences in biometrics and loading conditions, we focused on regional heterogeneity of estimated myocardial tissue properties rather than on absolute values. In brief, segmental contractility was defined as the maximum rate of active stress rise, which can be seen as the local tissue level equivalent of the maximum rate of ventricular systolic pressure rise (dp/dt_{max}). Segmental wall compliance was defined as the slope of the end-diastolic myofiber stress-strain relationship at time before first ventricular activation and can be interpreted as the regional tissue equivalent of the slope of the end-diastolic pressure-volume relation. Mechanical activation delay was defined as the time interval between the models intrinsic time of activation and the onset of local active stress development.²³

Statistical analysis

Statistical analyses were performed using IBM SPSS 26.0 (IBM Corp, Armonk, NY, USA) and Stata SE 16.1 (StataCorp LLC, TX, USA). Values were expressed as mean with standard deviation (SD) or, median with interquartile range (IQR), as appropriate, and were compared by Fisher's exact test for dichotomous variables and Kruskal Wallis test for continuous variables. After visually excluding the possibility of non-linear trends, we assessed progression in the three age-groups by entering the echocardiographic deformation parameters into a linear mixed model regression with exchangeable covariance structure and random effects at individual level. P-values were two-sided, and values <0.05 were considered significant.

RESULTS

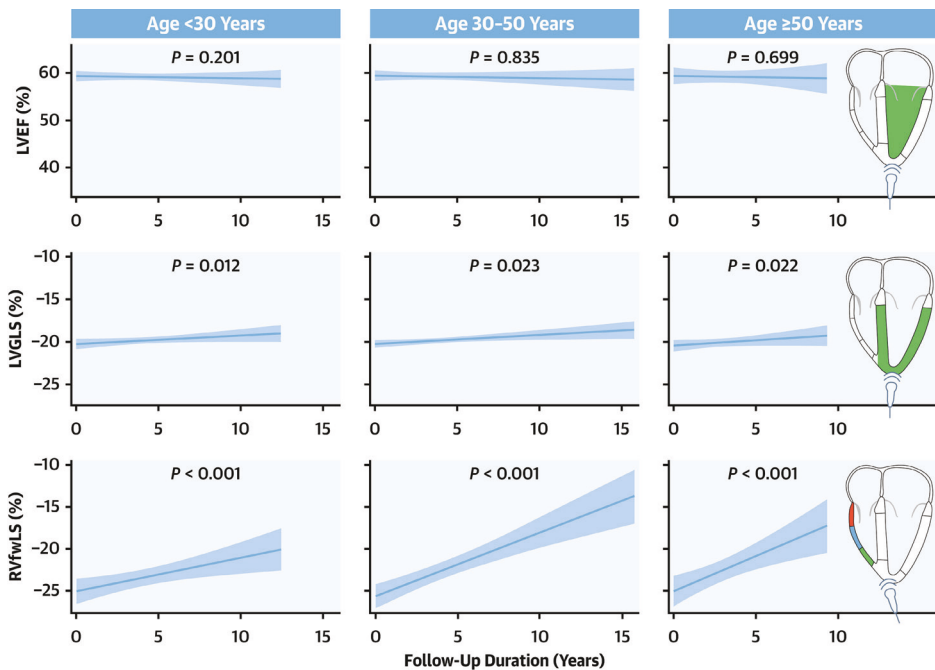
Clinical characteristics

We included 82 early-stage ARVC patients and genotype positive family members (57% female, age 39 ± 17 years, 10% probands, *Table 1*). Of 192 eligible patients, 110 were excluded due to VA or major structural TFC at or prior to first echocardiographic examination, or absence of a follow-up examination (*Supplemental Figure 1*). A (likely-)pathogenic variant was found in 92% of patients, mostly located in the PKP2 gene (84%). During a mean follow-up time of 6.7 ± 3.3 years, 355 echocardiograms were performed (average of 4 exams per patient, range 2 – 9). Forty-two exams were excluded due to inadequate visualization of one or more RV free wall segments ($n=33$), unavailability of raw echo data for deformation analysis ($n=7$), or irregular heart rhythm ($n=2$), leaving 313 exams appropriate for analysis.

Table 1. Baseline characteristics of 82 ARVC patients and family members, comparing three different age-groups

	total (n = 82)	Age <30 (n = 27)	Age 30-50 (n = 32)	Age ≥50 (n = 23)	p-value
Age (years)	39 ± 17	20 ± 6	39 ± 6	60 ± 7	
Female sex, n (%)	47 (57%)	15 (56%)	20 (63%)	12 (52%)	0.723
Proband, n (%)	8 (10%)	0 (0%)	4 (13%)	4 (17%)	0.064
Follow-up time (years)	6.5 ± 3.1	7.1 ± 2.9	6.9 ± 3.5	5.2 ± 2.5	0.109
VA during follow-up, n (%)	6 (7%)	0 (0%)	4 (13%)	2 (9%)	0.197
(Likely-)pathogenic variant, n (%)	75 (92%)	27 (100%)	29 (91%)	19 (83%)	0.077
PKP2, n (%)	69 (84%)	24 (89%)	28 (88%)	17 (74%)	0.326
DSG, n (%)	5 (6%)	2 (7%)	1 (3%)	2 (9%)	0.616
DSP, n (%)	1 (1%)	1 (4%)	0 (0%)	0 (0%)	0.610

Values are mean ± SD, median (IQR), or frequencies (%). Abbreviations: DSG, desmoglein-2 gene; DSP, desmoplakin gene; PKP2, plakophilin-2 gene; VA, life-threatening ventricular arrhythmia.

**Figure 1. Global myocardial disease progression**

Progression of left ventricular (LV) ejection fraction (LVEF), LV global longitudinal strain (LV GLS), and right ventricular free wall longitudinal strain (RV_{FW}LS), separated by age-group. P-values are for progression during follow-up. Deterioration in LVEF was not observed in any of the age-groups, but LV function deteriorated by absolute 0.1%-point per year (95% CI 0.05 to 0.15%-point) worsening of GLS. Deterioration was faster in the RV lateral wall, expressed by a mean worsening of absolute 0.6%-point per year (95% CI 0.46 to 0.70%-point). (Supplemental Table 1)

During follow-up, 6 patients experienced a first sustained VA, after a mean of 4.1 years (range 0.2 – 8.9 years). The mean age at event was 47 years (range 33 – 65 years).

Progression of deformation abnormalities

Both global (Figure 1) and segmental (Figure 2) deformation characteristics deteriorated during follow-up in all three age-groups. Deterioration in LVEF was not observed in any of the age-groups (-0.03% per year [95% CI -0.16 to 0.09]). However, LV function measured by LV GLS deteriorated slightly in all three age-groups by an average of 0.1%-point per year (95% CI 0.05 to 0.15%-point). Deterioration was more pronounced in the RV lateral wall in all age-groups, expressed by a mean worsening in $RV_{FW}LS$ of 0.6%-point per year (95% CI 0.46 to 0.70%-point). The three segmental deformation characteristics used to classify RV deformation type showed that the basal segment was most impaired in all age-groups, whereby an apex-to-base gradient was maintained during follow-up (Figure 2). When displaying progression of the deformation types during follow-up (Figure 3), the deformation pattern of the basal segment was most frequently impaired (type II or III). Progression to a more abnormal deformation pattern occurred in all age-groups, whereby the pattern in the basal segment deteriorated in about half of the cases and in the mid segment in about one third. Even in some subjects >50 years of age with normal RV deformation at first evaluation, progression towards abnormal deformation patterns was evident. Deformation in the apical segment was normal in most cases, and progression to an abnormal apical deformation pattern was rare. Yearly progression rates and mean values at inclusion and last follow-up are provided in Supplemental Table 1.

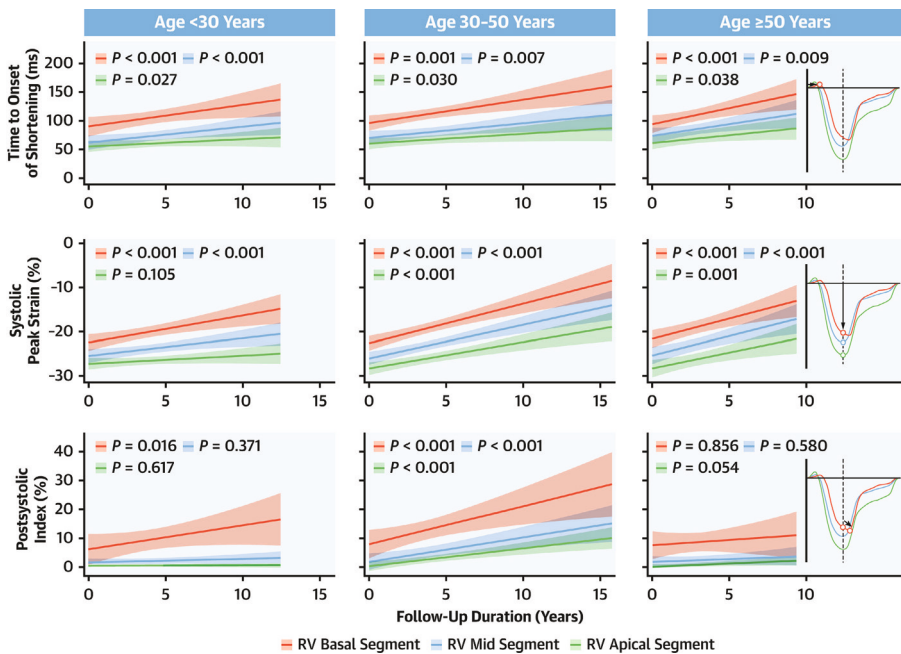


Figure 2. Segmental myocardial disease progression

Progression of segmental deformation parameters of the right ventricle (RV), separated by age-group. P-values are for progression during follow-up. The basal segment was most impaired in all age-groups, whereby an apex-to-base gradient was maintained during follow-up. (Supplemental Table 1)

When focusing on fulfilment of the 2010 TFC¹⁵, 16 subjects progressed towards a minor or major criterion for structural abnormalities during follow-up. All but one already showed abnormal deformation patterns before, or at the moment of TFC adjudication.

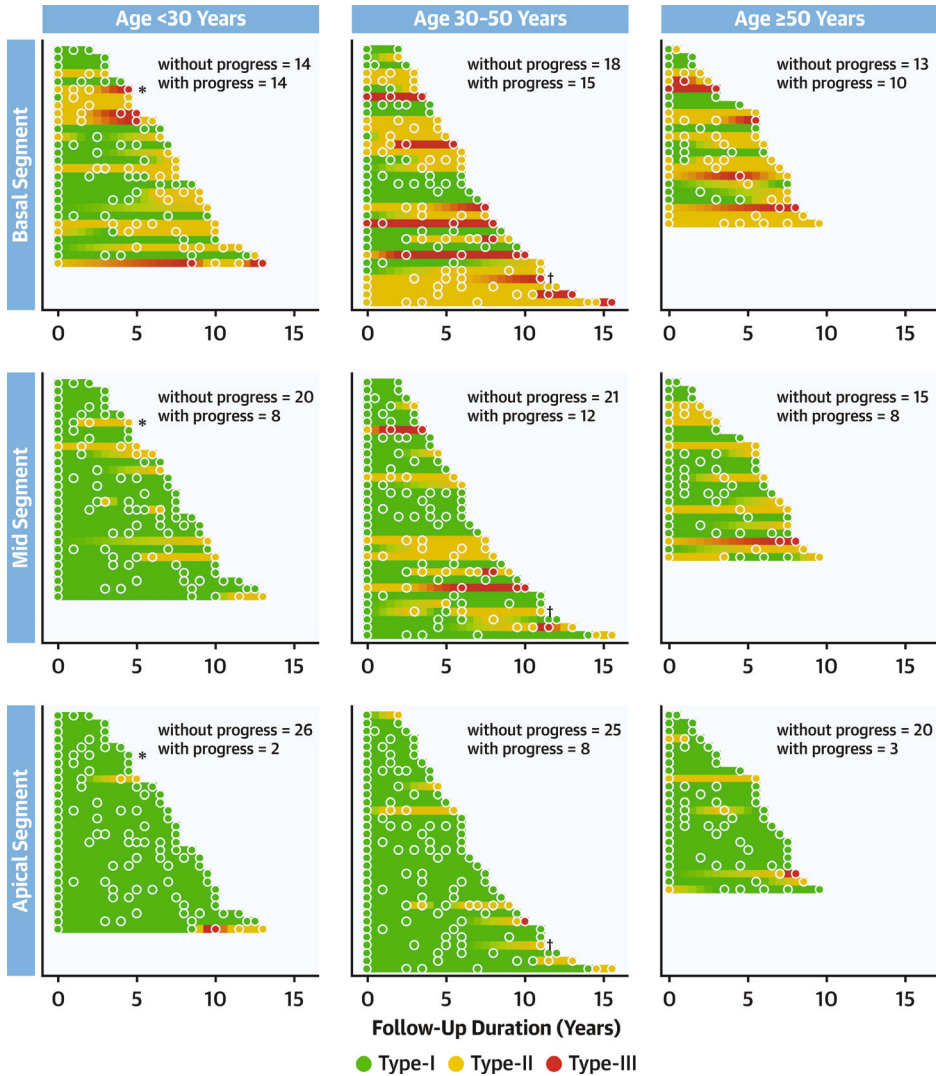


Figure 3. Progression of RV deformation patterns

Progression of right ventricular (RV) deformation types in the three RV free wall segments, separated by age-group. The deformation pattern of the basal segment was most frequently impaired (type II or III). Progression to a more abnormal deformation pattern occurred in all age-groups, whereby the pattern in the basal segment deteriorated in about half of the cases and in the mid segment in about one third. Deformation in the apical segment was normal in most cases, and progression to an abnormal apical deformation pattern was less likely. The * indicates case study 1 and ** indicates case study 2 as displayed in Figure 4.

Deformation characteristics of patients with ventricular arrhythmia

The 6 patients who experienced sustained VA during follow-up all showed abnormal RV deformation patterns at first evaluation. In the basal segment of the RV free wall, 4 patients showed a type II pattern and 2 patients a type III pattern. During follow-up, all of them progressed to a type III pattern. The small size of this subgroup prevents comparative analyses between subjects with and without VA during follow-up.

Progression of modelled RV tissue properties

To illustrate the application of longitudinal monitoring of myocardial disease on a patient-specific level, we first provide two representative case studies of subjects included in the cohort.

Patient 1 was a 20-year-old female followed in the outpatient department during 4.3 years (*Figure 4A*). At first evaluation, RV deformation was already slightly abnormal in the basal segment. During follow-up, the deformation pattern of especially the basal segment and to a lesser extent the mid segment became increasingly abnormal with strongly reduced peak strain. In the Digital Twin, it was estimated that the heterogeneity relied on mostly reduced contractility and only slightly on reduced compliance.

Patient 2 was a 36-year-old female who experienced sustained VA 2.9 years after first evaluation (*Figure 4B*). During the first examination, RV deformation was slightly abnormal in the basal segment, with delayed onset of shortening, slightly reduced peak strain and mild post-systolic shortening. During follow-up, deformation patterns became increasingly abnormal in all RV segments, whereby the basal pattern was most affected. This apex-to-base heterogeneity was expressed in the tissue substrate in the Digital Twin as well. Heterogeneity in estimated RV tissue properties was first observed in the activation delay and later also in contractility and compliance.

The increasing heterogeneity of estimated tissue properties within the RV free wall was also evident on a group level in all three age-groups (*Figure 5, Supplemental table 2*).

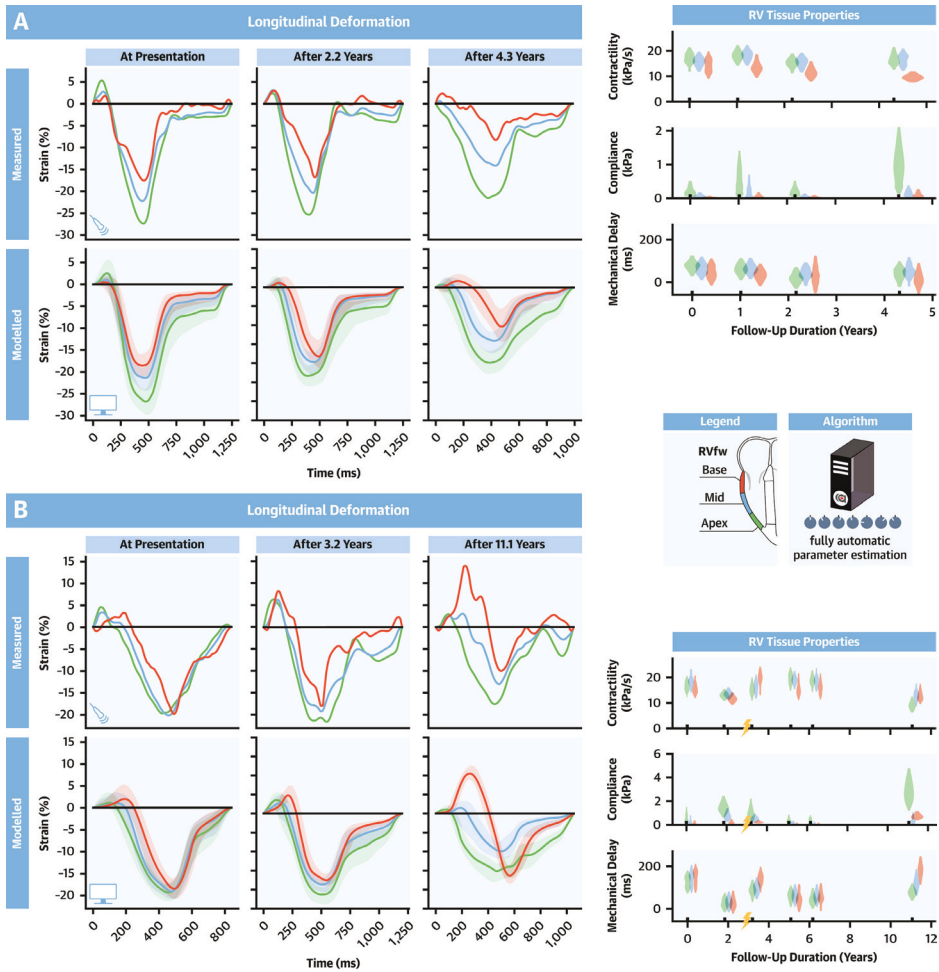


Figure 4. Myocardial disease progression in two patients with early ARVC

Panel A, case study 1. This 20-year-old patient was followed in the outpatient department during 4.3 years. At first evaluation, RV deformation was slightly abnormal in the basal segment. During follow-up, the deformation pattern of especially the basal segment and to a lesser extent the mid segment became increasingly abnormal with strongly reduced peak strain. In the Digital Twin, it was estimated that the heterogeneity relied on mostly reduced contractility and a little reduced compliance. **Panel B**, case study 2. This 36-year-old patient experienced a sustained ventricular arrhythmia 2.9 years after the first evaluation (yellow lightning bolt). During the first examination, RV deformation was slightly abnormal in the basal segment, with delayed onset of shortening, slightly reduced peak strain and mild post-systolic shortening. During follow-up, deformation patterns became increasingly abnormal in all RV segments, whereby the basal pattern was most affected (black panels). The apex-to-base heterogeneity was also expressed in the estimated RV tissue properties in the Digital Twin (panels on the right). Heterogeneity was first observed in the mechanical activation delay and later also in contractility and compliance.

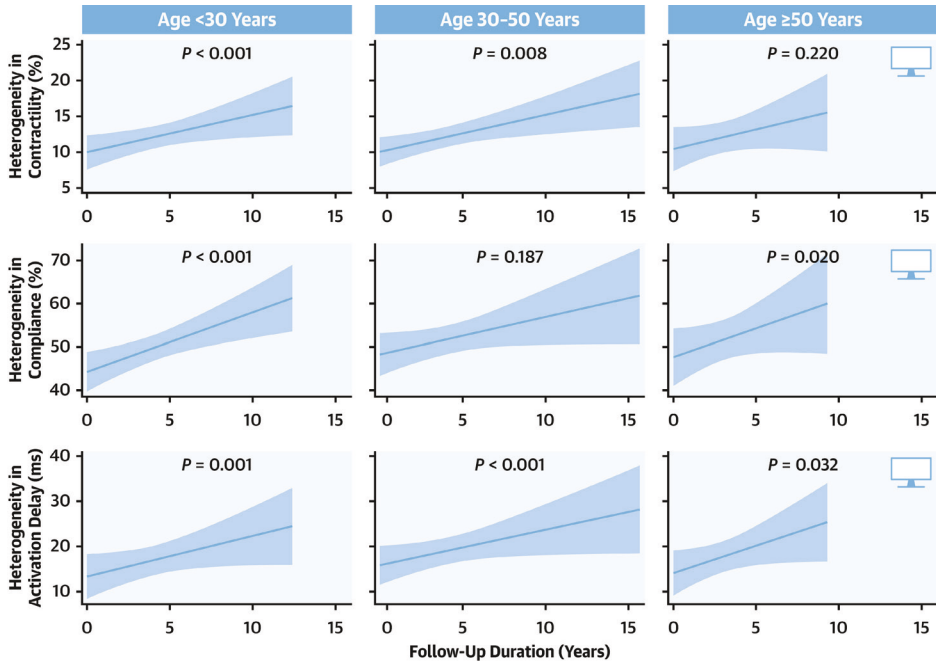


Figure 5. Progression of myocardial disease substrates in the Digital Twin

Progression of heterogeneity in estimated RV tissue properties between the three RV free wall segments, separated by age-group. A clear increase in heterogeneity was seen for all estimated RV tissue properties in the different age-groups. (Supplemental Table 2)

DISCUSSION

By monitoring myocardial disease progression in early ARVC, we found that LV GLS slightly deteriorated and especially RV deformation abnormalities progressed over time in all investigated age-groups. Digital Twins of the patient's hearts were created to link deformation abnormalities to underlying myocardial disease substrates, revealing local differences in contractility, compliance and mechanical activation delay. Based on our findings, age-based tailoring of follow-up intervals would not be indicated. On the contrary, progression continued throughout all age-groups and was in multiple cases followed by sustained VA, indicating the need for lifelong follow-up.

Progression of deformation abnormalities

Our study showed that deformation imaging is a useful technique for monitoring of myocardial disease progression in ARVC. In a previous study on serial evaluation of ARVC relatives, one-third showed electrical progression during a 4-year follow-up and structural progression was rare.²⁸ However, structural progression was measured by increase in 2010 TFC, which lack sensitivity for detection of early disease manifestation.¹⁷ We have previously shown that deformation imaging is superior for detection of early disease as compared to 2010 TFC.²⁹ Deformation analyses in the current study showed that abnormalities were often present before fulfilment of structural 2010 TFC. Progression of abnormalities occurred in all three age-groups in both

the LV and RV, but progression was more pronounced in the RV. This is in line with expectations, since primarily the RV myocardium is affected by fibrofatty replacement in ARVC.^{1,2} From *Figure 3* it can be appreciated that RV deformation types are a robust classification method during serial analyses, enabling detection of disease progression over time. This confirms that once abnormal, RV deformation patterns remain abnormal, as was previously shown in another cohort of ARVC patients with two sequential echocardiographic examinations.³⁰ Our segmental analysis consistently showed that all deformation parameters were worse in the basal segment and progressed over time from base to apex. This is in line with previous studies in other cohorts, which showed that the subtricuspid segment of the RV lateral wall is the earliest and most severely affected area in ARVC.^{13,19,30,31}

It is conceivable that longitudinal strain also slightly deteriorates over time in healthy individuals. While this has been shown for LV GLS³², the deterioration is small and probably not clinically relevant in the RV free wall³³. Importantly, the prolonged time to onset of shortening and post-systolic shortening, as observed in ARVC patients, are not observed in physiologic aging of the myocardium.

Progression of RV tissue substrates

Definitive diagnosis of ARVC is based on the presence of transmural fibro-fatty replacement of RV myocardium at biopsy, autopsy, or surgery.^{1,34} Since histology is not available in the vast majority of patients, TFC guide the diagnosis of ARVC.¹⁵ The use of personalized computational modelling can give more insight in the patient's underlying myocardial disease substrate through the estimated tissue properties being directly related to intrinsic myocardial function and composition.^{20,23,35} In the current study, we applied this Digital Twin approach on serial echocardiographic examinations in a large cohort to gain insight into the evolution of early myocardial disease substrates in ARVC. On a group level, we found increasing heterogeneity of both contractility, compliance, and activation delay in all three age-groups, indicating the progression of local RV tissue substrates. We presented two case studies of patients from the cohort. The first (*Figure 4A*) showed progression of deformation abnormalities, which were, according to estimations in the Digital Twin, caused by decreased contractility and to a lesser degree decreased compliance. The patient had no VA during follow-up. In the second case (*Figure 4B*), the patient experienced VA while having no overt structural phenotype according to conventional TFC. RV deformation abnormalities preceded the arrhythmic event and heterogeneity was most pronounced in the activation delay. These cases illustrate the potential use of the modelling approach on a patient-specific basis, as specific estimated tissue abnormalities which are present prior to an arrhythmic event may have predictive value. The number of events in this study on subjects with early-stage ARVC was, however, too low to draw any firm conclusions from these findings.

Clinical implications

Prevention of SCD is the most important goal of ARVC screening. Prior studies report SCD rates up to 23% at presentation, mainly in young ARVC patients.^{3,4} Cascade genetic screening provides clinicians with an increasing group of patients at risk of severe arrhythmic events, but without an overt phenotype at first evaluation. Since there is a clear correlation between structural disease expression and the risk of arrhythmias, these patients undergo frequent cardiac evaluations to detect early signs of disease penetrance. A recent expert consensus statement recommended clinical evaluation of relatives at risk with 12-lead ECG, ambulatory

ECG and cardiac imaging every 1-3 years starting at 10-12 years of age.⁷ In a cohort study of ARVC patients who presented ≥ 50 years of age, ventricular tachycardia and pre-existing structural abnormalities were common, but SCD was not observed during follow-up.⁵ The latter raises the question at what age you can stop the frequent and demanding screening of ARVC patients and relatives. In a position statement from 2010, it was suggested that serial screening of relatives can be stopped at the age of 50-60 years, due to completed penetrance.¹⁴

While *conventional* echocardiographic TFC lack sensitivity for detection of early disease substrates^{28,29}, this study supports the use of *deformation imaging* as a robust method for monitoring of ARVC patients and family members in the outpatient department. Our study showed similar patterns of myocardial disease progression in young, middle-aged, and older patients without an overt structural ARVC phenotype at first evaluation. These findings contradict the statement of completed penetrance after 50 years of age and do not support age-tailoring of cardiac imaging follow-up intervals at the outpatient department. Since other studies reported low risks of SCD in older relatives, structural progression in this group may be less alarming when compared to progression in younger relatives. However, of the 6 cases in which progression was followed by VA, two experienced a first event at the age of 64 and 65 years.

Deformation imaging provides an important additional tool for detection of ARVC disease manifestation and progression in an early stage, but should always be used in a multimodality setting, as described in the 2019 expert consensus statement⁷. When adhering to the recommended follow-up interval of 1-3 years, normal RV deformation can support clinicians in applying the longer interval whereas development of deformation abnormalities can be a warrant to reevaluate the patient earlier.

Based on deformation imaging characteristics, the Digital Twin can translate myocardial behaviour to valuable information on regional tissue properties. This can potentially be used to individualize risk assessment and to link genotype to phenotype. We have developed this method in subjects at risk of ARVC, but in the current era where family screening and genetic testing is increasingly performed, deformation imaging³⁶ and Digital Twins can be easily applied in other cardiomyopathies as well.

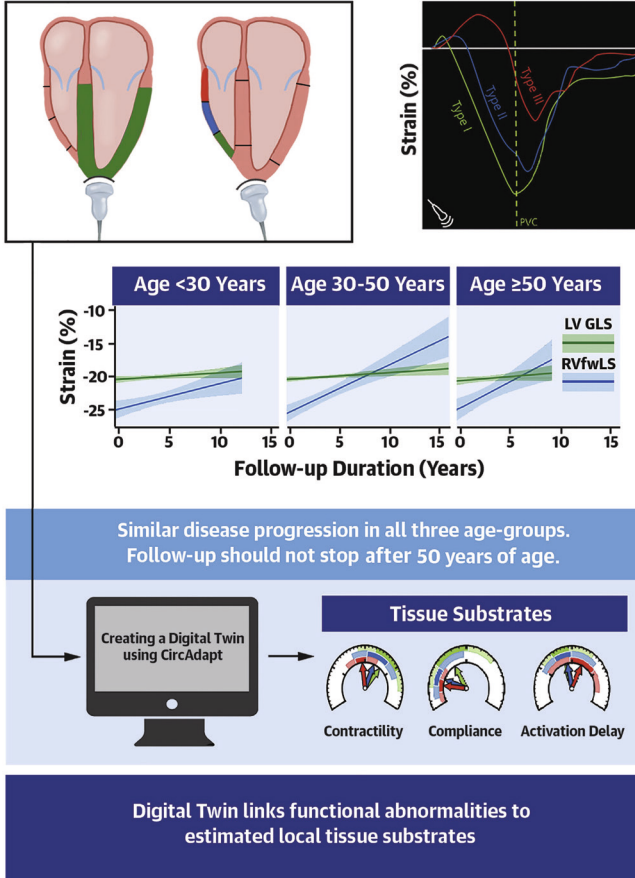
Limitations

The single-center design was a limitation to this study. Due to the high prevalence of patients with (likely-) pathogenic variants in the PKP2 gene, the generalizability to patient populations with other dominating variants is uncertain. Future multicenter cohort studies should perform a genotype-specific approach to test the generalizability to for instance DSP variant carriers, in which LV disease manifestation is often more pronounced.⁷

Since we excluded patients with overt structural disease or sustained VA at first evaluation, our cohort had a lower event rate than the average ARVC cohort. This resulted in a group of 6 patients who experienced sustained VA during follow-up, which is insufficient to search for risk factors in deformation imaging or estimated tissue properties on a group level.

CENTRAL ILLUSTRATION: Monitoring Age-Related Penetrance in Arrhythmogenic Right Ventricular Cardiomyopathy

82 Early Arrhythmogenic Right Ventricular Cardiomyopathy Subjects
7 years mean follow-up duration
313 echocardiographic assessments



Kirkels FP, et al. *J Am Coll Cardiol.* 2023;82(9):785-797.

Central Illustration. Monitoring age-related penetrance in ARVC

Patients with early arrhythmogenic right ventricular cardiomyopathy (ARVC) and genotype positive family members are frequently screened for structural abnormalities which are strongly associated with life-threatening ventricular arrhythmias. To find out whether this extensive screening can be stopped at older age, we performed biventricular deformation analyses in 313 longitudinal echocardiograms of 82 early ARVC patients and family members at risk divided over three age-groups. Digital Twins of the patients' hearts were created to reveal the local tissue substrates underlying myocardial deformation abnormalities. We found similar patterns of progression in both young, middle-aged and older subjects and first life-threatening arrhythmias still occurred in patients >50 years old, suggesting that follow-up of early ARVC patients and family members should not stop at older age.

CONCLUSION

ARVC disease progressed similarly in all age-groups of patients presenting with early ARVC disease during 7 years of follow-up. We created Digital Twins of the patients' hearts to link deformation abnormalities to underlying myocardial disease substrates, revealing local differences in contractility, compliance and mechanical activation delay. Potentially life-threatening arrhythmias also occurred in patients >50 years old without overt ARVC phenotype at first evaluation, with the oldest patient aged 65 years. Contradicting previously published statements, our study suggests that follow-up of ARVC patients and family members should not stop at older age.

CLINICAL PERSPECTIVES

Competency in Patient Care and Procedural Skills

In patients with arrhythmogenic right ventricular cardiomyopathy (ARVC) fibrofatty replacement of right ventricular myocardium progresses similarly across the age spectrum, and the initial presentation of life-threatening arrhythmias may emerge at any age, suggesting that clinical surveillance of patients with ARVC and their family members should not stop at older age.

Translational Outlook

The use of cascade genetic screening is exposing an expanding population at risk of ARVC. Echocardiographic deformation imaging is useful for monitoring of disease progression. Insight into the evolution of tissue substrates of individual patients may improve prediction of adverse outcomes.

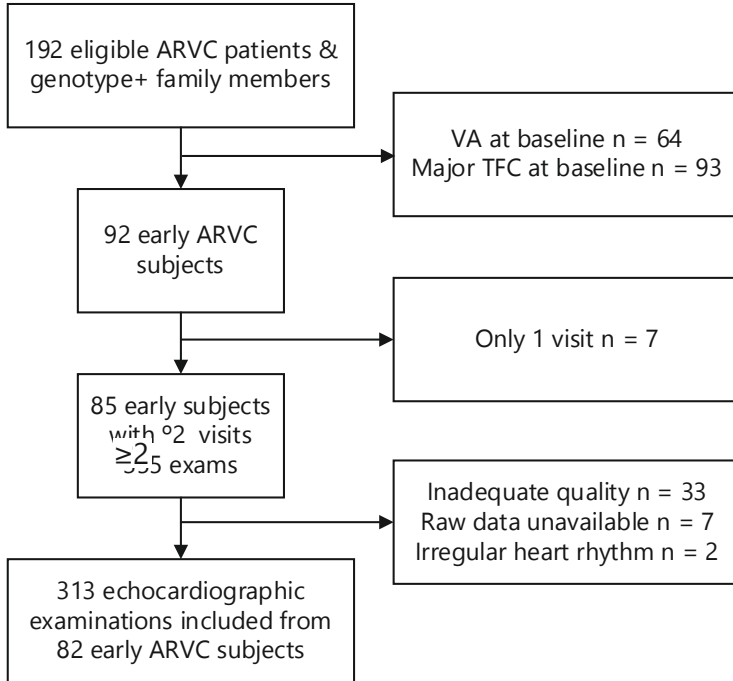
REFERENCES

1. Thiene G, Nava A, Corrado D, Rossi L, Pennelli N. Right Ventricular Cardiomyopathy and Sudden Death in Young People. *N Engl J Med*. 1988;318(3):129–33.
2. Basso C, Corrado D, Marcus FI. Arrhythmogenic right ventricular cardiomyopathy. *Lancet*. 2009;(373):1289–300.
3. Groeneweg JA, Bhonsale A, James CA, et al. Clinical Presentation, Long-Term Follow-Up, and Outcomes of 1001 Arrhythmogenic Right Ventricular Dysplasia/Cardiomyopathy Patients and Family Members. *Circ Cardiovasc Genet*. 2015;8(3):437–46.
4. Dalal D, Nasir K, Bomma C, et al. Arrhythmogenic right ventricular dysplasia: A United States experience. *Circulation*. 2005;12(25):3823–32.
5. van der Pols MJ, Mast TP, Loh P, et al. Clinical characterisation and risk stratification of patients with arrhythmogenic right ventricular dysplasia/cardiomyopathy ≥ 50 years of age. *Netherlands Heart J*. 2016;24(12):740–747.
6. Sen-Chowdry S, Syrris P, Ward D, Asimaki A, Sevdalis E, McKenna WJ. Clinical and genetic characterization of families with arrhythmogenic right ventricular dysplasia/cardiomyopathy provides novel insights into patterns of disease expression. *Circulation*. 2007;115(13):1710–20.
7. Towbin JA, McKenna WJ, Abrams DJ, et al. 2019 HRS expert consensus statement on evaluation, risk stratification, and management of arrhythmogenic cardiomyopathy. *Heart Rhythm*. 2019;16(11):e301–72.
8. Leren IS, Saberniak J, Haland TF, Edvardsen T, Haugaa KH. Combination of ECG and Echocardiography for Identification of Arrhythmic Events in Early ARVC. *JACC Cardiovasc Imaging*. 2017 May;10(5):503–13.
9. Lie ØH, Rootwelt-Norberg C, Dejgaard LA, et al. Prediction of Life-Threatening Ventricular Arrhythmia in Patients With Arrhythmogenic Cardiomyopathy: A Primary Prevention Cohort Study. *JACC Cardiovasc Imaging*. 2018;11(10):1377–86.
10. Chivulescu M, Lie ØH, Popescu BA, et al. High penetrance and similar disease progression in probands and in family members with arrhythmogenic cardiomyopathy. *Eur Heart J*. 2020;41(14):1401–1410.
11. Saguner AM, Vecchiati A, Baldinger SH, et al. Different prognostic value of functional right ventricular parameters in arrhythmogenic right ventricular cardiomyopathy/dysplasia. *Circ Cardiovasc Imaging*. 2014;7(2):230–9.
12. Pinamonti B, Dragos AM, Pyxaras SA, et al. Prognostic predictors in arrhythmogenic right ventricular cardiomyopathy: Results from a 10-year registry. *Eur Heart J*. 2011;32(9):1105–13.
13. Kirkels FP, Lie ØH, Cramer MJ, et al. Right Ventricular Functional Abnormalities in Arrhythmogenic Cardiomyopathy: Association With Life-Threatening Ventricular Arrhythmias. *JACC Cardiovasc Imaging*. 2021;14(5):900–910.
14. Charron P, Arad M, Arbustini E, et al. Genetic counselling and testing in cardiomyopathies: A position statement of the European Society of Cardiology Working Group on Myocardial and Pericardial Diseases. *Eur Heart J*. 2010;31(22):2715–28.
15. Marcus FI, McKenna WJ, Sherrill D, et al. Diagnosis of arrhythmogenic right ventricular cardiomyopathy/Dysplasia: Proposed modification of the task force criteria. *Circulation*. 2010;121(13):1533–41.
16. Borgquist R, Haugaa KH, Gilljam T, et al. The diagnostic performance of imaging methods in ARVC using the 2010 task force criteria. *Eur Heart J Cardiovasc Imaging*. 2014;15(11):1219–25.

17. Bosman LP, Cadrin-Tourigny J, Bourfiss M, et al. Diagnosing arrhythmogenic right ventricular cardiomyopathy by 2010 task force criteria: Clinical performance and simplified practical implementation. *Europace*. 2020;22(5):787–96.
18. Teske AJ, Cox MGPJ, Te Riele ASJM, et al. Early detection of regional functional abnormalities in asymptomatic ARVD/C gene carriers. *J Am Soc Echocardiogr*. 2012;25(9):997–1006.
19. Mast TP, Teske AJ, Walmsley J, et al. Right Ventricular Imaging and Computer Simulation for Electro-mechanical Substrate Characterization in Arrhythmogenic Right Ventricular Cardiomyopathy. *J Am Coll Cardiol*. 2016;68(20):2185–97.
20. Mast TP, Taha K, Cramer MJ, et al. The Prognostic Value of Right Ventricular Deformation Imaging in Early Arrhythmogenic Right Ventricular Cardiomyopathy. *JACC Cardiovasc Imaging*. 2019;12(3):446–55.
21. Voigt JU, Pedrizzetti G, Lysyansky P, et al. Definitions for a common standard for 2D speckle tracking echocardiography: consensus document of the EACVI/ASE/Industry Task Force to standardize deformation imaging. *Eur Heart J Cardiovasc Imaging*. 2015;16(1):1–11.
22. Malik N, Win S, James CA, et al. Right ventricular strain predicts structural disease progression in patients with arrhythmogenic right ventricular cardiomyopathy. *J Am Heart Assoc*. 2020;9(7):e015016.
23. Osta N van, Kirkels FP, Loon T van, et al. Uncertainty Quantification of Regional Cardiac Tissue Properties in Arrhythmogenic Cardiomyopathy Using Adaptive Multiple Importance Sampling. *Frontiers in Physiology*. 2021;12:738926.
24. Rootwelt-Norberg C, Lie ØH, Chivulescu M, et al. Sex differences in disease progression and arrhythmic risk in patients with arrhythmogenic cardiomyopathy. *Europace*. 2021;23(7):1084–1091.
25. Badano LP, Koliass TJ, Muraru D, et al. Standardization of left atrial, right ventricular, and right atrial deformation imaging using two-dimensional speckle tracking echocardiography: A consensus document of the EACVI/ASE/Industry Task Force to standardize deformation imaging. *Eur Heart J Cardiovasc Imaging*. 2018;19(6):591–600.
26. Mast TP, Teske AJ, Te Riele AS, et al. Prolonged Electromechanical Interval Unmasks Arrhythmogenic Right Ventricular Dysplasia/Cardiomyopathy in the Subclinical Stage. *J Cardiovasc Electrophysiol*. 2016;27(3):303–14.
27. Walmsley J, Arts T, Derval N, et al. Fast Simulation of Mechanical Heterogeneity in the Electrically Asynchronous Heart Using the MultiPatch Module. *PLoS Computational Biology*. 2015;11:1–23.
28. Te Riele ASJM, James CA, Rastegar N, et al. Yield of serial evaluation in at-risk family members of patients with ARVD/C. *J Am Coll Cardiol*. 2014;64(3):293–301.
29. Kirkels FP, Bosman LP, Taha K, et al. Improving Diagnostic Value of Echocardiography in Arrhythmogenic Right Ventricular Cardiomyopathy Using Deformation Imaging. *JACC Cardiovasc Imaging*. 2021;14(12):2481–2483.
30. Taha K, Mast TP, Cramer MJ, et al. Evaluation of Disease Progression in Arrhythmogenic Cardiomyopathy: The Change of Echocardiographic Deformation Characteristics Over Time. *JACC Cardiovasc Imaging*. 2019;13(2):631–4.
31. Te Riele ASJM, James CA, Philips B, et al. Mutation-positive arrhythmogenic right ventricular dysplasia/cardiomyopathy: The triangle of dysplasia displaced. *J Cardiovasc Electrophysiol*. 2013;24(12):1311–20.
32. D'Elia N, Caselli S, Kosmala W, et al. Normal Global Longitudinal Strain. *JACC Cardiovasc Imaging*. 2020;13(1):167–9.

33. Muraru D, Haugaa K, Donal E, et al. Right ventricular longitudinal strain in the clinical routine: a state-of-the-art review. *Eur Heart J Cardiovasc Imaging*. 2022;23(7):898–912.
34. Basso C, Burke M, Fornes P, et al. Guidelines for autopsy investigation of sudden cardiac death. *Virchows Archiv*. 2008;452(1):11–8.
35. Van Osta N, Kirkels FP, Lyon A, et al. Electromechanical substrate characterization in arrhythmogenic cardiomyopathy using imaging-based patient-specific computer simulations. *Europace*. 2021;23(Suppl1):i153-i160.
36. Taha K, Kirkels FP, Teske AJ, et al. Echocardiographic Deformation Imaging for Early Detection of Genetic Cardiomyopathies: JACC Review Topic of the Week. *J Am Coll Cardiol*. 2022;79(6):594-608.

SUPPLEMENTARY MATERIAL



Supplemental Figure 1. Flowchart of inclusion

Supplemental Table 1. Progression of deformation parameters

	At inclusion (n=82) (SD)	Progression rate, 1 year (SE)	At last follow-u (n=82) (SD)	p-value for progression
LVEF, %	59 (4)	0.0 (0.1)	59 (4)	0.603
Age 0-30	59 (4)	-0.1 (0.1)	59 (4)	0.201
Age 30-50	58 (4)	0.0 (0.1)	59 (4)	0.835
Age 50+	58 (6)	-0.1 (0.2)	59 (5)	0.699
LV GLS, %, n=313	-20.1 (1.9)	0.10 (0.02)	-19.6 (2.1)	<0.001
Age 0-30, n=108	-20.1 (1.8)	0.10 (0.04)	-19.6 (2.3)	0.012
Age 30-50, n=132	-20.0 (2.1)	0.08 (0.04)	-19.6 (1.8)	0.023
Age 50+, n=73	-20.1 (2.0)	0.15 (0.06)	-19.7 (2.3)	0.022
RV _{FW} LS, %	-25.3 (6.1)	0.58 (0.06)	-21.5 (5.9)	<0.001
Age 0-30	-25.6 (5.8)	0.43 (0.10)	-22.2 (5.4)	<0.001
Age 30-50	-25.6 (6.0)	0.65 (0.10)	-21.1 (6.5)	<0.001
Age 50+	-24.7 (6.6)	0.70 (0.13)	-21.2 (5.8)	<0.001
Peak systolic strain base	-22.8 (7.5)	0.71 (0.06)	-17.4 (6.5)	<0.001
Age 0-30	-23.2 (7.6)	0.67 (0.11)	-17.8 (6.6)	<0.001
Age 30-50	-23.0 (7.6)	0.70 (0.10)	-17.2 (6.9)	<0.001
Age 50+	-22.0 (7.6)	0.84 (0.13)	-17.2 (6.1)	<0.001
Peak systolic strain mid	-25.8 (6.3)	0.58 (0.07)	-21.8 (6.1)	<0.001
Age 0-30	-26.0 (6.0)	0.41 (0.10)	-22.6 (5.6)	<0.001
Age 30-50	-26.2 (6.2)	0.67 (0.10)	-21.6 (6.6)	<0.001
Age 50+	-25.0 (6.9)	0.72 (0.14)	-21.3 (6.2)	<0.001
Peak systolic strain apex	-27.5 (5.9)	0.43 (0.08)	-25.4 (6.0)	<0.001
Age 0-30	-27.6 (4.9)	0.19 (0.12)	-26.4 (4.6)	0.105
Age 30-50	-27.7 (6.0)	0.56 (0.12)	-24.7 (6.9)	<0.001
Age 50+	-27.3 (7.0)	0.59 (0.18)	-25.3 (6.3)	0.001
Onset base (ms)	96 (56)	4.1 (0.7)	122(55)	<0.001
Age 0-30	94 (64)	4.4 (1.2)	119 (63)	<0.001
Age 30-50	96 (59)	3.4 (1.0)	122 (54)	0.001
Age 50+	98 (45)	5.6 (1.3)	127 (50)	<0.001
Onset mid (ms)	69 (47)	3.3 (0.7)	87 (50)	<0.001
Age 0-30	56 (43)	3.7 (1.0)	84 (44)	<0.001
Age 30-50	73 (54)	3.0 (1.1)	89 (55)	0.007
Age 50+	80 (38)	3.7 (1.4)	90 (49)	0.009
Onset apex (ms)	58 (36)	2.1 (0.6)	73 (41)	<0.001
Age 0-30	51 (35)	2.2 (1.0)	67 (38)	0.027
Age 30-50	57 (36)	1.9 (0.9)	76 (47)	0.030
Age 50+	69 (34)	2.5 (1.2)	76 (35)	0.038
Post-systolic index base	7.9 (15.4)	0.76 (0.17)	11.6 (18.9)	<0.001
Age 0-30	5.7 (17.5)	0.60 (0.25)	11.0 (20.4)	0.016
Age 30-50	9.0 (15.4)	1.10 (0.27)	14.4 (20.6)	<0.001
Age 50+	8.9 (13.0)	0.07 (0.38)	8.5 (14.2)	0.856

Supplemental Table 1. Progression of deformation parameters (continued)

	At inclusion (n=82) (SD)	Progression rate, 1 year (SE)	At last follow-u (n=82) (SD)	p-value for progression
Post-systolic index mid	2.05 (5.3)	0.45 (0.12)	4.38 (12.7)	<0.001
Age 0-30	1.38 (5.2)	0.09 (0.10)	2.24 (4.2)	0.371
Age 30-50	2.10 (4.8)	0.85 (0.23)	7.15 (18.6)	<0.001
Age 50+	2.78 (6.1)	0.13 (0.23)	3.04 (8.1)	0.580
Post-systolic index apex	0.50 (1.2)	0.34 (0.07)	2.23 (7.2)	<0.001
Age 0-30	0.39 (0.8)	0.02 (0.03)	0.57 (1.5)	0.617
Age 30-50	0.68 (1.4)	0.63 (0.14)	4.30 (10.4)	<0.001
Age 50+	0.36 (1.3)	0.22 (0.12)	1.31 (4.9)	0.054

Values at inclusion and last follow-up are mean (SD). Yearly progression rate with standard errors (SE). P-values for progression are calculated by linear mixed model statistics with exchangeable covariance structure and random intercept. Abbreviations: LVEF, left ventricular ejection fraction; LV GLS, left ventricular global longitudinal strain; RV_{FW}LS, right ventricular free wall longitudinal strain.

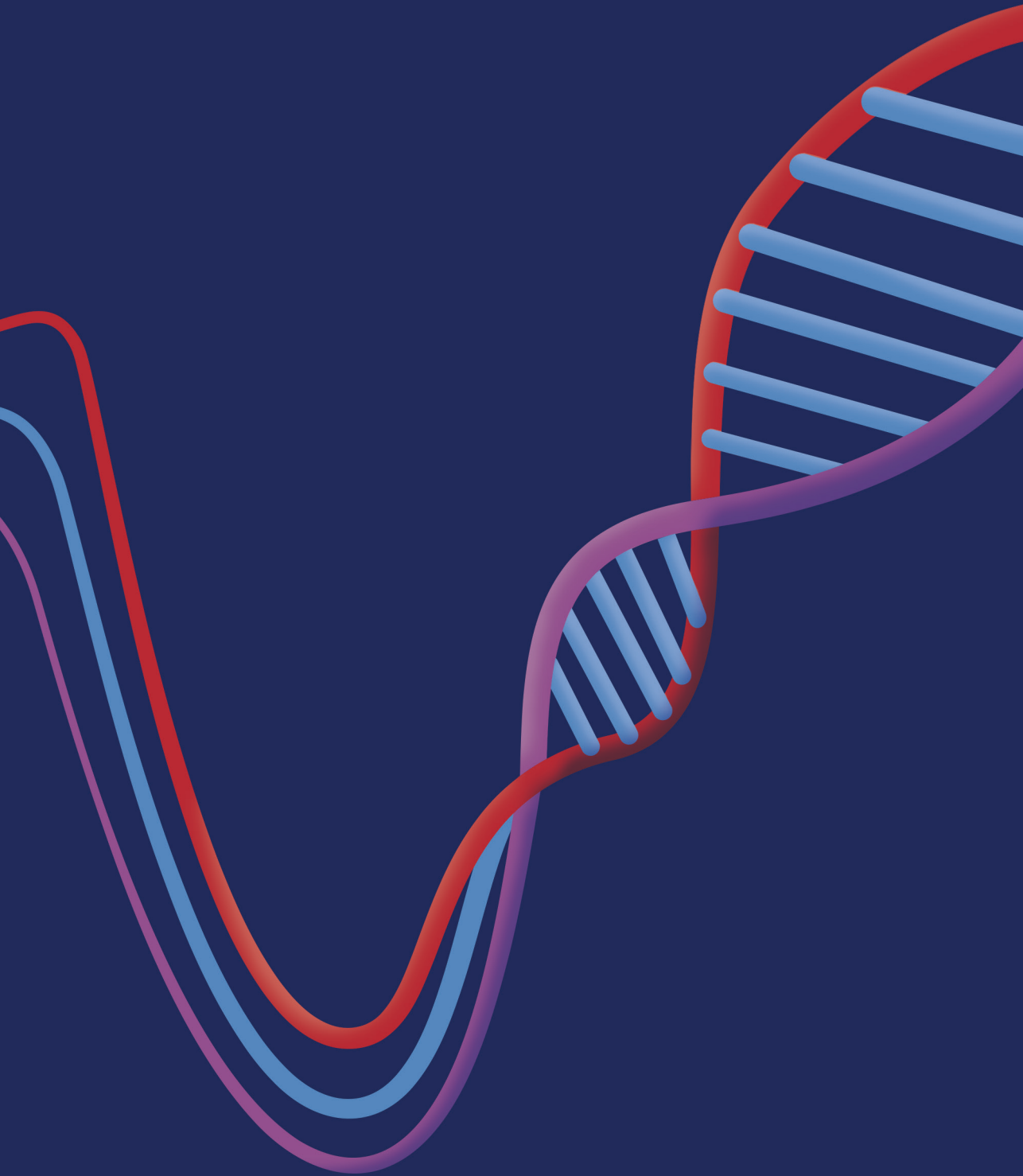
Supplemental Table 2. Progression of local differences in the modelled tissue substrate

	At inclusion (n=82)	Progression rate, 1 year(SE)	At last follow- up (n=82)	p-value for progression
Contractility normalized SD, %	10.99 (5.94)	0.46 (0.11)	13.26 (9.95)	<0.001
Age 0-30	10.67 (7.02)	0.51 (0.14)	13.68 (11.12)	<0.001
Age 30-50	10.63 (5.25)	0.47 (0.18)	13.98 (10.97)	0.008
Age 50+	11.86 (5.61)	0.38 (0.31)	11.78 (6.75)	0.220
Compliance normalized SD, %	44.84 (16.69)	1.07 (0.27)	55.53 (18.18)	<0.001
Age 0-30	43.10 (13.23)	1.53 (0.39)	56.33 (18.12)	<0.001
Age 30-50	46.94 (19.27)	0.55 (0.42)	52.96 (16.63)	0.187
Age 50+	43.96 (16.86)	1.69 (0.73)	58.19 (20.53)	0.020
Mechanical activation delay SD, ms	16.40 (16.56)	0.80 (0.25)	19.92 (19.51)	<0.001
Age 0-30	14.99 (11.24)	0.81 (0.40)	21.20 (29.58)	0.044
Age 30-50	18.11 (24.09)	0.71 (0.38)	20.16 (14.65)	0.057
Age 50+	15.67 (6.00)	1.10 (0.57)	18.09 (7.65)	0.052

Normalized heterogeneity between three RV free wall segments at inclusion and last follow-up are mean (SD). Yearly progression rate with standard errors. P-values for progression are calculated by linear mixed model statistics with exchangeable covariance structure and random intercept.

PART III.

**Towards clinical implementation of deformation
imaging**



CHAPTER 7

Echocardiographic Deformation Imaging for Early Detection of Genetic Cardiomyopathies: A Systematic Review

Feddo P. Kirkels, Karim Taha*, Arco J. Teske, Folkert W. Asselbergs, J. Peter van Tintelen, Pieter A. Doevendans, Shelby Kutty, Kristina H. Haugaa, Maarten J. Cramer*

** First authors contributed equally.*

J Am Coll Cardiol. 2022;79(6):594-608.

ABSTRACT

Clinical screening of the relatives of patients with genetic cardiomyopathies is challenging as they often lack detectable cardiac abnormalities at presentation. Life-threatening adverse events can already occur in these early stages of disease, so sensitive tools to reveal the earliest signs of disease are needed. The utility of echocardiographic deformation imaging for early detection has been explored for this population in multiple studies, but has not been broadly implemented in clinical practice. This article discusses contemporary evidence on the utility of deformation imaging in relatives of patients with genetic cardiomyopathies. The available body of data shows that deformation imaging reveals early disease-specific abnormalities in dilated cardiomyopathy, hypertrophic cardiomyopathy, and arrhythmogenic cardiomyopathy. Deformation imaging seems promising to enhance the screening and follow-up protocols in relatives, and we propose measures to accelerate its implementation in clinical care.

INTRODUCTION

It is recommended to screen relatives of patients with genetic cardiomyopathies, as they are at risk of developing a similar disease as the index patient.¹⁻³ If a (likely-)pathogenic genetic variant has been identified in the index patient, targeted genetic testing can be performed to identify relatives who carry the same variant and are therefore at high risk of developing the disease.⁴ However, management of these relatives is complicated as they often have no symptoms nor detectable cardiovascular abnormalities at presentation. In addition, penetrance is often incomplete, which implies that not all carriers of the (likely-)pathogenic variant will eventually develop the disease.^{3,5-7} It is important to identify the relatives who are at highest risk to develop the disease, as they may potentially benefit from early therapeutic intervention to prevent detrimental adverse events such as sudden cardiac death. To identify these relatives in an early stage, sensitive diagnostic tools that reveal the earliest signs of disease meet an important clinical need.

Cardiac imaging has a major role in genetic cardiomyopathies.⁸⁻¹⁰ It contributes not only to the diagnostic criteria of these cardiomyopathies, but also has important prognostic value. Unfortunately, conventional imaging modalities often lack sensitivity to detect early disease in relatives without overt disease expression.¹¹ This can be attributed to the fact that imaging parameters and their cut-off values are typically derived from affected individuals and therefore represent more established disease. Most relatives at early stages of disease fall in the grey zone or are even classified as normal when conventional imaging parameters are used.

Over the last decade, deformation imaging has emerged as more sensitive compared to conventional imaging for quantification of cardiac function.¹²⁻¹⁴ This allows quantification of global and regional myocardial deformation and may reveal subtle changes in the early stages of many cardiac diseases.^{13,14} Echocardiographic two-dimensional (2D) speckle tracking is the most commonly used tool for myocardial deformation imaging, and has been standardized for all cardiac chambers: the left and right ventricles (LV/RV), and the left and right atria (LA/RA).^{15,16} Echocardiographic speckle tracking is particularly attractive for routine clinical use because of its non-invasive nature, wide availability and low cost compared to other imaging modalities. Furthermore, speckle tracking derived indices have superior inter- and intra-observer reproducibility compared to conventional functional measurements.¹⁷

Deformation imaging has unequivocal diagnostic and prognostic value in patients with established genetic cardiomyopathies.¹⁸⁻²¹ Multiple studies suggest that it may also identify subtle mechanical alterations in the relatives of patients. However, deformation imaging has not been broadly implemented in the routine clinical screening of relatives. We conducted a systematic literature search on the use of echocardiographic deformation imaging in the screening of relatives, with the goals of evaluating the current evidence, identifying knowledge gaps, and determining future directions.

METHODOLOGY

A systematic search was conducted in the MEDLINE, Embase and Cochrane databases. The search queries included keywords and synonyms for (1) deformation imaging and (2) the most common genetic cardiomyopathies, including dilated cardiomyopathy (DCM), hypertrophic cardiomyopathy (HCM), arrhythmogenic cardiomyopathy (ACM) and non-compaction cardiomyopathy (NCCM).^{22,23} Full search queries for the different databases are provided in the *Supplementary methods*. The search was conducted on April, 1, 2021. After removing duplicates, records were independently screened by two observers (K.T. and F.K.) based on title and abstract. Studies were eligible when 2D speckle tracking was performed in relatives at risk for genetic cardiomyopathy, irrespective of their age and irrespective of whether genotyping was performed. Studies in cardiac storage diseases (e.g. Amyloidosis, Fabry), muscular dystrophy (e.g. Duchenne, Becker) or congenital heart diseases were excluded. Disagreement in abstract selection between the two observers was solved by consensus. Full papers were screened for eligibility and reference lists were screened to identify additional relevant articles that were not identified by the primary search. Abstracts without available full papers in English language, case reports/series, feasibility studies, reviews and editorials were excluded. Study quality and consequent risk of bias was assessed by two observers using the Newcastle-Ottawa scale for case-control studies and/or cohort studies (*Supplementary material*).

Included studies

In all, 29 studies were identified which were all published between 2009 and 2021 (flowchart in *Figure 1*). The studies are summarised per disease in *Tables 1-4*. Most studies included relatives who are at risk for HCM (11 studies)²⁴⁻³⁴ and ACM (11 studies)³⁵⁻⁴⁵, followed by DCM (6 studies)⁴⁶⁻⁵¹ and NCCM (1 study)⁵². All studies were case-control studies and/or longitudinal cohort studies, except for one which was a cross-sectional cohort study.³⁶ The number of included subjects at risk varied from 14 to 251 (median 41, interquartile range 24-73). The mean/median age of subjects at risk varied between 20 and 50 years in most studies, except for one study that included genotype-positive children at risk for HCM with a mean age of 9.8 ± 4.5 years.²⁶ Genetic data were reported in 26 studies.

Dilated cardiomyopathy

Most studies in DCM classified relatives as phenotype-negative on the basis of a preserved left ventricular ejection fraction (LVEF, *Table 1*). All studies showed that global deformation parameters of the LV, in particular global longitudinal strain (GLS), are reduced in relatives compared to controls (*Figure 2*). The largest study by Verdonschot et al.⁴⁶ investigated 251 first-degree relatives of genotyped DCM patients who all had normal LVEF ($\geq 55\%$) at baseline. The majority of these relatives was related to an index patient without a proven (likely-)pathogenic variant. GLS was reduced in relatives compared to matched controls. Abnormal baseline GLS in relatives was associated with deterioration of LVEF $< 55\%$ (with a minimum decrease of 5%) at a median follow-up of 36 months. Abnormal GLS at baseline was also associated with more cardiac hospitalizations and more deaths after a median follow-up of 40 months. While the results suggest that GLS can be used for risk stratification in relatives of DCM patients, occurrence of hard clinical endpoints during follow-up was infrequent, which is a common issue encountered in longitudinal studies of preclinical relatives. Studies with longer follow-up would strengthen the prognostic value of GLS in relatives at risk for DCM. Moreover, the role

of GLS within multi-modality risk calculators should be explored to define its added value on top of validated risk models.

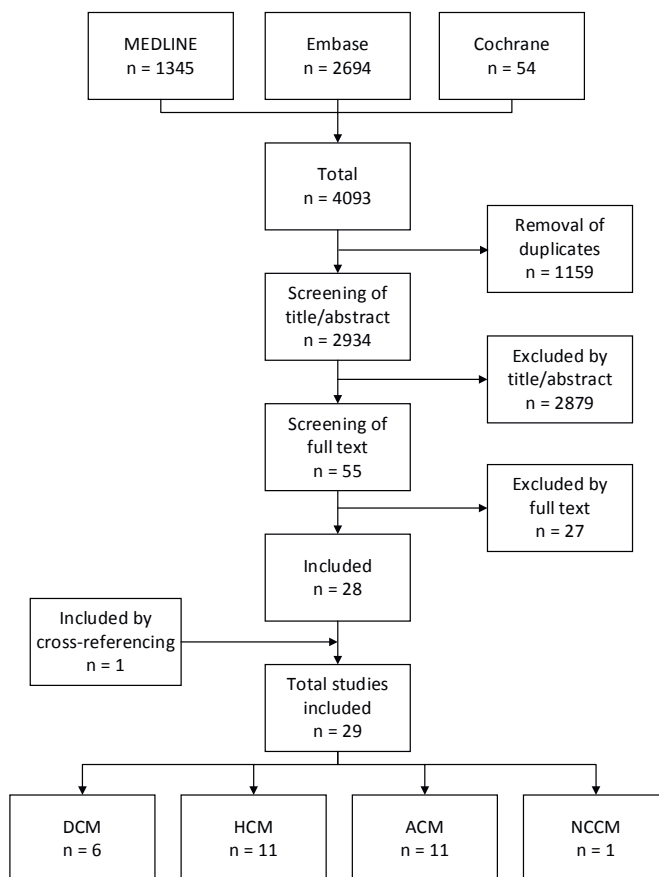


Figure 1. Flowchart

A systematic search was conducted in MEDLINE, Embase and Cochrane databases. After applying the inclusion and exclusion criteria, 29 studies were included, of which 6 were performed in DCM, 11 in HCM, 11 in ACM and 1 in NCCM. ACM, arrhythmogenic cardiomyopathy; DCM, dilated cardiomyopathy; HCM, hypertrophic cardiomyopathy, NCCM, noncompaction cardiomyopathy.

Regional deformation in DCM was investigated in one study. Taha et al.⁴⁷ evaluated 139 preclinical relatives who carried the pathogenic phospholamban (PLN) p.(Arg14del) variant, causing a risk of DCM with features of ACM. In one-third of presymptomatic genotype-positive relatives, regional post-systolic shortening was found in the LV apex (Figure 2), which was absent in controls. Presence of apical post-systolic shortening was the strongest echocardiographic predictor of ventricular arrhythmias in presymptomatic relatives. This genotype-specific approach has led to the identification of deformation patterns which are characteristic of individuals with a specific genetic variant, allowing a more tailored approach. It would be interesting to characterize genotype-specific strain patterns in other variants, for example *TTN* and *LMNA*, to optimize early detection in relatives with a particular pathogenic variant.

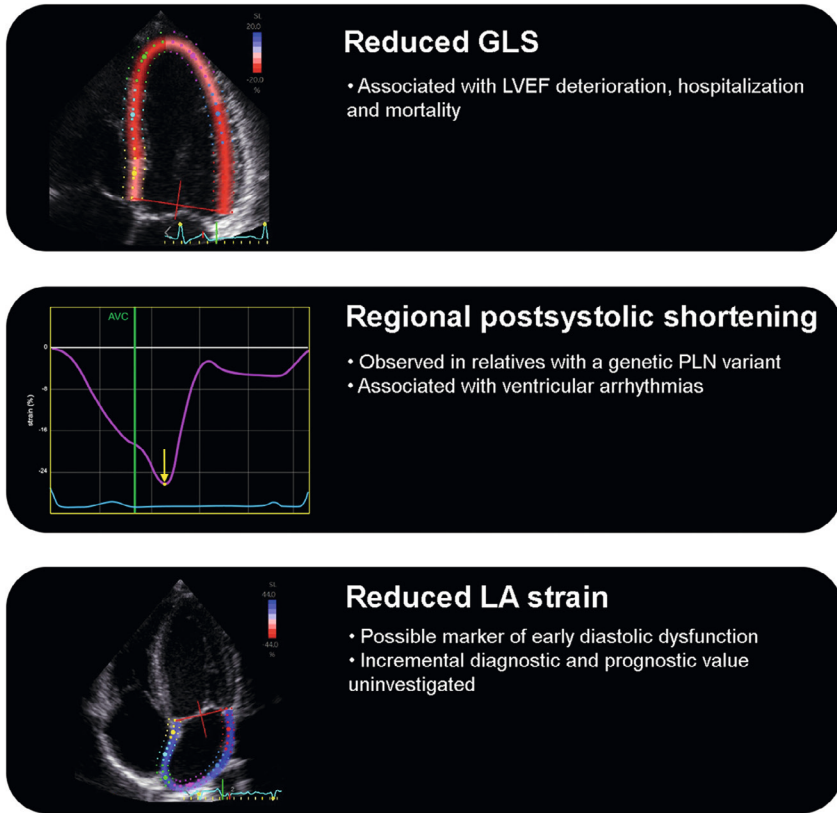


Figure 2. Reported early findings in relatives of DCM patients

The findings with echocardiographic deformation imaging that are reported in relatives of DCM patients are reduced GLS, regional postsystolic shortening and reduced LA strain. DCM, dilated cardiomyopathy; GLS, global longitudinal strain; LA, left atrium/atrial; PLN, phospholamban.

Paldino et al.⁵⁰ investigated atrial strain and showed impaired peak atrial longitudinal strain in 18% of the genotype-positive relatives of DCM patients, which possibly reflects early diastolic dysfunction (Figure 2). However, the additional value of this parameter on top of GLS has not been studied.

Hypertrophic cardiomyopathy

Most studies in HCM classified relatives as phenotype-negative when LV wall thickness was <12 or 13 mm (Table 2). Nine studies evaluated GLS, of which seven found no difference between genotype-positive relatives and controls. Haland et al.²⁵ observed reduced GLS in relatives without hypertrophy compared to healthy controls. In contrast, van Velzen et al.²⁴ reported higher GLS in relatives compared to controls, which was not associated with development of HCM during 5.6 ± 2.9 years of follow-up. The cause of these contradicting results remains speculative and may be explained by the continuum of HCM disease rather than the binary affected-not affected; the relatives could have been in different stages of disease when examined. Moreover, the considerable heterogeneity in HCM phenotypes may also have

contributed to the inconsistent findings.⁵³ While GLS has an unequivocal prognostic value in patients with overt HCM,¹⁸ its prognostic value in relatives represents a knowledge gap based on these results. A large multicentre study with in-depth multi-modality phenotyping could elucidate the precise role of GLS in genotype-positive HCM relatives.

Global circumferential and rotational function was investigated in five studies. Forsey et al.²⁶ and Williams et al.²⁸ reported enhanced systolic LV rotational function in mutation carriers without hypertrophy (*Figure 3*). This may be a consequence of increased Ca^{2+} affinity due to genetic variants in sarcomeres, as indicated in previous experimental studies.⁵⁴ However, Ho et al.²⁷, Yiu et al.³⁰, and Kauer et al.³¹ showed no systolic differences in rotation/twist. On the basis of available data, the added clinical value of circumferential and rotational function is unclear.

Six studies reported segmental strain parameters, of which four reported significantly lower strain in the basal septum (*Figure 3*).^{29,30,32,34} This was most pronounced in the basal anteroseptum. Early mechanical dysfunction in the basal septum is conceivable, as it has previously been identified as the most affected region in HCM.⁵⁵ Only one study found no difference in strain in the basal anteroseptum.²⁴ Forsey et al.²⁶ found no differences in 14 children who had an HCM-related genetic variant, but only the inferoseptum was evaluated. Reduced basal (antero)septal strain appears to be an early sign of disease in HCM relatives. This may not directly translate into reduced GLS in the early stage, presumably due to the typical focal character of the disease.

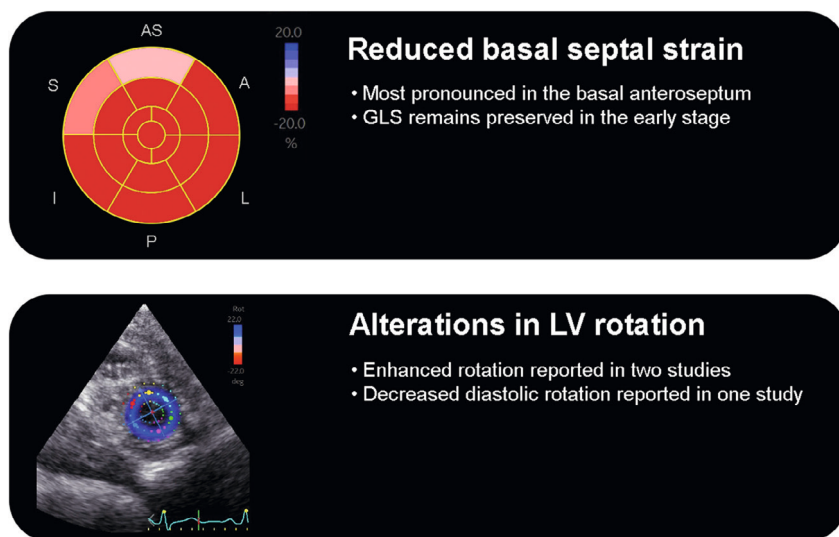


Figure 3. Reported early findings in relatives of HCM patients

The findings with echocardiographic deformation imaging that are reported in relatives of HCM patients are reduced basal septal strain and alterations in LV rotation. HCM, hypertrophic cardiomyopathy; LV, left ventricle/ventricular.

Arrhythmogenic cardiomyopathy

Early detection in relatives at risk for ACM is of particular interest, because these relatives are at risk of developing life-threatening ventricular arrhythmias before the onset of overt structural disease. Most studies on ACM and its right dominant subform arrhythmogenic right ventricular cardiomyopathy (ARVC) included relatives with (likely-)pathogenic variants in desmosomal genes (typically plakophilin-2, *Table 3*). Global RV deformation was investigated in four studies. Sarvari et al.⁴² and Reant et al.⁴³ found reduced RV free wall strain in genotype-positive relatives compared to control subjects (*Figure 4*). Lie et al.³⁵ investigated RV free wall strain in a subgroup of genotype-positive relatives and it was reduced in all four relatives who developed life-threatening ventricular arrhythmia during follow-up.

The reduction in RV free wall strain seems to be driven by regional alterations, particularly in the subtricuspid region. Mast et al.⁴⁴ described three distinct morphologies of regional deformation patterns in the RV: a type I pattern represents normal deformation while type II/III represents abnormal deformation. An abnormal deformation pattern was found in half of the preclinical relatives in the subtricuspid area (*Figure 4*). A follow-up study noted that normal deformation in the subtricuspid area could exclude disease progression with a high negative predictive value in relatives.³⁹ The role of the subtricuspid region is in line with cardiovascular magnetic resonance (CMR) and electrophysiological data that identified the subtricuspid region as one of the first affected regions in the disease.⁵⁶

Besides regional deformation patterns, the regional abnormalities can also be detected by measurement of contraction heterogeneity, expressed by RV mechanical dispersion (*Figure 4*). Sarvari et al.⁴² showed greater RV mechanical dispersion in genotype-positive relatives compared to healthy controls. RV mechanical dispersion was found to be an independent predictor of arrhythmic events in a mixed group of ACM patients and asymptomatic genotype-positive relatives. Leren et al.³⁶ showed that greater RV mechanical dispersion was associated with arrhythmic events in genotype-positive relatives, and had incremental value on top of electrical parameters according to the 2010 Task Force Criteria for ARVC.

The aforementioned methods of RV deformation were developed and tested in two centres and recently externally validated.⁵⁷ Both showed independent associations with life-threatening ventricular arrhythmias, and the combination of these methods increased the association with arrhythmia outcome. External validation has been a key step towards clinical implementation of deformation imaging in relatives at risk for ACM.

LV deformation has also been investigated in ACM relatives (*Figure 4*). Reduced GLS^{42,43}, impaired regional LV deformation^{37,43}, and increased LV mechanical dispersion (LVMD)⁴² was seen in relatives with (likely-) pathogenic variants of desmosomal genes. LVMD was greater in relatives who developed a life-threatening ventricular arrhythmia during follow-up, and predicted structural disease progression during follow-up.^{35,38}

Non-compaction cardiomyopathy

Relatives of NCCM patients were investigated in one study (*Table 4*).⁵² In 30 relatives, many deformation imaging parameters were slightly more abnormal compared to controls, including GLS, global circumferential and rotational strain. These results have not yet been replicated by other studies.

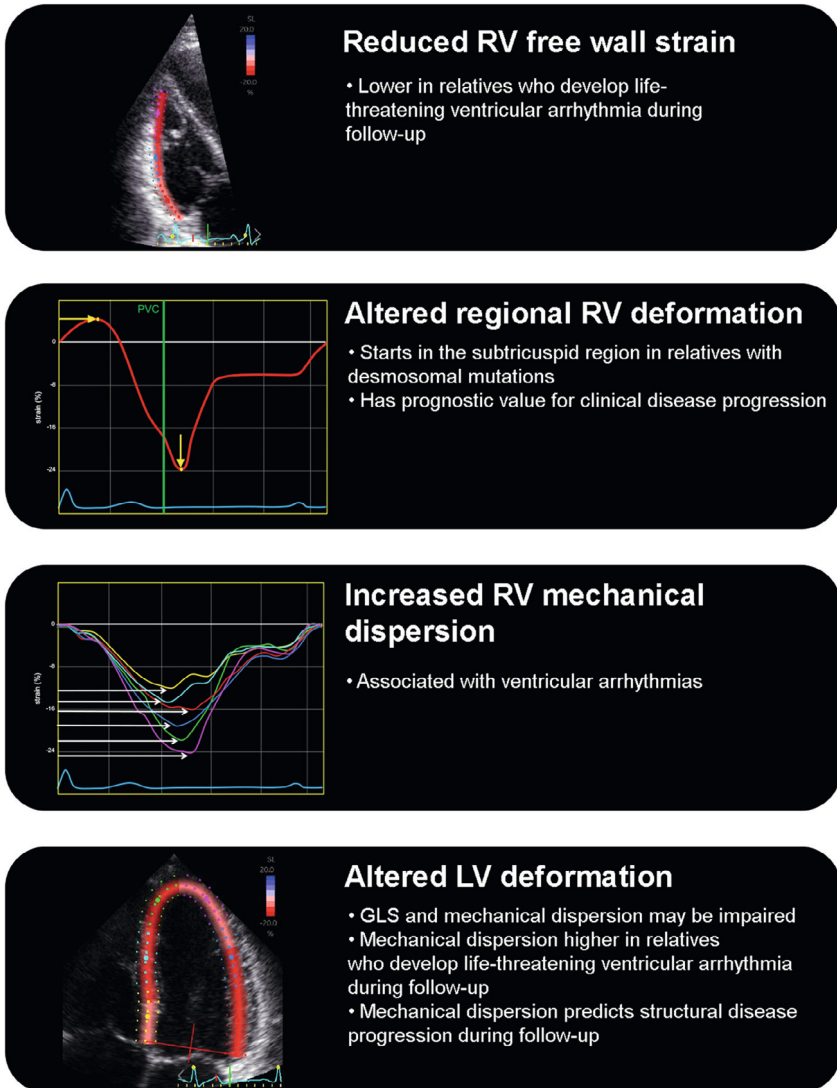


Figure 4. Reported early findings in relatives of ACM patients

The findings with echocardiographic deformation imaging that are reported in relatives of ACM patients are reduced RV free wall strain, increased RV mechanical dispersion, alterations in regional RV deformation, and alterations in LV deformation. ACM, arrhythmogenic cardiomyopathy; GLS, global longitudinal strain; LV, left ventricle/ventricular; RV, right ventricle/ventricular.

Clinical implications and future perspectives

Early detection of disease expression in relatives of patients with a genetic cardiomyopathy is of great importance, as these relatives are at risk of detrimental adverse events such as sudden cardiac death. Based on currently available literature, deformation imaging enables identification of an early disease substrate in these relatives. This seems to be true across

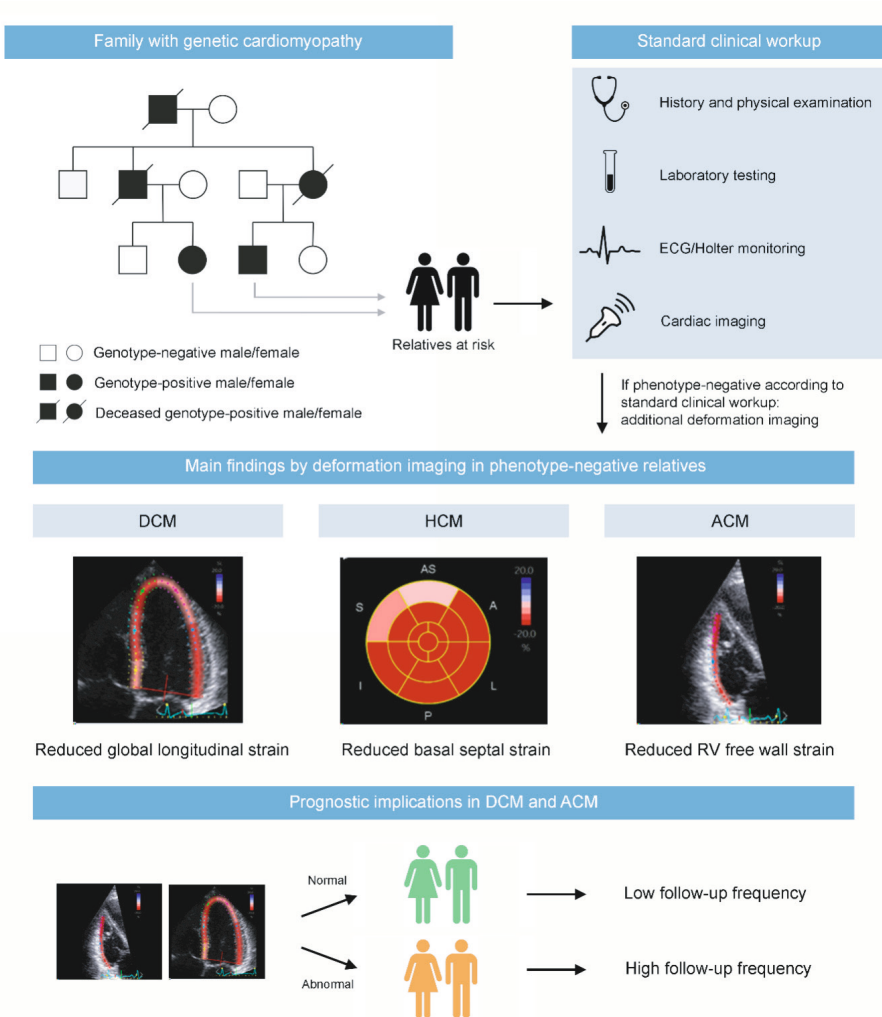
the various genetic cardiomyopathies, possibly reflecting early cardiomyocyte loss in DCM, myocardial disarray and interstitial fibrosis in HCM, and desmosomal dysfunction in ACM. Multiple deformation parameters are available, but the main findings reproduced by the different studies are: (1) reduced GLS in relatives at risk for DCM, (2) reduced basal (antero) septal strain in relatives at risk for HCM and (3) reduced RV free wall strain in relatives at risk for ACM (*Central Illustration*).

With regard to risk stratification, the prognostic value of deformation imaging has most extensively been investigated in DCM and ACM, showing a benign prognosis when deformation abnormalities are absent. Prognostic data for deformation imaging in HCM relatives are limited, making its role in clinical risk stratification uncertain. Since life-threatening arrhythmias rarely occur in early stages of HCM⁵⁸, follow-up of septal thickness may be sufficient for arrhythmic risk stratification. At this point, the presence or absence of deformation abnormalities may be helpful for determining follow-up strategies in DCM and ACM relatives. Considering the high negative prognostic value of deformation imaging in the available studies, relatives who have normal findings by deformation imaging may be offered lower follow-up intensity than relatives who have subclinical deformation abnormalities. The exact follow-up strategies, including the required intervals, remain to be investigated in longer longitudinal studies. In addition, more studies in younger subjects are needed to gain further knowledge about the penetrance in the pediatric population and the required age to start screening, since our systematic search only yielded one pediatric study.

Identification of an early disease substrate has the most potential to lead to therapeutic strategies in relatives at risk for DCM or ACM. Thereby, these relatives can potentially be offered early heart failure medication to prevent end-stage heart failure, or antiarrhythmic medication and implantable cardioverter defibrillator implantation to prevent sudden cardiac death.^{35,46} However, since the numbers of hard end-points are low in the published studies, the prognostic value of deformation imaging should be confirmed in larger studies, preferably with longer follow-up intervals. Deformation imaging may also soon become relevant for patient selection in HCM, given the promising trials on medical treatment of early stage HCM.^{59,60}

We encourage the authors of reported studies to investigate and publish the long term (>10 years) outcomes of their cohorts whenever possible. Moreover, we strongly encourage collaborations between different research groups to create larger cohorts and to create a platform for external validation. We would like to emphasize that deformation imaging should not be used as stand-alone parameter, but interpreted in the context of other clinical variables, and in conjunction with other examinations such as electrocardiography and CMR. Studies implementing relevant deformation imaging parameters into multi-modality risk prediction models are therefore of great interest.

Finally, we would like to encourage the use of machine learning approaches to improve the classification of deformation curves of relatives.⁶¹ Machine learning models may detect hidden patterns in deformation curves and improve the classification of these curves, potentially leading to earlier identification of high-risk relatives. Besides using machine learning merely for classification purposes, specific techniques can be applied to visualize the features that are detected by the machine learning model.⁶² The application of such techniques will enrich our knowledge of hidden features in the deformation curves of relatives, which will enhance the clinical utility of deformation imaging in this population.



Central illustration. The clinical utility of deformation imaging in relatives at risk for genetic cardiomyopathies

Deformation imaging on top of the standard clinical workup reveals early signs of disease in relatives of patients with genetic cardiomyopathy. These early mechanical abnormalities have prognostic value in DCM and ACM, and may be used in these relatives to tailor follow-up protocols. ACM, arrhythmogenic cardiomyopathy; DCM, dilated cardiomyopathy; ECG, electrocardiogram; HCM, hypertrophic cardiomyopathy; RV, right ventricle/ventricular.

Limitations

All studies included in this review are retrospective observational studies, mostly with small sample sizes. The majority of the studies were performed in single centres, and the authors of this review were involved in 10 of the 29 included studies, particularly in the field of ACM. An inherent limitation of studies in relatives is that the rates of hard end-points are generally

low. To investigate the clinical significance of deformation imaging in relatives with regard to hard end-points, larger studies with longer follow-up are needed. Due to the heterogeneity in definitions and methods between the studies, we could not perform a meta-analysis, nor could we extract cut-off values from the published data. Finally, when applying these results into clinical practice, it should be taken into account that different software packages were used among the different studies. While the inter-vendor differences for global measurements are small,¹⁷ there is still considerable variability in the detection of regional functional abnormalities among different vendors.⁶³

CONCLUSION

Deformation imaging can unmask early signs of disease in relatives of DCM, HCM and ACM patients. The main observations in these relatives are (1) reduced GLS in relatives at risk for DCM, (2) reduced basal (antero)septal strain in relatives at risk for HCM, and (3) reduced RV free wall strain in relatives at risk for ACM. Considering the prognostic value in early stages of DCM and ACM, we recommend routine measurement of disease-specific deformation parameters in these relatives. Collaborations between research groups are needed to create opportunities for larger studies and to create a platform for external validation.

Table 1. Included DCM studies

First author, year, journal	Design	Study population	Number	Age (years)	Genotype
Verdonschot, 2020, JACC cvi	CCS + LCS	First-degree relatives with LVEF $\geq 55\%$	251	46 \pm 17	Genetic testing in 44 relatives (18%), of which 32 (13%) genotype-positive (predominantly <i>TTN</i>)
Taha, 2021, JACC cvi	CCS + LCS	Genotype-positive relatives (PLN p.Arg14del) without a history of VA, premature ventricular complex count <500/24h, LVEF $\geq 45\%$	139	33 [IQR 21-41]	All <i>PLN</i> p.(Arg14del)
Okten, 2017, Herz	CCS	First-degree relatives with LVEF $\geq 55\%$	77	35 [IQR 15]	Not reported
van der Bijl, 2019, EHJ cvi	CCS	Genotype-positive relatives with LVEF $\geq 55\%$	50	50 \pm 15	Predominantly <i>TTN</i> (48%) and <i>LMNA</i> (20%)
Paldino 2021, Int J Cardiology	CCS + LCS	Genotype-positive relatives with normal ECG and echocardiographic findings	41	37 \pm 14	<i>TTN</i> , <i>LMNA</i> , <i>FLNC</i> , <i>MYH7</i> , <i>TNNT2</i> , <i>MYBPC3</i> , <i>DSP</i> , <i>SCN5A</i> , <i>TMEM43</i> , <i>RBM20</i>
Lakdawala, 2012, Circ Cardiovasc Img	CCS	Genotype-positive relatives with LVEF $\geq 55\%$ and normal dimensions	12	25 \pm 19	<i>MYH7</i> (75%) and <i>TPM1</i> (25%)

Abbreviations: CCS = case-control study, DCM = dilated cardiomyopathy, ECG = electrocardiogram, GCS = global circumferential strain, GLS = global longitudinal strain, GRS = global radial strain, IQR = interquartile range, LCS = longitudinal cohort study, LV = left ventricle/ventricular, LVEF = left ventricular ejection fraction, LVMD = left ventricular mechanical dispersion, RVFWLS = right ventricular free wall longitudinal strain VA = ventricular arrhythmia.

Software	Global deformation parameters	Regional deformation parameters	Control group	Main result(s)
TomTec	GLS	none	251 patients referred for chest pain, dyspnea or palpitations, with LVEF $\geq 55\%$	GLS reduced in relatives ($P < 0.001$). Reduced GLS associated with LVEF deterioration and adverse events (cardiac hospitalization and death) during follow-up
GE Echopac	GLS, LVMD, RVFWLS	post-systolic shortening	70 healthy volunteers and patients from the outpatient clinic without cardiac disease	Post-systolic shortening present in the LV apex in 31% of relatives with the <i>PLN</i> p.(Arg14del) variant; presence associated with nonsustained VA during follow-up.
GE EchoPAC	GLS, GLS rate, GCS, GCS rate, GRS, GRS rate, peak torsion	none	86 healthy subjects with normal ECG and echo, and no family history of heart failure	All global parameters significantly reduced in relatives
GE EchoPAC	GLS	none	28 genotype-negative relatives	GLS reduced in genotype-positive relatives ($P = 0.036$)
TomTec	GLS, peak atrial longitudinal strain	none	52 healthy volunteers and 17 genotype negative relatives	GLS and peak atrial longitudinal strain reduced in genotype-positive relatives
GE EchoPAC	GLS, GLS rate, GCS, GCS rate, GRS, GRS rate	none	29 genotype-negative relatives	All parameters (except for GCS rate) reduced in genotype-positive relatives ($P = 0.018$ for GLS)

Table 2. Included HCM studies

First author, year, journal	Design	Study population	Number	Age (years)	Genotype	Software
van Velzen, 2019, Neth Heart J	CCS + LCS	HCM genotype-positive individuals with LV wall thickness <13 mm and LVEF \geq 50%	120	41 \pm 13	Predominantly <i>MYBPC3</i> (77%)	TomTec
Haland, 2017, Open Heart	CCS	Sarcomere mutation carriers with LV wall thickness <13 mm and no symptoms	100	36 \pm 15	Predominantly <i>MYBPC3</i> (58%) and <i>MYH7</i> (29%)	GE EchoPAC
Ho, 2009, Circ Cardiovasc Genet	CCS	Genotype-positive relatives with LV wall thickness <12 mm	68	24 \pm 12	Predominantly <i>MYH7</i> (50%) and <i>MYBPC3</i> (37%)	GE EchoPAC
Williams, 2018, Am J Cardiol	CCS	Genotype-positive relatives with LV wall thickness <12 mm	60	30 \pm 10	Majority <i>MYBPC3</i> and <i>MYH7</i> (rates not specified)	Siemens VVI
Baudry, 2020, EHJ cvi	CCS	Genotype-positive relatives with LV wall thickness <13 mm	53 (20 derivation cohort, 33 validation cohort)	Derivation cohort: 31 [IQR 24-44], validation cohort: 42 [IQR 34-47]	Predominantly <i>MYBPC3</i> (53%) and <i>MYH7</i> (28%)	GE EchoPAC
Yiu, 2012, PLoS one	CCS	Genotype-positive first-degree relatives without HCM diagnosis	47	42 \pm 17	<i>MYBPC3</i> (83%) and <i>MYH7</i> (17%)	GE EchoPAC
Kauer, 2017, EHJ cvi	CCS	Genotyped relatives without major or minor criteria for HCM	41	37 \pm 11	Mutations in 56%, predominantly <i>MYBPC3</i> (46%).	Philips QLAB

Global deformation parameters	Regional deformation parameters	Control group	Main result(s)
GLS, average basal, mid and apical longitudinal strain	LV basal anteroseptal longitudinal strain	110 volunteers with normal physical examination, normal ECG and LVEF $\geq 50\%$	GLS increased in mutation carriers ($P < 0.001$), but not associated with development of HCM phenotype during follow-up (5.6 ± 2.9 years)
GLS	none	80 healthy volunteers	GLS reduced in mutation carriers ($P = 0.001$)
GLS, GLS rate, GCS, GRS	LV septal, lateral, inferior and anterior longitudinal strain and strain rate (averaged over wall)	38 genotype-negative relatives	No significant differences between genotype-positive and genotype-negative relatives. GLS reduced in relatives with <i>MYBPC3</i> variant compared to <i>MYH7</i> ($P < 0.001$)
GLS, GLS rate, GCS (multi-layer), global mechanical synchrony index, rotation, twist	none	60 healthy subjects without family history of HCM and normal echocardiogram	Enhanced circumferential systolic function ($P < 0.001$), increased twist ($P < 0.001$) and more myocardial dyssynchrony ($P < 0.001$) in relatives
GLS	Longitudinal strain in 17 LV segments	49 genotype-negative relatives and healthy volunteers with no history of cardiovascular disease and normal echocardiography (21 in derivation cohort, 28 in validation cohort)	Regional strain reduced in genotype-positive relatives in basal anteroseptal wall and basal inferoseptal wall ($P = 0.035$ and $P = 0.002$ in validation cohort)
GLS, GCS, GRS	LV basal anteroseptal and basal posterior peak longitudinal systolic strain	25 subjects referred for atypical chest pain, palpitations or syncope with normal echo	Basal anteroseptal longitudinal strain reduced in relatives ($P < 0.01$)
Twist, twist rate, untwist, untwist rate, unstrain, unstrain rate	LV inferoseptal, anterolateral, inferolateral and anteroseptal unstrain, unstrain rate and longitudinal strain (averaged over wall)	41 healthy, non-obese volunteers, with normal LA/LV volumes and function, and normal ECG	Early diastolic untwist rate reduced in relatives ($P < 0.05$), untwist delayed ($P < 0.005$). Late diastolic unstrain rate increased and delayed in all walls, except for anterolateral wall

Table 2. Included HCM studies (continued)

First author, year, journal	Design	Study population	Number	Age (years)	Genotype	Software
De, 2011, Am Heart J	CCS	Genotype-positive relatives (<i>MYBPC3</i> c.3330+2T>G) with LV wall thickness <13 mm and no clinical signs or symptoms consistent with obstructive HCM	35	30 ± 14	All <i>MYBPC3</i> c.3330+2T>G	GE EchoPAC
Grover, 2019, EHJ cvi	CCS	Genotype-positive relatives (<i>MYBPC3</i>) without LVH	18	38 ± 14	All <i>MYBPC3</i>	GE EchoPAC
Peyrou, 2016, Int J Cardiovasc Img	CCS	Genotype-positive first-degree relatives with LV wall thickness <13 mm	14	43 ± 16	<i>MYH7</i> (57%), <i>MYBPC3</i> (29%) and <i>TNNT2</i> (14%)	GE EchoPAC
Forsey, 2014, JASE	CCS	Genotype-positive first-degree relatives (children) without LVH	12	10 ± 5	<i>MYBPC3</i> (43%), <i>MYH7</i> (36%), <i>MYHC</i> (14%) and <i>TPM1</i> (7%)	GE EchoPAC

Abbreviations: CCS = case-control study, ECG = electrocardiogram, GCS = global circumferential strain, GLS = global longitudinal strain, GRS = global radial strain, HCM = hypertrophic cardiomyopathy, IQR = interquartile range, LCS = longitudinal cohort study, LA = left atrium/atrial LV = left ventricle/ventricular, LVEF = left ventricular ejection fraction, LVH = left ventricular hypertrophy.

Global deformation parameters	Regional deformation parameters	Control group	Main result(s)
GLS	Longitudinal strain in 18 LV segments	30 healthy volunteers with normal echo	Basal septal longitudinal strain reduced in relatives (P=0.02), whereas basal posterior and mid posterior longitudinal strain increased (both P=0.001)
GLS	Longitudinal strain in 6 LV walls (averaged over wall)	11 genotype-negative siblings and 11 volunteers without cardiac disease or cardiovascular risk factors	No significant differences reported
GLS	Longitudinal strain in 18 LV segments	32 healthy volunteers without LVH, without hypertension and without family history of HCM	Basal inferoseptal and basal anteroseptal longitudinal strain reduced in relatives (p<0.05)
Mean circumferential strain (basal/mid/apical), mean longitudinal strain (apical 4-chamber), basal/apical rotation and rotation rate, twist	Circumferential strain in 18 segments, longitudinal strain in 6 segments (apical 4-chamber)	28 healthy volunteers from a normal control database	Mean apical circumferential strain increased in relatives (P=0.04). Basal and apical rotation and LV twist increased in relatives, most marked at the apex (P=0.0001).

Table 3. Included ACM studies

First author, year, journal	Design	Study population	Number	Age (years)	Genotype	Software
Lie, 2018, JACC CVI	LCS	Genotype-positive relatives without life-threatening VA at baseline	83	39 ± 16 for total cohort (including 34 probands)	All desmosomal mutation carriers (not specified)	GE EchoPAC
Leren, 2017, JACC CVI	CSCS	Early ACM (possible/ borderline diagnosis), of which 79% are genotype-positive relatives	73	41 ± 16 for total cohort (also including 86 probands)	All desmosomal mutation carriers (not specified)	GE EchoPAC
Chivulescu, 2019, EHJ	LCS	Genotype-positive relatives without major structural TFC	73	38 ± 18 for all relatives (also including 3 relatives with major structural TFC)	<i>PKP2</i> (92%), <i>DSP</i> (4%), <i>DSG2</i> (4%)	GE EchoPAC
Mast, 2019, JACC cvi	LCS	First-degree relatives without electrical or structural TFC (possible ACM)	37	26 ± 14	Predominantly <i>PKP2</i> (65%). Also 22% relatives of gene-elusive index patients	GE EchoPAC
Taha, 2020, JACC cvi	LCS	Genotype-positive relatives without definite TFC diagnosis (possible and borderline ACM)	34	Not reported	Predominantly desmosomal (not specified)	GE EchoPAC
Mast, 2016, J Cardiovasc Electrophysiol	CCS + LCS	Genotype-positive first-degree relatives without definite TFC diagnosis and without VA or symptoms (possible and borderline ACM)	31	30 ± 14	<i>PKP2</i> (90%) and <i>DSG2</i> (10%)	GE EchoPAC
Sarvari, 2011, EHJ	CCS	Genotype-positive first-degree relatives without palpitations, syncope, arrhythmias or heart failure (possible and borderline ACM)	27	38 ± 18	<i>PKP2</i> (89%), <i>DSP</i> (11%)	GE EchoPAC

Global deformation parameters	Regional deformation parameters	Control group	Main result(s)
GLS, LVMD, RVMD, RVFWLS	none	N/A	4 relatives with VA during follow-up. LVMD higher and RVFWLS lower in these relatives
GLS, LVMD, RVGLS (6 segments), RVMD	None	N/A	15 subjects with arrhythmic events. RVMD lower in subjects with arrhythmic events (P = 0.003).
GLS, LVMD	None	N/A	25 relatives had structural progression during follow-up. Higher LVMD at baseline predicted structural progression in relatives (P = 0.02).
none	Basal RV deformation pattern	N/A	Basal RV deformation patterns have high negative predictive value for disease progression during 3.7 ± 2.1 years follow-up
none	Basal, mid, apical RV deformation pattern	N/A	Basal RV deformation patterns reveal disease progression during 6.6 ± 3.1 years follow-up, conventional measurements remain unchanged
none	Basal, mid, apical RV electromechanical interval	30 healthy volunteers without history of heart disease	Electromechanical interval prolonged in relatives in RV basal area (P<0.001). Prolonged electromechanical interval associated with arrhythmic outcome during 4.2 ± 3.1 years follow-up
GLS, LVMD, RVFWLS, RVMD	none	10 genotype-negative relatives and 30 healthy volunteers	All parameters impaired in relatives (P<0.001). RVMD strongest association with arrhythmias.

Table 3. Included ACM studies (continued)

First author, year, journal	Design	Study population	Number	Age (years)	Genotype	Software
Reant, 2016, Int J Cardiovasc Img	CCS	Genotype-positive relatives without TFC (possible ACM)	27	40 ± 20	All desmosomal mutation carriers (not specified)	GE EchoPAC
Mast, 2016, JACC	CCS	Genotype-positive relatives without TFC (possible ACM)	21	27 ± 14	<i>PKP2</i> and <i>DSG2</i> (not specified)	GE EchoPAC
Aneq, 2012, cardiovascular ultrasound	CCS	First degree male relatives not fulfilling TFC diagnosis (possible or borderline ACM)	19	median 29 (range 19-73)	Not reported	GE EchoPAC
Mast, 2015, JASE	CCS	Mutation-positive relatives without definite Task Force diagnosis (possible or borderline ACM)	16	32 ± 14	<i>PKP2</i> (75%), <i>PLN</i> (12.5%), <i>DSG2</i> (6.25%), <i>DSC2</i> (6.25%)	GE EchoPAC

Abbreviations: ACM = arrhythmogenic cardiomyopathy, CCS = case-control study, CSCS = cross-sectional cohort study, ECG = electrocardiogram, GLS = global longitudinal strain, LCS = longitudinal cohort study, LV = left ventricle/ventricular, LVMD = left ventricular mechanical dispersion, RV = right ventricle/ventricular, RVFWLS = right ventricular free wall longitudinal strain, RVMD = right ventricular mechanical dispersion, TFC = Task Force Criteria, VA = ventricular arrhythmia.

Global deformation parameters	Regional deformation parameters	Control group	Main result(s)
GLS (multilayer), RVFWLS	Longitudinal strain in 17 LV segments (multilayer) and basal, mid and apical RV longitudinal strain	26 healthy volunteers, asymptomatic without history of premature cardiovascular disease	Global parameters reduced in relatives. Regional parameters also reduced in LV free wall segments (epicardial more than endocardial), septal segments and RV mid and apical segments.
none	Basal RV time to onset shortening, (systolic) peak strain, post-systolic shortening and deformation pattern	84 healthy unrelated controls	Abnormal deformation patterns more frequent in relatives than in controls (48% vs. 4%)
none	Longitudinal strain in basal/mid segments of LV lateral wall, septum and RV lateral wall	Asymptomatic healthy male volunteers without family history of premature cardiovascular disease, no ECG abnormalities and no cardiac medication	Reduced strain in basal septum of relatives
Mean LV systolic peak strain (mean of 18 segments)	Systolic peak strain and strain rate, and post-systolic shortening in 18 LV segments	Healthy control subjects free of any cardiovascular disease (volunteers, unrelated to cases)	Global strain equal, LV involvement in 25% relatives (vs 0% in controls)

Table 4. Included NCCM studies

First author, year, journal	Design	Study population	Number	Age (years)	Genotype
Akhan, 2021, Int J Cardiovasc Img	CCS	First-degree relatives of NCCM patients	30	46 ± 17	Not reported

Abbreviations: CCS = case-control study, GCS = global circumferential strain, GLS = global longitudinal strain, GRS = global radial strain, NCCM = noncompaction cardiomyopathy

Software	Global deformation parameters	Regional deformation parameters	Control group	Main result(s)
GE EchoPAC	GLS, GLS rate, GCS, GCS rate, GRS, GRS rate	none	31 healthy volunteers	Many conventional parameters and all strain parameters impaired in relatives compared to controls

REFERENCES

1. Nava A, Bauce B, Basso C, et al. Clinical profile and long-term follow-up of 37 families with arrhythmogenic right ventricular cardiomyopathy. *J Am Coll Cardiol*. 2000;36(7):2226-2233.
2. Michels V, Olson TM, Miller FA, Ballman K, Rosales AG, Driscoll DJ. Frequency of development of idiopathic dilated cardiomyopathy among relatives of patients with idiopathic dilated cardiomyopathy. *Am J Cardiol*. 2003;91(11):1389-1392.
3. Maron BJ, Niimura H, Casey SA, et al. Development of left ventricular hypertrophy in adults with hypertrophic cardiomyopathy caused by cardiac myosin-binding protein C gene mutations. *J Am Coll Cardiol*. 2001;38(2):315-321.
4. Hershberger RE, Givertz MM, Ho CY, et al. Genetic evaluation of cardiomyopathy: a clinical practice resource of the American College of Medical Genetics and Genomics (ACMG). *Genet Med*. 2018;20(9):899-909.
5. Rankin J, Auer-Grumbach M, Bagg W, et al. Extreme phenotypic diversity and nonpenetrance in families with the LMNA gene mutation R644C. *Am J Med Genet Part A*. 2008;146A(12):1530-1542.
6. Dalal D, James C, Devanagondi R, et al. Penetrance of Mutations in Plakophilin-2 Among Families With Arrhythmogenic Right Ventricular Dysplasia/Cardiomyopathy. *J Am Coll Cardiol*. 2006;48(7):1416-1424.
7. Lorenzini M, Norrish G, Field E, et al. Penetrance of Hypertrophic Cardiomyopathy in Sarcomere Protein Mutation Carriers. *J Am Coll Cardiol*. 2020;76(5):550-559.
8. Donal E, Delgado V, Bucciarelli-Ducci C, et al. Multimodality imaging in the diagnosis, risk stratification, and management of patients with dilated cardiomyopathies: an expert consensus document from the European Association of Cardiovascular Imaging. *Eur Heart J Cardiovasc Imaging*. 2019;20(10):1075-1093.
9. Haugaa KH, Basso C, Badano LP, et al. Comprehensive multi-modality imaging approach in arrhythmogenic cardiomyopathy-an expert consensus document of the European Association of Cardiovascular Imaging. *Eur Heart J Cardiovasc Imaging*. 2017;18(3):237-253.
10. Cardim N, Galderisi M, Edvardsen T, et al. Role of multimodality cardiac imaging in the management of patients with hypertrophic cardiomyopathy: an expert consensus of the European Association of Cardiovascular Imaging Endorsed by the Saudi Heart Association. *Eur Heart J Cardiovasc Imaging*. 2015;16(3):280-280.
11. te Riele ASJM, James CA, Rastegar N, et al. Yield of serial evaluation in at-risk family members of patients with ARVD/C. *J Am Coll Cardiol*. 2014;64(3):293-301.
12. Cikes M, Solomon SD. Beyond ejection fraction: an integrative approach for assessment of cardiac structure and function in heart failure. *Eur Heart J*. 2016;37(21):1642-1650.
13. Collier P, Phelan D, Klein A. A Test in Context: Myocardial Strain Measured by Speckle-Tracking Echocardiography. *J Am Coll Cardiol*. 2017;69(8):1043-1056.
14. Potter E, Marwick TH. Assessment of Left Ventricular Function by Echocardiography. *JACC Cardiovasc Imaging*. 2018;11(2):260-274.
15. Voigt J-U, Pedrizzetti G, Lysyansky P, et al. Definitions for a common standard for 2D speckle tracking echocardiography: consensus document of the EACVI/ASE/Industry Task Force to standardize deformation imaging. *J Am Soc Echocardiogr*. 2015;28(2):183-193.

16. Badano LP, Koliaas TJ, Muraru D, et al. Standardization of left atrial, right ventricular, and right atrial deformation imaging using two-dimensional speckle tracking echocardiography: a consensus document of the EACVI/ASE/Industry Task Force to standardize deformation imaging. *Eur Heart J Cardiovasc Imaging*. 2018;19(6):591-600.
17. Farsalinos KE, Daraban AM, Ünlü S, Thomas JD, Badano LP, Voigt J-U. Head-to-Head Comparison of Global Longitudinal Strain Measurements among Nine Different Vendors: The EACVI/ASE Inter-Vendor Comparison Study. *J Am Soc Echocardiogr*. 2015;28(10):1171-1181.
18. Tower-Rader A, Mohananey D, To A, Lever HM, Popovic ZB, Desai MY. Prognostic Value of Global Longitudinal Strain in Hypertrophic Cardiomyopathy. *JACC Cardiovasc Imaging*. 2019;12(10):1930-1942.
19. Malik N, Win S, James CA, et al. Right Ventricular Strain Predicts Structural Disease Progression in Patients With Arrhythmogenic Right Ventricular Cardiomyopathy. *J Am Heart Assoc*. 2020;9(7).
20. Lie ØH, Chivulescu M, Rootwelt-Norberg C, et al. Left Ventricular Dysfunction in Arrhythmogenic Cardiomyopathy: Association With Exercise Exposure, Genetic Basis, and Prognosis. *J Am Heart Assoc*. 2021;10(8):e018680.
21. Marrow BA, Cook SA, Prasad SK, McCann GP. Emerging Techniques for Risk Stratification in Nonischemic Dilated Cardiomyopathy. *J Am Coll Cardiol*. 2020;75(10):1196-1207.
22. Elliott P, Andersson B, Arbustini E, et al. Classification of the cardiomyopathies: a position statement from the european society of cardiology working group on myocardial and pericardial diseases. *Eur Heart J*. 2007;29(2):270-276.
23. Maron BJ, Towbin JA, Thiene G, et al. Contemporary Definitions and Classification of the Cardiomyopathies. *Circulation*. 2006;113(14):1807-1816.
24. van Velzen HG, Schinkel AFL, van Grootel RWJ, et al. Five-year prognostic significance of global longitudinal strain in individuals with a hypertrophic cardiomyopathy gene mutation without hypertrophic changes. *Netherlands Heart J*. 2019;27(3):117-126.
25. Haland TF, Hasselberg NE, Almaas VM, et al. The systolic paradox in hypertrophic cardiomyopathy. *Open Heart*. 2017;4(1):e000571.
26. Forsey J, Benson L, Rozenblyum E, Friedberg MK, Mertens L. Early Changes in Apical Rotation in Genotype Positive Children with Hypertrophic Cardiomyopathy Mutations without Hypertrophic Changes on Two-Dimensional Imaging. *J Am Soc Echocardiogr*. 2014;27(2):215-221.
27. Ho CY, Carlsen C, Thune JJ, et al. Echocardiographic Strain Imaging to Assess Early and Late Consequences of Sarcomere Mutations in Hypertrophic Cardiomyopathy. *Circ Cardiovasc Genet*. 2009;2(4):314-321.
28. Williams LK, Misurka J, Ho CY, et al. Multilayer Myocardial Mechanics in Genotype-Positive Left Ventricular Hypertrophy-Negative Patients With Hypertrophic Cardiomyopathy. *Am J Cardiol*. 2018;122(10):1754-1760.
29. Baudry G, Mansencal N, Reynaud A, et al. Global and regional echocardiographic strain to assess the early phase of hypertrophic cardiomyopathy due to sarcomeric mutations. *Eur Heart J Cardiovasc Imaging*. Published online May 2019.
30. Yiu KH, Atsma DE, Delgado V, et al. Myocardial Structural Alteration and Systolic Dysfunction in Preclinical Hypertrophic Cardiomyopathy Mutation Carriers. *PLoS One*. 2012;7(5):e36115.

31. Kauer F, van Dalen BM, Michels M, et al. Delayed and decreased LV untwist and unstrain rate in mutation carriers for hypertrophic cardiomyopathy. *Eur Heart J Cardiovasc Imaging*. Published online December 2016;jew213.
32. De S, Borowski AG, Wang H, et al. Subclinical echocardiographic abnormalities in phenotype-negative carriers of myosin-binding protein C3 gene mutation for hypertrophic cardiomyopathy. *Am Heart J*. 2011;162(2):262-267.e3.
33. Grover S, Lloyd R, Perry R, et al. Assessment of myocardial oxygenation, strain, and diastology in MYBPC3-related hypertrophic cardiomyopathy: a cardiovascular magnetic resonance and echocardiography study. *Eur Heart J Cardiovasc Imaging*. 2019;20(8):932-938.
34. Peyrou J, Réant P, Reynaud A, et al. Morphological and functional abnormalities pattern in hypertrophy-free HCM mutation carriers detected with echocardiography. *Int J Cardiovasc Imaging*. 2016;32(9):1379-1389.
35. Lie ØH, Rootwelt-Norberg C, Dejgaard LA, et al. Prediction of Life-Threatening Ventricular Arrhythmia in Patients With Arrhythmogenic Cardiomyopathy: A Primary Prevention Cohort Study. *JACC Cardiovasc Imaging*. 2018;11(10):1377-1386.
36. Leren IS, Saberniak J, Haland TF, Edvardsen T, Haugaa KH. Combination of ECG and Echocardiography for Identification of Arrhythmic Events in Early ARVC. *JACC Cardiovasc Imaging*. 2017;10(5):503-513.
37. Mast TP, Teske AJ, vd Heijden JF, et al. Left Ventricular Involvement in Arrhythmogenic Right Ventricular Dysplasia/Cardiomyopathy Assessed by Echocardiography Predicts Adverse Clinical Outcome. *J Am Soc Echocardiogr*. Published online 2015.
38. Chivulescu M, Lie ØH, Popescu BA, et al. High penetrance and similar disease progression in probands and in family members with arrhythmogenic cardiomyopathy. *Eur Heart J*. 2020;41(14):1401-1410.
39. Mast TP, Taha K, Cramer MJ, et al. The Prognostic Value of Right Ventricular Deformation Imaging in Early Arrhythmogenic Right Ventricular Cardiomyopathy. *JACC Cardiovasc Imaging*. 2019;12(3):446-455.
40. Taha K, Mast TP, Cramer MJ, et al. Evaluation of Disease Progression in Arrhythmogenic Cardiomyopathy. *JACC Cardiovasc Imaging*. 2020;13(2):631-634.
41. Mast TP, Teske AJ, Te Riele AS, et al. Prolonged Electromechanical Interval Unmasks Arrhythmogenic Right Ventricular Dysplasia/Cardiomyopathy in the Subclinical Stage. *J Cardiovasc Electrophysiol*. 2016;27(3):303-314.
42. Sarvari SI, Haugaa KH, Anfinsen O-G, et al. Right ventricular mechanical dispersion is related to malignant arrhythmias: a study of patients with arrhythmogenic right ventricular cardiomyopathy and subclinical right ventricular dysfunction. *Eur Heart J*. 2011;32(9):1089-1096.
43. Réant P, Hauer AD, Castelletti S, et al. Epicardial myocardial strain abnormalities may identify the earliest stages of arrhythmogenic cardiomyopathy. *Int J Cardiovasc Imaging*. 2016;32(4):593-601.
44. Mast TP, Teske AJ, Walmsley J, et al. Right Ventricular Imaging and Computer Simulation for Electromechanical Substrate Characterization in Arrhythmogenic Right Ventricular Cardiomyopathy. *J Am Coll Cardiol*. 2016;68(20):2185-2197.
45. Aneq MÅ, Engvall J, Brudin L, Nylander E. Evaluation of right and left ventricular function using speckle tracking echocardiography in patients with arrhythmogenic right ventricular cardiomyopathy and their first degree relatives. *Cardiovasc Ultrasound*. 2012;10(1):37.

46. Verdonschot JAJ, Merken JJ, Brunner-La Rocca H-P, et al. Value of Speckle Tracking–Based Deformation Analysis in Screening Relatives of Patients With Asymptomatic Dilated Cardiomyopathy. *JACC Cardiovasc Imaging*. 2020;13(2):549-558.
47. Taha K, te Rijdt WP, Verstraelen TE, et al. Early Mechanical Alterations in Phospholamban Mutation Carriers. *JACC Cardiovasc Imaging*. 2021;14(5):885-896.
48. Sefa Okten M, Tuluze K, Yakar Tuluze S, et al. Screening first-degree relatives of patients with idiopathic dilated cardiomyopathy. *Herz*. 2017;42(7):669-676.
49. van der Bijl P, Bootsma M, Hiemstra YL, Ajmone Marsan N, Bax JJ, Delgado V. Left ventricular 2D speckle tracking echocardiography for detection of systolic dysfunction in genetic, dilated cardiomyopathies. *Eur Heart J Cardiovasc Imaging*. 2019;20(6):694-699.
50. Paldino A, De Angelis G, Dal Ferro M, et al. High prevalence of subtle systolic and diastolic dysfunction in genotype-positive phenotype-negative relatives of dilated cardiomyopathy patients. *Int J Cardiol*. 2021;324:108-114.
51. Lakdawala NK, Thune JJ, Colan SD, et al. Subtle Abnormalities in Contractile Function Are an Early Manifestation of Sarcomere Mutations in Dilated Cardiomyopathy. *Circ Cardiovasc Genet*. 2012;5(5):503-510.
52. Akhan O, Demir E, Dogdus M, Cakan FO, Nalbantgil S. Speckle tracking echocardiography and left ventricular twist mechanics: predictive capabilities for noncompaction cardiomyopathy in the first degree relatives. *Int J Cardiovasc Imaging*. 2021;37(2):429-438.
53. Bos JM, Towbin JA, Ackerman MJ. Diagnostic, prognostic, and therapeutic implications of genetic testing for hypertrophic cardiomyopathy. *J Am Coll Cardiol*. 2009;54(3):201-211.
54. Robinson P, Griffiths PJ, Watkins H, Redwood CS. Dilated and Hypertrophic Cardiomyopathy Mutations in Troponin and α -Tropomyosin Have Opposing Effects on the Calcium Affinity of Cardiac Thin Filaments. *Circ Res*. 2007;101(12):1266-1273.
55. Klues HG, Schiffrers A, Maron BJ. Phenotypic spectrum and patterns of left ventricular hypertrophy in hypertrophic cardiomyopathy: Morphologic observations and significance as assessed by two-dimensional echocardiography in 600 patients. *J Am Coll Cardiol*. 1995;26(7):1699-1708.
56. Te Riele ASJM, James CA, Philips B, et al. Mutation-positive arrhythmogenic right ventricular dysplasia/cardiomyopathy: the triangle of dysplasia displaced. *J Cardiovasc Electrophysiol*. 2013;24(12):1311-1320.
57. Kirkels FP, Lie ØH, Cramer MJ, et al. Right Ventricular Functional Abnormalities in Arrhythmogenic Cardiomyopathy. *JACC Cardiovasc Imaging*. 2021;14(5):900-910.
58. Spirito P, Bellone P, Harris KM, Bernabò P, Bruzzi P, Maron BJ. Magnitude of Left Ventricular Hypertrophy and Risk of Sudden Death in Hypertrophic Cardiomyopathy. *N Engl J Med*. 2000;342(24):1778-1785.
59. Argirò A, Zampieri M, Berteotti M, et al. Emerging Medical Treatment for Hypertrophic Cardiomyopathy. *J Clin Med*. 2021;10(5):951.
60. Ho CY, Day SM, Axelsson A, et al. Valsartan in early-stage hypertrophic cardiomyopathy: a randomized phase 2 trial. *Nat Med*. 2021;27(10):1818-24.
61. Tabassian M, Sunderji I, Erdei T, et al. Diagnosis of Heart Failure With Preserved Ejection Fraction: Machine Learning of Spatiotemporal Variations in Left Ventricular Deformation. *J Am Soc Echocardiogr*. 2018;31(12):1272-84.
62. van de Leur R, Taha K, Bos MN, et al. Discovering and Visualizing Disease-specific Electrocardiogram Features Using Deep Learning: Proof-of-concept in Phospholamban Gene Mutation Carriers. *Circ Arrhythm Electrophysiol*. 2021; 14(2):e009056.

63. Mirea O, Pagourelis ED, Duchenne J, et al. Intervendor Differences in the Accuracy of Detecting Regional Functional Abnormalities: A Report From the EACVI-ASE Strain Standardization Task Force. *JACC Cardiovasc Imaging*. 2018;11(1):25-34.

SUPPLEMENTARY MATERIAL

Supplementary methods

Search queries

MEDLINE

(strain[tiab] OR deformation imaging[tiab] OR speckle tracking[tiab] OR GLS[tiab] OR mechanical dispersion[tiab]) AND ((genetic cardiomyopathy[tiab] OR inherited cardiomyopathy[tiab]) OR ("Cardiomyopathy, Hypertrophic"[Mesh] OR hypertrophic cardiomyopathy[tiab] OR HCM[tiab] OR hypertrophic obstructive cardiomyopathy[tiab] OR HOCM[tiab]) OR ("Cardiomyopathy, Dilated"[Mesh] OR dilated cardiomyopathy[tiab] OR DCM[tiab]) OR ("Arrhythmogenic Right Ventricular Dysplasia"[Mesh] OR arrhythmogenic cardiomyopathy[tiab] OR ACM[tiab] OR arrhythmogenic right ventricular cardiomyopathy[tiab] OR ARVC[tiab] OR arrhythmogenic right ventricular dysplasia[tiab] OR ARVD[tiab] OR ARVD/C[tiab]) OR (non-compaction[tiab] OR NCCM[tiab] OR LVNC[tiab] OR RVNC[tiab]))

Embase

(strain:ab,ti OR 'deformation imaging':ab,ti OR 'speckle tracking':ab,ti OR gls:ab,ti OR 'mechanical dispersion':ab,ti) AND ('genetic cardiomyopathy':ab,ti OR 'inherited cardiomyopathy':ab,ti OR 'hypertrophic cardiomyopathy':ab,ti OR hcm:ab,ti OR 'hypertrophic obstructive cardiomyopathy':ab,ti OR hocm:ab,ti OR 'dilated cardiomyopathy':ab,ti OR dcm:ab,ti OR 'arrhythmogenic cardiomyopathy':ab,ti OR acm:ab,ti OR 'arrhythmogenic right ventricular cardiomyopathy':ab,ti OR arvc:ab,ti OR 'arrhythmogenic right ventricular dysplasia':ab,ti OR arvd:ab,ti OR 'arvd/c':ab,ti OR 'non compaction':ab,ti OR nccm:ab,ti OR lvnc:ab,ti OR rvnc:ab,ti)

Cochrane

((strain OR deformation imaging OR speckle tracking OR GLS OR mechanical dispersion) AND ((genetic cardiomyopathy OR inherited cardiomyopathy) OR (hypertrophic cardiomyopathy OR HCM OR hypertrophic obstructive cardiomyopathy OR HOCM) OR (dilated cardiomyopathy OR DCM) OR (arrhythmogenic cardiomyopathy OR ACM OR arrhythmogenic right ventricular cardiomyopathy OR ARVC OR arrhythmogenic right ventricular dysplasia OR ARVD OR ARVD*C) OR (non-compaction OR NCCM OR LVNC OR RVNC)));ti,ab,kw

Quality assessment

The Newcastle – Ottawa Quality Assessment Scale (NOS) for case-control studies was used for assessment of case-control studies, and the NOS for cohort studies was used for (longitudinal) cohort studies. In case of a study with a mixed case-control design and a cohort study design, the study was assessed with both scales. The quality assessment was performed by two independent observers (K.T. and F.K.) and disagreement was solved by consensus.

Newcastle – Ottawa Quality Assessment Scale for case-control studies

Selection, Q1: Is the case definition adequate? (1p)

A point was awarded if the included relatives were identified through screening of the family of an index patient.

Selection, Q2: Representativeness of the cases (1p)

Cases were considered representative if relatives were consecutively included over a certain time period, or in case of a random sample of relatives.

Selection, Q3: Selection of controls (1p)

Studies that included mutation-positive relatives were awarded a point if the control group consisted of genotype-negative relatives. In case of non-genotyped relatives, a control group with community controls (i.e. healthy volunteers) was considered to be an appropriate control group.

Selection, Q4: Definition of controls (1p)

A point was awarded if control subjects were genotype-negative and/or not related to a patient with genetic cardiomyopathy.

Comparability, Q1: Comparability of cases and controls (2p)

Studies were awarded points on the basis of comparability between relatives and controls at baseline. One point was awarded per variable (typically age and sex) that was comparable between relatives and controls (with a significance level of $p > 0.05$) or adjusted for confounding, with a maximum of two points.

Exposure, Q1: Ascertainment of exposure (1p)

Exposure was defined as the presence of abnormalities measured by deformation imaging. A point was awarded when the deformation imaging analysis was performed blind for the case/control status and for other relevant clinical data.

Exposure, Q2: Same method for ascertainment of cases and controls (1p)

A point was awarded if the same method for deformation imaging was used in relatives and control subjects.

Exposure, Q3: Non-response rate (1p)

In this question we assessed exclusion of cases because of insufficient image quality. Studies were awarded a point if it was reported that the exclusion rate was comparable between relatives and control subjects.

Newcastle – Ottawa Quality Assessment Scale for cohort studies*Selection, Q1: Representativeness of the exposed cohort (1p)*

Exposure was defined as the presence of abnormalities measured by deformation imaging at baseline. A point was awarded if relatives were consecutively or randomly included at baseline, regardless of their measurements by deformation imaging.

Selection, Q2: Selection of the non-exposed cohort (1p)

A point was awarded if the study reported comparative analysis of exposed and non-exposed relatives (i.e. relatives with and without deformation imaging abnormalities).

Selection, Q3: Ascertainment of exposure (1p)

Studies were awarded a point if it was reported that deformation imaging was performed blind for outcomes.

Selection, Q4: Demonstration that outcome of interest was not present at start of the study (1p)

A point was awarded if the outcome of interest was absent at the start of the study.

Comparability, Q1: Comparability of cohorts (2p)

Studies were awarded points if they reported data on comparability at baseline between the group with vs. the group without deformation imaging abnormalities. One point was awarded per variable that was comparable between the groups (with a significance level of $p > 0.05$) or adjusted for confounding, with a maximum of two points

Outcome, Q1: Assessment of outcome (1p)

Studies were awarded points in case of independent or blind assessment of the outcome, or by confirmation of the outcome by reference to secure records.

Outcome, Q2: Was follow-up long enough for outcomes to occur (1p)

Since the outcomes of interest were different among the studies, we could not define one acceptable length of follow-up for all studies. This question was therefore assessed per study by two independent observers and disagreement was solved by consensus.

Outcome, Q3: Adequacy of follow-up cohorts (1p)

Studies were awarded a point if the follow-up rate was deemed high enough to avoid selection bias. In case of a low follow-up rate, we evaluated follow-up rates of the exposed and non-exposed cohort to assess the risk of bias (if needed we requested this data from the author).

Supplementary results

Quality assessment

The Newcastle-Ottawa scale for case-control studies was used to assess the risk of bias in 24 studies (**Supplementary table 1**). The median score for case-control studies was 7 out of 9 points (ranging between 6 and 9 points). Most points were lost because the rate of echocardiogram exclusion due to insufficient image quality was not reported. Moreover, many studies investigating genotype-positive relatives lost points due to inclusion of healthy volunteers as control subjects instead of genotype-negative relatives. Last, more than half of the studies did not report whether analyses were performed blind for clinical data.

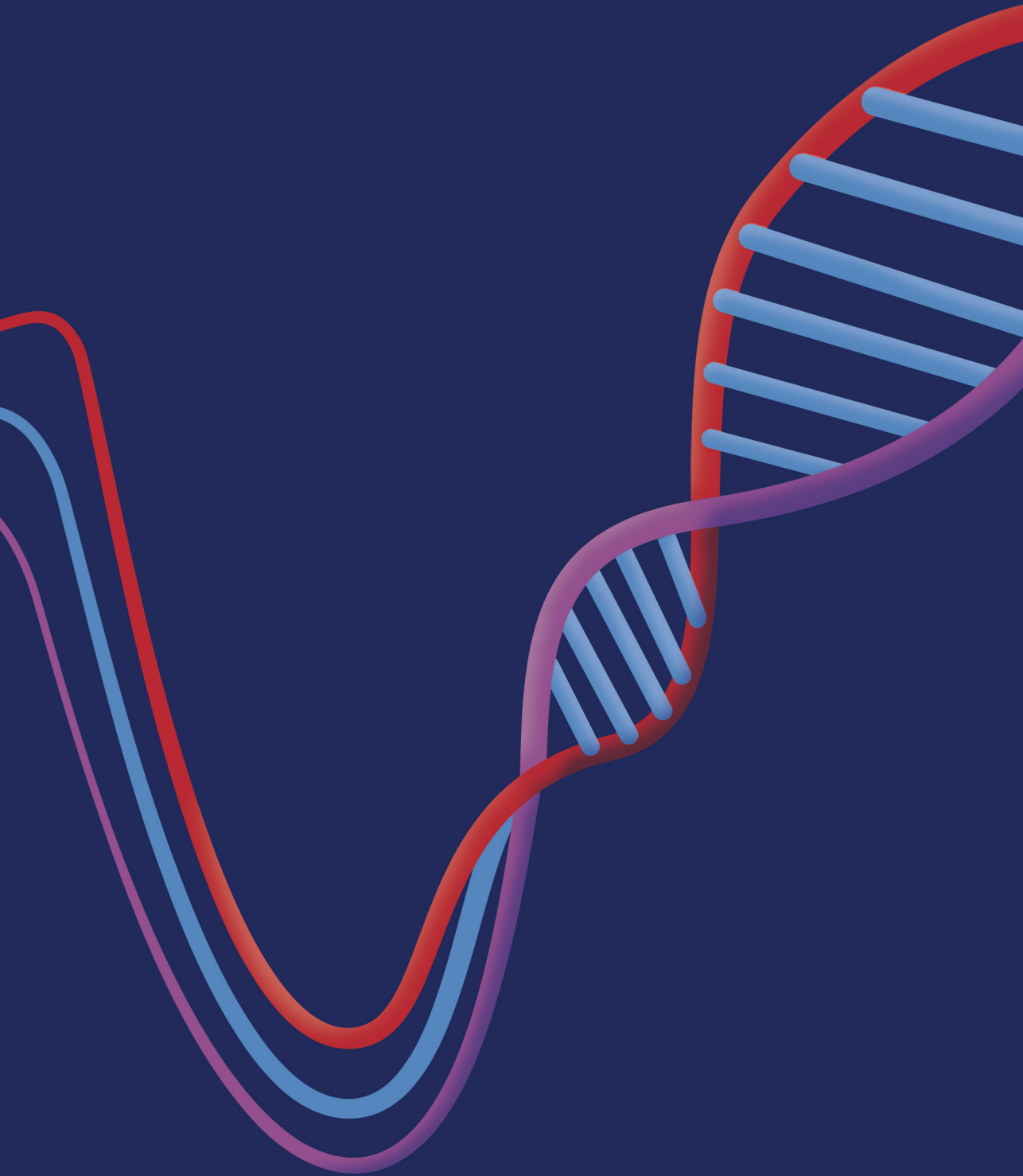
The Newcastle-Ottawa scale for cohort studies was used in 10 studies (**Supplementary table 2**). The median score for cohort studies was 7 out of 9 points (ranging between 6 and 8 points). Most points were lost because it was not reported whether clinical characteristics of the two groups of relatives that were followed (often relatives with normal vs. abnormal strain) were comparable. Moreover, many studies lost points because follow-up was deemed not long enough for outcomes to occur

Supplementary table 1. Quality assessment case-control studies

Study	Selection				Comparability		Exposure			Total score
	Q1	Q2	Q3	Q4	Q1	Q1	Q2	Q3		
HCM										
van Velzen, 2019	●	●		●	●●		●	●	7	
Haland, 2017	●	●		●	●		●	●	6	
Ho, 2009	●	●	●	●	●●	●	●		8	
Williams, 2018	●	●		●	●●		●		6	
Baudry, 2020	●	●		●	●●	●	●		7	
Yiu, 2012	●	●		●	●●		●		6	
Kauer, 2017	●	●		●	●●		●		6	
De, 2011	●			●	●●	●	●		6	
Grover, 2019	●	●	●	●	●●		●		7	
Peyrou, 2016	●	●		●	●●		●		6	
Forsey, 2014	●	●		●	●●		●		6	
ACM										
Mast, 2016	●	●		●	●	●	●		6	
Sarvari, 2011	●	●		●	●●	●	●		7	
Reant, 2016	●	●		●	●●	●	●		7	
Mast, 2016	●	●		●	●●	●	●		7	
Aneq, 2012	●	●	●	●	●●	●	●	●	9	
Mast, 2015	●	●		●	●	●	●		6	
DCM										
Verdonschot, 2020	●	●		●	●●		●		6	
Taha, 2020	●	●		●	●●	●	●		7	
Okten, 2017	●	●	●	●	●●	●	●		8	
van der Bijl, 2019	●	●	●	●	●●		●		7	
Paldino 2020	●	●	●	●	●●	●	●		8	
Lakdawala, 2012	●	●	●	●	●●	●	●	●	9	
NCCM										
Akhan, 2020	●	●	●	●	●●		●		7	

Supplementary table 2. Quality assessment cohort studies

Study	Selection				Comparability Q1	Outcome			Total score
	Q1	Q2	Q3	Q4		Q1	Q2	Q3	
HCM									
van Velzen, 2019	●	●		●		●	●	●	6
ACM									
Lie, 2018	●	●	●	●	●●	●		●	8
Leren, 2017	●	●	●	●		●	●	●	7
Chivulescu, 2019	●	●	●	●		●	●	●	7
Mast, 2019	●	●	●	●		●	●	●	7
Taha, 2020	●	●	●	●			●	●	6
Mast, 2016	●	●	●	●		●	●	●	7
DCM									
Verdonschot, 2020	●	●		●	●●	●		●	7
Taha, 2020	●	●	●	●	●●	●		●	8
Paldino 2020	●	●	●	●	●●	●			7



CHAPTER 8

The Added Value of Abnormal Regional Myocardial Function for Risk Prediction in Arrhythmogenic Right Ventricular Cardiomyopathy

Feddo P. Kirkels, Christine Rootwelt-Norberg, Laurens P. Bosman, Eivind W. Aabel, Steven A. Muller, Anna I. Castrini, Karim Taha, Nick van Osta, Øyvind H. Lie, Folkert W. Asselbergs, Joost Lumens, Anneline S.J.M. te Riele, Nina E. Hasselberg, Maarten J. Cramer, Kristina H. Haugaa, Arco J. Teske**

** Shared last authorship*

Eur Heart J Cardiovasc Imaging. 2023;24(12):1710-1718.

ABSTRACT

Background & aims

A risk calculator for individualized prediction of first-time sustained ventricular arrhythmia (VA) in arrhythmogenic right ventricular cardiomyopathy (ARVC) patients has recently been developed and validated (www.ARVCrisk.com). This study aimed to investigate whether regional functional abnormalities, measured by echocardiographic deformation imaging, can provide additional prognostic value.

Methods & results

From two referral centres, 150 consecutive patients with a definite ARVC diagnosis, no prior sustained VA and an echocardiogram suitable for deformation analysis were included (aged 41 ± 17 years, 50% female). During a median follow-up of 6.3 (IQR 3.1-9.8) years, 37 (25%) experienced a first-time sustained VA. All tested left and right ventricular (LV, RV) deformation parameters were univariable predictors for first-time VA. While LV function did not add predictive value in multivariable analysis, two RV deformation parameters did; RV free wall longitudinal strain and regional RV deformation patterns remained independent predictors after adjusting for the calculator-predicted risk (HR 1.07 [1.02-1.11]; $p = 0.004$ and 4.45 [1.07-18.57]; $p = 0.040$, respectively) and improved its discriminative value (from C-statistic 0.78 to 0.82 in both. Akaike information criterion change >2). Importantly, all patients who experienced VA within 5 years from the echocardiographic assessment had abnormal regional RV deformation patterns at baseline.

Conclusion

This study showed that regional functional abnormalities measured by echocardiographic deformation imaging can further refine personalized arrhythmic risk prediction when added to the ARVC risk calculator. The excellent negative predictive value of normal RV deformation could support clinicians considering timing of ICD implantation in patients with intermediate arrhythmic risk.

INTRODUCTION

Arrhythmogenic right ventricular cardiomyopathy (ARVC) is an inherited heart disease which predisposes patients to life-threatening ventricular arrhythmias (VA) and progressive cardiac failure.¹ The disease is characterized by fibrofatty replacement and subsequent structural and functional alterations of primarily right ventricular (RV) myocardium. VA can occur already in an early stage of the disease, making it a leading cause of sudden cardiac death in especially the young and seemingly healthy.^{1,2} Consideration of an implantable cardioverter defibrillator (ICD) is a central component of clinical management of ARVC patients, but selecting the optimal candidates, especially for primary prevention of sudden cardiac death, has proven difficult.³ To support clinicians and patients in this process, a multimodality risk calculation tool was published in 2019⁴ and its utility has been replicated in multiple independent cohorts.⁵⁻⁸ In addition, a recent study validated the risk calculator as an accurate tool to repeatedly calculate arrhythmic risk during follow-up.⁹

Visualisation of the structural disease substrate is an important part of arrhythmic risk stratification in ARVC. RV ejection fraction (RVEF), measured by cardiac magnetic resonance imaging (CMR), is currently the only imaging parameter included in the ARVC risk calculator. While global systolic function of the RV is well reflected in the EF, we know that life-threatening VA can already occur early in the disease. In this stage, fibrofatty replacement of myocardial tissue leads to regional wall motion abnormalities while the global systolic function is preserved. Echocardiographic deformation imaging has developed as a more sensitive method for detection of regional abnormalities in myocardial function. Regional deformation abnormalities have been associated to arrhythmia in ARVC patients, whereby especially negative predictive value of normal deformation was high.¹⁰⁻¹³ Although results of previous studies were promising, the added predictive value of echocardiographic deformation imaging should be tested in a multimodality approach and on top of current clinical practice. The purpose of this study was to test the predictive value of echocardiographic deformation imaging in a primary prevention cohort of patients with ARVC, and to further improve arrhythmic risk stratification by investigating whether it has prognostic value independent of the ARVC VA risk calculator.

METHODS

Study design and population

We included consecutive patients with definite ARVC who presented to the University Medical Centre Utrecht in the Netherlands and the Oslo University Hospital in Norway up until January 1st 2023. These patients were partially included in previous studies.^{10,11,14,15} ARVC diagnosis was defined according to the 2010 Task Force Criteria (TFC).¹⁶ Patients with previous myocardial infarction or congenital heart disease were excluded. Date of inclusion was defined as the date of echocardiographic examination closest to date of diagnosis and available for performing deformation imaging. Patients with VA prior to baseline evaluation were excluded. Dutch patients were included in the UCC-UNRAVEL biobank for inherited heart diseases. The study was approved by both local institutional ethics review boards and complies with the Declaration of Helsinki.

Data collection

For each patient, baseline demographics, treatment with antiarrhythmic medication, and presence of an ICD were recorded. ECG, Holter and CMR data from the study closest to baseline echocardiography and prior to occurrence of primary outcome were used. The 7 variables included in the ARVC risk calculator (www.ARVCrisk.com) were collected independently in each centre according to uniform definitions, and included: age at diagnosis, sex, recent syncope (<1 year ago), number of inferior/anterior leads with T-wave inversion, non-sustained ventricular tachycardia (NSVT), 24-hour premature ventricular complex (PVC) count and RVEF measured by CMR. All genetic variants reported were adjudicated according to the American College of Medical Genetics and Genomics guidelines.¹⁷

The echocardiographic deformation imaging protocol was previously described in more detail.^{12,15} We used a GE Vivid 7, E9 or E95 scanner and loops were stored for post-processing with EchoPac version 203 (GE Healthcare, Horten, Norway). All measurements were performed by a single observer according to the current guidelines^{18,19} and blinded to clinical outcome. Data on inter- and intra-observer variability are provided in *Supplemental Table 1*. Myocardial deformation was assessed in three apical views of the left ventricle (LV) and in the RV focused 4-chamber view. Predictive value of the following five deformation parameters was tested: LV global longitudinal strain (GLS), LV and RV mechanical dispersion (LVMD and RVMD, respectively), RV free-wall longitudinal strain (RV_{FW}LS) and regional RV deformation patterns. LV GLS was calculated as the peak negative strain from the averaged regional 16-segment LV model.¹⁸ Mechanical dispersion was calculated as the standard deviation (SD) of the segmental time intervals until maximum shortening of 16 segments in the LV and 6 segments in the RV.¹² RV_{FW}LS was defined as the peak negative strain from the averaged regional RV free wall deformation curve. Deformation patterns were analysed in the basal, mid and apical segment of the RV free wall. The RV deformation pattern was classified as normal if the pattern was normal in all three segments and abnormal if at least one segment showed abnormal deformation (*Figure 1*).^{10,15}

Missing data

Missing data were assumed to be missing at random and imputed using multiple imputation with chained equations as described previously.⁴ The multiple imputation model included all pre-specified predictors, proband status and genotype together with the outcome, and cumulative baseline hazard estimation.^{20,21} A total of 25 imputed datasets were generated, and the final inference estimations were combined using Rubin's rules.²²

All covariates of the ARVC risk calculator and the deformation imaging variables had <5% missingness, except for 24-hour PVC count (11%) and RVEF by CMR (19%). Complete case analyses without imputation and 24-hour PVC count and RVEF were performed as sensitivity analyses (*Supplemental Table 2*).

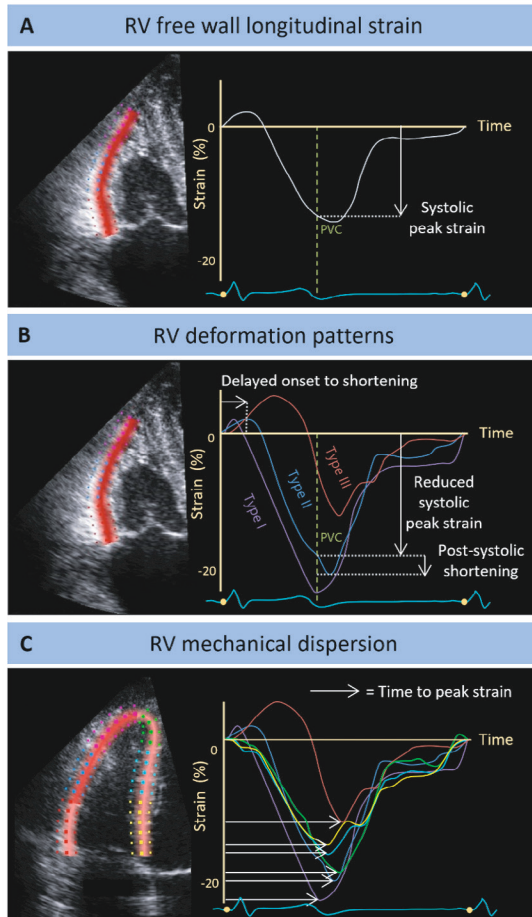


Figure 1. Echocardiographic deformation imaging in an RV focused view

Colours represent different myocardial regions. **Panel A.** RV free wall longitudinal strain was calculated as the systolic peak strain from the averaged regional RV free wall deformation characteristic. **Panel B.** Based on predefined criteria, a division into 3 different deformation patterns was identified in all three segments of the RV lateral wall.¹⁵ Type I is normal deformation. Type II and III are abnormal deformation, whereby type II is characterized by delayed onset of shortening, reduced systolic peak strain, and minor post-systolic shortening; type III is characterized by little or no systolic peak strain, predominantly systolic stretching, and major post-systolic shortening. **Panel C.** For RV mechanical dispersion, a 6-segment model of the RV was used, including both the lateral wall and the interventricular septum. It was calculated as the SD of the segmental time intervals from onset Q/R on the surface ECG to peak negative strain and expressed in ms.¹² Abbreviations: PVC = pulmonic valve closure.

Study Outcomes

The primary outcome of the study was first sustained VA after TFC-based ARVC diagnosis. In accordance with the published ARVC risk calculator, sustained VA was defined as sustained ventricular tachycardia lasting ≥ 30 s at ≥ 100 bpm, aborted cardiac arrest, or appropriate ICD therapy. Incident heart transplantation, cardiovascular mortality and all-cause mortality were also recorded during follow-up. Follow-up duration was defined as the time interval between baseline echocardiography and VA or censoring, which was defined as last clinical visit if lost to follow-up or 1st of January 2023.

Statistical analysis

Analyses were performed with RStudio (v. 2022.12.0, Boston, USA) and Stata (v. 16.0, Statacorp, Texas, USA). Continuous variables were expressed as mean with SD or median with interquartile range (IQR) and compared using independent sample t-test or Mann–Whitney U test. Categorical variables were presented as frequencies (%) and compared using the Fisher exact test. VA-free survival probability was estimated using the Kaplan–Meier method and Cox proportional hazard regression analysis. For Kaplan–Meier analysis of continuous variables, categorization was based on threshold regression analysis. All deformation imaging variables were subjected to linearity and proportional hazards assumption testing criteria. P-values were two-sided, and values < 0.05 were considered significant.

Model testing

The overall discriminative performance of the ARVC risk calculator was measured using the optimism-corrected Harrell's C-statistic. The 5-year risk of sustained VA for an individual patient as per the published model was calculated using the following equation⁴:

$$5 \text{ year VA risk} = 1 - 0.84 \exp(PI)$$

where the prognostic index (PI) was calculated according to the equation:

$$PI = \text{male sex} * 0.49 - \text{age} * 0.022 + \text{cardiac syncope} * 0.66 + \text{NSVT} * 0.81 +$$

$$\ln(24\text{-h PVC count}) * 0.17 + \text{TWI} * 0.11 - \text{RVEF} * 0.025$$

Based on the 5-year risk of sustained VA, patients were stratified into low risk ($< 5\%$), intermediate risk (5 – 25%) and high risk ($> 25\%$) subgroups. Of note, the baseline hazard for 5-year prediction (0.84) has been corrected since the initial publication in 2019.²³

To assess the predictive ability of deformation imaging for VA events, Cox proportional hazards models of VA events were fitted to deformation imaging results. The strongest deformation imaging parameters were identified by stepwise backward selection in a multivariable Cox proportional hazards model and tested for prognostic value independent of the ARVC risk calculator PI (incorporated as a fixed offset variable). Model discriminations were assessed using a nonparametric concordance-based C-statistic. The added value of deformation imaging to the ARVC risk calculator for predicting VA events was assessed by comparison of optimism-corrected C-statistics. The Akaike information criterion (AIC) was estimated for the risk models, for which a reduction of > 2 was considered a significant improvement.

RESULTS

Clinical characteristics

From 439 eligible patients, 130 were excluded due to prior VA, 146 were family-members carrying a pathogenic or likely pathogenic (P/LP) genetic variant who did not fulfil a definite TFC diagnosis and 13 were excluded due to various other reasons as shown in *Supplemental Figure 1*. Hence, the final cohort consisted of 150 patients (*Table 1*, see *Supplemental Table 3* for data per centre) with a definite ARVC diagnosis and no prior VA who underwent echocardiographic deformation imaging. Mean age at baseline echocardiography was 41 ± 17 years, 75 (50%) patients were male, and 51 (34%) were proband. Median follow-up duration was 6.3 (IQR 3.1 – 9.8) years. The majority of patients (86%) were carriers of a P/LP genetic variant, of which mutations in the *PKP2* gene (66%) were most prevalent.

Table 1. Baseline characteristics of ARVC patients without and with sustained VA during follow-up

	All (n=150)	No VA (n=113)	VA (n=37)	p-value
Demographics				
Age at echocardiography, yrs	41.3 ± 17.1	41.8 ± 17.3	39.8 ± 16.8	0.558
Male	75 (50)	54 (48)	21 (57)	0.449
Probands	51 (34)	30 (27)	21 (57)	0.002
Genetic status				
P/LP variant	129 (86)	102 (90)	27 (73)	0.018
PKP2	99 (66)	74 (66)	25 (68)	
DSP	3 (2)	3 (3)	0 (0)	
DSG2	5 (3)	5 (4)	0 (0)	
PLN	18 (12)	16 (14)	2 (5)	
Multiple	1 (1)	1 (1)	0 (0)	
Other	3 (2)	3 (3)	0 (0)	
Clinical history				
Any cardiac symptoms	105 (70)	73 (65)	32 (87)	0.021
Recent cardiac syncope	12 (8)	2 (2)	10 (27)	<0.001
Treatment at baseline				
ICD	19 (13)	12 (11)	7 (19)	0.302
Anti-arrhythmic drugs	24 (16)	18 (16)	6 (16)	1
Beta-blockers	45 (30)	33 (30)	12 (32)	0.893
Clinical phenotype				
Total TFC score	5 (4-6)	5 (4-6)	7 (5-8)	<0.001
Age at diagnosis	40.7 ± 16.7	41.3 ± 16.6	38.8 ± 17.1	0.436
ECG				
TWI in ≥3 precordial leads	57 (38)	38 (34)	19 (51)	0.078
TWI in ≥2 inferior leads	22 (15)	14 (12)	8 (22)	0.185
PVC count per 24h	497 (48 – 2322)	281 (31 – 1496)	894 (757 – 7884)	<0.001

Table 1. Baseline characteristics of ARVC patients without and with sustained VA during follow-up (continued)

	All (n=150)	No VA (n=113)	VA (n=37)	p-value
NSVT	67 (45)	46 (41)	21 (57)	0.141
CMR (n = 141)				
RVEF, %	46 ± 10	48 ± 9	39 ± 10	<0.001
RVEDVi, ml	109 ± 29	105 ± 29	125 ± 24	0.002
LVEF, %	54 ± 9	54 ± 8	52 ± 10	0.387
LGE	23 (20)	16 (18)	7 (25)	0.419
Traditional echocardiography				
LVEF, %	55 ± 8	55 ± 7	53 ± 12	0.216
RVFAC, %	39 ± 9	40 ± 9	35 ± 8	0.017
RVOT, mm	35 ± 7	34 ± 6	37 ± 7	0.058
Echocardiographic deformation imaging				
LV GLS, %	-18.2 ± 3.2	-18.7 ± 2.5	-16.7 ± 4.3	0.001
LVMD, ms	38(31 – 47)	38 (30 – 46)	42 (36 – 49)	0.107
RV _{FW} LS, %	-19.5 ± 7.0	-21.0 ± 6.3	-15.0 ± 6.9	<0.001
RVMD, ms	33 (23 – 44)	30 (21 – 43)	43 (29 – 67)	0.003
RV deformation pattern abnormal	97 (66)	63 (56)	34 (94)	<0.001
Type I	51 (35)	50 (45)	2 (6)	
Type II	65 (44)	50 (45)	15 (42)	
Type III	32 (22)	13 (12)	19 (53)	

Values are n (%), mean ± standard deviation or median (25th, 75th percentiles) according to the distribution of normality. Abbreviations: ARVC = arrhythmogenic right ventricular cardiomyopathy, CMR = cardiac magnetic resonance, DSG2 = desmoglein-2, DSP = desmoplakin, EDVi = end diastolic volume indexed, EF = ejection fraction, FAC = fractional area change, GLS = global longitudinal strain, LGE = late gadolinium enhancement, LV = left ventricular, MD = mechanical dispersion, NSVT = non-sustained ventricular tachycardia, PKP2 = plakophilin-2, P/LP = pathogenic or likely pathogenic, PVC = premature ventricular complex, RV = right ventricular, RV_{FW}LS = right ventricular free wall longitudinal strain, RVOT = right ventricular outflow tract, TFC = task force criteria, TWI = T-wave inversion, VA = ventricular arrhythmia.

Outcomes

Thirty-seven patients (25%) experienced the primary outcome of first sustained VA after a median follow-up of 2.9 years (IQR 0.9 – 6.0) (Figure 2, see Supplemental Figure 2 for data per centre). The corresponding annual event rate of the primary endpoint was 3.6% (95% CI 2.6 – 5.0%). The most common primary endpoint was appropriate ICD therapy (n = 26, 70%), followed by sustained VA (n = 10, 27%) and sudden cardiac arrest (n = 1, 3%). At last follow-up, half of the patients (n = 75, 50%) had received an ICD. Eight (5%) patients had died of mostly non-cardiac cause (n = 6, 4%) and three (2%) had undergone heart transplantation.

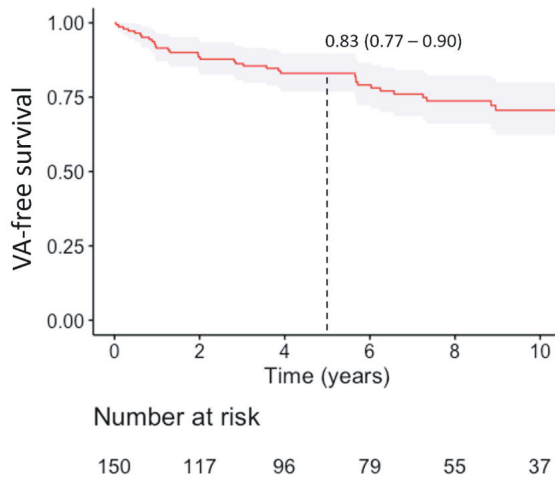


Figure 2. Kaplan-Meier estimate of ventricular arrhythmia (VA) free survival for patients with arrhythmogenic right ventricular cardiomyopathy without prior sustained VA

Dotted line represents cumulative 5-year survival.

Deformation imaging and incidence of VA

One patient was excluded because of insufficient image quality for any deformation analyses. Of included patients, LV deformation imaging was feasible in 146 patients (97%) and RV deformation imaging in 148 patients (99%). For the LV deformation parameters, LV GLS was worse in patients who later experienced VA, while LVMD was not (*Table 1*). All three RV deformation parameters ($RV_{FW}LS$, RVMD and RV deformation pattern) were more abnormal in patients with VA during follow-up. Regional RV deformation patterns were abnormal (i.e. type II or type III) at baseline in 94% of patients with VA anytime during follow-up against 56% in patients without VA. Moreover, all patients who experienced the primary outcome within 5 years from the echocardiographic assessment had abnormal RV deformation patterns at baseline. Nevertheless, the positive predictive value of an abnormal RV deformation pattern for VA within 5 years was low with 0.41 (95% CI 0.32 – 0.50). The worst outcome was seen in patients with the most abnormal type III deformation pattern (*Figure 3, panel B*). For the Kaplan-Meier plot of $RV_{FW}LS$ (*Figure 3, panel A*), threshold regression analysis identified two optimal cut-offs for increased arrhythmic risk (-24% and -17%).

Univariable survival analysis showed increased hazard of VA occurrence for all tested deformation parameters, as expressed by hazard ratios (*Table 2*).

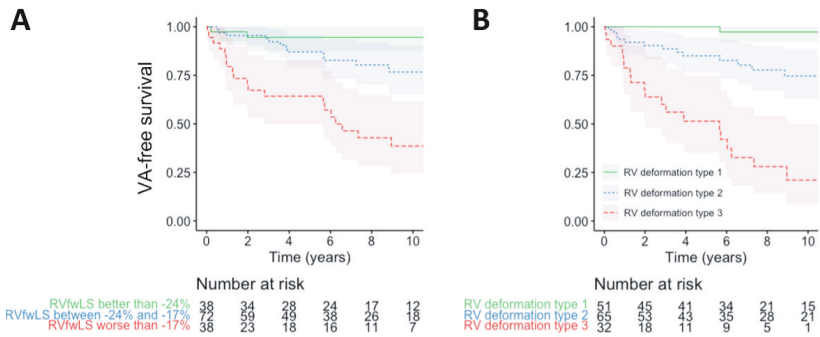


Figure 3. Ventricular arrhythmia (VA) free survival in presence of abnormal RV function measured by deformation imaging

Panel A. When dividing RV free wall longitudinal strain (RV_{FWLS}) into three groups, a clear difference in VA-free survival was seen. **Panel B.** A normal RV deformation pattern (type 1) was associated with excellent negative predictive value (0.96, 95% CI 0.87 – 0.99). Especially the most abnormal type 3 deformation was associated with worse outcome.

Deformation imaging in personalized risk prediction

Discriminative value of the current ARVC risk calculator model was good in this cohort with a C-statistic of 0.78 (95% CI 0.71 – 0.86), consistent with prior results.(4)

The strongest predictors of VA among the deformation parameters were RV_{FWLS}, abnormal RV deformation pattern and LV GLS. Incremental predictive value was found when adding RV_{FWLS} or abnormal RV deformation pattern to the risk calculator. Adding LV GLS, however, did not seem to improve prediction of VA (Table 3). The resulting adjusted HR was 1.07 ([95% CI 1.02 – 1.11], p = 0.004) per % worsening of RV_{FWLS} and 4.45 ([95% CI 1.07 – 18.57], p = 0.040) in case of an abnormal regional deformation pattern. Optimism-corrected C-statistics were higher when RV_{FWLS} or RV deformation pattern was added to the model (in both cases 0.82 [95% CI 0.75 – 0.88]). Also, both RV parameters reduced the model AIC by >2, which was not the case for LV GLS.

The intermediate arrhythmic risk subgroup (5-year VA risk 5 – 25% as per the ARVC risk calculator) consisted of 73 patients. In this subgroup, no events occurred in the 28 patients who had normal regional RV deformation patterns. In the 7 intermediate risk patients who did experience VA during follow-up we observed abnormal regional RV deformation patterns, resulting in a specificity of 0.41 (95% CI 0.31 – 0.57) and positive predictive value of 0.16 (95% CI 0.14 – 0.19).

Table 2 . Associations between deformation parameters and first sustained VA

	HR (95% CI)	p-value	
LV GLS	1.20 (1.10 – 1.31)	<0.001	per % worsening
LVMD (ln)	2.73 (1.07 – 6.98)	0.036	per ln(ms) increase
RV _{FW} LS	1.12 (1.08 – 1.17)	<0.001	per % worsening
RVMD (ln)	3.09 (1.73 – 5.53)	<0.001	per ln(ms) increase
RV deformation pattern	10.94 (2.63 – 45.56)	<0.001	when abnormal

Hazard ratios (HR) are presented with 95% CIs. Since linearity and proportional hazards assumption testing criteria showed signs of non-linearity for mechanical dispersion, the timing variables LVMD and RVMD were subjected to log-transformation. Abbreviations: GLS = global longitudinal strain, LV = left ventricular, MD = mechanical dispersion, RV = right ventricular, RV_{FW}LS = right ventricular free wall longitudinal strain, VA = ventricular arrhythmia.

Table 3. The added value of deformation imaging for personalized arrhythmic risk prediction in ARVC

	Adjusted HR (95% CI)	p-value	C-statistic (95% CI)	AIC
Risk calculator model	0.78 (0.71 – 0.86)	299.2
+ RV _{FW} LS per % worsening	1.07 (1.02 – 1.11)	0.004	0.82 (0.75 – 0.88)	-7.2
+ RV deformation abnormal	4.45 (1.07 – 18.57)	0.040	0.82 (0.75 – 0.88)	-6.6
+ LV GLS per % worsening	1.07 (0.98 – 1.18)	0.138	0.79 (0.72 – 0.86)	-1.3

Hazard ratios (HR) are adjusted for the calculator-predicted risk. HR and optimism corrected C-statistic are presented with 95% CIs. Abbreviations: AIC = Akaike information criterion, ARVC = arrhythmogenic right ventricular cardiomyopathy, LV GLS = left ventricular global longitudinal strain, RV = right ventricular, RV_{FW}LS = right ventricular free wall longitudinal strain.

DISCUSSION

In this study, we showed that echocardiographic deformation imaging can further refine personalized arrhythmic risk prediction when added to the ARVC risk calculator. Both abnormal regional RV deformation patterns and RV_{FW}LS as a continuous indicator of RV function showed independent predictive value on top of the risk calculator and improved its discriminative value. Measures of LV deformation, on the other hand, did not add predictive value in this cohort. Importantly, all patients who experienced VA within 5 years from the echocardiographic assessment showed abnormal RV deformation patterns at baseline.

Risk stratification in patients with ARVC

Arrhythmic risk prediction is a central part of clinical management of ARVC patients, in order to determine if and when an ICD is warranted. Especially in this disease, risk prediction is challenging, since life-threatening arrhythmias can already occur early in the disease.² Predictors of unfavourable outcome which were identified over the past decades were recently summarized in a meta-analysis²⁴ and subsequently used for the development of a

multimodality risk calculation tool.⁴ This published ARVC risk calculator (www.ARVCrisk.com), which aims to predict the 5-year risk of first sustained VA in patients with definite ARVC, has since been validated in different settings and showed superior performance when compared to existing risk stratification algorithms.⁵⁻⁸ In the current cohort, annual event rate was slightly lower compared to the initial risk calculator study⁴ (3.6% [95% CI 2.6 – 5.0] vs 5.6% [95% CI 4.7 – 6.6]), which may be caused by a larger proportion of diagnosed family members in the current cohort, identified through cascade genetic testing. Still, the discriminative value was comparable (0.78 [95% CI 0.71 – 0.86] vs 0.77 [95% CI 0.73 – 0.81]).

Deformation imaging in ARVC arrhythmic risk stratification

Echocardiography has an important role in the diagnosis and follow-up of ARVC patients. However, traditional echocardiographic parameters, such as RV fractional area change and RV outflow tract diameter, may lack sensitivity with regards to detection of early disease substrates.^{4,25,26} Over the past two decades, echocardiographic deformation imaging has evolved into a sensitive method to detect regional abnormalities in myocardial function, reflecting structural disease manifestation in ARVC.²⁶⁻²⁸ Distinct abnormalities in regional myocardial function have been identified, which were associated with disease severity. These regional deformation patterns with delayed onset to shortening, reduced peak strain and post-systolic shortening (*Figure 1*) most likely reflect pathologic changes on tissue level which form the substrate for VA.¹⁵ An exploratory study sought to explain these specific deformation types by computer simulation using the CircAdapt model. Indeed, loss in contractility and increase in local myocardial stiffness characterized the regional function abnormalities. Studies consistently showed that the first and most severely affected area was the subtricuspid region of the RV lateral wall^{10,15,29}, a well known predilection site for the earliest disease manifestation of ARVC.³⁰ Echocardiographic deformation imaging is well suited to evaluate this specific region. Of interest, deformation abnormalities appear already early in the development of this disease and remain stable or progress over time.^{29,31} These observations and modelling data indicate that this specific functional assessment might be of incremental value in predicting VA, since it seems to reflect the microscopic alterations that form the substrate for re-entry tachycardia. Indeed multiple indicators of myocardial deformation have been associated to VA.¹⁰⁻¹³ In a previous primary prevention study including both ARVC patients and family members at risk, both LVMD and RV_{FW}LS were strong predictors of arrhythmic outcome.¹¹ In a combined cohort with patients from our two centres, especially negative predictive value of normal regional deformation patterns for prior VA (98%) was high.¹⁰ The current prediction study is unique since it included only patients with a definite TFC diagnosis, which explains the high prevalence of abnormal regional RV deformation patterns (65%). Importantly, it confirmed the high negative predictive value of normal deformation, since all patients with VA within 5 years from baseline evaluation already showed regional abnormalities in the RV. In line with previous ARVC studies, the subtricuspid was consistently first and most severely affected. Up to now, added value of deformation imaging has never been tested on top of current clinical practice. The multimodality ARVC risk score⁴, a validated tool for clinical risk prediction tool guiding management and ICD necessity, created this opportunity.

Deformation imaging added to the ARVC risk calculator

In a multivariable model, RV deformation patterns and RV_{FW}LS were the strongest independent predictors of first sustained VA. The superiority of RV parameters was not surprising given the

fact that patients were selected by the RV focused 2010 TFC and mostly *PKP2* variant carriers were included, who typically present with the classical right dominant ARVC phenotype. Previous papers showed that the ARVC risk calculator performs well in *PKP2* dominated cohorts, while for patients with a different genetic background incorporation of measures of LV function might be important.^{8,32}

When integrated with the ARVC risk calculator, both indices of regional RV deformation still showed independent prognostic value. Models that combined the ARVC risk calculator-predicted risk with regional RV deformation patterns or $RV_{FW}LS$ were superior at predicting VA compared to either of these predictors alone. This confirms our hypothesis that inclusion of measures of regional RV function can improve arrhythmic risk prediction in ARVC.

Clinical implications

This was the first study showing added value of deformation imaging in a clinical practice-based, multimodality approach. Both RV deformation patterns and $RV_{FW}LS$ were able to refine risk stratification when added to the existing ARVC risk calculator. Especially negative predictive value of deformation imaging was high; none of the patients with normal regional RV deformation patterns at baseline experienced VA within 5 years from the echocardiogram. The existing risk calculator already performs very well when it comes to guiding ICD implantation in the high- and low-risk group. In the intermediate arrhythmic risk group (5-25% at 5 years), the timing of ICD implantation is most challenging. With a two-step approach, this additional stratification tool can probably be of greatest use in this intermediate arrhythmic risk group as predicted by the ARVC risk calculator. Normal RV deformation could in this case reassure both clinician and patient in a watchful waiting strategy regarding ICD implantation. While echocardiographic deformation imaging has shown the ability to reveal early signs of disease associated to arrhythmic outcome in multiple genetic cardiomyopathies^{27,33,34}, predictive value when added to clinical risk prediction tools in these diseases is yet to be investigated.

Limitations

Due to the high prevalence of patients with P/LP variants in the *PKP2* gene (66%), generalizability to patient populations with other dominating variants is uncertain. A genotype specific approach might improve predictive value especially for non-*PKP2* patients, as pointed out in a recent validation of the ARVC risk calculator⁸, but is hindered by lack of power.

The feasibility of echocardiographic deformation imaging depends on image quality. With >95% for both LV and RV deformation imaging, feasibility was high in the ARVC cohorts included in this study. If centres do not routinely perform dedicated RV focused images, feasibility may drop. Missing data also represent a limitation of this retrospective cohort. Although a complete case analysis demonstrates a similar trend towards added value of deformation imaging, missing data could influence the relative benefit.

Despite our efforts to assemble the largest cohort of definite ARVC patients with deformation imaging to date, this study is underpowered for development of a new ARVC-risk calculator with incorporation of RV deformation imaging. Larger multi-centre collaborations are much needed.

Last, this was an observational study with inherent limitations by study design. Validation in an external cohort will be important for the clinical implementation of integrating deformation imaging with the ARVC risk calculator.

CONCLUSION

This study showed that inclusion of regional abnormalities in RV function can further refine personalized arrhythmic risk prediction in ARVC. Both regional deformation patterns and longitudinal strain of the RV free wall improved prediction of arrhythmic outcome beyond the ARVC risk calculator. With a two-step approach, the excellent negative predictive value of normal RV deformation could support clinicians considering timing of ICD implantation in patients with intermediate arrhythmic risk.

Key Question

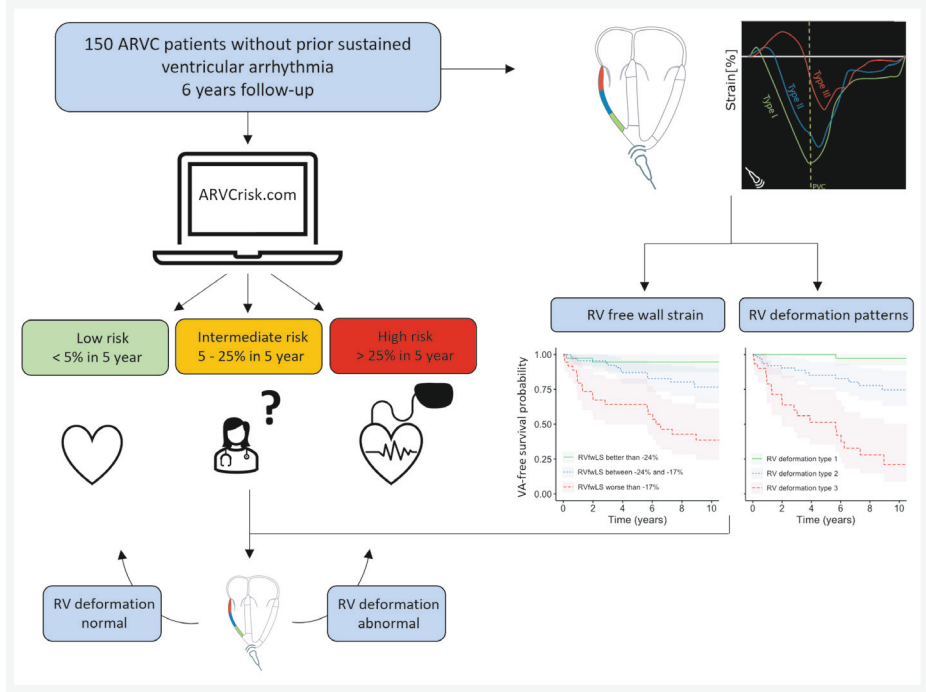
Can the published arrhythmogenic right ventricular cardiomyopathy risk calculator (www.ARVCrisk.com) be improved by addition of regional functional abnormalities measured by echocardiographic deformation imaging?

Key Finding

- 1) RV deformation abnormalities were independent risk predictors and improved discriminative value of the ARVC risk calculator.
- 2) Normal RV deformation had excellent negative predictive value for incident life-threatening ventricular arrhythmia and can support a watchful waiting strategy regarding ICD implantation.

Take Home Message

Addition of regional RV functional abnormalities can further refine personalized risk prediction with the ARVC risk calculator.



Central illustration

ARVC = arrhythmogenic right ventricular cardiomyopathy; RV = right ventricular; RVEF = right ventricular ejection fraction; RVFWLS = right ventricular free wall longitudinal strain; VA = ventricular arrhythmia.

REFERENCES

1. Corrado D, Link MS, Calkins H. Arrhythmogenic Right Ventricular Cardiomyopathy. *N Engl J Med*. 2017 Jan 5;376(1):61-72.
2. Groeneweg JA, Bhonsale A, James CA, et al. Clinical Presentation, Long-Term Follow-Up, and Outcomes of 1001 Arrhythmogenic Right Ventricular Dysplasia/Cardiomyopathy Patients and Family Members. *Circ Cardiovasc Genet*. 2015;8(3):437-46.
3. Calkins H, Corrado D, Marcus F. Risk Stratification in Arrhythmogenic Right Ventricular Cardiomyopathy. *Circulation*. 2017;136(21):2068-82.
4. Cadrin-Tourigny J, Bosman LP, Nozza A, et al. A new prediction model for ventricular arrhythmias in arrhythmogenic right ventricular cardiomyopathy. *Eur Heart J*. 2019;40(23):1850-1858.
5. Baudinaud P, Laredo M, Badenco N, et al. External Validation of a Risk Prediction Model for Ventricular Arrhythmias in Arrhythmogenic Right Ventricular Cardiomyopathy. *Canadian Journal of Cardiology*. 2021;37(8):1263-6.
6. Aquaro GD, de Luca A, Cappelletto C, et al. Comparison of different prediction models for the indication of implanted cardioverter defibrillator in patients with arrhythmogenic right ventricular cardiomyopathy. *ESC Heart Fail*. 2020;7(6):4080-8.
7. Jordà P, Bosman LP, Gasperetti A, et al. Arrhythmic risk prediction in arrhythmogenic right ventricular cardiomyopathy: external validation of the arrhythmogenic right ventricular cardiomyopathy risk calculator. *Eur Heart J*. 2022;43(32):3041-52.
8. Protonotarios A, Bariani R, Cappelletto C, et al. Importance of genotype for risk stratification in arrhythmogenic right ventricular cardiomyopathy using the 2019 ARVC risk calculator. *Eur Heart J*. 2022;43(32):3053-67.
9. Carrick RT, te Riele ASJM, Gasperetti A, et al. Longitudinal Prediction of Ventricular Arrhythmic Risk in Patients With Arrhythmogenic Right Ventricular Cardiomyopathy. *Circ Arrhythm Electrophysiol*. 2022;15(11):e011207.
10. Kirkels FP, Lie ØH, Cramer MJ, et al. Right Ventricular Functional Abnormalities in Arrhythmogenic Cardiomyopathy. *J Am Coll Cardiol Img*. 2021;14(5):900-10.
11. Lie ØH, Rootwelt-Norberg C, Dejgaard LA, et al. Prediction of Life-Threatening Ventricular Arrhythmia in Patients With Arrhythmogenic Cardiomyopathy: A Primary Prevention Cohort Study. *J Am Coll Cardiol Img*. 2018;11(10):1377-86.
12. Sarvari SI, Haugaa KH, Anfinson OG, et al. Right ventricular mechanical dispersion is related to malignant arrhythmias: A study of patients with arrhythmogenic right ventricular cardiomyopathy and subclinical right ventricular dysfunction. *Eur Heart J*. 2011;32(9):1089-96.
13. Leren IS, Saberniak J, Haland TF, Edvardsen T, Haugaa KH. Combination of ECG and Echocardiography for Identification of Arrhythmic Events in Early ARVC. *J Am Coll Cardiol Img*. 2017 May;10(5):503-13.
14. Rootwelt-Norberg C, Lie ØH, Chivulescu M, et al. Sex differences in disease progression and arrhythmic risk in patients with arrhythmogenic cardiomyopathy. *Europace*. 2021;23(7):1084-91.
15. Mast TP, Teske AJ, Walmsley J, et al. Right Ventricular Imaging and Computer Simulation for Electromechanical Substrate Characterization in Arrhythmogenic Right Ventricular Cardiomyopathy. *J Am Coll Cardiol*. 2016 Nov;68(20):2185-97.

16. Marcus FI, McKenna WJ, Sherrill D, et al. Diagnosis of arrhythmogenic right ventricular cardiomyopathy/Dysplasia: Proposed modification of the task force criteria. *Circulation*. 2010;121(13):1533–41.
17. Richards S, Aziz N, Bale S, et al. Standards and guidelines for the interpretation of sequence variants: A joint consensus recommendation of the American College of Medical Genetics and Genomics and the Association for Molecular Pathology. *Genet Med*. 2015;17(5):405–24.
18. Voigt JU, Pedrizzetti G, Lysyansky P, et al. Definitions for a common standard for 2D speckle tracking echocardiography: consensus document of the EACVI/ASE/Industry Task Force to standardize deformation imaging. *Eur Heart J Cardiovasc Imaging*. 2015;16(1):1–11.
19. Badano LP, Koliás TJ, Muraru D, et al. Standardization of left atrial, right ventricular, and right atrial deformation imaging using two-dimensional speckle tracking echocardiography: A consensus document of the EACVI/ASE/Industry Task Force to standardize deformation imaging. *Eur Heart J Cardiovasc Imaging*. 2018;19(6):591–600.
20. Van Buuren S, Boshuizen HC, Knook DL. Multiple imputation of missing blood pressure covariates in survival analysis. *Stat Med*. 1999;18:681–94.
21. White IR, Royston P, Wood AM. Multiple imputation using chained equations: Issues and guidance for practice. *Stat Med*. 2011;30:377–99.
22. Rubin DB. Multiple Imputation for Nonresponse in Surveys. New York: John Wiley and Sons. 1987.
23. Corrigendum to: A new prediction model for ventricular arrhythmias in arrhythmogenic right ventricular cardiomyopathy. *Eur Heart J*. 2022;43(28):2712.
24. Bosman LP, Sammani A, James CA, et al. Predicting arrhythmic risk in arrhythmogenic right ventricular cardiomyopathy: A systematic review and meta-analysis. *Heart Rhythm*. 2018;15(7):1097–107.
25. Borgquist R, Haugaa KH, Gilljam T, et al. The diagnostic performance of imaging methods in ARVC using the 2010 task force criteria. *Eur Heart J Cardiovasc Imaging*. 2014;15(11):1219–25.
26. Kirkels FP, Bosman LP, Taha K, et al. Improving Diagnostic Value of Echocardiography in Arrhythmogenic Right Ventricular Cardiomyopathy Using Deformation Imaging. *J Am Coll Cardiol Img*. 2021;14(12):2481–83.
27. Taha K, Kirkels FP, Teske AJ, et al. Echocardiographic Deformation Imaging for Early Detection of Genetic Cardiomyopathies: JACC Review Topic of the Week. *J Am Coll Cardiol*. 2022;79(6):594–608.
28. Haugaa KH, Basso C, Badano LP, et al. Comprehensive multi-modality imaging approach in arrhythmogenic cardiomyopathy - an expert consensus document of the European Association of Cardiovascular Imaging. *Eur Heart J Cardiovasc Imaging*. 2017;18(3):237–53.
29. Taha K, Mast TP, Cramer MJ, et al. Evaluation of Disease Progression in Arrhythmogenic Cardiomyopathy: The Change of Echocardiographic Deformation Characteristics Over Time. *J Am Coll Cardiol Img*. 2020;13(2):631–34.
30. te Riele ASJM, James CA, Philips B, et al. Mutation-positive arrhythmogenic right ventricular dysplasia/cardiomyopathy: The triangle of dysplasia displaced. *J Cardiovasc Electrophysiol*. 2013;24(12):1311–20.
31. Mast TP, Taha K, Cramer MJ, et al. The Prognostic Value of Right Ventricular Deformation Imaging in Early Arrhythmogenic Right Ventricular Cardiomyopathy. *J Am Coll Cardiol Img*. 2019;12(3):446–55.
32. Aquaro GD, de Luca A, Cappelletto C, et al. Prognostic Value of Magnetic Resonance Phenotype in Patients With Arrhythmogenic Right Ventricular Cardiomyopathy. *J Am Coll Cardiol*. 2020;75(22):2753–65.

33. Tower-Rader A, Mohanane D, To A, Lever HM, Popovic ZB, Desai MY. Prognostic Value of Global Longitudinal Strain in Hypertrophic Cardiomyopathy. *J Am Coll Cardiol Img.* 2019;12(10):1930–42.
34. Kawakami H, Nerlekar N, Haugaa KH, Edvardsen T, Marwick TH. Prediction of Ventricular Arrhythmias With Left Ventricular Mechanical Dispersion. *J Am Coll Cardiol Img.* 2020;13(2):562–72

SUPPLEMENTARY MATERIAL

Supplemental Table 1. Intra- and inter-observer variability in deformation imaging measurements

		Utrecht				Oslo	
		INTRA_1	INTRA_2	INTER_1_2		INTER	
GLS	ICC + 95%CI	0.95 [0.81;0.98]	0.96 [0.91;0.98]	0.94 [0.89;0.96]		0.92 [0.81;0.97]	
LVMD	ICC + 95%CI	0.96 [0.91;0.99]	0.99 [0.96;0.99]	0.92 [0.86;0.96]		0.87 [0.71;0.95]	
RVMD	ICC + 95%CI	0.87 [0.71;0.95]	x	0.84 [0.64;0.93]		0.91 [0.78;0.96]	
RV patterns	difference	3/20	0/20	3/40		2/20	
	K	0.74 p <0.001	1.00 p <0.001	0.87 p <0.001	0.85 p <0.001		
	weighted K	0.78 p <0.001	1.00 p <0.001	0.89 p <0.001	0.89 p <0.001		

Abbreviations: GLS = global longitudinal strain, ICC = intraclass correlation coefficient, K = kappa statistic, LV = left ventricle, MD = mechanical dispersion, RV = right ventricle.

Supplemental Table 2. Complete case analyses without imputation of RVEF and 24-hour PVC count

	RVEF imputation using MICE multivariable analysis		Complete case multivariable analysis	
	Adjusted HR (95% CI)	p-value	Adjusted HR (95% CI)	p-value
Risk calculator model				
+ RV _{FW} LS per % worsening	1.07 (1.02 – 1.11)	0.004	1.08 (1.02 – 1.13)	0.004
+ RV deformation abnormal	4.45 (1.07 – 18.57)	0.040	3.32 (0.79 – 13.98)	0.102
+ LV GLS per % worsening	1.07 (0.98 – 1.18)	0.138	1.06 (0.95 – 1.18)	0.277

Hazard ratios (HR) are adjusted for the calculator-predicted risk. HR are presented with 95% CIs. Abbreviations: LV GLS = left ventricular global longitudinal strain, RV = right ventricular, RVEF = right ventricular ejection fraction, RV_{FW}LS = right ventricular free wall longitudinal strain.

	24-hour Holter count imputation using MICE multivariable analysis		Complete case multivariable analysis	
	Adjusted HR (95% CI)	p-value	Adjusted HR (95% CI)	p-value
Risk calculator model				
+ RV _{FW} LS per % worsening	1.07 (1.02 – 1.11)	0.004	1.07 (1.02 – 1.13)	0.007
+ RV deformation abnormal	4.45 (1.07 – 18.57)	0.040	3.72 (0.88 – 15.77)	0.074
+ LV GLS per % worsening	1.07 (0.98 – 1.18)	0.138	1.04 (0.93 – 1.17)	0.451

Hazard ratios (HR) are adjusted for the calculator-predicted risk. HR are presented with 95% CIs. Abbreviations: LV GLS = left ventricular global longitudinal strain, RV = right ventricular, RV_{FW}LS = right ventricular free wall longitudinal strain.

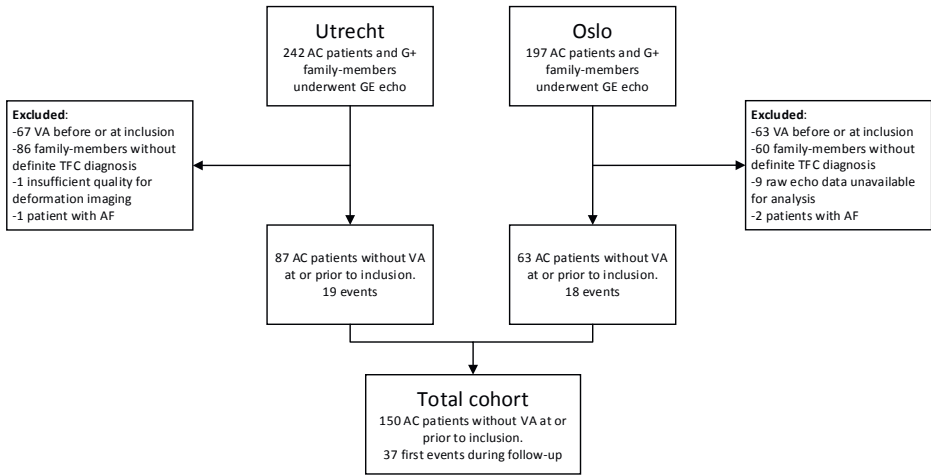
Supplemental Table 3. Baseline characteristics separated by centre

	All (n=150)	Utrecht (n=87)	Oslo (n=63)	p-value
Demographics				
Age at echocardiography, yrs	41.3 ± 17.1	40.3 ± 16.3	42.7 ± 18.3	0.409
Male	75 (50)	39 (45)	36 (57)	0.186
Proband	51 (34)	25 (29)	26 (41)	0.154
Follow-up duration, yrs	6.3 (3.1 – 9.8)	7.2 (3.8 – 10.3)	4.5 (2.0 – 9.1)	0.042
Genetic status				
P/LP variant	129 (86)	81 (93)	48 (76)	0.007
PKP2	99 (66)	57 (66)	42 (67)	
DSP	3 (2)	2 (2)	1 (2)	
DSG2	5 (3)	2 (2)	3 (5)	
PLN	18 (12)	18 (21)	0 (0)	
Multiple	1 (1)	0 (0)	1 (2)	
Other	3 (2)	2 (2)	1 (2)	
Clinical history				
Any cardiac symptoms	105 (70)	58 (67)	47 (75)	0.386
Recent cardiac syncope	12 (8)	5 (6)	7 (11)	0.373
Clinical phenotype				
Total TFC score (IQR)	5 (4-6)	5 (4-7)	5 (4-6)	0.227
Age at diagnosis	40.7 ± 16.7	39.6 ± 15.4	42.2 ± 18.3	0.343
ECG				
TWI in ≥3 precordial leads	57 (38)	30 (35)	27 (43)	0.312
TWI in ≥2 inferior leads	22 (15)	10 (12)	12 (19)	0.244
PVC count	497 (48 – 2322)	555 (126 – 2261)	409 (20 – 3201)	0.597
NSVT	67 (45)	39 (45)	28 (45)	1
CMR				
RVEF, %	46 ± 10	46 ± 9	45 ± 13	0.830
RVEDVi, ml	109 ± 29	108 ± 26	111 ± 37	0.568
LVEF, %	54 ± 9	53 ± 8	55 ± 9	0.372
LGE	23 (20)	17 (22)	6 (15)	0.465
Traditional echocardiography				
LVEF, %	55 ± 8	54 ± 8	56 ± 9	0.216
RVFAC, %	39 ± 9	40 ± 9	38 ± 9	0.207
RVOT, mm	35 ± 7	33 ± 6	37 ± 7	<0.001
Echocardiographic deformation imaging				
LV GLS, %	-18.2 ± 3.2	-18.5 ± 3.2	-17.9 ± 3.2	0.224
LVMD, ms	38(31 – 47)	38 (29 – 48)	39 (33 – 47)	0.571
RV _{FW} LS, %	-19.5 ± 7.0	-20.4 ± 6.0	-18.3 ± 8.0	0.072

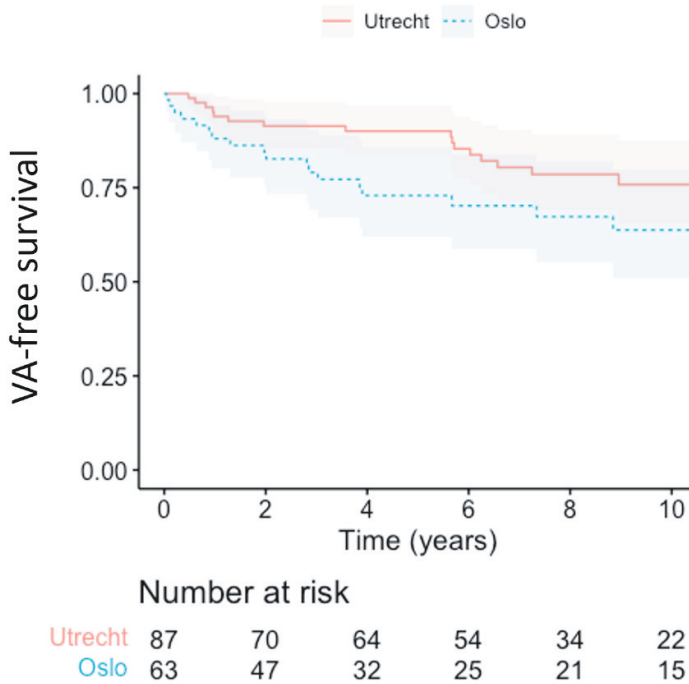
Supplemental Table 3. Baseline characteristics separated by centre (continued)

	All (n=150)	Utrecht (n=87)	Oslo (n=63)	p-value
RVMD, ms	33 (23 – 44)	32 (24 – 43)	36 (23 – 51)	0.373
RV deformation pattern abnormal	97 (65)	50 (58)	47 (76)	0.040
Type I	51 (35)	50 (45)	2 (6)	
Type II	65 (44)	50 (45)	15 (42)	
Type III	32 (22)	13 (12)	19 (53)	

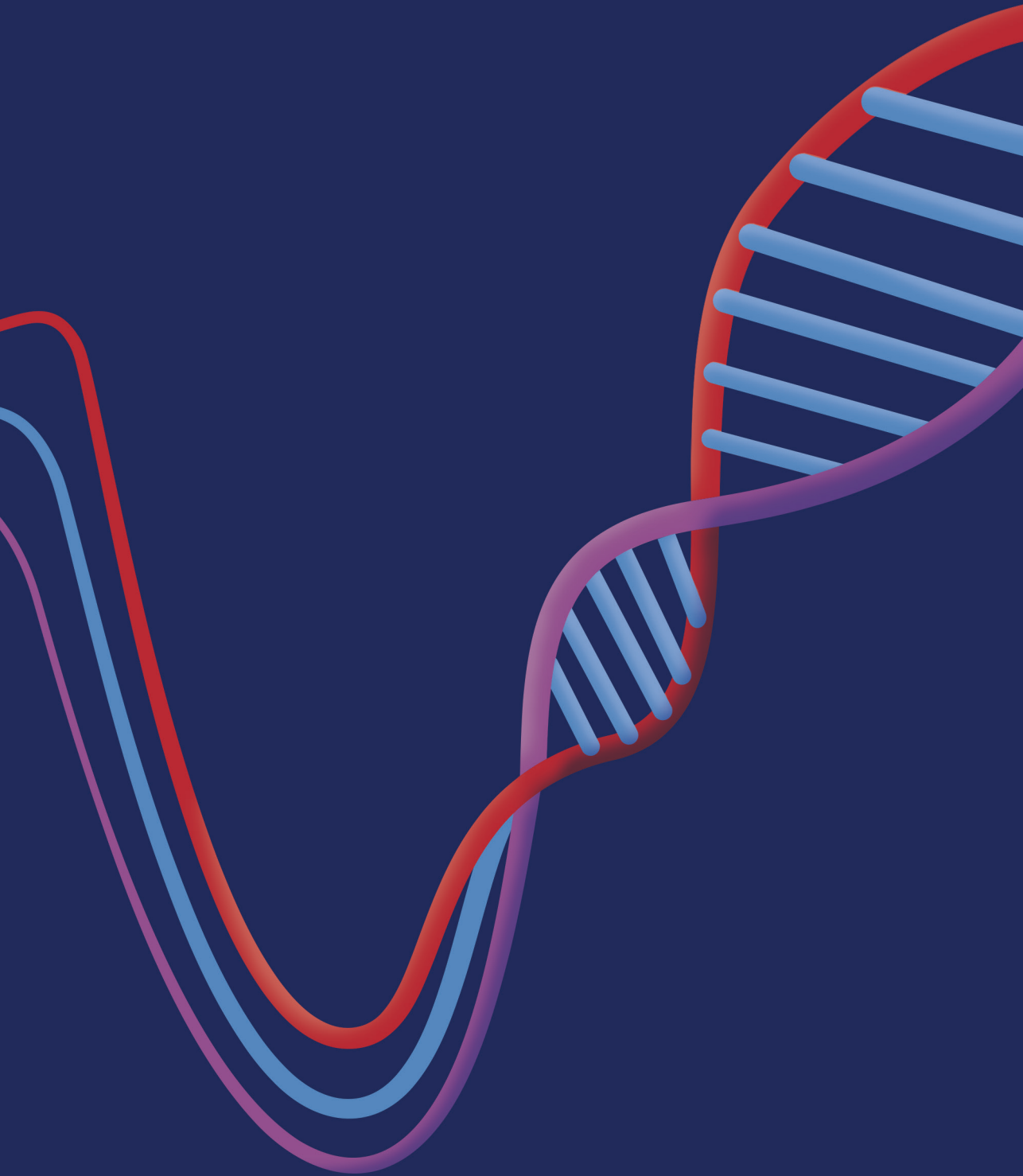
Values are n (%), mean \pm standard deviation or median (25th, 75th percentiles) according to the distribution of normality. Abbreviations: CMR = cardiac magnetic resonance, DSG2 = desmoglein-2, DSP = desmoplakin, EDVi = end diastolic volume indexed, EF = ejection fraction, FAC = fractional area change, GLS = global longitudinal strain, LGE = late gadolinium enhancement, LV = left ventricular, MD = mechanical dispersion, NSVT = non-sustained ventricular tachycardia, PKP2 = plakophilin-2, P/LP = pathogenic or likely pathogenic, PVC = premature ventricular complex, RV = right ventricular, RV_{FW}LS = right ventricular free wall longitudinal strain, RVOT = right ventricular outflow tract, TFC = task force criteria, TWI = T-wave inversion, VA = ventricular arrhythmia.



Supplemental Figure 1. Flowchart of inclusion



Supplemental Figure 2. Survival analysis separated by centre



CHAPTER 9

General Discussion and Future Perspectives

Introduction

In this thesis, arrhythmogenic right ventricular cardiomyopathy (ARVC) was used as a disease model to demonstrate the added clinical value of echocardiographic deformation imaging in early diagnosis and risk prediction of genetic cardiomyopathies in general. The chapters of this thesis all contribute to the process of wider clinical implementation in their own way. Besides studies of added clinical value, validation of the technique as well as pathophysiological background of our findings are addressed. Based on the research presented in this thesis, the following chapter will discuss several important aspects and future perspectives in the field. First, the role of genotypic basis in disease definition is discussed. Second, the role of computer modelling and a multimodality approach are addressed. Third, vulnerable arrhythmogenic spots of the heart and the influence of exercise on disease progression will be discussed. Finally, the future steps towards wider clinical implementation of deformation imaging will be addressed.

Genotype vs Phenotype

The classical approach of inherited heart muscle diseases, or cardiomyopathies, is based on phenotype. Based on morphological and functional features, a distinction is made between hypertrophic cardiomyopathy (HCM), dilated cardiomyopathy (DCM), right-sided cardiomyopathy (ARVC) and restrictive cardiomyopathy.¹ While the first two are characterized by mainly structural abnormalities with hypertrophy and dilatation of the left ventricle (LV), respectively, ARVC patients may experience life-threatening arrhythmias before the occurrence of clear structural abnormalities, hence the addition “arrhythmogenic”. The problem with this phenotypic approach is that not all cardiomyopathies can be classified within one of these three categories. Not all left-sided cardiomyopathies show clear dilatation before functional impairment or arrhythmia occur, and not all cardiomyopathies evolve into isolated left- or right-dominant involvement. The problems with this phenotypic approach are well reflected in the changing terminology in the field of ARVC over the past decades, as addressed in the introduction of this thesis. Due to the diverse phenotypic manifestations observed among patients sharing a similar genetic background, the term “ARVC” had become insufficiently comprehensive. Not only the right ventricle (RV) was affected, but also the LV could be involved. Sometimes predominant or even isolated LV disease was observed. This led to the broader term arrhythmogenic cardiomyopathy (AC), which was also used in some chapters of this thesis. Since myriad unrelated diseases which can cause ventricular dysfunction and arrhythmias (including DCM) could now be classified as AC², the field moved back to ARVC to address that one disease and a distinct arrhythmogenic left ventricular cardiomyopathy (ALVC). However, phenotypic expression may be dynamic and often progresses over time. Besides, this approach complicates familial screening, since phenotypic expression may differ within families carrying the same genetic basis for a disease. In the most recent 2023 guideline for the management of cardiomyopathies³, the category of non-dilated left ventricular cardiomyopathy (NDLVC) is added to the existing four phenotype-based categories. Besides, the guideline proposes to start the diagnostic process by integrating symptoms, incidental findings like ECG abnormalities and arrhythmia, and family history to the imaging findings in a so-called *clinical scenario*, which should lead to a phenotype-based diagnosis.

Based on advances in medical technology, clinicians do no longer have to rely on merely phenotypical expression of disease. In the era of increasing availability of genetic testing, disease-causing genetic variants can be identified in many familial (cardiomyopathy) cases.

The genetic basis of the disease has become an important part in both diagnosis and risk stratification. Moreover, in the foreseeable future, treatment approaches are expected to undergo a paradigm shift from one-size-fits-all to individualized treatments based on molecular characteristics of the disease. Treatment will be targeted at the cause of disease, rather than the consequence (dilatation or hypertrophy). It is therefore very likely that the classical phenotypical disease classification will be replaced by a genotype-based disease classification. This is already common practice when a pathogenic variant in the phospholamban or lamin A/C gene is identified (*PLN*- or *LMNA*-cardiomyopathy, respectively). In line with most research which has been performed to this date, the studies included in this thesis are based on the phenotypical approach. The diagnostic 2010 Task Force Criteria⁴ which were tested in **Chapter 2** and used for patient inclusion in most of the other chapters, disregard genotype and focus merely on phenotypical expression of right-sided heart disease. Patients with (likely-)pathogenic variants in genes coding for the cardiac desmosome were treated similarly to patients with non-desmosomal genetic variants or patients without a known disease causing variant. Even within the group of patients with a disease causing genetic variant in the cardiac desmosome, there is considerable heterogeneity. While variants in the plakophilin-2 (*PKP2*) gene typically lead to a classical right-sided ARVC phenotype, variants in the desmoplakin (*DSP*) gene often appear to lead to predominant LV impairment.⁵ It might therefore be more appropriate to distinguish *PKP2*-cardiomyopathy from *DSP*-cardiomyopathy, instead of classifying both as ARVC. Grouping all patients with a TFC-based diagnosis together may lead to important features in genetic subgroups being unrecognized. Patients with a variant in the plakophilin-2 (*PKP2*) gene represent the majority in most cohorts studied in this thesis. The typical abnormal deformation patterns in the subtricuspid segment of the RV lateral wall which were first classified by Mast et al.⁶ are commonly found as one of the first signs of disease manifestation in *PKP2* variant carriers, as described in **Chapter 3** and **Chapter 7**. While different genotypic forms of ARVC all have a final common pathway of myocardial fibro-fatty replacement and ventricular arrhythmias, the disease mechanism may be different among these patients. Not all non-*PKP2* patients show typical abnormal deformation patterns in the subtricuspid segment in the early disease phase. Extrapolation of the sensitivity of subtricuspid RV deformation patterns for detection of early disease in subgroups with another genetic basis should therefore be met with caution. In future research, a genotype-specific approach might reveal specific deformation abnormalities which are characteristic for specific genetic variants. In *PLN* patients and family members, this approach has recently been successfully applied.⁷ Post-systolic shortening in the LV apex showed to be a characteristic finding in *PLN p.Arg14del* variant carriers, preceding any other symptom or sign of disease.

In **Chapter 9**, we demonstrated the added value of deformation imaging on top of the ARVC risk predictor in a cohort of patients with an ARVC phenotype. In line with the studies in which the risk predictor was developed and validated, all patients fulfilled a definite ARVC diagnosis according to the 2010 TFC.⁴ In a validation study of the risk calculator it was pointed out that genotype should be included in future models for ARVC, since risk prediction appeared to be better in *PKP2* patients compared to for instance *DSP* patients.⁸ In another recent study, it was shown that risk stratification of familial cardiomyopathies in a genotype-based approach outperformed the classical phenotype-based approach.⁹ Although the differences between genetic subgroups were largely driven by highly pathogenic variants in for instance the *LMNA* gene, this study might be an example for future approaches to risk stratification in genetic cardiomyopathies. Unfortunately, the general obstacle of this approach is that it is very difficult

to assemble a genotypically homogeneous cohort of sufficient size, in order to perform statistically powered studies. Characterization of deformation patterns and subsequent risk-prediction in a genotype-specific approach will only be feasible for disease causing variants with high prevalence and requires global multi-center collaborations, on a much larger scale than currently seen.

Computer modelling of the disease substrate

To characterize the disease substrate in cardiomyopathies, histology should be performed on tissue obtained by myocardial biopsy, autopsy or surgery. A definite diagnosis of ARVC is based on the presence of transmural fibro-fatty replacement of RV myocardium.¹⁰ Since histology is not available in the vast majority of patients, non-invasive imaging, integrated in the TFC, guides the diagnosis. In search of alternative ways to characterize the disease substrate on a cellular level, collaboration between engineers from Maastricht University and clinicians from the University Medical Center Utrecht led to the application of a computer model of the human heart and circulation, called CircAdapt (www.circadapt.org). In 2016, it was hypothesized that this model could be used for *in silico* myocardial disease substrate characterization at an individual patient level, based on generic simulations of the characteristic regional RV deformation abnormalities observed in ARVC patients and family members.⁶ Since the existing paradigm was that electrical abnormalities precede structural abnormalities in ARVC, it was expected that local electrical activation delay would be the cause of abnormal deformation patterns in early ARVC. Surprisingly, characteristic abnormal deformation patterns (type II and III) could be simulated by solely decreasing myocardial contractility and increasing passive stiffness in the model, challenging the existing paradigm. This modelling approach could be very useful to provide a form of “non-invasive biopsy” based on myocardial deformation data. Insight into the local disease substrate might have predictive value for disease progression and might refine arrhythmic risk stratification. In order to bring the modelling approach to clinical application, we wanted to move from generic simulations based on predefined parameter manipulations to a patient-specific approach based on a patient’s Digital Twin (Figure 1). Furthermore, we added local activation delay to the model to get an impression of the contribution of electrical versus mechanical substrates in ARVC.

We first performed a feasibility study, in which we evaluated whether the model could simulate RV myocardial deformation of 10 individual patients by manipulating regional myocardial contractility and passive stiffness as published in 2016.¹¹ Since the CircAdapt model contains many parameters with complex interactions, the focus on two pre-specified parameters in the RV lateral wall disregards many other potentially relevant model parameters. Therefore, we performed a sensitivity analysis to select the most important model parameters for accurate simulation of a patient’s myocardial deformation based on objective mathematical criteria.¹² Starting from a total of 110 parameters representing vascular, valvular and myocardial tissue properties, the final subset included 23 parameter representing regional tissue contractility, compliance, activation delay and wall volume. Subsequently, as reported in **Chapter 4**, we applied this patient-specific modelling approach in the cohort of ARVC patients and family members which was used for the general simulations in 2016. The model indeed showed reduced regional contractile function and tissue compliance in carriers of a pathogenic genetic variant. A characteristic apex-to-base heterogeneity of tissue abnormalities was found, with the basal region of the RV free wall most affected. The next step was to estimate the disease substrate in a longitudinal study, in order to test reproducibility on repeated

examinations and to evaluate disease progression over time. Since both measurements and model estimations introduce uncertainty, in **Chapter 5** the introduction of uncertainty to estimations of tissue properties is described. This was a necessary step towards longitudinal follow-up of the disease substrates presented in **Chapter 6**. The heterogeneity in estimated tissue properties progressed over time in early ARVC subjects in different age groups. While case studies showed that heterogeneity in regional tissue properties in the Digital Twin preceded overt disease and arrhythmia, the added value of absolute values of estimated properties was still limited. Since the model is based on deformation characteristics, which are load dependent, more information on loading conditions during the examination will probably support the interpretation of absolute values, rather than heterogeneity alone. In addition to the phenomenological model used in our Digital Twin approach, computer modelling can also further elucidate the electromechanical coupling which is a central component in the pathophysiology of ARVC.¹³ With the coupling between an electromechanical cardiomyocyte model and a mechanical sarcomere model, myocardial deformation can be related to disease specific changes in cellular electrophysiology and calcium handling within cardiomyocytes.¹⁴

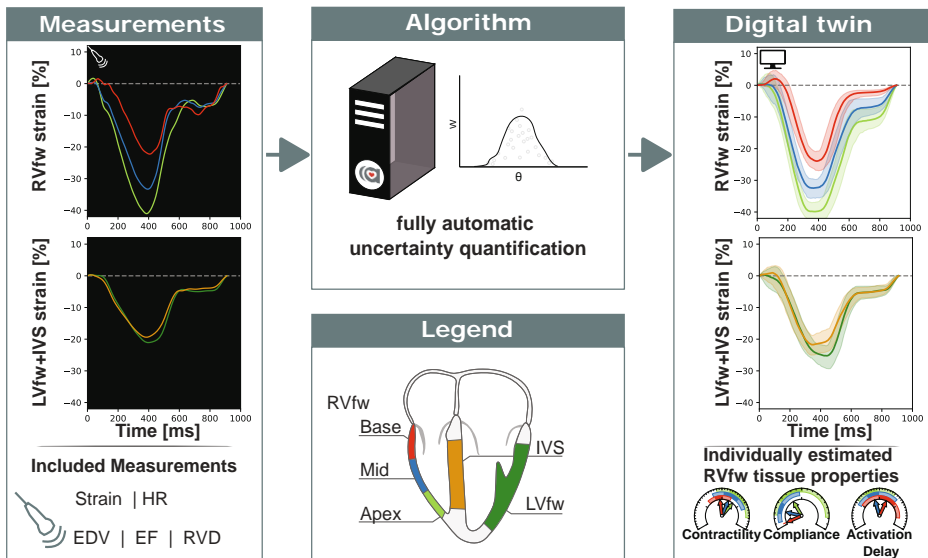


Figure 1. The Digital Twin model as was used after introducing uncertainty into the algorithm¹⁵

Non-invasive measurements were used as input for a fully automated algorithm. The Digital Twin estimated individual tissue properties for the three segments of the RV free wall (RVfw), the inverventricular septum (IVS) and the LV free wall (LVfw). HR = heart rate, EDV = end diastolic volume, EF = ejection fraction, RVD = RV diameter.

Multimodality approach

While a diagnosis of DCM or HCM can usually be made based on one single imaging modality, diagnosis of ARVC and risk assessment in all genetic cardiomyopathies requires a multimodality approach. The aforementioned electromechanical coupling illustrates that both imaging and electrocardiographic diagnostics are needed to perform a complete risk assessment. Over the years, the Utrecht University has developed into a unique environment for ARVC research since

researchers with divergent backgrounds became engaged in investigating the disease, profiting from each other's insights and expertise. New insights in the value of echocardiographic deformation imaging in ARVC could be integrated with the work of other clinical researchers investigating the value of new cardiac magnetic resonance (CMR) techniques¹⁶ or novel electrocardiographic techniques¹⁷. Furthermore, preclinical studies from colleagues from the medical physiology lab provided us with new insights into the role of calcium transients¹³ and colleagues from the Hubrecht lab elucidated disease pathways which are responsible for the decreased contractility which we observe in *PKP2* variant carriers¹⁸.

An ongoing question in the field of ARVC is whether electrical abnormalities precede structural abnormalities. We do see regional deformation abnormalities in a very early stage, even in the absence of electrical abnormalities according to the 2010 TFC (the "subclinical stage" in **Chapter 3**). However, it could be that these deformation abnormalities actually rely on delayed electrical activation rather than a structural substrate. Impairment of the cardiac desmosome can lead to both structural abnormalities and electrical conduction abnormalities.¹⁸ Another question is whether it matters for a patient's prognosis whether electrical delay or a local substrate of decreased contractility causes deformation abnormalities. One method we have applied to try to answer these questions is the use of model estimations of the CircAdapt model. In **Chapter 6** we presented two cases of ARVC patients with early deformation abnormalities. In the Digital Twin of the first patient, abnormal regional myocardial function was estimated to result from reduced contractility with little contribution of mechanical activation delay. The second patient showed heterogeneous mechanical activation in an early stage and experienced a life-threatening arrhythmia shortly after. While hypotheses on the arrhythmogenicity of different substrates have to be tested in cohorts with more events, it shows the potential clinical value of unraveling the electro-mechanical coupling.

Another approach to distinguish electrical from structural disease substrates would be the integration of multimodality data. Colleagues from the department of electrophysiology in the University Medical Center Utrecht have developed a non-invasive ECG imaging method using 67 electrode body surface potential mapping (BSM). While it is difficult to derive information on electrical conduction of the RV on a regular 12-lead surface ECG, this new method allows more detailed evaluation of RV electrical disease. *Figure 2* shows an example of a patient in an early stage of ARVC disease in whom CMR imaging, ECG imaging and echocardiography were performed on the same day. Estimations of tissue properties in the patient's Digital Twin showed only little electrical delay, while regional contractility of the subtricuspid segment was clearly diminished. While the presented case represents only one time point in one patient, it shows the potential of integrating data from different diagnostics in a way that makes sense from a clinical perspective. Besides, it fits nicely into the strategy of the 2023 cardiomyopathy guideline³, which proposes to start with a clinical scenario by combining incidental findings from different diagnostic modalities.

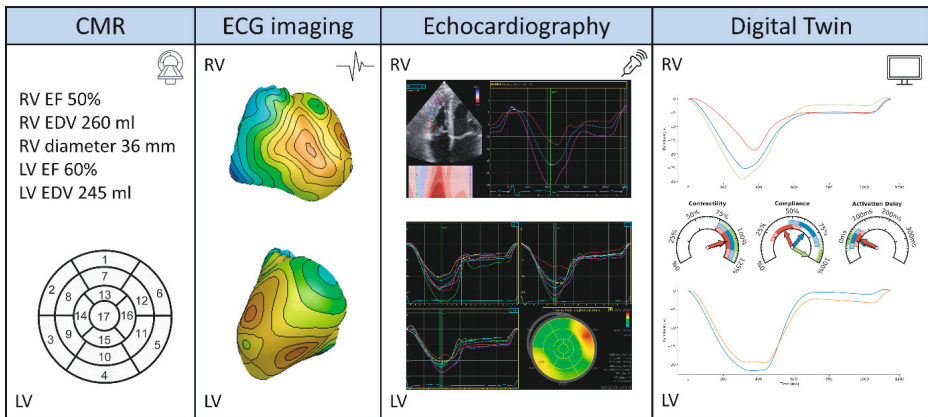


Figure 2. Integration of multimodality data

The displayed data are from an early ARVC patient who underwent CMR, ECG imaging and echocardiography on the same day. The carrier of a pathogenic variant was diagnosed with ARVC based on family history (major TFC), prolonged terminal activation duration on the ECG (minor TFC) and >500 premature ventricular beats on the surface ECG (minor TFC). CMR showed no signs of fibrosis, a preserved ejection fraction of both ventricles and no regional akinesia or dyskinesia. ECG imaging showed relatively homogeneous electrical activation with the subtricuspid segment of the RV lateral wall and the basal segment of the anterolateral being the latest activated regions. Echocardiographic deformation imaging showed indeed slightly delayed mechanical activation of these areas. Besides, longitudinal strain was clearly diminished in the subtricuspid region with slight post-systolic shortening. In the Digital Twin model, these deformation abnormalities were estimated to result from decreased myocardial compliance, rather than an electrical disease substrate.

Achilles heels of the heart

The human heart has adapted to highly specific requirements in order to survive under all kinds of extreme conditions.¹⁹ Although evolution lead to an intricate design which seems optimally adapted to our needs, the cardiac diseases discussed in this thesis reveal several potential weak spots or “Achilles heels” of the heart. The most extensively discussed weak spot is the thin RV free wall, more specifically the subtricuspid segment. The early and predominant impairment of the subtricuspid segment was a consistent finding in ARVC patients with a pathogenic variant in desmosomal genes, which became especially evident in **Chapter 6**. Besides the thin aspect of the RV free wall, the anatomical location of the subtricuspid segment may result in disproportionately high wall stress. Swiss researchers used silicone anatomical RV models of ARVC patients and healthy controls to evaluate wall shear stress in different segments.²⁰ They observed the highest wall shear stress in the RV outflow tract, followed by the subtricuspid region. In general, these are the earliest affected regions in ARVC and a common origin of arrhythmia.²¹ On the other hand, wall shear stress in the RV apex and septal region was negligible in the silicone RV models. In the LV, completing the so-called triangle of dysplasia, a common predisposition site for ARVC disease manifestation is the basal segment of the LV posterolateral wall.^{21,22} The fact that this region mirrors the subtricuspid segment of the RV lateral wall on the left side might support similar hypotheses; systolic flow direction from apex to base might result in disproportionately high wall stress in both the RV and LV basal segments.

In the addendum of this thesis, **Chapter 10** addresses mitral annular disjunction. In this condition, the mitral valve hinge points are displaced towards the atrium (*Figure 3*). While this condition may involve variable parts of the annular circumference, it mainly seems to be associated with severe arrhythmic events when present in the posterolateral wall.^{23,24} So again, the basal segment of the LV posterolateral seems to be an Achilles heel for cardiac arrhythmias.

Recognition of the weak spots of the heart is important in clinical practice to guide focus of early detection of disease in genetic cardiomyopathies. While global diagnostic indices are still preserved, abnormalities in these predilection sites may already introduce an important arrhythmic risk. In **Chapter 2** we emphasized that visual assessment of regional abnormalities is difficult and highly dependent on the observer's experience. Throughout this thesis, echocardiographic deformation imaging repeatedly showed to be a highly sensitive technique for assessment of disease manifestation in the Achilles heels of the heart.

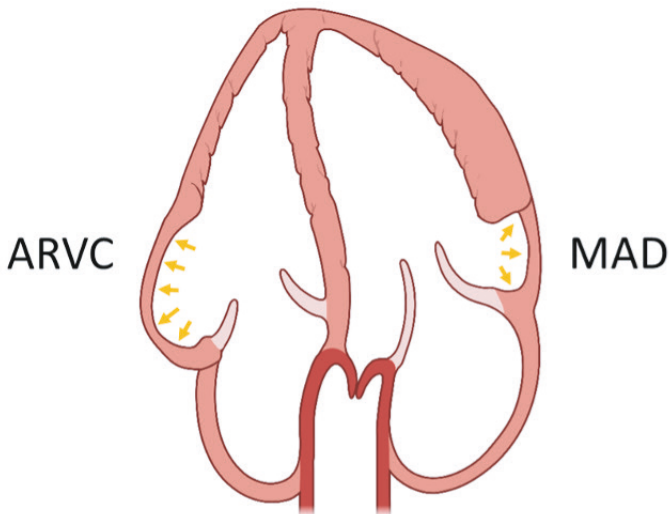


Figure 3. Two Achilles heels of the heart: the subtricuspid segment of the RV free wall and the submitral segment of the posterolateral wall in the LV

The first is a common predilection site for ARVC disease manifestation in patients with genetic variants impairing desmosomal function. The second is often the first involved LV region in ARVC and can be the source of arrhythmia in case of atrial displacement of the mitral valve annulus (MAD). In both cases, ventricular flow dynamics and a thin wall may lead to high wall stress. This stress can lead to formation of scar tissue in already vulnerable myocardium, which in turn forms a pro-arrhythmic substrate.

The influence of exercise

While exercise is associated with unequivocal health benefits in the general population, this may not necessarily be the case in patients with genetic cardiomyopathies. If the Achilles heel of the heart is already under stress in rest, the effects of exercise may be an extra trigger for worse outcome. Especially in ARVC, a history of frequent vigorous exercise has been associated with more pronounced phenotypes and worse prognosis.²⁵⁻²⁷ In preclinical studies in mice expressing a mutated human PKP-2 gene, the abnormal phenotype could be triggered by repeated exercise.^{28,29} In the presence of dysfunctional cardiac desmosomes, exercise

imposes high wall stress causing cardiomyocyte detachment and gap junction remodeling, triggering apoptosis and fibroadiposis. Afterload and hence systolic wall stress increases to a disproportionately greater extent in the RV compared to the LV.³⁰ Moreover, even without a known genetic cause of desmosomal dysfunction, excessive wall stress on the thin-walled RV may cause an ARVC phenotype with malignant arrhythmias originating from the RV, the so-called exercise-induced ARVC.³¹

These effects of exercise in patient with ARVC or a genetic predisposition to develop the disease may not only be important in advising exercise restriction; the detrimental effect of exercise may also have consequences for diagnostic testing. Early disease manifestation might already be detectable during exercise, while the functional abnormalities are too subtle to be detected in rest. Another hypothesis, in line with the findings by La Gerche et al. in exercise-induced ARVC³¹, is that significant progression of RV dysfunction during exercise is associated with worse outcome. Preliminary computer simulations with the CircAdapt model seem to support these hypotheses: when introducing a mild disease substrate in the basal segment of the RV free wall, stepwise increasing cardiac output from 5L to 15L per minute results in increasingly abnormal regional deformation. During peak exercise, the simulated deformation shows a clearly abnormal type III with systolic stretching, while the disease substrate on tissue level did not change.

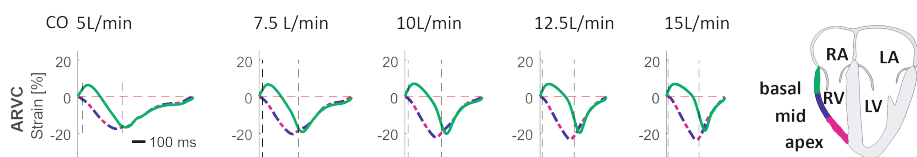


Figure 4. Simulated regional RV deformation in early ARVC during exercise

A mild disease substrate is introduced in the basal segment of the RV free wall. In rest, deformation in the basal segment is slightly abnormal with delayed onset of shortening (type II). By increasing the cardiac output and keeping other factors constant, a highly pathologic RV deformation pattern develops with predominantly systolic stretching (type III). CO = cardiac output.

Electrocardiography is already routinely performed during exercise in order to detect arrhythmia in ARVC patients and family members at risk. Concurrently, ultrasound machines deployed in clinical settings are well-suited for exercise imaging of the RV. Given the infrastructure already being present in most hospitals, an intriguing avenue for research arises—namely, the exploration of the additional diagnostic and prognostic insights offered by RV deformation imaging during exercise for ARVC patients and family members at risk.

Towards clinical implementation

After more than two decades of research on echocardiographic deformation imaging, the technique is now starting to be integrated into clinical practice. An important contributing factor to wider implementation is the increasing availability of speckle tracking deformation imaging in standard clinical ultrasound machines. Another factor is that semi-automated analyses make it less time-consuming. On this aspect, there is still more to gain with the introduction of fully automated analyses which will be both time-saving and less observer dependent. Deep-learning based automated analysis will probably enter the clinical arena soon, since great

interest from both vendors and academic researchers already led to great achievements in this field. To identify knowledge gaps and the necessary steps to accelerate clinical implementation of the technique, we conducted a systematic review in **Chapter 7**, focusing on the utility of deformation imaging for family screening in genetic cardiomyopathies. The main observations that were reproduced in different cohorts were (1) reduced global longitudinal LV strain in relatives at risk of DCM, (2) reduced basal septal strain in relatives at risk of HCM, (3) reduced RV free wall strain in relatives at risk of ARVC.

The next step towards wider implementation of the technique most likely is inclusion in clinical guidelines. Along with guideline recognition, reimbursement of the technique is another hurdle which has recently been successfully taken in the United States. The recently updated *2023 European guideline on the management of genetic cardiomyopathies* already mentions the added value of deformation imaging as a sensitive marker to detect subtle ventricular dysfunction in genotype-positive HCM, DCM and ARVC family members.³ Furthermore, mechanical dispersion (**Chapter 3, 7 and 8**) is mentioned as a marker of contraction inhomogeneity that might highlight fine structural changes that may be missed by other modalities. In the *2022 European guideline on management of patients with ventricular arrhythmias and the prevention of sudden cardiac death*³², it is stated that global longitudinal strain can be used as a measure to detect subtle changes while ejection fraction is still preserved and mechanical dispersion as an index associated with increased risk of ventricular arrhythmia. To let deformation imaging play a decisive role in clinical management, added value of the technique on top of current clinical practice should be shown with regard to hard clinical endpoints. **Chapter 8** might be an example of such a study, being the first to show added value of deformation imaging in a clinical practice-based, multimodality approach. External validation of these results in a large multicenter cohort will be the next important step. Another focus for future studies is to test the predictive value of deformation imaging in other cardiomyopathies. Moreover, rather than using a phenotypical approach, these studies might have to shift towards a gene-based (or even gene variant-based) risk stratification approach.

Closing remarks

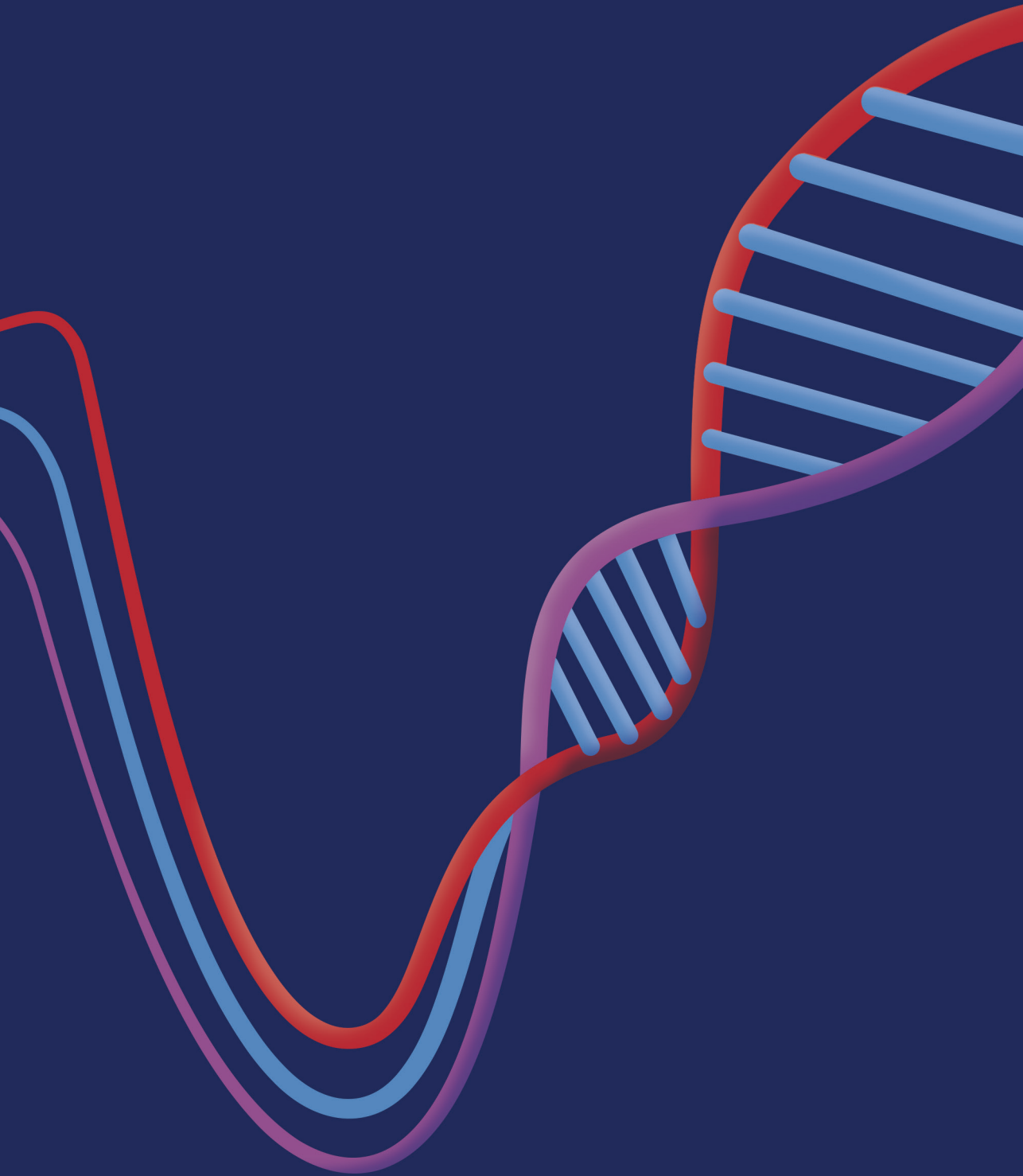
If there is one thing that I have learned from doing research in the field of genetic cardiomyopathies, it is that collaboration is the central and most important theme. All chapters in this thesis are the result of collaborations between research groups, both national and international. Looking at the future steps which should be taken, global collaboration is becoming even more essential. The shift towards practicing precision medicine creates a need for ever larger multicenter cohorts with more events. In addition to willingness to share data, this requires an effort in harmonization of databases, not to mention infrastructure and legislation that facilitate collaborations exceeding the hospital walls.

REFERENCES

1. Elliott P, Andersson B, Arbustini E, et al. Classification of the cardiomyopathies: a position statement from the European Society of Cardiology working group on myocardial and pericardial diseases. *Eur Heart J*. 2008;29(2):270–6.
2. Towbin JA, McKenna WJ, Abrams DJ, et al. 2019 HRS expert consensus statement on evaluation, risk stratification, and management of arrhythmogenic cardiomyopathy. *Heart Rhythm*. 2019;16(11):e301–72.
3. Arbelo E, Protonotarios A, Gimeno JR, et al. 2023 ESC Guidelines for the management of cardiomyopathies. *Eur Heart J*. 2023;44(37):3503–626.
4. Marcus FI, McKenna WJ, Sherrill D, et al. Diagnosis of arrhythmogenic right ventricular cardiomyopathy/Dysplasia: Proposed modification of the task force criteria. *Circulation*. 2010;121(13):1533–41.
5. Lie ØH, Chivulescu M, Rootwelt-Norberg C, et al. Left Ventricular Dysfunction in Arrhythmogenic Cardiomyopathy: Association With Exercise Exposure, Genetic Basis, and Prognosis. *J Am Heart Assoc*. 2021;10(8).
6. Mast TP, Teske AJ, Walmsley J, et al. Right Ventricular Imaging and Computer Simulation for Electromechanical Substrate Characterization in Arrhythmogenic Right Ventricular Cardiomyopathy. *J Am Coll Cardiol*. 2016;68(20):2185–97.
7. Taha K, te Rijdt WP, Verstraelen TE, et al. Early Mechanical Alterations in Phospholamban Mutation Carriers. *JACC Cardiovasc Imaging*. 2021;14(5):885–96.
8. Protonotarios A, Bariani R, Cappelletto C, et al. Importance of genotype for risk stratification in arrhythmogenic right ventricular cardiomyopathy using the 2019 ARVC risk calculator. *Eur Heart J*. 2022;43(32):3053–67.
9. Paldino A, Dal Ferro M, Stolfo D, et al. Prognostic Prediction of Genotype vs Phenotype in Genetic Cardiomyopathies. *J Am Coll Cardiol*. 2022;80(21):1981–94.
10. Basso C, Corrado D, Marcus FI. Arrhythmogenic right ventricular cardiomyopathy. *Lancet*. 2009;373(9673):1289–300.
11. Van Osta N, Kirkels FP, Lyon A, et al. Personalization of Biomechanical Models for Early Detection of Disease. In: *Computing in Cardiology Conference*. 2018.
12. Van Osta N, Lyon A, Kirkels FP, et al. Parameter subset reduction for patient-specific modelling of arrhythmogenic cardiomyopathy-related mutation carriers in the CircAdapt model: Parameter Subset Reduction. *Philosophical Transactions of the Royal Society A*. 2020;378(2173):20190347.
13. van Opbergen CJM, Delmar M, van Veen TAB. Potential new mechanisms of pro-arrhythmia in arrhythmogenic cardiomyopathy: focus on calcium sensitive pathways. *Netherlands Heart Journal*. 2017;25(3):157–69.
14. Lyon A, Dupuis LJ, Arts T, et al. Differentiating the effects of β -adrenergic stimulation and stretch on calcium and force dynamics using a novel electromechanical cardiomyocyte model. *Am J Physiol Heart Circ*. 2020;319(3):H519–30.
15. Osta N van, Kirkels FP, Loon T van, et al. Uncertainty Quantification of Regional Cardiac Tissue Properties in Arrhythmogenic Cardiomyopathy Using Adaptive Multiple Importance Sampling. *Front Physiol*. 2021;12:738926.

16. Taha K, Bourfiss M, te Riele ASJM, et al. A head-to-head comparison of speckle tracking echocardiography and feature tracking cardiovascular magnetic resonance imaging in right ventricular deformation. *Eur Heart J Cardiovasc Imaging*. 2021;22(8):950–8.
17. Kloosterman M, Boonstra MJ, Roudijk RW, et al. Body surface potential mapping detects early disease onset in Plakophilin-2 pathogenic variant carriers. *Europace*. 2023;25(7):euaad197.
18. Tsui H, van Kampen SJ, Han SJ, et al. Desmosomal protein degradation as an underlying cause of arrhythmogenic cardiomyopathy. *Sci Transl Med*. 2023;15(688):eadd4248.
19. Schut B. *Pump: A Natural History of the Heart*. New York: Algonquin books; 2021.
20. Gülan U, Saguner AM, Akdis D, et al. Hemodynamic Changes in the Right Ventricle Induced by Variations of Cardiac Output: A Possible Mechanism for Arrhythmia Occurrence in the Outflow Tract. *Sci Rep*. 2019;9(1):100.
21. Te Riele ASJM, James CA, Philips B, et al. Mutation-positive arrhythmogenic right ventricular dysplasia/cardiomyopathy: The triangle of dysplasia displaced. *J Cardiovasc Electrophysiol*. 2013;24(12):1311–20.
22. Mast TP, Teske AJ, Vd Heijden JF, et al. Left Ventricular Involvement in Arrhythmogenic Right Ventricular Dysplasia/Cardiomyopathy Assessed by Echocardiography Predicts Adverse Clinical Outcome. *J Am Soc Echocardiogr*. 2015;28(9):1103–1113.
23. Dejgaard LA, Skjølsvik ET, Lie ØH, et al. The Mitral Annulus Disjunction Arrhythmic Syndrome. *J Am Coll Cardiol*. 2018;72(14):1600–9.
24. Essayagh B, Sabbag A, El-Am E, Cavalcante JL, Michelena HI, Enriquez-Sarano M. Arrhythmic mitral valve prolapse and mitral annular disjunction: pathophysiology, risk stratification, and management. *Eur Heart J*. 2023;44(33):3121–35.
25. James CA, Bhonsale A, Tichnell C, et al. Exercise increases age-related penetrance and arrhythmic risk in arrhythmogenic right ventricular dysplasia/cardiomyopathy-associated desmosomal mutation carriers. *J Am Coll Cardiol*. 2013;62(14):1290–7.
26. Lie ØH, Dejgaard LA, Saberniak J, et al. Harmful Effects of Exercise Intensity and Exercise Duration in Patients With Arrhythmogenic Cardiomyopathy. *JACC Clin Electrophysiol*. 2018;4(6):744–53.
27. Bosman LP, Wang W, Lie ØH, et al. Integrating Exercise Into Personalized Ventricular Arrhythmia Risk Prediction in Arrhythmogenic Right Ventricular Cardiomyopathy. *Circ Arrhythm Electrophysiol*. 2022;15(2):e010221.
28. Cruz FM, Sanz-Rosa D, Roche-Molina M, et al. Exercise Triggers ARVC Phenotype in Mice Expressing a Disease-Causing Mutated Version of Human Plakophilin-2. *J Am Coll Cardiol*. 2015;65(14):1438–50.
29. van Opbergen CJM, Bagwan N, Maurya SR, et al. Exercise Causes Arrhythmogenic Remodeling of Intracellular Calcium Dynamics in Plakophilin-2–Deficient Hearts. *Circulation*. 2022;145(19):1480–96.
30. La Gerche A, Heidbuchel H, Burns A, et al. Disproportionate Exercise Load and Remodeling of the Athlete's Right Ventricle. *Med Sci Sports Exerc*. 2011 Jun;43(6):974–81.
31. La Gerche A, Claessen G, Dymarkowski S, et al. Exercise-induced right ventricular dysfunction is associated with ventricular arrhythmias in endurance athletes. *Eur Heart J*. 2015;36(30):1998–2010.
32. Zeppenfeld K, Tfelt-Hansen J, de Riva M, et al. 2022 ESC Guidelines for the management of patients with ventricular arrhythmias and the prevention of sudden cardiac death. *Eur Heart J*. 2022;43(40):3997–4126.

Addendum: Left sided wall stress causing arrhythmia



CHAPTER 10

Prevalence of Mitral Annulus Disjunction and Mitral Valve Prolapse in Patients with Idiopathic Ventricular Fibrillation

Feddo P. Kirkels, Sanne A. Groeneveld*, Maarten J. Cramer, Reinder Evertz, Kristina H. Haugaa, Pieter G. Postema, Niek H.J. Prakken, Arco J. Teske, Arthur A.M. Wilde, Birgitta K. Velthuis, Robin Nijveldt, Rutger J. Hassink*

** The first two authors contributed equally*

J Am Heart Assoc. 2022;11(16):e025364.

ABSTRACT

Background

Idiopathic ventricular fibrillation (IVF) is diagnosed in patients with ventricular fibrillation of which the origin is not identified after extensive evaluations. Recent studies suggest an association between mitral annulus disjunction (MAD), mitral valve prolapse (MVP) and ventricular arrhythmias. The prevalence of MAD and MVP in IVF patients in this regard, is not well established. We aimed to explore the prevalence of MAD and MVP in a consecutive cohort of IVF patients compared to matched controls.

Methods and Results

In this retrospective multicenter cohort study, cardiac magnetic resonance images from IVF patients (i.e., negative for ischemia, cardiomyopathy and channelopathies) and age- and sex-matched control subjects were analyzed for the presence of MAD (≥ 2 mm) and MVP (> 2 mm).

In total, 72 patients (mean age 39 ± 14 years, 42% female) and 72 control subjects (mean age 41 ± 11 years, 42% female) were included. MAD in the inferolateral wall was more prevalent in IVF patients versus healthy controls (7 [11%] vs. 1 [1%], $p=0.024$). MVP was only seen in IVF patients and not in controls (5 [7%] vs. 0 [0%], $p=0.016$). MAD was observed in both patients with ($n=4$) and without ($n=3$) MVP.

Conclusion

Inferolateral MAD and MVP were significantly more prevalent in IVF patients compared to healthy controls. The authors advocate that evaluation of the mitral valve region deserves extra attention in the extensive screening of patients with unexplained cardiac arrest. These findings support further exploration of the pathophysiological mechanisms underlying a subset of IVF that associates with MAD and MVP.

INTRODUCTION

Idiopathic ventricular fibrillation (IVF) is diagnosed in patients with ventricular fibrillation of unknown origin that remains unidentified after extensive diagnostic testing.^{1,2} The diagnosis IVF depends on the absence of a substrate for VF by exclusion of both structural cardiac diseases and primary arrhythmia syndromes. In the follow-up of these patients, a continuing search for previously unknown pro-arrhythmic factors is driven by the evolution of medical knowledge and diagnostic techniques.³

Decades ago, mitral valve prolapse (MVP) and mitral annulus disjunction (MAD) have already been associated with ventricular arrhythmias and sudden cardiac arrest (SCA) in young patients.^{4–13} In recent years, MAD regained attention in association with MVP and ventricular arrhythmias.^{8,14–17} MAD is defined as an abnormal atrial displacement of the mitral valve leaflet hinge point, away from the ventricular myocardium. Close relation has been shown to MVP and SCA but recent studies also showed an association with ventricular arrhythmias independently of MVP.^{8–10}

Imaging with cardiac magnetic resonance imaging (CMR) and echocardiography is included in the standard work-up for IVF patients. Previous studies have reported a high prevalence of MVP in patients with aborted cardiac arrest of unexplained etiology⁹, but until now no specific attention has been given to the presence of MAD in IVF patients. We hypothesize that this abnormality might often have been overlooked in the routine clinical work up of IVF patients. The aim of this study was to describe MAD and MVP prevalence and morphology in a multicenter cohort of IVF patients and matched controls.

METHODS

Study population

Patients were derived from a large Dutch registry of IVF patients. Details of the cohort have been published in previous studies.^{2,18} In summary, we enrolled patients with an unexplained cardiac arrest with an initial rhythm of ventricular fibrillation, in whom known cardiac, respiratory, metabolic, and toxicological causes were excluded at first presentation. Comprehensive clinical investigation was performed, and accepted diagnostic criteria were used to exclude specific disease.¹⁹

For this multicenter retrospective cohort study, we included IVF patients who were evaluated in three tertiary referral centers in the Netherlands (University Medical Center Utrecht, Amsterdam University Medical Center and Radboud University Medical Center) between September 2004 and December 2020 and underwent CMR imaging of sufficient image quality (*Figure 1*). Age- and sex-matched controls with no history of cardiovascular disease were selected from a previous prospectively included cohort of healthy non-athletes.^{20,21} The study complied with the Declaration of Helsinki and was approved by the Regional Committee for Medical Research Ethics in all participating centers and the subjects gave informed consent when appropriate. The data that support the findings of this study are available from the corresponding author upon reasonable request.

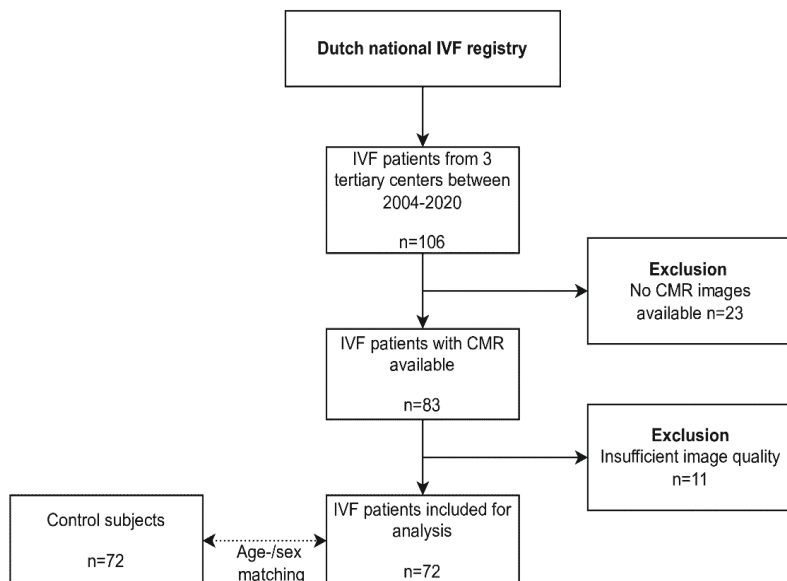


Figure 1. Inclusion flowchart

IVF patients included in a large national registry from three tertiary centers were included. Abbreviations: CMR = cardiac magnetic resonance, IVF = idiopathic ventricular fibrillation.

CMR imaging

All included subjects underwent CMR examination on a clinical 1.5T or 3T MR scanner using electrocardiographic gating and a phased array cardiac receiver coil according to standardized cardiac protocols.²² Breath-hold balanced steady-state free-precession (bSSFP) cine images covering both the ventricles and atria were acquired (4-chamber long-axis view, 2- and 3-chamber long-axis LV views and multi-slice full coverage of the LV in short axis orientation). The voxel size of the cine sequences used was dependent on the local clinical scan protocol and was typically around $1.5 \times 1.5 \times 5\text{--}8 \text{ mm}^3$. In addition, late gadolinium enhancement (LGE) imaging was performed at least 10 minutes after intravenous administration of a gadolinium-based contrast agent in identical views. LGE imaging was not performed in control subjects.

Ventricular metrics and ejection fraction (EF) were measured in a standardized way using semi-automated contour tracing software.²³ Ventricular end-diastolic volumes were indexed for body surface area (EDVi). Patients with major LGE (sufficient for a specific diagnosis) were not included in the IVF registry, while patients with minor LGE of uncertain pathogenicity were included in this study. The LGE images were re-evaluated for any myocardial fibrosis in the left ventricle and papillary muscles by an experienced cardiac radiologist. Mild insertion fibrosis was deemed insignificant for this study.

Two blinded observers analyzed CMR images for presence and longitudinal distance of MAD and MVP. Longitudinal MAD distance was measured on all three long-axis cine views from the left atrial wall mitral valve leaflet junction to the top of the left ventricular wall at end-systole. Presence of MAD was defined as a longitudinal displacement of $>1 \text{ mm}$ (Figure

2). Presence of MVP was defined as displacement of >2 mm of one or both leaflets beyond the annular hinge points at end-systole, measured perpendicular to the annular plane in the 3-chamber view (Figure 2).²⁴ Presence of the curling sign, defined as an unusual systolic motion of the inferior mitral annulus on the adjacent ventricular wall, was identified by visual assessment (online video A).^{8,25}

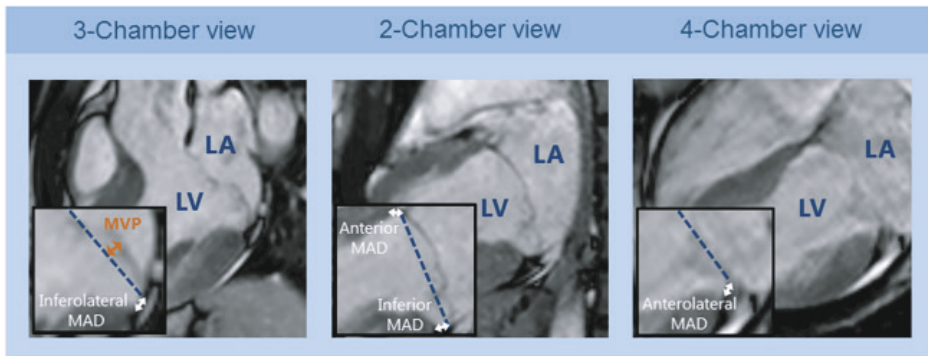


Figure 2. Measurements of longitudinal MAD and MVP distance on CMR imaging

All images are obtained at end-systole. The blue line connects the annular hinge points of the mitral valve, the white arrows are longitudinal MAD measurements, the orange arrow is the MVP measurement. Abbreviations: CMR = cardiac magnetic resonance, LA = left atrium, LV = left ventricle, MAD = mitral annulus disjunction, MVP = mitral valve prolapse.

Clinical characteristics

Clinical data was derived from the IVF registry. Enrolled patients all underwent detailed investigation of the medical history, physical examination, 12-lead ECG, laboratory testing, echocardiography, coronary angiography (or CT angiography) and CMR. All patients underwent echocardiographic imaging according to the standard clinical protocol.^{26,27} Additional investigations such as exercise ECG, sodium channel blocker provocation, endomyocardial biopsy and genetic testing were performed at the treating physician's discretion.^{2,18} T-wave abnormalities were defined as inverted or biphasic T-waves. Genetic testing consisted of single targeted gene testing or next generation sequencing of a larger panel of genes, depending on the center where the genetic testing was performed. In line with previous studies, we also included patients with the DPP6 haplotype, a genetic variant associated with short-coupled Torsade de Pointes/IVF.^{1,28} Although we previously proposed that Ito overexpression particularly in Purkinje plays an essential role in these patients²⁹, the underlying pathophysiological mechanism for VF remains uncertain.

Follow-up data was retrospectively collected from all patients. All electrocardiographic data on ECGs, cardiac telemetry during admission, exercise ECG and Holter monitoring was analyzed for the occurrence of PVCs. A high PVC burden was defined as more than 1000 PVCs per 24 hours on Holter monitoring. In patients without Holter monitoring, a high PVC burden was defined as more than 20 PVCs during an exercise test or bigeminy or trigeminy on ECG or cardiac telemetry. Non sustained ventricular tachycardia was defined as three or more ventricular beats with a maximum duration of 30 seconds.³⁰ Appropriate ICD therapy was defined as anti-tachycardia pacing or shock during a ventricular tachycardia or ventricular fibrillation.

Statistical analysis

Parametric data were presented as mean \pm standard deviation, median [interquartile range] or number (%). Comparisons were performed using a Student's t-test, Mann-Whitney U test, or Fisher exact test as appropriate. Analyses were performed with SPSS version 24.0 (SPSS Inc., Chicago, Illinois). Intra- and inter-observer variability was expressed by intraclass correlation coefficients (ICC). Two-sided p values <0.05 were considered significant.

RESULTS

Study population

After screening 106 IVF patients from three centers, a total of 72 patients (mean age 39 ± 14 years, 42% female) and 72 age- and sex-matched control subjects (mean age 41 ± 11 years, 42% female) were included (Figure 1). In total, 23 patients were excluded due to CMR unavailability and 11 patients were excluded due to insufficient image quality. An ICD for secondary prevention was implanted in all but one of the IVF patients (99%) (Table 1).

Table 1. Baseline characteristics of idiopathic ventricular fibrillation patients

Characteristics	All (n=72)
Age, yrs	39 \pm 14
Female, n (%)	30 (42)
<i>Circumstances event, n (%)</i>	
- Rest	43 (60)
- Exercise	16 (22)
- Asleep	9 (12)
- Emotions	4 (6)
<i>Genetic testing</i>	
- DPP6 haplotype	9 (13)
<i>Electrocardiogram</i>	
- Heart rate, bpm	69 \pm 13
ICD implantation	71 (99)

Values are, n (%), mean \pm standard deviation. Abbreviations: bpm = beats per minute, ICD = implantable cardioverter defibrillator.

Prevalence of mitral valve disease

MAD was commonly measured in the anterior, inferior and anterolateral wall in both IVF patients and healthy controls (Table 2). The inferolateral wall was the only distinctive location for the presence of MAD between IVF patients and controls (7 [11%] vs. 1 [1%], $p=0.024$). In addition, IVF patients showed a higher prevalence of MVP (5 [8%] vs. 0 [0%], $p=0.016$). A curling sign of the inferior wall was observed in three IVF patients with MAD and not in controls. One control subject showed MAD in the inferolateral wall of 2 mm, without signs of other mitral valve disease. In seven IVF patients with inferolateral MAD, other mitral valve disease was prevalent; four (57%) also had MVP, of which three females with bi-leaflet MVP, and four patients (57%) showed signs of mitral regurgitation. One patient with MVP did not have inferolateral MAD.

Characteristics of subjects with MAD and/or MVP are described in *Table 3*. In two subjects with MAD/MVP, a variant of uncertain significance was found with genetic testing (*Table S1*). Three subjects with MAD/MVP underwent electrophysiology study. Voltage mapping of the LV was not performed. One subject underwent radiofrequency ablation due to frequent PVCs in the anterolateral RVOT. Seven subjects with MAD/MVP underwent exercise stress testing, zero showed NSVT or multifocal PVCs.

Table 2. Comparison between idiopathic ventricular fibrillation (IVF) patients and matched controls

Characteristics	IVF patients (n=72)	Controls (n=72)	p-value
Age, yrs	39 ± 14	41 ± 11	0.290
Female, n(%)	30 (42)	30 (42)	1.000
BSA, m ²	2.0 ± 0.2	1.9 ± 0.2	0.571
Cardiac magnetic resonance			
LVEF, %	57 ± 15	60 ± 7	0.180
LVEDVi, ml/m ²	85 ± 16	93 ± 14	0.005
Late gadolinium enhancement, n (%)	8 (13)	n/a	n/a
Mitral annulus disjunction, n (%)	40 (56)	44 (61)	0.612
- Anterolateral wall (n=141*)	17 (24)	13 (18)	0.417
- Anterior wall (n=132*)	21 (33)	32 (46)	0.156
- Inferior wall (n=135*)	26 (40)	29 (41)	1.000
- Inferolateral wall (n=133*)	7 (11)	1 (1)	0.024
Mitral valve prolapse, n (%)	5 (8)	0 (0)	0.016
Bi-leaflet mitral valve prolapse, n (%)	3 (5)	0 (0)	0.096
Curling sign, n (%)	3 (5)	0 (0)	0.096

Values are, n (%), mean ± standard deviation. Abbreviations: BSA = body surface area, LVEF = left ventricular ejection fraction, LVEDVi = indexed left ventricular end diastolic volume. *Missing values due to unavailable views or insufficient image quality.

Table 3. Characteristics of 8 subjects with MVP and/or MAD in the inferolateral wall on CMR

Subject N=7	Sex	MAD (mm)				MVP (mm)	Bi-leaflet MVP	Curling sign	MR*	LGE	ECG T-wave Abnormalities	Ventricular ectopy
		AL	ANT	INF	IL							
Control 1	M	2	2	3	2	0	No	No	No	n/a	n/a	n/a
IVF 1	F	3	0	0	2	5	Yes	No	Moderate	Basal septal LV	Yes (inferior)	No
IVF 2	M	3	0	5	3	3	No	No	Mild	No	No	Yes (basal LV)
IVF 3	M	3	0	8	3	0	No	No	Mild	No	No	No
IVF 4	F	3	3	2	2	0	No	Yes	No	No	No	Yes (RVOT)
IVF 5	F	1	2	5	3	6	Yes	Yes	No	No	Yes (inferior)	Yes (basal LV)
IVF 6	M	2	5	1	2	0	No	No	No	No	Yes (inferior)	Yes (RVOT)
IVF 7	F	2	2	2	2	7	Yes	Yes	Mild	No	No	Yes (LV apex)
IVF 8	M	0	0	4	0	4	No	No	No	No	No	Yes (RVOT)

Abbreviations: AL = anterolateral wall, ANT = anterior wall, INF = inferior wall, IL = inferolateral wall, MAD = mitral annulus disjunction, MVP = mitral valve prolapse, CMR = cardiac magnetic resonance, ECG = electrocardiogram, LGE = late gadolinium enhancement, MR = mitral regurgitation. n/a = not available. MAD, MVP and the curling sign were assessed on CMR. * Mitral regurgitation was determined on echocardiography.

Comparison between IVF patients with and without mitral valve disease

Mitral regurgitation was more prevalent in patients with MAD and/or MVP compared to patients without (4 [50%] vs. 7 [14%], $p=0.024$) (Table 4). In addition, inverted or biphasic T-waves were more frequently observed in IVF patients with MAD/MVP compared to patients without (3 [38%] vs. 2 [3%], $p=0.009$). LGE imaging was available for analysis in the majority of IVF patients ($n=61$). In eight (13%) IVF patients, small LGE spots of uncertain pathogenicity were reported (Table 4). There was no difference in the occurrence of LGE between patients with MAD/MVP compared to patients without (1 [13%] vs. 7 [13%], $p=1.000$). One patient with inferolateral MAD showed midwall LGE in the LV basal inferoseptal myocardium (Figure S1) LGE was seen in seven patients without MAD: location and pattern of LGE ranged from small mid-wall or epicardial foci in 3 patients (basal inferolateral twice and basal inferior wall); three patients had a small subendocardial scar in the respectively basal inferior, apical septal and apical inferior segments, and one patient had a small transmural scar in the basal inferolateral segment. The patient with possible basal subendocardial LGE could also be slow flow in a basal crypt (Figure S1). The four patients with subendocardial to transmural LGE had no coronary artery disease on catheter angiography or coronary CT angiography.

Table 4. Comparison between IVF patients with and without MAD and/or MVP

Characteristics	IVF with MAD/MVP (n=8)	IVF without MAD/MVP (n=64)	p-value
Age, yrs	38 ± 17	39 ± 14	0.890
LVEF, %	54 ± 15	56 ± 8	0.430
Female, n (%)	4 (50)	25 (39)	0.706
Late gadolinium enhancement, n(%)	1 (13)	7 (13)	1.000
Mitral regurgitation, n (%)	4 (50%)	7 (14%)	0.024
Inverted/biphasic T waves, n (%)	3 (38%)	2 (3%)	0.009
<i>Follow-up data</i>			
Follow-up duration, yrs	7 [4-11]	7 [2-12]	0.886
PVC count per hour on Holter monitoring, n	228 [71-676]	1 [0-18]	0.016
High PVC burden on ECG, telemetry, exercise test or Holter	6 (75%)	8 (16%)	0.001
LV basal	2 (25%)	0 (0%)	n/a
RVOT	3 (38%)	3 (6%)	n/a
Other	0 (0%)	5 (10%)	n/a
Multiform	1 (12%)	0 (0%)	n/a
Non-sustained ventricular tachycardia	4 (50%)	17 (31%)	0.423
Appropriate ICD therapy, n (%)	1 (13%)	15 (24%)	0.670
Ventricular tachycardia	1 (13%)	5 (8%)	n/a
Ventricular fibrillation	0 (0%)	10 (16%)	n/a
Atrial fibrillation, n (%)	1 (13%)	5 (9%)	0.567

Values are, n (%), mean ± standard deviation or median [interquartile range]. Abbreviations: BSA = body surface area, ECG = electrocardiogram, ICD = implantable cardioverter defibrillator, LV = left ventricle, LVEF = left ventricular ejection fraction, PVC = premature ventricular complex, RVOT = right ventricular outflow tract.

Follow-up

The mean follow-up duration of the IVF cohort was seven (IQR 2-12) years. Patients with MAD/MVP more frequently showed a high PVC burden (6 [75%] vs 7 [13%], $p=0.001$). In patients with MAD/MVP the PVCs more frequently originated from the basal LV or RVOT (Table S2 and Figure S2). There were no significant differences between IVF patients with MAD/MVP compared to patients without MAD/MVP with regard to the occurrence of non-sustained VTs or appropriate ICD therapy during follow-up (Table 4).

Intra- and inter-observer agreement

We showed excellent reproducibility of longitudinal MAD distance measurements. The intra-observer agreement on 80 segments from 20 patients was 0.92, 95% CI (0.88 - 0.95), $p<0.001$ and the inter-observer agreement was also 0.92, 95% CI (0.88 - 0.95), $p<0.001$.

DISCUSSION

Our study is the first to compare prevalence of MAD and MVP in a consecutive multicenter cohort of IVF patients to a healthy control population. The most important finding was the increased prevalence of MAD in the inferolateral wall and MVP compared to controls (Figure 3). Subjects with MAD in the inferolateral wall also showed high prevalence of other mitral valve disease and ventricular ectopy. This is in line with previous studies suggesting a correlation between mitral valve disease and IVF. MAD in the anterior, inferior and anterolateral wall was commonly measured in both IVF patients and healthy controls.

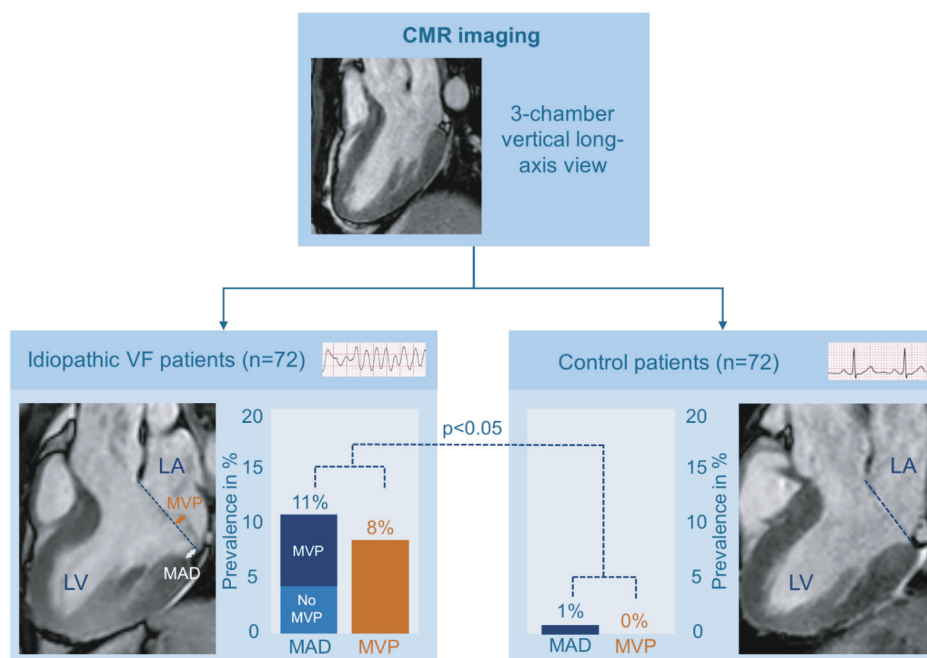


Figure 3. Prevalence of MAD and MVP in IVF patients compared to healthy controls

In total, 144 patients were enrolled in the study; 72 idiopathic ventricular fibrillation (IVF) patients and 72 healthy controls. All patients were screened for presence of mitral annulus disjunction (MAD) and mitral valve prolapse (MVP) on CMR by two blinded observers. MAD in the inferolateral wall was more prevalent in IVF patients compared to controls ($p = 0.024$). MVP was also more prevalent in IVF patients compared to controls ($p = 0.016$).

Location of mitral annulus disjunction

Previous studies showed that MAD distance can vary considerably along the annulus circumference. This was shown with an extensive CMR protocol design assessing the mitral annulus every 30 degrees.⁸ Although we did not assess the mitral annulus every 30 degrees due to unavailability of these acquisitions or 3D CMR data in this retrospective study, we also observed considerable differences in longitudinal MAD distance over the mitral annulus (Table 3). The aforementioned study showed that MAD located in the inferolateral wall assessed by CMR was an independent risk marker for ventricular arrhythmias.⁸ In our cohort, the inferolateral

wall visualized in the 3-chamber long-axis view was found to be the only distinctive location for MAD between IVF patients and controls. In the other walls, gaps of 1-3 mm between the LV myocardium and the mitral annulus hinge points were frequently seen in both patients and controls. Where the 3-chamber view (or parasternal long-axis view in echo) is generally considered to be the most standardized for measurements of the mitral valve, the other views are less reproducible when it comes to measurements on the saddle shaped valve and might therefore be more subjected to errors.^{24,31} This might have contributed to our finding that the inferolateral wall was the only distinctive location for MAD between IVF patients and controls, which is in line with previous studies.^{8,9,25,32} Additionally, a recent study applying a comprehensive 3D analysis on cardiac computed tomography images of 98 structurally normal hearts also showed high prevalence of MAD in the anterior to anterolateral and inferior to inferoseptal segments (77.5% and 87.8%, respectively), while inferolateral MAD was less common in healthy subjects (11.2%).³³

The cut-off to determine presence of MAD on CMR is another point of discussion. We considered longitudinal distances of >1 mm significant, given the spatial resolution of CMR¹⁸, but general consensus is lacking. The voxel size of cine sequences acquired in routine clinical care limits reliability of measurements below 1.5 mm. Besides, longitudinal distances measured by CMR and echocardiography cannot be used interchangeably, as shown by differences in measured distances by the two modalities in a previous study.⁸ Larger CMR based population studies are needed to determine the upper limit of normal.

Mitral annulus disjunction and the relation to mitral valve prolapse

The concept of MAD as an arrhythmic factor was introduced for the first time around the 1980s.^{11,12,34} Since then, it has been closely linked to MVP and other mitral valve disease.²⁵ During the last years, MAD has regained interest and multiple reports indicate that MAD may also be present without MVP.^{8,35} This is in line with our findings, as 43% of IVF patients with MAD did not show MVP. The distinction between MAD and MVP can however be difficult, especially when determining the exact hinge point of a prolapsed mitral valve that parallels the atrial wall. If the prolapse distance is measured from the myocardial edge, MVP will always be found in presence of MAD.²⁵ We measured longitudinal MAD distance from the myocardial edge to the annular hinge point and MVP beyond the annular hinge point, allowing a distinction between the two.⁸ Although the distinction between MAD and MVP can be challenging, the increased prevalence of both entities in IVF that was found in this study is remarkable.

The pro-arrhythmic substrate

The exact proarrhythmic mechanism of MAD is unknown. It has been hypothesized that hypermobility of the mitral valve causes mechanical stretch on the myocardial wall. This may directly induce ventricular ectopy which can potentially trigger VF. On the long term, mechanical stretch may also result in myocyte hypertrophy and fibrosis, creating another potential cause for myocardial electrical instability and arrhythmias.^{9,25} Previous studies related papillary muscle fibrosis to arrhythmic events in the presence of MAD and MVP, but severe arrhythmias were also observed in patients without visible papillary muscle fibrosis on CMR.^{8,14,25} In this study, we did not observe any papillary muscle fibrosis in IVF patients with MAD. However, we did observe more frequently ventricular ectopy and T-wave abnormalities in the inferolateral leads in MAD/MVP patients, which was also observed in previous studies.^{9,25}

While PVCs from the basal LV correspond with the anatomical location of MAD, this relation is less clear for PVCs from the RVOT. The latter were previously reported in MAD, but mainly with concurrent LVOT PVCs.⁹ Ventricular ectopy from areas in close proximity to the mitral annular region and papillary muscles has been attributed to mechanical traction in a subgroup of IVF patients with bi-leaflet MVP⁹ and the same mechanism of traction induced ectopy may be present in MAD.³⁶ Bi-leaflet MVP was present in three female IVF patients in our cohort, in consistence with the previous description of the ‘malignant bi-leaflet MVP syndrome’, which was characterized by bi-leaflet MVP, frequent ventricular ectopy and female sex.⁹

Clinical implications

A previous report demonstrated a case of unexplained cardiac arrest in an otherwise healthy patient, whereby clear MAD was found upon secondary evaluation of cardiac imaging data.³⁷ We confirm that in 11% of our IVF cohort, MAD and/or MVP can be observed during focused analysis of CMR images, while it was previously left unrecognized in a thorough diagnostic process. In a matched cohort of healthy controls, MAD and MVP were rarely found. Overt MVP in combination with extensive myocardial fibrosis in the annular region and papillary muscles was not observed in our IVF cohort. These subjects were most likely already diagnosed with an arrhythmic mitral valve prolapse according to current clinical standards and did not end up in the IVF cohort.^{9,38} Our findings suggest that mitral valve disease may still contribute as pro-arrhythmic factor in a subset of IVF patients. However, one could still argue that minor degrees of MAD are a bystander in IVF. A future, larger prospective study is needed to further evaluate our findings. We advocate that evaluation of the mitral valve region deserves extra attention in the extensive screening of patients with unexplained sudden cardiac arrest. The direct therapeutic consequences for IVF patients may be limited as they generally have a clear indication for secondary prevention ICD implantation. However, knowledge about the correlation between MAD and arrhythmias may yield prognostic value for IVF patients and might especially be important to identify a possible arrhythmogenic risk in family members.

Limitations

Although this is one of the largest IVF cohorts worldwide, the number of patients included is relatively small due to the rarity of the disease. Due to the retrospective nature of this study, image plane acquisition was already performed. Therefore, MAD measurements were confined to available CMR views. In addition, LGE imaging was not standardly performed in the older CMRs and in some cases could not be interpreted due to artefacts. Other studies suggest that MAD is also easily detectable on echocardiography, but the quality and focus of the images acquired are of great importance.^{8,35} We did not use echocardiography because we concluded that measurement of MAD distance on retrospective exams without focused images was not feasible. Holter monitoring was not routinely performed due to the retrospective set-up of the study. In addition, the number of patients with MAD or MVP was relatively small, hampering strong conclusions on clinical follow-up data. Larger prospective follow-up studies are needed to determine the potential impact of MAD/MVP on the prognosis of IVF patients.

CONCLUSION

Inferolateral mitral annulus disjunction (MAD) and mitral valve prolapse (MVP) were significantly more prevalent in a large multicenter cohort of IVF patients compared to healthy controls. Our findings support further exploration of the pathophysiological mechanisms underlying a subset of IVF that associates with MAD and MVP. The clinical implications of the presence of MAD for recurrences of ventricular arrhythmias and treatment strategies remain to be elucidated.

REFERENCES

1. Visser M, Heijden JF Van Der, Doevendans PA, Loh P, Wilde AA, Hassink RJ. Idiopathic Ventricular Fibrillation: The Struggle for Definition, Diagnosis, and Follow-Up. *Circ Arrhythmia Electrophysiol.* 2016;9(5):1–11.
2. Blom LJ, Visser M, Christiaans I, et al. Incidence and predictors of implantable cardioverter-defibrillator therapy and its complications in idiopathic ventricular fibrillation patients. *Europace.* 2019;21(10):1519–26.
3. Groeneveld SA, Ree MH van der, Taha K, et al. Echocardiographic deformation imaging unmasks global and regional mechanical dysfunction in patients with idiopathic ventricular fibrillation: A multicenter case-control study. *Heart Rhythm.* 2021;18(10):1666–72.
4. Vohra J, Sathe S, Warren R, Tatoulis J, Hunt D. Malignant Ventricular Arrhythmias in Patients with Mitral Valve Prolapse and Mild Mitral Regurgitation. *Pacing Clin Electrophysiol.* 1993;16(3):387–93.
5. Dollar AL, Roberts WC. Morphologic comparison of patients with mitral valve prolapse who died suddenly with patients who died from severe valvular dysfunction or other conditions. *J Am Coll Cardiol.* 1991;17(4):921–31.
6. Pocock WA, Bosman CK, Chesler E, Barlow JB, Edwards JE. Sudden death in primary mitral valve prolapse. *Am Heart J.* 1984;107(2):378–82.
7. Kleid JJ. Sudden Death and the Floppy Mitral Valve Syndrome. *Angiology.* 1976;27(12):734–7.
8. Dejgaard LA, Skjølsvik ET, Lie ØH, et al. The Mitral Annulus Disjunction Arrhythmic Syndrome. *J Am Coll Cardiol.* 2018;72(14):1600–9.
9. Sriram CS, Syed FF, Ferguson ME, et al. Malignant bileaflet mitral valve prolapse syndrome in patients with otherwise idiopathic out-of-hospital cardiac arrest. *J Am Coll Cardiol.* 2013;62(3):222–30.
10. Essayagh B, Sabbag A, Antoine C, et al. Presentation and Outcome of Arrhythmic Mitral Valve Prolapse. *J Am Coll Cardiol.* 2020;76(6):637–49.
11. Hutchins GM, Moore GW, Skoog DK. The association of floppy mitral valve with disjunction of the mitral annulus fibrosus. *N Engl J Med.* 1986;314(9):535–40.
12. Angelini A, Ho SY, Anderson RH, Becker AE, Davies MJ. Disjunction of the mitral annulus in floppy mitral valve. *N Engl J Med.* 1988;318(3):188–9.
13. Bharati S, Granston AS, Liebson PR, Loeb HS, Rosen KM, Lev M. The conduction system in mitral valve prolapse syndrome with sudden death. *Am Heart J.* 1981;101(5):667–70.
14. Bennett S, Thamman R, Griffiths T, et al. Mitral annular disjunction: A systematic review of the literature. *Echocardiography.* 2019;36(8):1549–58.
15. Basso C, Perazzolo Marra M. Mitral Annulus Disjunction: Emerging Role of Myocardial Mechanical Stretch in Arrhythmogenesis. *J Am Coll Cardiol.* 2018;72(14):1610–2.
16. Haugaa KH, Aabel EW. Mitral Annulus Disjunction. *JACC Cardiovasc Imaging.* 2021;14(11):2088–90.
17. Muthukumar L, Jahangir A, Jan MF, Perez Moreno AC, Khandheria BK, Tajik AJ. Association Between Malignant Mitral Valve Prolapse and Sudden Cardiac Death. *JAMA Cardiol.* 2020;5(9):1053.
18. Visser M, Heijden JF Van Der, Smagt JJ Van Der, et al. Long-Term Outcome of Patients Initially Diagnosed with Idiopathic Ventricular Fibrillation. *Circ Arrhythmia Electrophysiol.* 2016;9(10):e004258.

19. Priori SG, Wilde AA, Horie M, et al. Executive summary: HRS/EHRA/APHRS expert consensus statement on the diagnosis and management of patients with inherited primary arrhythmia syndromes. *Europace*. 2013;15(10):1389–406.
20. Prakken NH, Velthuis BK, Teske AJ, Mosterd A, Mali WP, Cramer MJ. Cardiac MRI reference values for athletes and nonathletes corrected for body surface area, training hours/week and sex. *Eur J Cardiovasc Prev Rehabil*. 2010;17(2):198–203.
21. Prakken NH, Cramer MJ, Teske AJ, Arend M, Mali WP, Velthuis BK. The effect of age in the cardiac MRI evaluation of the athlete's heart. *Int J Cardiol*. 2011;149(1):68–73.
22. Kramer CM, Barkhausen J, Bucciarelli-Ducci C, Flamm SD, Kim RJ, Nagel E. Standardized cardiovascular magnetic resonance imaging (CMR) protocols: 2020 update. *J Cardiovasc Magn Reson*. 2020;22(1):17.
23. Schulz-Menger J, Bluemke DA, Bremerich J, et al. Standardized image interpretation and post-processing in cardiovascular magnetic resonance - 2020 update. *J Cardiovasc Magn Reson*. 2020;22(1):19.
24. Han Y, Peters DC, Salton CJ, et al. Cardiovascular Magnetic Resonance Characterization of Mitral Valve Prolapse. *JACC Cardiovasc Imaging*. 2008;1(3):294–303.
25. Perazzolo Marra M, Basso C, Lazzari M, et al. Morphofunctional Abnormalities of Mitral Annulus and Arrhythmic Mitral Valve Prolapse. *Circ Cardiovasc Imaging*. 2016;9(8).
26. Lang RM, Badano LP, Mor-Avi V, et al. Recommendations for Cardiac Chamber Quantification by Echocardiography in Adults: An Update from the American Society of Echocardiography and the European Association of Cardiovascular Imaging. *Eur Hear J Cardiovasc Imaging*. 2015;16(3):233–71.
27. Evangelista A, Flachskampf F, Lancellotti P, et al. European Association of Echocardiography recommendations for standardization of performance, digital storage and reporting of echocardiographic studies. *Eur J Echocardiogr*. 2008;9(4):438–48.
28. Sande JNT, Postema PG, Boekholdt SM, et al. Detailed characterization of familial idiopathic ventricular fibrillation linked to the DPP6 locus. *Heart Rhythm*. 2016;13(4):905–12.
29. Xiao L, Koopmann TT, Ördög B, et al. Unique cardiac Purkinje fiber transient outward current β -subunit composition: A potential molecular link to idiopathic ventricular fibrillation. *Circ Res*. 2013;112(10):1310–22.
30. Pedersen CT, Kay GN, Kalman J, et al. EHRA/HRS/APHRS Expert Consensus on Ventricular Arrhythmias. *Heart Rhythm*. 2014;11(10):e166–96.
31. Parwani P, Avierinos J-F, Levine RA, Delling FN. Mitral Valve Prolapse: Multimodality Imaging and Genetic Insights. *Prog Cardiovasc Dis*. 2017;60(3):361–9.
32. Essayagh B, Sabbag A, Antoine C, et al. The Mitral Annular Disjunction of Mitral Valve Prolapse. *JACC Cardiovasc Imaging*. 2021;14(11):2073–87.
33. Toh H, Mori S, Izawa Y, et al. Prevalence and extent of mitral annular disjunction in structurally normal hearts: comprehensive 3D analysis using cardiac computed tomography. *Eur Hear J Cardiovasc Imaging*. 2021;00:1–9.
34. Bharati S, Bauernfiend R, Scheinman M, Wu D, Lev M, Rosen KM. Congenital Abnormalities of the Conduction System in Two Patients with Tachyarrhythmias. *Circulation*. 1979;59:593–606.
35. Konda T, Tani T, Suganuma N, et al. The analysis of mitral annular disjunction detected by echocardiography and comparison with previously reported pathological data. *J Echocardiogr*. 2017;15(4):176–85.
36. Thamman R. A New Malignant MVP Phenotype? *JACC Case Reports*. 2021;3(2):247–9.

37. Bennett S, Phan T, Patwala A, Thamman R, Kwok CS. Surviving cardiac arrest from mitral annular disjunction: A case report. *Echocardiography*. 2019;36(7):1405–8.
38. Basso C, Perazzolo Marra M, Rizzo S, et al. Arrhythmic Mitral Valve Prolapse and Sudden Cardiac Death. *Circulation*. 2015;132(7):556–66.

SUPPLEMENTAL MATERIAL

Table S1. Variants of uncertain significance found in patients with MAD/MVP

Patient	Mutation	Gene		
IVF survivor 3	VUS	TMEM43	c.428C>T	p.(Thr143Met)
	VUS	DSP	c.3230C>A	p.(Ala1077Glu)
IVF survivor 4	VUS	TTN	c.76352dupC	Pro25452fs

Table S2. Morphologic PVC criteria in patients with MAD/MVP

Patient	VE	BBB pattern	Precordial transition	Axis	Estimated origin
IVF survivor 1	No	N/A	N/A	N/A	N/A
IVF survivor 2	Yes	RBBB	V4	Superior	LV inferoseptal
		LBBB	V5	Inferior	RVOT
IVF survivor 3	No	N/A	N/A	N/A	N/A
IVF survivor 4	Yes	LBBB	V3	Inferior	RVOT (distal)
IVF survivor 5	Yes	RBBB	Positive conc.	Intermediar/ superior	LV mid posterior
IVF survivor 6	Yes	LBBB	V4	Inferior	RVOT (distal)
IVF survivor 7	Yes	RBBB	V5	Superior	LV apex
IVF survivor 8	Yes	LBBB	V4	Inferior	RVOT distal lateral DD LVOT RCC

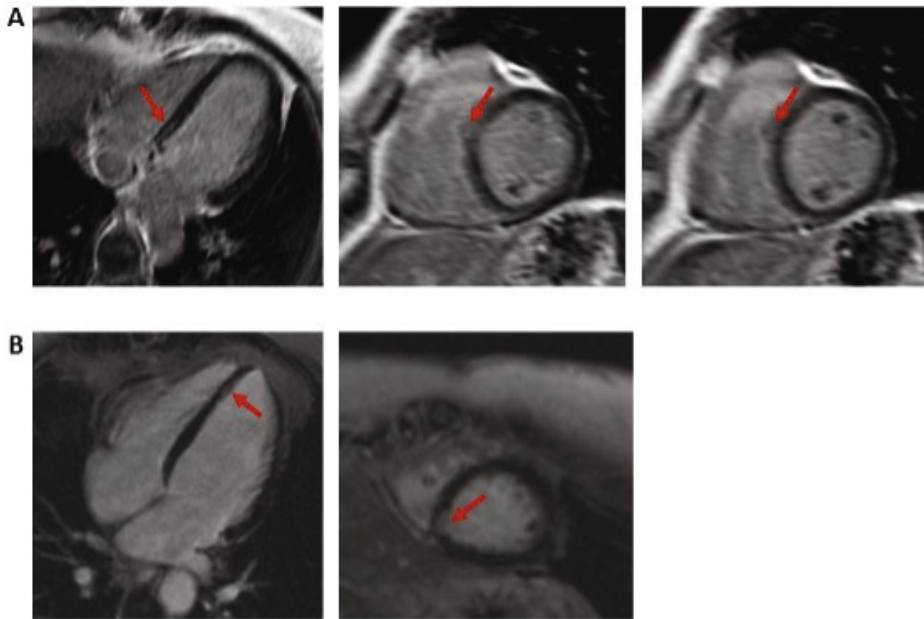


Figure S1. Example of two IVF patients with LGE

A: One patient with inferolateral MAD showed midwall LGE in the LV basal inferoseptal myocardium. B: One patient without MAD/MVP showed possible basal subendocardial LGE. However, this could also be due to slow flow in a basal crypt.

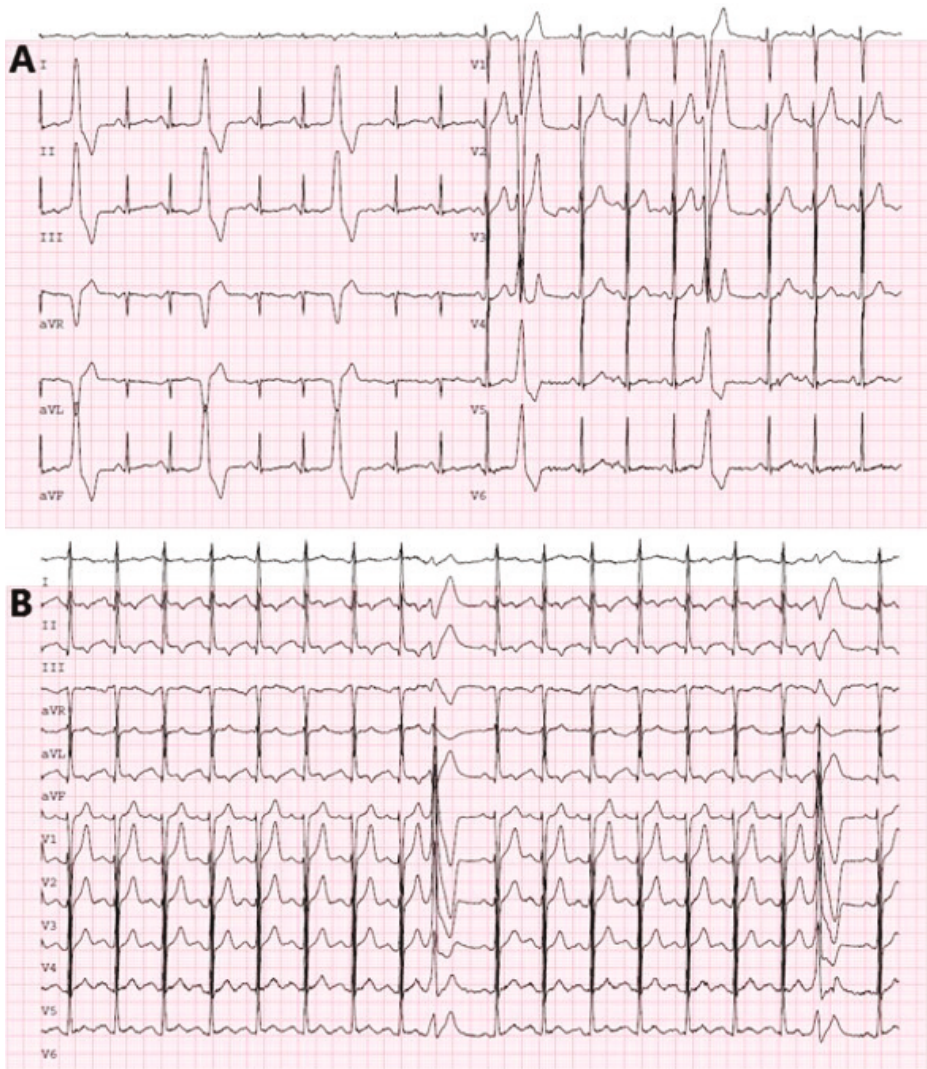


Figure S2. Example of two patients with MAD/MVP and PVCs

A: The electrocardiogram shows PVCs with a LBBB morphology and an inferior axis of an IVF patient with MAD/MVP. B: The electrocardiogram shows PVCs with an RBBB morphology and a horizontal axis of an IVF patient with MAD/MVP.

APPENDIX

Nederlandstalige samenvatting

List of Publications

Dankwoord/Acknowledgements

Curriculum Vitae

NEDERLANDSTALIGE SAMENVATTING

Plotse hartdood bij jonge, ogenschijnlijk gezonde personen heeft een enorme impact. Families en artsen blijven achter met veel onbeantwoorde vragen: Hebben we tekenen over het hoofd gezien? Had het voorkomen kunnen worden? En wie loopt nog meer risico? In Nederland wordt geschat dat elke drie dagen een persoon onder de 40 jaar overlijdt aan plotse hartdood. De meest voorkomende oorzaken van plotse hartdood bij deze jonge patiënten bestaan uit een aangeboren (anatomische) hartafwijking, een genetisch bepaalde hartritmestoornis, of een erfelijke hartspierziekte.

Binnen de erfelijke hartspierziekten wordt onderscheid gemaakt tussen gedilateerde cardiomyopathie (DCM), hypertrofe cardiomyopathie (HCM) en aritmogene cardiomyopathie, ook bekend als aritmogene rechter ventrikel cardiomyopathie (ARVC). De laatstgenoemde ziekte betreft een groot deel van de in dit proefschrift beschreven populatie. In vergelijking met de andere hartspierziekten wordt ARVC gekenmerkt door het optreden van potentieel levensbedreigende hartritmestoornissen in een vroege fase van de ziekte, zonder dat er vooraf sprake was van symptomen of evidente structurele afwijkingen aan het hart. Achteruitgang van de pompfunctie, in sommige gevallen leidend tot ernstig hartfalen, treedt pas laat in het ziekteproces op. De diagnose ARVC is niet eenvoudig te stellen, waarbij deze berust op een aantal criteria waaraan punten worden toegekend volgens een wereldwijd overeengekomen richtlijn, die bijgesteld kan worden op grond van nieuwe studies.

Doordat het voorkomen van ARVC erfelijk bepaald is, lopen familieleden van patiënten ook risico de ziekte te ontwikkelen. Op dit moment kan in ongeveer twee derde van de patiënten een genetisch defect (mutatie) worden aangetoond dat ten grondslag ligt aan het ziektebeeld. Voor de meeste vormen van ARVC geldt dat een eerstegraads familielid 50% kans heeft om drager te zijn van de genetische aanleg voor de ziekte. Verschillende genetische defecten kunnen tot hetzelfde beeld van ARVC leiden, maar niet alle dragers van zo'n mutatie ontwikkelen klachten of uitingen van de ziekte (onvolledige penetrantie). Deze genetische defecten coderen vrijwel allemaal voor eiwitten die een belangrijke rol spelen in de functie en opbouw van het desmosoom, een eiwitcomplex dat zorgt voor de mechanische (en elektrische) verbinding tussen twee hartspiercellen. Wanneer in een patiënt een genetische mutatie is gevonden die de ziekte veroorzaakt, kan genetisch onderzoek in familieleden worden verricht om dragerschap vast te stellen. Patiënten en familieleden met een risico op het ontwikkelen van de ziekte ondergaan frequent uitgebreid cardiologisch onderzoek om ARVC-gerelateerde afwijkingen in een vroeg stadium op te sporen. Dit bestaat onder andere uit electrocardiografie (ECG), Holteronderzoek, en beeldvorming van het hart middels echocardiografie en/of magnetische resonantie beeldvorming (MRI). Aangezien ARVC niet genezen kan worden is het belangrijkste doel na vaststellen van de aanleg voor deze ziekte het voorkomen van plotse hartdood. Dit kan middels een implanteerbare cardioverter-defibrillator (ICD). Daarnaast wordt intensief sporten afgeraden voor ARVC patiënten en familieleden die risico lopen de aandoening te ontwikkelen, aangezien dit de ziekteprogressie kan versnellen. Omdat juist bij ARVC een levensbedreigende ritmestoornis de eerste uiting kan zijn van de ziekte, is extra aanvullend onderzoek nodig gericht op een betere risicostratificatie.

Deformatiebeeldvorming

Een techniek die kan helpen om uitingsvormen van hartspierziekten in een vroeg stadium aan het licht te brengen is echocardiografische deformatiebeeldvorming. Deze techniek is gericht op het kwantificeren van mechanische vervorming (deformatie) van de hartspier gedurende de hartcyclus. Eerdere studies hebben laten zien dat hiermee subtiele mechanische afwijkingen ontmaskerd kunnen worden, die bij visuele beoordeling van beelden onopgemerkt zouden blijven. Ondanks het niet-invasieve karakter, de lage kosten en de brede beschikbaarheid, wordt in de klinische praktijk wordt nog maar beperkt gebruik gemaakt van deformatiebeeldvorming. Waarschijnlijk komt dit onder andere doordat de waarde van de meeste parameters slechts in één cohort is aangetoond, zonder externe validatie. Daarnaast hebben eerdere studies nog niet de toegevoegde waarde in vergelijking met de huidige klinische praktijk onderzocht, waarin meerdere modaliteiten naast elkaar worden gebruikt.

In dit proefschrift wordt ARVC als ziektemodel gebruikt om het pad naar de klinische toepassing van deformatiebeeldvorming bij (erfelijke) hartspierziekten te beschrijven. Hierbij worden diverse doelen beoogd: verbetering van vroege herkenning van ARVC, verbetering van risicof stratificatie ten aanzien van levensbedreigende ritmestoornissen, en tot slot ook meer bekendheid en bredere toepassing van deformatiebeeldvorming bij verdenking op hartspierziekten in de algemene cardiologische praktijk.

Deel I – Deformatiebeeldvorming in ARVC

ARVC begint in specifieke regio's van met name de rechterkamer (RV) en verspreidt zich steeds verder over zowel de rechter- als de linkerkamer. Visuele beoordeling van wandbewegingsstoornissen in de dunwandige RV is erg lastig, maar wel een vereiste binnen de criteria om de diagnose ARVC te stellen. In **Hoofdstuk 2** onderzoeken wij of het gebruik van RV deformatiebeeldvorming kan leiden tot betere detectie van ARVC patiënten middels echocardiografie. Hierbij bleek dat alle patiënten die de diagnose ARVC kregen volgens een expert panel al (subtiele) afwijkende RV deformatiepatronen lieten zien. Het was dus een hele gevoelige (sensitieve) methode. Er moeten echter altijd meerdere modaliteiten naast elkaar gebruikt worden om de diagnose te stellen, omdat afwijkende RV deformatie op zichzelf geen betrouwbaar onderscheid kan maken tussen ARVC en andere RV gerelateerde ziekten (niet specifiek).

Er zijn het afgelopen decennium twee verschillende methoden ontwikkeld om regionale afwijkingen in de RV te classificeren. In een cohort in Utrecht werden drie karakteristieke regionale deformatiepatronen onderscheiden en in een cohort in Oslo werd gefocust op mechanische dispersie, een maat voor heterogeniteit van de contractie. Beide methoden waren echter nog niet extern gevalideerd of met elkaar vergeleken. **Hoofdstuk 3** beschrijft de succesvolle externe validatie van beide methoden. In een gecombineerd cohort van patiënten uit Oslo en Utrecht laten we daarnaast zien dat het combineren van de twee technieken aanvullende waarde kan hebben. Als het regionale deformatiepatroon normaal is, bleek het risico op een ernstige hartritmestoornis zeer laag. Wanneer het patroon afwijkend is kan de mechanische dispersie verder onderscheid maken tussen een matig en een hoog risico op ernstige ritmestoornissen.

Deel II – Karakteriseren van het onderliggende ziektesubstraat

Omdat onderzoek van het hartspierweefsel middels een biopt vanwege de risico's in de meeste gevallen geen optie is, moet gezocht worden naar niet-invasieve manieren om het ziektesubstraat te karakteriseren. Eerder hebben simulaties met een computermodel laten zien dat afwijkingen in de deformatie waarschijnlijk een reflectie zijn van het onderliggende substraat. Een verrassende bevinding bij dit onderzoek was dat verminderde contractiliteit en toegenomen stijfheid van het weefsel al zeer vroeg in het ziektebeloop leken voor te komen, terwijl de heersende opvatting tot dat moment was dat in eerste instantie alleen elektrische afwijkingen optreden bij ARVC. In deel II van dit proefschrift beschrijven we verschillende stappen waarin wordt toegewerkt naar een persoonlijke simulatie van het ziektesubstraat met potentiële klinische toepassingen, de zogenaamde Digitale Tweeling. Het uiteindelijke doel was om met behulp van het computermodel een onderscheid te maken tussen veranderingen die gepaard gaan met een hoog risico op ritmestoornissen en meer onschuldige veranderingen in het weefsel die tot een afwijkende deformatie leiden. In **Hoofdstuk 4** passen we deze patiëntspecifieke benadering toe in een cohort van dragers van een desmosomale mutatie. Op basis van deformatiedata maakt het model een inschatting van het onderliggende ziektesubstraat in een specifieke patiënt. Uit een grote hoeveelheid variabelen die het model in acht neemt bleken regionale veranderingen in contractiliteit en compliantie van het weefsel het ziektesubstraat in ARVC het beste te karakteriseren. **Hoofdstuk 5** beschrijft de introductie van onzekerheid in het model. Aangezien zowel de metingen als de simulaties onzekerheid met zich meebrengen, was deze stap noodzakelijk om uiteindelijk het substraat over de tijd de kunnen vervolgen. In **Hoofdstuk 6** hebben we deformatiedata en simulaties van het onderliggende ziektesubstraat gecombineerd om het tot uiting komen van de ziekte in verschillende leeftijdsgroepen te onderzoeken. Eerder werd gesuggereerd dat screenen na de leeftijd van 50 tot 60 jaar niet meer nodig is, maar in deze studie laten wij zien dat ARVC ook op latere leeftijd nog tot uiting kan komen met potentieel levensbedreigende ritmestoornissen tot gevolg.

Deel III – Implementatie van deformatiebeeldvorming in de klinische praktijk

Het laatste deel van dit proefschrift is gericht op het naar de dagelijkse klinische praktijk brengen van deformatiebeeldvorming. Een belangrijke stap naar bredere implementatie zou opname in klinische richtlijnen zijn. Hiervoor is overtuigend bewijs van de toegevoegde waarde van de techniek nodig. Een belangrijke kracht van deformatiebeeldvorming is dat het een gevoeligere methode is voor detectie van vroege ziektemanifestaties in vergelijking met conventionele beeldvorming. In **Hoofdstuk 7** hebben we op basis van literatuuronderzoek het beschikbare bewijs samengevat voor de toepassing van deformatiebeeldvorming bij vroege detectie van genetische hartspierziekten bij familieleden. Met name bij DCM en ARVC zijn er specifieke parameters die van meerwaarde zijn bij vroege detectie van ziekte en bovendien aanvullende prognostische waarde hebben met betrekking tot (levensbedreigende) hartritmestoornissen.

Hoewel de waarde van deformatiebeeldvorming als een op zichzelf staande index meerdere malen is gepubliceerd, ontbreekt het aan studies die de klinische praktijk nabootsen, waarbij meerdere modaliteiten naast elkaar worden gebruikt. Opname in klinische richtlijnen vereist bewijs dat de techniek de huidige klinische praktijk verbetert. In **Hoofdstuk 8** hebben we ARVC gebruikt als model om de toegevoegde waarde van deformatiebeeldvorming voor

het voorspellen van ritmestoornissen te onderzoeken in een multimodale benadering. We integreerden deformatiebeeldvorming met de gevalideerde ARVC risicocalculator om aanvullende waarde in de klinische praktijk te onderzoeken. In deze studie bleek dat het toevoegen van RV deformatie de gepersonaliseerde risicopredictie bij ARVC patiënten kan verbeteren. Gezien de zeer goede negatief voorspellende waarde kan normale RV deformatie artsen ondersteunen in een afwachtend beleid met betrekking tot ICD implantatie bij patiënten met een laag of matig risico op ritmestoornissen.

In **Hoofdstuk 9** worden aan de hand van de in dit proefschrift opgenomen studies enkele belangrijke kwesties in het onderzoeksveld bediscussieerd. Op dit moment worden hartspierziekten met name op basis van het fenotype geclassificeerd, terwijl we door toenemend gebruik van genetisch onderzoek in de toekomst waarschijnlijk naar een benadering op basis van genotype zullen gaan. Daarnaast worden in dit hoofdstuk enkele zwakke plekken van het hart besproken, waaronder de regio waar ARVC vaak het eerst tot uiting komt. Tijdens inspanning kunnen deze zwakke plekken nog extra onder druk komen te staan, wat invloed kan hebben op progressie van de ziekte. In het **Addendum** van dit proefschrift beschrijven wij hoe een andere zwakke plek, aan de linkerzijde van het hart, mogelijk op een vergelijkbare manier tot ritmestoornissen kan lijden.

Conclusie

Deformatiebeeldvorming stelt ons in staat expressie van erfelijke hartspierziekten in een vroeger stadium op te sporen dan met de conventionele onderzoeken en technieken. Dit kan helpen bij het plannen van follow-up van familieleden met (erfelijke) hartspierziekten. Ook kan het ondersteuning geven in beslissingen rondom preventief therapeutisch ingrijpen, zoals het implanteren van een ICD. Er is echter meer onderzoek nodig om beslissingen rondom therapeutisch ingrijpen te ondersteunen en daarvoor is nationale en internationale samenwerking essentieel. Het vereist namelijk zeer grote cohorten van patiënten en familieleden om uiteindelijk de zorg voor dragers van specifieke genetische mutaties te personaliseren.

Deformatiebeeldvorming verdient een belangrijkere plaats in de richtlijnen voor diagnostiek van hartspierziekten in het algemeen. Mede door verregaande automatisering is de meting goed toepasbaar in de algemene praktijk, waardoor functionele veranderingen objectiever kunnen worden vastgelegd dan met visuele beoordeling van een echocardiogram.

LIST OF PUBLICATIONS

Sabbag A*, Aabel EW*, Castrini AI, Siontis KC, Laredo M, Nizard J, Duthoit G, Asirvatham S, Sehrawat O, **Kirkels FP**, van Rosendaal PJ, Beinart R, Acha MR, Peichl P, Lim HS, Sohns C, Martins R, Font J, Truong NNK, Estensen M, Haugaa KH. Mitral Valve Prolapse: Arrhythmic Risk during Pregnancy and Postpartum. *Eur Heart J*. 2024 Apr 15. [Epub ahead of print]. (doi: 10.1093/eurheartj/ehae224)

Verheul LM, Guglielmo M, Groeneveld SA, **Kirkels FP**, Scrocco C, Cramer MJ, Bootsma M, Kapel GFL, Alings M, Evertz R, Mulder BA, Prakken NHJ, Balt JC, Volders PGA, Hirsch A, Yap SC, Postema PG, Nijveldt R, Velthuis BK, Behr ER, Wilde AAM, Hassink RJ. Mitral Annular Disjunction in Idiopathic Ventricular Fibrillation Patients: Just a Bystander or a Potential Cause? *Eur Heart J Cardiovasc Imaging*. 2024 Feb 27;jeae054 [Epub ahead of print]. (doi: 10.1093/ehjci/jeae054)

Kirkels FP, Rootwelt-Norberg C, Bosman LP, Aabel EW, Muller SA, Castrini AI, Taha K, van Osta N, Lie ØH, Asselbergs FW, Lumens J, Te Riele ASJM, Hasselberg NE, Cramer MJ, Haugaa KH**, Teske AJ**. The Added Value of Abnormal Regional Myocardial Function for Risk Prediction in Arrhythmogenic Right Ventricular Cardiomyopathy. *Eur Heart J Cardiovasc Imaging*. 2023;24(12):1710-1718. (doi: 10.1093/ehjci/jead174)

Kirkels FP*, van Osta N*, Rootwelt-Norberg C, Chivulescu M, van Loon T, Aabel EW, Castrini AI, Lie ØH, Asselbergs, FW, Delhaas T, Cramer MJ, Teske AJ, Haugaa KH**, Lumens J**. Monitoring of Myocardial Involvement in Early Arrhythmogenic Right Ventricular Cardiomyopathy Across the Age Spectrum. *J Am Coll Cardiol*. 2023;82(9):785-97. (doi: 10.1016/j.jacc.2023.05.065)

Kloosterman M, Boonstra MJ, Roudijk RW, Bourfiss M, van der Schaaf I, Velthuis BK, Eijsvogels TMH, **Kirkels FP**, van Dam PM, Loh P. Body surface potential mapping detects early disease onset in plakophilin-2-pathogenic variant carriers. *Europace*. 2023;25(7):euad197 [Epub ahead of print]. (doi: 10.1093/europace/euad197)

Kirkels FP*, Taha K*, Teske AJ, Asselbergs FW, van Tintelen JP, Doevendans PA, Kutty S, Haugaa KH, Cramer MJ. Echocardiographic Deformation Imaging for Early Detection of Genetic Cardiomyopathies: JACC Review Topic of the Week. *J Am Coll Cardiol*. 2022;79(6):594-608. (doi: 10.1016/j.jacc.2021.11.045)

Verheul LM, Groeneveld SA, **Kirkels FP**, Volders PGA, Teske AJ, Cramer MJ, Guglielmo M, Hassink RJ. State-of-the-Art Multimodality Imaging in Sudden Cardiac Arrest with Focus on Idiopathic Ventricular Fibrillation: A Review. *J Clin Med*. 2022;11(16):4680. (doi: 10.3390/jcm11164680)

Kirkels FP*, Groeneveld SA*, Cramer MJ, Evertz R, Haugaa KH, Postema PG, Prakken NHJ, Teske AJ, Wilde AAM, Velthuis BK, Nijveldt R, Hassink RJ. Prevalence of Mitral Annulus Disjunction and Mitral Valve Prolapse in Patients With Idiopathic Ventricular Fibrillation. *J Am Heart Assoc*. 2022;11(16):e025364. (doi: 10.1161/JAHA.121.025364)

Koopsen T, Van Osta N, Van Loon T, Van Nieuwenhoven FA, Prinzen FW, Van Klarenbosch BR, **Kirkels FP**, Teske AJ, Vernooij K, Delhaas T, Lumens J. A Lumped Two-Compartment Model for

Simulation of Ventricular Pump and Tissue Mechanics in Ischemic Heart Disease. *Frontiers in Physiology*. 2022;13:782592. (doi: 10.3389/fphys.2022.782592)

Kirkels FP, Bosman LP, Taha K, Cramer MJ, van der Heijden JF, Hauer RNW, Asselbergs FW, Te Riele ASJM, Teske AJ. Improving Diagnostic Value of Echocardiography in Arrhythmogenic Right Ventricular Cardiomyopathy Using Deformation Imaging. *JACC Cardiovascular Imaging*. 2021;14(12):2481-2483. (doi: 10.1016/j.jcmg.2021.07.002)

Kirkels FP, Lie ØH, Cramer MJ, Chivulescu M, Rootwelt-Norberg C, Asselbergs FW, Teske AJ, Haugaa KH. Right Ventricular Functional Abnormalities in Arrhythmogenic Cardiomyopathy: Association With Life-Threatening Ventricular Arrhythmias. *JACC Cardiovasc Imaging*. 2021;14(5):900-910. (doi: 10.1016/j.jcmg.2020.12.028)

Kirkels FP*, van Osta N*, Lyon A, Koopsen T, van Loon T, Cramer MJ, Teske AJ, Delhaas T, Lumens J. Electromechanical Substrate Characterization in Arrhythmogenic Cardiomyopathy Using Imaging-Based Patient-Specific Computer Simulations. *Europace*. 2021;23(Suppl1):i153-i160. (doi: 10.1093/europace/euaa407)

Kirkels FP*, van Osta N*, van Loon T, Koopsen T, Lyon A, Meiburg R, Huberts W, Cramer MJ, Delhaas T, Haugaa KH, Teske AJ, Lumens J. Uncertainty Quantification of Regional Cardiac Tissue Properties in Arrhythmogenic Cardiomyopathy Using Adaptive Multiple Importance Sampling. *Frontiers in Physiology*. 2021;12:738926. (doi: 10.3389/fphys.2021.738926)

van Osta N, Lyon A, **Kirkels FP**, Koopsen T, van Loon T, Cramer MJ, Teske AJ, Delhaas T, Huberts W, Lumens J. Parameter subset reduction for patient-specific modelling of arrhythmogenic cardiomyopathy-related mutation carriers in the CircAdapt model. *Philos Trans A Math Phys Eng Sci*. 2020;378(2173):20190347. (doi: 10.1098/rsta.2019.0347)

van Osta N, **Kirkels FP**, Lyon A, Koopsen T, Delhaas T, Cramer MJ, Teske AJ, Lumens J. Personalization of Biomechanical Models for Early Detection of Disease in Arrhythmogenic Cardiomyopathy. *2018 Computing in Cardiology Conference proceedings*. (doi: 10.22489/CinC.2018.400)

*Shared first authorship

**Shared last authorship

DANKWOORD / ACKNOWLEDGEMENTS

Met het schrijven van dit dankwoord komt mijn promotietraject ten einde en kan ik terugkijken op een bijzondere tijd waarin ik veel inspirerende mensen heb ontmoet. Bovenal is dit proefschrift het resultaat van samenwerking, waarbij ik de luxe heb gehad mij thuis te voelen in drie heel verschillende onderzoeksgroepen. Ik wil graag iedereen bedanken die direct, dan wel indirect, heeft bijgedragen aan dit proefschrift. Allereerst wil ik de patiënten en familieleden bedanken die mee hebben gewerkt aan de onderzoeken en toestemming gaven voor het gebruik van hun gegevens. Alleen op deze manier kunnen we verder komen in de geneeskunde. Daarnaast wil ik een aantal mensen in het bijzonder noemen:

Mijn promotoren **prof. dr. F.W. Asselbergs** en **prof. dr. ir. J.E. Lumens**:

Beste **Folkert**, de eerste keer dat ik je ontmoette kwam ik als student langs voor een oriënterend gesprek. Je stelde voor dat ik de volgende dag op het vliegtuig kon stappen om onderzoek te doen bij jouw groep in Londen, maar dat vereiste wel dat ik "uit mijn comfortzone" zou stappen. Het alternatief dat je schetste was dat ik in mijn comfortzone in het "echokliniekje van Maarten Jan" zou blijven. Ik koos de laatste optie, maar ben blij dat dit toch heeft geleid tot een promotietraject met jou als promotor. Hierbij ben ik uiteindelijk toch ook nog 500km verder van huis terechtgekomen ten opzichte van jouw voorstel. Dank voor je betrokkenheid de afgelopen jaren. Ik heb bewondering voor jouw vermogen om vele taken te combineren, waarbij je ook nog ieder moment van de dag klaar stond voor je promovendi. Je denkt altijd aan het grotere plaatje en bent vaak al vele denkstappen verder dan je gesprekspartner. Uiteindelijk was Utrecht helaas te klein voor je, maar jouw overstap creëert ook weer nieuwe kansen voor samenwerkingen tussen Utrecht en Amsterdam.

Beste **Joost**, door jouw goede banden met de cardiologen uit Utrecht en Oslo kon mijn promotietraject in deze driehoekssamenwerking vorm krijgen. Al vele malen maakte jij de reis vanuit het verre zuiden om te filosoferen over toepassingen van het CircAdapt model en jouw kennis over de cardiomechanica te delen. Je koppelde mij al vroeg aan jouw nieuwe promovendus om deze ideeën samen uit te werken en hebt mij later ook verwelkomd binnen jouw onderzoeksgroep. Helaas verliep mijn aanstelling in Maastricht grotendeels digitaal vanwege Covid-19, maar jij hebt ervoor gezorgd dat ik mij altijd thuis heb gevoeld binnen de onderzoeksgroep. Je bent als geen ander in staat een brug te slaan tussen klinici en engineers wat zorgt voor een mooie kruisbestuiving.

Mijn copromotoren **dr. M.J. Cramer** en **dr. A.J. Teske**:

Beste **Maarten-Jan**, jouw ongeëvenaarde enthousiasme en netwerkcapaciteiten zijn de basis geweest voor vele onderzoeksprojecten en samenwerkingen, waaronder al het werk wat in dit proefschrift is beschreven. Op ieder congres moesten we weer even op de foto met de onderzoeksgrootheden en door jouw toedoen zijn er al heel wat tulpenvazen en Domtorens de wereld over gevlogen. Nadat ik op zondag regelmatig een mail of belletje kreeg als je weer inspiratie had opgedaan na het lezen van JACC is het erg mooi dat twee van de hoofdstukken in dit proefschrift ook in je favoriete tijdschrift terecht zijn gekomen. Bedankt voor jouw warme en persoonlijke begeleiding en de kansen die je mij geboden hebt de afgelopen jaren.

Beste **Arco**, ik mag mij gelukkig prijzen dat ik heb mogen leren van een echogoeroe als jij. Jouw kritische blik en inhoudelijke basis hebben belangrijke invloed gehad op dit proefschrift. Je vormde een ideale combinatie met Maarten-Jan, waarbij jij met je koersvastheid ervoor zorgde dat we niet afdwaalden en altijd weer terugkwamen tot de kern. Jouw kennis van de echocardiografie en cardiomechanica heeft mijn enthousiasme voor cardiale beeldvorming aangewakkerd en ik hoop in de toekomst nog veel met je samen te mogen werken.

Ik wil de leden van de leescommissie **prof. dr. S.A.J. Chamuleau**, **prof. dr. P.A.F.M. Doevendans**, **prof. dr. M.C. Post**, **prof. dr. J.P. van Tintelen** en **prof. dr. Velthuis** bedanken dat zij de tijd hebben genomen om dit proefschrift te lezen en beoordelen.

Oslo

Prof. dr Haugaa, dear **Kristina**, I feel very lucky that I have had the opportunity to work under your supervision. From the first time you welcomed me in Oslo as a medical student you made me feel part of the group. I am very thankful for the opportunities you provided me and your efforts to extent the collaboration between Oslo, Maastricht and Utrecht. Your work ethic and passion for science with clinical impact is inspiring. I hope you are still able to work after 4pm now that my supply of stroopwafels has stopped. It was also interesting to see that over the past years, your office looked more and more like a museum of Dutch traditional objects due to Maarten-Jan. I hope that the projects we did together are the start of many more collaborative efforts in the field of genetic cardiomyopathies. Tusen takk!

I would also like to thank my other colleagues in Oslo. Even after the majority of our work was finished, you were the reason I kept looking for excuses to visit Oslo. **Øyvind**, thank you your help and supervision when I came to Oslo as a student. You were an inspiring mentor, not only because of your knowledge of statistics, which had a large influence on many chapters in this thesis, but also as a person, of which your performance at the Julebord was a good example. **Isotta**, I am thankful for the time we spent together in Oslo. From studying together in BI for the echo exam to the nice dinners with your family. While I only wrote this book, you managed to write a thesis and brought two beautiful boys into this world. I am looking forward to your defence. **Maria**, thank you for welcoming me not only in the research lab, but also in the greatest town on earth, your hometown Drammen. Tusen takk **Christine**, **Monica**, **Eivind**, **Marianne**, **Eystein**, **Margareth**, **Lars**, **Alessia**, **Esther**, **Jorun**, **Nina**, **Tove-Elisabeth**, **Anders** and **prof. dr. Thor Edvardsen**.

Erik, with your profession of opera singing, I cannot really qualify you as a colleague. I am very happy though that my stay in the student housing in Oslo lead to our friendship. I am thankful for the many moments we share, including the canoe fishing trip at your parents' home, the camping trip to Lund and your opera singing in our nearly sinking boat in the canals of Utrecht.

Maastricht

Nick, het heeft heel wat Zoomsessies en retourtjes Utrecht-Maastricht gekost, maar na lang discussiëren lukte het ons altijd weer onze twee verschillende werelden bij elkaar te brengen. Deze discussies over mechanica en fysiologie hebben mijn passie voor de cardiologie vergroot. En ondanks het gemis van een technische achtergrond ben ik dankbaar dat jullie mij toch in de groep hebben opgenomen **Aurore**, **Tijmen**, **Tim**, **Ahmed**, **Claudia**, **Melania**, **Anneloes**,

Andrija, Roel, Erik en **prof. dr. Tammo Delhaas**. Een groot deel van mijn aanstelling ondervonden we beperkingen door de pandemie, maar gelukkig hebben we ook nog genoeg mooie momenten beleefd, van ambtenarencarnaval op het Vrijthof tot schapendrijven in het Limburgse heuvelland.

Utrecht

De projecten beschreven in dit proefschrift zouden niet mogelijk zijn geweest zonder de lange geschiedenis van onderzoek op het gebied van genetische hartspierziekten in het UMC Utrecht. Veel dank aan **prof. dr. R.N.W. Hauer, prof. dr. J.P. van Tintelen, prof. dr. P.A.F.M. Doevendans, dr. K.P. Loh, dr. J.F. van der Heijden, dr. A.A.B. van Veen, prof. dr. Velthuis, dr. M. Harakalova, dr. A.F. Baas** en alle andere betrokkenen. **Dr. A.S.J.M. te Riele, Anneline**, met jouw drive en je onderzoeksprestaties ben je gekroond tot de nieuwe ARVC-queen. Bedankt voor je betrokkenheid en enthousiasme en ik heb er alle vertrouwen in dat jij gaat bijdragen aan nog vele jaren hoogwaardig onderzoek naar genetische hartspierziekten in Utrecht. **Dr. T.P. Mast**, beste **Thomas**, jij hebt mij in de bunker voor het eerst laten kennismaken met de echocardiografie en jouw beschrijving van de strainpatroon heeft een belangrijke basis gelegd voor veel hoofdstukken in dit proefschrift, inclusief het contact met de onderzoeksgroepen in Oslo en Maastricht. Dank daarvoor!

De promovendi uit de Asselbergsgroep, oftewel Folkerts studieleger, wil ik bedanken voor het hechte groepsgevoel, waardoor het doen van een promotietraject nooit eenzaam voelde. **Mimount**, van de MRI strain heb je weinigen kunnen overtuigen, maar ik ben wel heel blij je nu in het Diak én straks in het UMC weer als collega naast mij te hebben! **Arjan & Lieke**, toch mooi dat we met wat activisme en ondernemerschap de voorpagina van de Telegraaf hebben gehaald met onze stichting. **Mark**, nooit verlegen om een kleine discussie, waarbij **Machteld** waarschijnlijk voornamelijk in voor haar gebruikelijke straattaal antwoordt. **Rob** en **Janine**, ik zie jullie vast snel weer als jullie het verre oosten vertegenwoordigen op de NVVC-dagen. **Marijke**, ik begin mij nu toch af te vragen of je eerder je beide promoties afrondt of eerder professor wordt. **Laurens**, jij hebt in ieder geval al het agendabeheer van een ware verstrooide professor en in **Steven** heb je een waardige opvolger gevonden. **Fahima, Iris** en **Manon**, succes met jullie PhD's! (Waarschijnlijk hebben jullie mij inmiddels wel bijna ingehaald)

Sanne, heel wat avonden aan MAD-metingen op de radiologie hebben we samen doorstaan. Ik weet alleen niet of ik ooit nog tegenover je durf te staan op de tennisbaan. **Philippe**, ik zal je binnenkort maar eens vragen dit proefschrift op CD te branden. **Nicole, Justin, Rutger, Marijn, Anne-Mar, Evangeline, Hugo, Thomas, Max, Rosanne, Timion, René, Odette, Bas, Lennart, Melle, Markella, Aria, Lisa, Diantha, Aernoud**, dank voor de vele gezellige borrels, congressen en PhD-weekenden. Ik kijk ernaar uit om met veel van jullie weer in de kliniek te werken de komende jaren!

De laboranten van de hartfunctie, waarmee ik inmiddels mijn 12.5-jarig jubileum mag vieren, wil ik bedanken voor hun rol bij het verzamelen van data en de begeleiding tijdens mijn eerste periode als echolaborant. Bedankt voor de mooie echo's **Ineke, Jeannette, Elly, Grianne, Roshni, Vasudha** en alle anderen.

De dames van het secretariaat **Christa, Jantine, Katinka, Sylvia** en **Tamara** wil ik bedanken voor hun hulp tijdens mijn promotietraject en ANIOS-periode.

Naast alle collega's waar ik in de kliniek mee heb gewerkt wil ik in het bijzonder mijn opleiders van de afdeling cardiologie in het UMC Utrecht, **dr. G.Tj. Sieswerda** en **dr. N. Clappers**, en mijn opleiders van de vooropleiding interne geneeskunde in het Diaconessenhuis, **dr. G.A.J. van Boekel** en **dr. L.H. van Huis**, danken voor de tijd die zij mij hebben gegeven om naast het klinische werk aan dit proefschrift te werken.

Daarnaast is dit ook de plek om mijn vrienden te bedanken voor al het andere wat belangrijk is in het leven. De BROK koffieclub, **Floris, Cas, Yvette, Joep, Geert**, doordat we tegelijk aan onze promoties begonnen begrepen we elkaars frustraties, maar konden we toch vooral ook samen genieten van de flexibiliteit van het PhD-life. Mijn tennisteam wil ik danken voor de uitlaatklep en de flexibiliteit als ik weer eens een deadline had. De Blazeboys, **Jonas, Jasper, Tycho, Joris, Kasper, Jef, Lex, Luuk, Nol, Okke, Thom, Kim, Cedric** en **Maurits**, ik ben dankbaar dat we inmiddels al zo lang zo'n hechte vriendengroep hebben. Het was altijd weer een verademing om op vrijdagavond bij jullie aan tafel te zitten, waarbij jullie begrip van mijn werk zich had gevormd tot iets als het verkopen van MRI-scanners, en ik ben blij dat deze traditie niet verbroken wordt nu er een totale babyboom aan de gang is. Ook de bewoners van de **Braamstraat**, de **Feministen**, de vrienden van het **Jordan** en de andere vrienden van **Geneeskunde** ben ik dankbaar voor al het moois wat we samen hebben meegemaakt en voor hoe vertrouwd het altijd is als we elkaar weer zien. Het Oudwijcker eetgezelschap, **Bob** en **Stijn**, ik weet dat jullie hier graag als paranimfen hadden gestaan, maarja, je kan niet alles hebben. Ik vind het prachtig dat jullie inmiddels bijna deel van de familie zijn geworden en jullie tripjes naar Noorwegen waren hoogtepunten van de tijd die ik daar doorbracht.

Paranimfen

Karim, eigenlijk ben je al vijf jaar lang mijn paranimf. Doordat je al eerder kon echoën, eerder in de bunker de kunst van het strainen van Thomas en Arco had geleerd, eerder begon met je promotie en je ANIOS-periode en ik al eerder aan jouw zijde heb mogen staan tijdens je verdediging heb ik eigenlijk alles van je af kunnen kijken. Folkert had nog wel eens moeite om ons als twee afzonderlijke personen te zien, maar dat heb ik nooit een probleem gevonden. Ik ben blij dat ik mij kon optrekken aan iemand met jouw kwaliteiten, die zo relaxed is en zo trouw. Ik kijk ernaar uit om de komende jaren ook eindelijk in de kliniek samen te werken!

Cas, toen ik er in de introductieweek van geneeskunde achter kwam dat jij één van de Culemborgers was die mijn klasgenoten opwachtte buiten het schoolplein had ik niet verwacht hier nu samen te staan. Het enige wat ik mij nu nog afvraag is hoe het kon dat iemand jou niet mocht. Met je oprechtheid en enthousiasme zorg je overal waar je komt voor verbinding. Doordat we tegelijk aan onze promotie begonnen hielden we gelukkig enige flexibiliteit om dingen buiten werk te ondernemen. Ondanks enkele gemiste kampioenschappen van Ajax kan ik jarenlang samenwonen op de Braamstraat, een reis naar Cuba en vele (zelf georganiseerde) festivals later terugkijken op oneindig veel mooie momenten samen.

Familie

Mijn schoonfamilie, **Remco** en **Petra**, dank voor al jullie onvoorwaardelijke steun en interesse. Het is altijd fijn om weer even tot rust te komen in jullie oase in het bos, die binnenkort nog veel mooier zal zijn! **Robert** en **Özden**, gelukkig was de vakantie die we samen hebben doorgebracht wat comfortabeler dan jullie gemiddelde bergactiviteit en ik ben blij jullie weer bij ons in het land terug te hebben.

Lieve **Corry**, zonder jou als 2e moeder denk ik niet dat we met alle drie de kinderen de beroepskeuze van onze ouders zouden hebben gevolgd. Jij zorgde voor de hoognodige rust en regelmatig waardoor wij geen last van hadden van hun diensten en lange werkdagen. Ik denk ook niet dat jouw record van 27 jaar oppassen bij één gezin ooit nog verbroken gaat worden. Dankjewel dat jij er altijd voor ons bent geweest!

Onne en **Jasper**, naast de gezelligheid wil jullie bedanken voor de steun die jullie altijd zijn geweest voor mijn zusjes en de rest van de familie. Ik kan het jullie niet kwalijk nemen dat jullie soms even afdwalen als het aan tafel onbedoeld weer over geneeskunde gaat.

Lieve **Harmke**, toen jij nog mijn grote zus was vervulde het mij altijd met een gevoel van trots als ik je op school of op zeilkamp zag. Dit gevoel van trots is sindsdien eigenlijk alleen maar groter geworden. Je bent de sterkste en meest veerkrachtige persoon die ik ken en ik ben dankbaar voor de sterke band die wij hebben. Niet alleen vanuit onze kindertijd, maar ook als huisgenoten in onze studententijd ("ik ga naar mijn ouders"). Wat mooi om te zien dat jij het aanstekelijke enthousiasme wat je van mama hebt nu ook weer doorgeeft aan de volgende generatie. **Madée**, vrolijk mensje, op het moment van schrijven ben je nog maar 6 maanden oud, maar met je uitgesproken karakter en je onderzoekende blik ben je nu al een mooie aanvulling op onze familie.

Lieve **Yanne**, we lijken zoveel op elkaar en toch ook weer zo weinig. Goed dat je na het zien van beeldmateriaal uit onze jeugd toch ook vooral je eigen aandeel onderkent in plaats van alleen een pestende grote broer. Er zijn inmiddels wat jaren verstreken, maar ik vind het nog steeds moeilijk voor te stellen dat mijn kleine zusje nu in opleiding tot huisarts is. Ik ben dankbaar dat we met zijn drieën zo dicht bij elkaar wonen en zo betrokken zijn bij elkaars leven.

En dan mijn ouders, **Hans** en **Rian**, het is moeilijk om te ontkennen dat jullie ons geïnspireerd hebben in het leven. Dank dat jullie altijd voor ons klaar staan en dank voor het bijzondere, hechte gezin wat jullie op de wereld hebben gezet.

Lieve papa, wat bijzonder om nu in hetzelfde vakgebied te werken als jij. Ik heb regelmatig de vraag gekregen of het niet vervelend is vergeleken te worden met je vader of dat de lat dan te hoog wordt gelegd. Ik kan niet ontkennen dat het grote schoenen zijn om te vullen, maar als collega's of patiënten over jou vertellen kan ik alleen maar trots zijn op zo'n vader. In het begin van mijn promotietijd zijn het even spannende tijden geweest, maar ik ben heel dankbaar jou nu zo ontspannen in Friesland te zien, het plekje waar je altijd al van droomde en waar ik de afgelopen jaren ook mijn toevlucht toe zocht als er aan dit proefschrift geschreven moest worden.

Lieve mama, je bent op zoveel vlakken een voorbeeld voor mij. Ik moet zeggen dat met de passie die jij hebt voor je vak en het enthousiasme wat je uitdraagt, het lastig was een andere richting te kiezen dan de huisartsgeneeskunde. Jij hebt mij altijd geleerd "voor in de bus" te zitten in het leven en ik hoop dat ik wat stukjes levenslust en activisme van jou heb

meegekregen. De momenten met jou, Yanne, Harmke en mijn vrienden samen op de vele festivals in de zomer vormen mijn dierbaarste herinneringen!

Lieve **Yvette**, het is moeilijk om in woorden te vatten hoe blij ik ben dat wij elkaar gevonden hebben. Bij onze eerste ontmoeting toen ik 8 was zat ik nog even niet op te letten, maar gelukkig is daarna alles goed gekomen. Wat was het fijn om de afgelopen jaren tegelijk te promoveren. Waar we normaal gesproken al geen woorden nodig hebben om elkaar te begrijpen was dat hierbij niet anders. Ik kon altijd rekenen op jouw hulp als ik het weer eens lastig vond om knopen door te hakken, of mijn uitstelgedrag er weer voor zorgde dat alles op de avond voor de deadline moest gebeuren. Het was niet altijd makkelijk als we weer van elkaar gescheiden werden doordat ik naar Noorwegen ging of jij naar Tanzania, maar de quote van Erik klopt, de liefde wordt er alleen maar sterker van. Waar we uiteindelijk ook terecht komen, of wat we uiteindelijk ook gaan doen, als ik met jou ben is het goed.

CURRICULUM VITAE

Feddo Kirkels was born on the 27th of May 1993 in Utrecht to Hans Kirkels and Rian van Kessel. He grew up in Zeist together with his sisters Harmke and Yanne. After graduating with honours from the Herman Jordan Lyceum Zeist in 2011, he started medical school at the University of Utrecht.

He participated in the Bachelor Honours program with research on optimal lead positioning in cardiac resynchronization therapy under supervision of Prof. Mathias Meine. He combined his studies with a love for traveling by doing clinical rotations in Ho Chi Minh City, Vietnam and Nkhoma, Malawi. During his Master's degree, he met Dr. Maarten-Jan Cramer, who, together with Dr. Thomas Mast and Dr. Arco Teske, introduced him into the world of echocardiographic deformation imaging. During his final year, Feddo performed a scientific internship in the Oslo University Hospital in Norway under supervision of Prof. Kristina Haugaa and Dr. Øyvind Lie. At that time, the plan for a PhD trajectory was set out in which Feddo would work within a triangular collaboration between Oslo, Utrecht and the group of mechanical engineers led by Prof. Joost Lumens from Maastricht University in the Netherlands. After graduating medical school in 2018, he started his PhD track investigating the added clinical value of deformation imaging in genetic cardiomyopathies under supervision of Prof. Folkert Asselbergs, Prof. Joost Lumens, Dr. Maarten-Jan Cramer and Dr. Arco Teske. During this time, he obtained the accreditation in adult transthoracic echocardiography by the European Association of Cardiovascular Imaging (EACVI). He spent one year working in the University Hospital Oslo under supervision of Prof. Kristina Haugaa, with an interruption due to the Covid-19 pandemic.

After working as a cardiology resident (ANIOS), Feddo started his cardiology training in June 2023 in the University Medical Center Utrecht under supervision of Dr. Gertjan Sieswerda and Dr. Nick Clappers. Feddo lives in Utrecht together with Yvette Löwensteyn.

